University of Nottingham
UK | CHINA | MALAYSIA

Engineering *Cupriavidus necator* for Butanediol Production

Ph.D. Thesis

Joshua Luke Gascoyne, MSc, BEng

2021

Thesis submitted to the University of Nottingham

for the degree of Doctor of Philosophy, March 2021

Acknowledgements

I would like to thank my primary supervisor Dr Naglis Malys for his continued support, encouragement and guidance during this PhD project. I would not be the scientist I am today without the mentoring provided by Dr Naglis Malys, giving me the confidence and knowledge needed to undertake this project. Additionally, I wish to thank my co-supervisor Assistant Professor Stephan Heeb and my bench supervisor Dr Rajesh Bommareddy for their valued contributions throughout the project. I am also grateful for the funding provided by the BBSRC and EPSRC that enabled this research at the University of Nottingham.

I would also like to thank my family, particularly my father Timothy John Gascoyne for his unfaltering support and reassurance during my studies. I would also like to thank close friends at Nottingham who have made my time thoroughly enjoyable, in particular Callum McGregor, Sean Craig, Charlie Wickam-Smith, Rajan Patel. Finally, I would like to thank my close friends Edwin and Harry for always keeping me going.

Declaration

I declare that this thesis has been composed solely by myself and that it has not been submitted, in whole or in part, in any previous application for a degree. Except where stated otherwise by reference or acknowledgement, the work presented is entirely my own.

Joshua Luke Gascoyne

Abstract

The increase in atmospheric greenhouse gases such as carbon dioxide (CO_2) is a major factor contributing to global warming. Harnessing CO_2-fixing microorganisms to produce platform chemicals, typically synthesised from petrochemicals, can simultaneously reduce greenhouse gas emissions and dependence on non-renewable sources. In this work, the conversion of CO_2 to the platform chemical butanediol (BDO) facilitated by the chemolithoautotrophic bacterium *Cupriavidus necator* H16 has been investigated.

First, *C. necator* H16 was evaluated for potential deployment as a chassis to produce (*R*)-1,3-BDO and other BDOs, through consumption and toxicity assays. To aid the engineering of *C. necator* H16, two inducible gene expression systems, TF/P_{yhjX} from *Escherichia coli* and AcoR/P_{acoA} system from *Acetobacterium woodii* were used to develop genetically encoded biosensors. These biosensors were then evaluated for potential use in BDO detection and monitoring.

Next, *C. necator* H16 was metabolically engineered to produce the optically active (*R*)-1,3-BDO. Bioproduction of (*R*)-1,3-BDO was achieved using two synthetic metabolic pathways consisting of a butanal dehydrogenase, pyruvate decarboxylase, deoxyribose-5-phosphate aldolase and an aldehyde reductase. Carbon flux towards (*R*)-1,3-BDO was significantly increased through deletion of the P3HB synthase encoded by *phaC1* and the succinyl-CoA synthetase encoded by *sucCD*. To increase genetic stability, genes encoding (*R*)-1,3-BDO biosynthesis pathways were integrated into the *C. necator* H16 genome. Chromosomally integrated strains were then cultivated heterotrophically

and autotrophically for bioproduction of (*R*)-1,3-BDO. This is the first report of production of (*R*)-1,3-BDO using CO_2 as the carbon source.

Finally, *C. necator* H16 energy metabolism was investigated to ascertain NADPH regeneration mechanism during BDO production from CO_2. To elucidate the role of four putative transhydrogenase's (PntAB1234) and their involvement in NADPH regeneration, a Δ*pntAB1234* strain was generated and characterised. A *meso*-2,3-BDO and (*R*, *R*)-2,3-BDO biosynthetic pathways were employed to evaluate transhydrogenase deletion strain ability regenerating NADH and NADPH, respectively.

This research shows that through the stepwise engineering, *C. necator* H16 can be developed as a chassis for platform chemical production demonstrating its potential for biosynthesis of (*R*)-1,3-BDO from CO_2.

Contents

List of Figures

List of Tables

Abbreviations

1,3-BDO	1,3-butanediol
1,4-BDO	1,4-butanediol
2,3-BDO	2,3-butanediol
4H2B	4-hydroxy-2-butanone
A.U.	Arbritrary unit
BDO	Butanediol
bp	base pairs
CBB	Calvin-Benson-Bassham
d	Day(s)
DCW	Dry cell weight
DNA	Deoxyribonucleic acid
DO	Dissolved oxygen
FMM	Fermentation minimal media
GC-MS	Gas chromatography-mass spectrometry
h	Hour(s)
HPLC	High performance liquid chromatography
LB	Lysogeny broth
LC-MS	Liquid chromatography-mass spectrometry
min	Minute(s)
MM	Minimal media
M9MM	M9 minimal media
NADH	Nicotinamide adenine dinucleotide + hydrogen
NADPH	Nicotinamide adenine dinucleotide phosphate + hydrogen
NCBI	National Centre for Biotechnology Information
NLMM	Nitrogen limiting minimal media
OD	Optical density
P3HB	Poly[(*R*)-3-hydroxybutyrate]
PCR	Polymerase chain reaction
(*R*)-3-HBCoA	(*R*)-3-hydroxubutyryl-CoA
RBS	Ribosomal binding site
RFP	Red fluorescent protein
RI	Refractive Index
SDS-PAGE	Sodium dodecyl sulphate-polyacrylamide gel electrophoresis
T_m	Melting temperature
TLC	Thin layer chromatography
TR	Transcriptional regulator
UV	Ultraviolet
v/v	Volume per volume
w/v	Weight per volume
μ	Specific growth rate

1 Introduction

1.1 Context

Climate change caused by the increase in atmospheric greenhouse gases (GHG) is an extremely serious risk facing humankind. In 2015, the United Nations (UN) Paris Agreement declared that an international effort is needed to limit global temperature increase to 1.5 ˚C above pre-industrial levels (UNFCCC, 2015). The climate change specifically caused by increase in the GHG carbon dioxide (CO_2) is reported to be largely irreversible (Solomon *et al.*, 2009). Indeed, cessation of CO_2 emissions and subsequent removal of atmospheric CO_2 would decrease heat lost to the ocean, resulting in significant drops in atmospheric temperatures taking 1000 years to be seen.

In order to tackle global warming, several countries have introduced initiatives and/or legislation, aiming to reduce atmospheric CO_2 levels. This includes the international research and innovation programmes that are aimed to guide the transition towards an optimal use of renewable biological resources whilst simultaneously reducing reliance on fossil carbon resources through development of the bioeconomy. One specific strategy for developing the bioeconomy is recycling and reutilisation of industrially emitted CO_2 as a carbon source and material for biosynthesis ('Horizon 2020: EU framework programme for research and innovation,' 2014).

To establish a successful bioeconomy, there has been considerable research into the use of microorganisms for increased biological production of compounds of interest. Indeed, one approach was to limit the nitrogen levels during autotrophic fermentation of *Cupriavidus necator* that increased accumulation of the bioplastic poly[(*R*)-3-hydroxybutyrate] (P3HB) (Volova *et al.*, 2013). An alternative approach is alteration

of a microorganism's DNA to re-wire its' metabolism for directing carbon towards a desired product. One example of this is use of enzymes encoded by heterologous genes for production of the platform chemical acetoin from CO_2 by *C. necator* (Windhorst and Gescher, 2019). To develop strains for production of chemicals from waste CO_2, the synthetic biology design-build-test-learn cycle (Figure 1.1) can be a useful tool, aiming to improve results from each previous iteration (Opgenorth *et al.*, 2019).

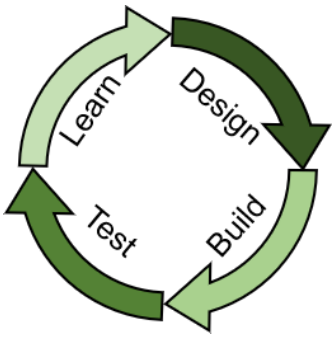

Figure 1.1 Design-build-test-learn cycle, supported by improvements made in synthetic biology is a framework for metabolic engineering of a microorganism. Each cycle aims to improve upon the previous iteration using a more systematic and efficient approach towards strain development.

The engineering of microorganisms to produce platform chemicals is one approach that can be adopted to reduce reliance on non-renewable petrochemical sources. The deployment of microorganisms that can fix CO_2 for production of platform chemicals will simultaneously reduce the demand for fossil fuels and utilise GHG. There are various microorganisms capable of fixing atmospheric CO_2 such as algae, cyanobacteria and chemolithoautotrophic bacteria. During assimilation of CO_2, energy is required due to the high oxidation state of the carbon atoms. Reducing power is supplied by organisms in various forms: hydrogen-oxidising bacteria utilise molecular hydrogen (H_2); photoautotrophs harness light to split water; acetogens utilise carbon

monoxide (CO) and H_2; and nitrifying, sulphur or iron-oxidising bacteria utilise inorganic ammonia, sulphur or iron (Nybo *et al.*, 2015). Chemolithoautotrophs are unique in that they do not require light for fixation of CO_2, increasing their rate to fix carbon achieve high biomass levels quicker, proving advantageous over light-dependent microorganisms.

1.2 The platform chemicals: butanediols

Butanediol (BDO) is a platform chemical traditionally derived from non-renewable petrochemical sources butane, acetylene and propylene (Yim *et al.*, 2011). There are four stable structural isomers of BDO: 1,2-BDO, 1,3-BDO, 1,4-BDO and 2,3-BDO (Figure 1.2). Bioproduction of 2,3-BDO has been studied for a number of decades due to natural production by several types of bacteria, providing a wealth of literature (Sabra, Groeger and Zeng, 2016; Sun *et al.*, 2015; Hakizimana, Matabaro and Lee, 2020; Ji, Huang and Ouyang, 2011). In the past decade there has been increased interest in microbial production of 1,4-BDO and 1,3-BDO which has been achieved through metabolic engineering. This section details the reported production of 1,3-BDO, 2,3-BDO and 1,4-BDO, highlighting significant scientific breakthroughs with BDO bioproduction summarised in Table 1.1.

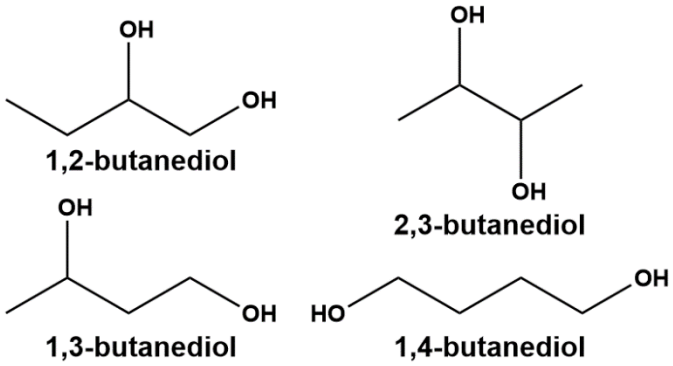

Figure 1.2 Skeletal structure of butanediol structural isomers 1,2-BDO, 1,3-BDO, 1,4-BDO and 2,3-BDO.

1.2.1 1,3-butanediol

1,3-BDO has many industrial applications. Notably, it is used for chemical conversion to the highly important 1,3-butadiene (estimated at 10 million metric tonnes in 2012) (Duan et al., 2016). Further uses rely on the optically active *R*- form of 1,3-BDO that is used for production of insecticides, pheromones, fragrances (Matsuyama, Kobayashi and Ohnishi, 1993) and antibiotics (Llarrull *et al.*, 2010). Importantly, 1,3-BDO was listed within the top 10 biobased chemical opportunities in 2017 by the Lignocellulosic Biorefinery Network (LBNet, 2017). Typical petrochemical methods for purification of 1,3-BDO produce a mixture of *R*- and *S*- optical isomers (Figure 1.3). By utilising a biological enzymatic approach for production of (*R*)-1,3-BDO, enantiomeric purity can be greatly increased.

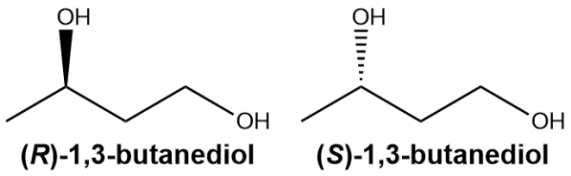

Figure 1.3 Skeletal structure of 1,3-BDO optical isomers (*R*)-1,3-BDO and (*S*)-1,3-BDO

(*R*)-1,3-BDO can be biosynthesized from 4-hydroxy-2-butanone (4H2B) in single reaction using whole cell biocatalysis. This was demonstrated using *Pichia jadinii* cells, which yielded 425 mM (*R*)-1,3-BDO of 100% optical purity from 510 mM 4H2B achieving >80% conversion (Yang et al., 2014). Similarly, a strain of *Candida krusei* was used to convert 510 mM 4H2B to 430 mM *R*-1,3-BDO with a 99 % stereochemical specificity (Zheng et al., 2012).

Several potential 1,3-BDO metabolic pathways were patented by Burgard and co-workers under patent publication number US 2012/0329113 A1 (Burgard *et al.*, 2012). However, only two biosynthetic pathways have been reported for production of (*R*)-1,3-BDO to date (Figure 1.4), both of which have been employed in *E. coli*. One pathway utilises acetyl-CoA as the precursor which is converted to acetoacetyl-CoA and then (*R*)-3-hydroxybutyryl-CoA by a β-ketothiolase and acetoacetyl-CoA reductase, respectively (Kataoka *et al.*, 2013). Another reported pathway utilises pyruvate as the precursor for conversion to acetaldehyde and then (*R*)-3-hydrobutyryl-CoA by a pyruvate decarboxylase and aldolase, respectively. Final reduction to (*R*)-1,3-BDO in both pathways is completed by an aldehyde reductase or alcohol dehydrogenase (Nemr *et al.*, 2018; Kim *et al.*, 2017).

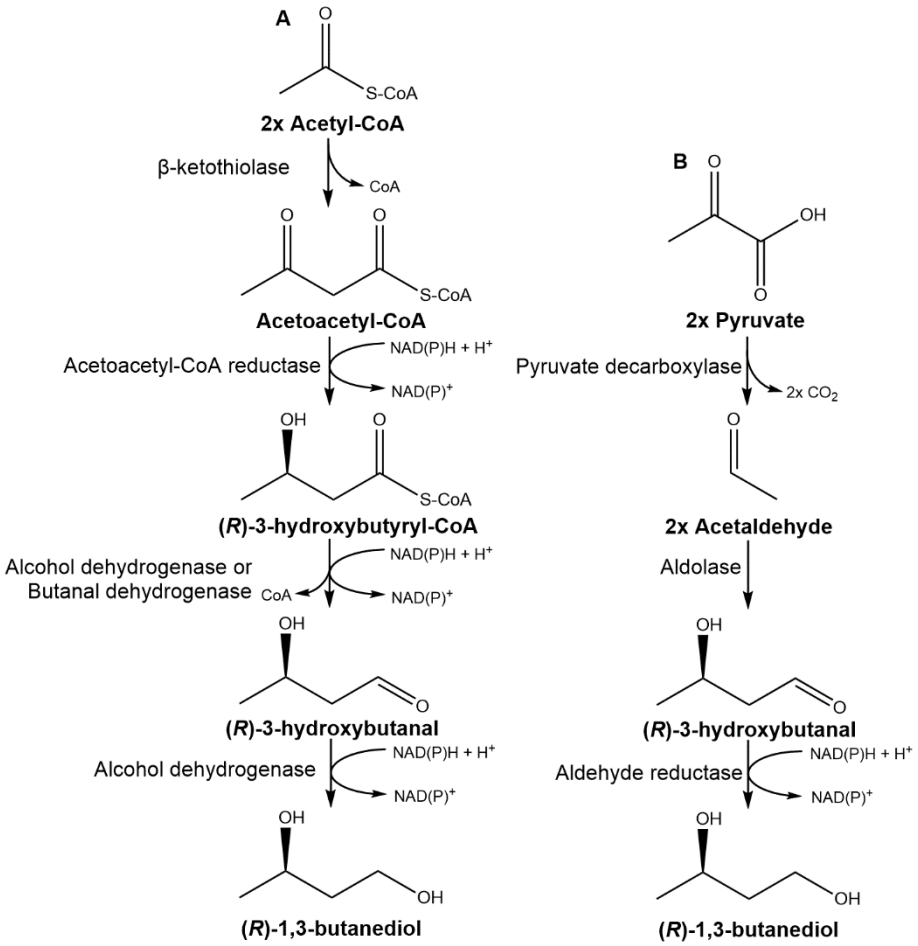

Figure 1.4 Metabolic pathways employed for microbial biosynthesis of (*R*)-1,3-BDO by Kataoka and co-workers (A) or Kim and co-workers (B).

Microbial production of (*R*)-1,3-BDO using glucose as a carbon source was first reported by Kataoka and co-workers employing the acetyl-CoA-dependent pathway in *E. coli* reaching a concentration of 100 mM with 98.5 % *R*-stereo specificity (Kataoka *et al.*, 2013). This was achieved using a β-ketothiolase encoded by *phaA* and acetoacetyl-CoA reductase encoded by *phaB1*, both from *C. necator* H16, which enabled conversion of acetyl-CoA to (*R*)-3-hydroxybutryl-CoA. A CoA-acylating butyraldehyde reductase encoded by *bld* from *Clostridium saccharoperbutylacetonicum* N1-4(HMT) then catalysed conversion of (*R*)-3-hydroxybutryl-CoA to (*R*)-3-hydroxybutanal. Final conversion to (*R*)-1,3-BDO was

accomplished by an unknown endogenous aldehyde reductase activity (Kataoka *et al.*, 2013). The *phaA, phaB1* and *bld* genes were assembled on a medium copy number plasmid and heterologous expression was carried out using IPTG inducible *lacZ*/$P_{A1lacO-1}$ gene expression system (Figure 1.5). During cultivation, acetate was identified as the primary byproduct within this system, with formate and ethanol also produced, all reaching concentrations >30 mM (Kataoka *et al.*, 2013). Accumulation of acetate in this system may be overflow metabolism resulting from high glucose consumption rates and subsequent decrease in carbon flux towards (*R*)-1,3-BDO (Vemuri *et al.*, 2006). Further research was undertaken to optimise fermentation conditions. Production of (*R*)-1,3-BDO increased >1.5-fold through optimisation of both oxygen transfer rate (K_La) and pH within the bioreactors (Kataoka *et al.*, 2014). Maintaining K_La at 82.3 h^{-1} resulted in the highest concentration of 91.8 mM (*R*)-1,3-BDO. Notably, as K_La values increased up to 97.2 h^{-1}, corresponding (*R*)-1,3-BDO production decreased to 41.3 mM. This demonstrates the importance of cultivation conditions when aiming to improve carbon flux towards a synthetic pathway. After optimal K_La value was identified, maintaining a pH of 5.5 was found to drastically reduce accumulation of by-product acetate during fermentation from a concentration of 43.1 mM to 27.2 mM. This corresponded to an increase in (*R*)-1,3-BDO concentration to 98.5 mM and it was hypothesised that minimising acetate accumulation reduced the inhibitory effect acetate can have on *E. coli* growth and recombinant protein production (Kataoka *et al.*, 2014).

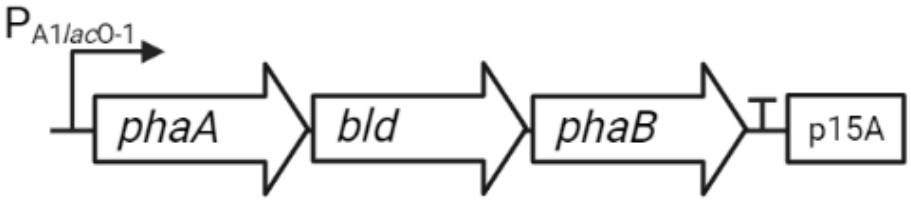

Figure 1.5 Plasmid design employed by Kataoka and co-workers for (*R*)-1,3-BDO bioproduction. Heterologous genes *phaA, bld* and *phaB* were assembled on a plasmid with p15A ori and gene expression was driven by the IPTG inducible promoter $P_{A1/lacO-1}$ (Kataoka *et al.*, 2013).

Notably, Bld from *C. saccharoperbutylacetonicum* N1-4(HMT) has been employed in metabolic pathways for production of alternative compounds: (*R*)-1,2,4-butanetriol, (*R*)-1,3-pentanediol, 4-methyl-(*R*)-1,3-pentanediol (Kataoka *et al.*, 2017); isobutanol, *n*-butanol (Black *et al.*, 2018) and 1,4-BDO (Hwang *et al.*, 2014). To improve production of 1,4-BDO, Bld was subjected to error-prone mutagenesis with a single amino acid mutation (L273T) resulting in over 4-fold increase in 1,4-BDO titres (Hwang *et al.*, 2014). The specific activity of wild type Bld and L273T mutant for conversion of 4-hydroxybutyrl-CoA to 4-hydroxybutanal were characterised under anaerobic conditions that were 2.0 ± 0.48 and 3.0 ± 0.47 pmol mg^{-1} min^{-1}, respectively. Characterisation of Bld was also attempted by Kataoka and co-workers during development of 1,3-BDO production pathway in *E. coli* that was unsuccessful due to enzyme instability, possibly due to aerobic assay conditions. However, oxygen sensitivity of Bld is still unclear with previous reports demonstrating increased oxygen availability subsequently increased 1,3-BDO production in *E. coli* cells utilising Bld (Kataoka *et al.*, 2013).

Bioproduction of (*R*)-1,3-BDO has also been reported by Nemr and co-workers utilising the pyruvate-dependent pathway with glucose as the carbon source, producing a concentration of 26.6 mM (*R*)-1,3-BDO in the host chassis *E. coli* during fermentation (Nemr *et al.*, 2018). This was achieved by using a pyruvate decarboxylase encoded by *pdc* sourced from *Zymomonas mobilis* which facilitated conversion of pyruvate to acetaldehyde. Deoxyribose-5-phosphate aldolase (DERA) encoded by *dra* from *Bacillus halodurans* facilitated conversion of acetaldehyde to (*R*)-3-hydroxybutanal. An aldo-keto reductase encoded by *PA1127* from *Pseudomonas aeruginosa* facilitated conversion of (*R*)-3-hydroxybutanal to (*R*)-1,3-BDO. The genes *pdc*, *dra* and *PA1127* were assembled on a high copy number plasmid and heterologous gene expression was achieved using the IPTG inducible *lacI*/P_{trc} gene expression system (Figure 1.6) (Nemr *et al.*, 2018). Nemr and co-workers hypothesised pyruvate decarboxylase enabled conversion of pyruvate to pathway by-products acetoin and subsequent conversion to *meso*-2,3-BDO, (*R, R*)-2,3-BDO or (*S, S*)-2,3-BDO facilitated by an unknown alcohol dehydrogenase. During strain development, to increase pyruvate accumulation in *E. coli* genes *ldhA, pflB* and *ilvB* were deleted in addition to deletion of *adhE, yqhD, eutG, adhP* and *yjgB* to decrease production of by-product ethanol. To further increase (*R*)-1,3-BDO yield, copy number of *dra* and *PA1127* was doubled to increase enzyme biosynthesis and subsequent carbon flux through the pyruvate-dependent pathway (Nemr *et al.*, 2018).

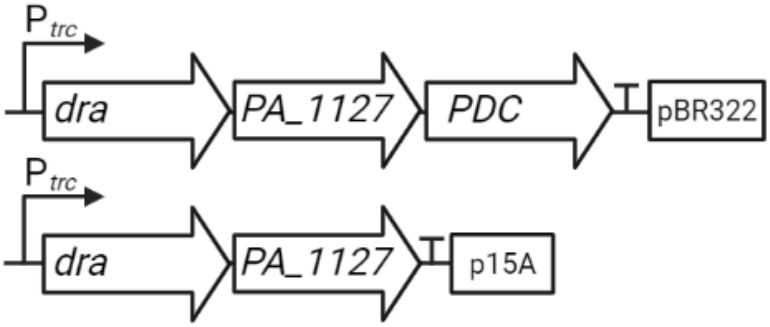

Figure 1.6 Design of two plasmids reported by Nemr and co-workers for (*R*)-1,3-BDO bioproduction. Heterologous genes *dra*, *PA1127* and *PDC* were assembled on a single plasmid with pBR322 ori and gene expression was driven by the IPTG inducible promoter P_{trc}. A second copy of *dra* and *PA1127* was assembled on another plasmid with p15A ori to increase gene dosage and subsequent DERA and aldo-keto reductase synthesis, respectively (Nemr *et al.*, 2018).

1.2.2 2,3-butanediol

2,3-BDO has 3 optical isomers: (*R, R*)-2,3-BDO, *meso*-2,3-BDO and (*S, S*)-2,3-BDO (Figure 1.7). The estimated annual global market of 2,3-BDO is 32 million tons (Bhatia et al., 2016). Examples of uses include aiding in the manufacture of printing ink, perfumes and pharmaceuticals. 2,3-BDO is also used as a precursor for chemical conversion to 1,3-butadiene and specifically, (*R, R*)-2,3-BDO is commonly used as antifreeze (Sun et al., 2015).

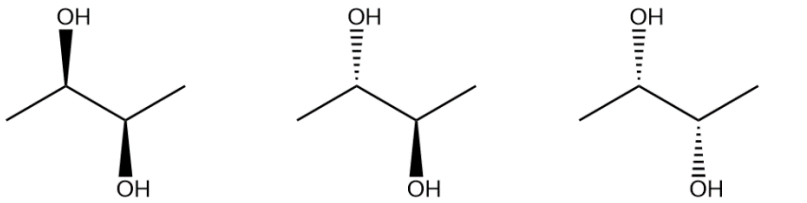

Figure 1.7 Skeletal structure of 2,3-BDO optical isomers (*R, R*)-2,3-BDO, *meso*-2,3-BDO and (*S, S*)-2,3-BDO

Of the butanediol isomers, bioproduction of *meso*-2,3-BDO and (*R, R*)-2,3-BDO are the most widely researched and current strategies for microbial production has been reviewed recently (Hakizimana, Matabaro and Lee, 2020). There are several species that naturally produce 2,3-BDO, these include bacteria from the *Bacillus* and *Lactobacillus* genus as well as *Klebsiella pneumoniae* (de Oliveira and Nicholson, 2016, Gaspar et al., 2011, Ma et al., 2009). The primary metabolic pathway for 2,3-BDO bioproduction in bacteria is from the precursor pyruvate which is converted to α-acetolactate and acetoin by an α-acetolactate synthase and then an α-acetolactate decarboxylase, respectively (Hakizimana, Matabaro and Lee, 2020). The final conversion to either *meso*-2,3-BDO, (*R, R*)-2,3-BDO or (*S, S*)-2,3-BDO is facilitated by an acetoin reductase or butanediol dehydrogenase (Hakizimana, Matabaro and Lee, 2020).

Bioproduction of *meso*-2,3-BDO was reported by Sadaharu and co-workers utilising pyruvate as the pathway precursor and glucose as the carbon source reaching a concentration of 196 mM in the host chassis *E. coli* (Sadaharu et al., 1997). This was achieved by using an α-acetolactate decarboxylase, α-acetolactate synthase and a *meso*-2,3-butanediol dehydrogenase encoded by the gene operon *budABC* from *K. pneumoniae*, respectively. A 6 Kb DNA fragment containing *budABC* was cloned into

a high copy number plasmid and it was hypothesised heterologous gene expression was achieved by an uncharacterised promoter from the *K. pneumoniae* genome. Whilst an IPTG inducible system was intended to promote expression of *budABC*, addition of IPTG had a negative or no effect on *meso*-2,3-BDO production.

Bioproduction of optically active (*R, R*)-2,3-BDO was reported by Yan and co-workers utilising pyruvate as the pathway precursor and glucose as the carbon source (Yan, Lee and Liao, 2009). In this study, stereoselectivity of four secondary alcohol dehydrogenases (sADH) for production of either *meso*-2,3-BDO or (*R, R*)-2,3-BDO from (*R*)-acetoin was investigated. This was accomplished by using an α-acetolactate synthase and α-acetolactate decarboxylase encoded by *alsS* and *alsD* from *B. subtilis*, respectively, for conversion of pyruvate to (*R*)-acetoin *via* α-acetolactate. The final enzymatic conversion to either *meso*-2,3-BDO or (*R, R*)-2,3-BDO was accomplished by one of four candidate sADH encoded by *bdhA* from *B. subtilis*, *adh* from *Clostridium beijerinckii* (adh_{Cb}), *adh* from *Thermoanaerobacter brockii* (adh_{Tb}) or *budC* from *K. pneumonia*. Upon testing, a concentration of 111 mM *meso*-2,3-BDO with >99 % enantiomeric purity was achieved by the strain containing *budC* from *K. pneumoniae*,. (*R, R*)-2,3-BDO concentrations of 57-68 mM with >99 % enantiomeric excess were achieved for strains containing the three alternative sADH, with expression of adh_{Tb} achieving the highest titre of 68 mM (Yan, Lee and Liao, 2009). The genes *alsSD* and either *bdhA*, adh_{Cb}, adh_{Tb} or *budC* were assembled on a high copy number plasmid and heterologous gene expression was achieved using the IPTG inducible *lacI*/P_{Llac01} gene expression system (Yan, Lee and Liao, 2009). Notably, *budC* has the highest catalytic efficiency of 68 mM^{-1} s^{-1}, with adh_{Tb} catalytic efficiency reported to be 4.0 mM^{-1} s^{-1}

(Yan, Lee and Liao, 2009). Furthermore, catalytic efficiency for *bdhA* is similar to adh_{Tb} at 3.8 mM^{-1} s^{-1} with adh_{Cb} comparatively lower at 0.99 mM^{-1} s^{-1}.

One of the highest titres of 2,3-BDO was achieved using non-engineered *K. pneumoniae* using glucose as the carbon source, reaching a concentration of 1664 mM after 38 h of fermentation (Ma et al., 2009). This was achieved through optimisation of media components with corn steep liquor powder and $(NH_4)_2HPO_4$ deemed the most significant media components for increasing 2,3-BDO titres. The enantiomeric purity of the produced 2,3-BDO was not reported.

Bioproduction of (*R, R*)-2,3-BDO was reported by Oliver and co-workers in the cyanobacterium *Synechococcus elongates* using CO_2 as the carbon source achieving a titre of 26.4 mM after 21 days of cultivation in the presence of constant light (Oliver *et al.*, 2013). This was achieved by using an α-acetolactate synthase encoded by *alsS* from *B. subtilis*, α-acetolactate decarboxylase encoded by *alsD* from *Aeromonas hydrophila* and sADH encoded by *adh* from *Clostridium beijerinckii*. The genes *alsS, alsD* and *adh* were inserted into the *S. elongates* chromosome and heterologous gene expression was achieved using the IPTG inducible *lacI*/P_{Llac01} gene expression system. Notably in this study, use of NADPH-dependent sADH was favourable due to increased availability of NADPH during photosynthesis (Oliver *et al.*, 2013).

1.2.3 1,4-butanediol

The platform chemical 1,4-BDO has an estimated annual production of 2 million tonnes and is typically used for automotive and electronic plastics, solvents and polyesters such as spandex (Burgard et al., 2016, Sun et al., 2015). Burk and co-workers have

developed bioproduction of 1,4-BDO at an industrial scale patenting the technology under patent publication number US 7,858,350 B2 (Burk *et al.*, 2010).

The microbial production of 1,4-BDO has been extensively studied primarily within the model organism *E. coli* due to its robustness and ease of genetic manipulation. The first successful 1,4-BDO metabolic pathway utilising succinyl semialdehyde as the precursor was reported a decade ago (Yim *et al.*, 2011). Conversion to 1,4-BDO was achieved by three enzymatic steps from succinyl semialdehyde through the intermediates 4-hydroxybutryate, 4-hydroxybutyryl-CoA and 4-hydroxybutanal. An alternative non-phosphorylative pathway for 1,4-BDO bio-production was developed in *E. coli* from the precursor 2,5-dioxopentanoate (2,5-DPO) produced from metabolism of xylose, arabinose and galacturonate (Tai *et al.*, 2016). The 2,5-DPO-dependent 1,4-BDO biosynthesis pathway requires two enzymatic steps through the intermediate butanedial.

Bioproduction of 1,4-BDO was first reported by Yim and co-workers utilising succinyl semialdehyde as the pathway precursor with glucose as the carbon source reaching a concentration of 199 mM in the host chassis *E. coli* (Yim *et al.*, 2011). This was achieved by using a 4-hydroxybutyrate dehydrogenase and 4-hydroxubutyrate transferase encoded by *4hbd* and *cat2* from *Porphyromonas gingivalis*, respectively, which facilitated conversion of succinyl semialdehyde to 4-hydroxybutryly-CoA *via* the intermediate 4-hydroxybutyrate. Conversion of 4-hydroxybutyryl-CoA to 4-hydroxybutanal was facilitated by an aldehyde dehydrogenase encoded by *ald* from *C. beijerinckii* with final enzymatic conversion to 1,4-BDO hypothesised to be facilitated be unknown homologous *E. coli* alcohol dehydrogenase(s) (Yim *et al.*, 2011). To increase the pool of the precursor succinyl semialdehyde, increased biosynthesis of

succinyl-CoA synthase and succinate semialdehyde dehydrogenase was achieved through overexpression of *sucCD* from *E. coli* as well as heterologous expression of *sucD* from *P. gingivalis*. A 2-oxoglutarate decarboxylase encoded by *sucA* from *Mycobacterium bovis* was also utilised for conversion of α-ketoglutarate to the pathway precursor succinyl semialdehyde. To achieve biosynthesis of 1,4-BDO *E. coli* cells were transformed with two plasmids containing genes responsible that allowed for balancing of pathway enzymes. The genes *sucCD* from *E. coli*, *sucD* from *P. gingivalis*, *4hbd* and *sucA* were assembled on one low copy number plasmid gene expression was achieved using the IPTG inducible *lacI*/$P_{A1lac0\text{-}1}$ gene expression system. In addition, the genes *cat2* and *ald* were assembled on a high copy number plasmid using the same IPTG inducible *lacI*/$P_{A1lac0\text{-}1}$ gene expression system. To increase carbon flux towards 1,4-BDO, *E. coli* genes *adhE, ldhA, pflB, mdh* and *arcA* were deleted. Furthermore, the endogenous *lpdA* was replaced with a *lpdA* from *K. pneumoniae* with a D354K mutation and *gltA* was mutated (R163L) to reduce NADH sensitivity and NADH inhibition, respectively (Yim *et al.*, 2011). During fermentation pyruvate, acetate and the pathway intermediate 4-hydroxybutyrate were found to be the primary pathway by-products with each compound accumulating to concentrations >75 mM, indicating a pathway bottleneck is present (Yim *et al.*, 2011). Initially, pyruvate accumulates then gradually decreases corresponding to an increase in acetate concentration, presumably acting as carbon storage for the cells when cultivated under microaerobic conditions.

Further development and optimisation of the pathway significantly increased 1,4-BDO bioproduction, achieving concentrations of 1098 mM 1,4-BDO reaching commercially viable production (Burgard *et al.*, 2016). Transferring from laboratory scale production to a commercial scale required several further metabolic modifications to reduce overall

production costs. This included genomic integration of all enzymes required to overcome genome instabilities and balancing enzyme expression driven by constitutive promoters.

Bioproduction of 1,4-BDO was reported by Tai and co-workers utilising 2,5-DPO as the pathway precursor with galacturonate used as the carbon source reaching a concentration of 183 mM in the host chassis *E. coli* (Tai *et al.*, 2016). This was achieved using a 2-ketoacid decarboxylase (KDC) facilitating conversion of 2,5-DPO to butanedial and final conversion to 1,4-BDO facilitated by an alcohol dehydrogenase (ADH). Employment of the 2,5-DPO-dependent pathway for 1,4-BDO biosynthesis first required screening of several KDC and ADH enzyme combinations. From screening, the highest 1,4-BDO concentration was achieved by a combination of α-ketoisovalerate decarboxylase encoded by *kivD* from *Lactoccocus lactis* and overexpression of the endogenous NADPH-dependent aldehyde reductase encoded by *yqhD* (Tai et al., 2016). The genes *kivd* and *yqhD* were assembled on a high copy number plasmid and gene expression was achieved using the IPTG inducible *lacI*/P_{Llac01} gene expression system. One notable by-product formed in this system was 1,2,4-butanetriol (1,2,4-BTO) due to decarboxylation of 2-keto-3-deoxy-D-xylonate by Kivd as a preferred substrate. To increase specificity of Kivd for 2,5-DPO, protein engineering was undertaken with a V461I mutation resulting in a 2-fold increase in 1,4-BDO production due to an extra methyl group in isoleucine shrinking the binding pocket (Tai *et al.*, 2016).

Wang and co-workers reported an alternative 1,4-BDO biosynthetic pathway reaching a concentration of 2.3 mM using xylose as the carbon source in the host chassis *E. coli* using an entirely synthetic metabolic pathway (Wang *et al.*, 2017). This was achieved

by conversion of xylose to 3,4-dihydorxybutanal *via* the intermediates xylonic acid and 3-deoxy-glycero-pentulosonic acid facilitated by a xylose dehydrogenase and xylonate dehydratase and an α-ketoisovalerate decarboxylase, respectively. Xylose dehydrogenase and xylonate dehydratase were encoded by *xylBC* and *xylD* from *Caulobacter crescentus*. The α-ketoisovalerate decarboxylase was encoded by *kivD* from *L. lactis*. Next, 3,4-dihydroxybutanal is converted to 1,2,4-BTO facilitated by an NADPH-depdendent aldehyde reductase encoded by *yqhD* from *E. coli*. 1,2,4-BTO is then converted to the 1,4-BDO pathway intermediate 4-hydroxybutanal by a diol dehydratase encoded by three genes: *ppdA-C-B* from *Klebsiella oxytoca*. The final enzymatic step is the conversion of 4-hydroxynutanal to 1,4-BDO, also facilitated by YqhD (Wang *et al.*, 2017).

Notably, the NADPH-dependent aldehyde reductase encoded by *yqhD* from *E. coli* has been reported to reduce several aldehydes including butyraldehyde, isobutyraldehyde, 3-hydroxypropionaldehyde (3HPA) and acetaldehyde to their respective alcohols (Perez *et al.*, 2008; Atsumi *et al.*, 2010; Li, Chen and Li, 2008; Jarboe, 2011). It is hypothesised YqhD contributes to cellular metabolism by reducing accumulation of toxic compounds in the form of aldehydes, such as butyraldehyde and glyoxal (Perez *et al.*, 2008). Indeed, YqhD was reported to have a high catalytic efficiency for butyraldehyde of 87 s^{-1} mM^{-1}, facilitating conversion to butanol (Perez *et al.*, 2008). However, metabolic engineers have successfully employed YqhD for production of chemicals of interest, with researchers at DuPont first identifying YqhD as facilitating conversion of 3HPA to 1,3-propanediol (1,3-PDO (Emptage *et al.*, 2003). The capability of YqhD to convert 3HPA to 1,3-PDO was further investigated with research from Li and co-workers reporting YqhD to have a catalytic efficiency of 1.3 $x10^{-4}$ mM^{-}

^{1} s^{-1} for 3HPA (Li, Chen and Li, 2008). To increase the catalytic efficiency, *yqhD* was subjected to error prone PCR that resulted in a >4-fold increase for YqhD with mutations D99Q and N147H. Further research was undertaken by Miller and co-workers that reported ability of YqhD to reduce furfural that was linked to availability of NADPH, leading to the conclusion YqhD is NADPH dependent when converting aldehydes and has a K_m value of 0.008 mM for NADPH (Miller *et al.*, 2009).

Table 1.1 Summary of reported bioproduction of the BDO structural isomers 1,3-BDO, 1,4-BDO and 2,3-BDO. Substrate and pathway precurosor are identified demonstrating the various pathways and carbon sources that have been utilisised for production of different BDO's.

Diol	Microorganism	Substrate	Pathway precursor	Titre (mM)	Reference
1,3-BDO	*Escherichia coli* BW25113 *lacI*^{q}	Glucose	Acetyl-CoA	100	(Kataoka *et al.*, 2013)
	Escherichia coli BW25113 *lacI*^{q}	Glucose	Acetyl-CoA	174	(Kataoka *et al.*, 2014)
	Escherichia coli MG1655	Glucose	Pyruvate	26.6	(Nemr *et al.*, 2018)
	Pichia jadinii HBY61	-	4H2B	425	(Yang *et al.*, 2014)
	Candida krusei ZJB-09162	-	4H2B	430	(Zheng *et al.*, 2012)
2,3-BDO	*Escherichia coli* JM109	Glucose	Pyruvate	190	(Sadaharu *et al.*, 1997)
	Escherichia coli JCL260	Glucose	Pyruvate	68	(Yan, Lee and Liao, 2009)
	Synechococcus elongates PCC7942	CO_2	Pyruvate	26	(Oliver *et al.*, 2013)
	Klebsiella pneumoniae SDM	Glucose	Pyruvate	1664	(Ma *et al.*, 2009)
1,4-BDO	*Escherichia coli* ECKh-422	Glucose	Succinyl semialdehyde	199	(Yim *et al.*, 2011)
	Escherichia coli MG1655	Glucose	Succinyl semialdehyde	1098	(Burgard *et al.*, 2016)
	Escherichia coli W023	Glucose	Succinyl semialdehyde	7.32	(Hwang *et al.*, 2014)
	Escherichia coli BW25113	Galacturonate	2,5-DPO	183	(Tai *et al.*, 2016)
	Escherichia coli BW25113	Xylose	Xylose	2.32	(Wang *et al.*, 2017)

1.2.4 Detection and quantification of butanediols

For quantification of BDO produced during microbial fermentation, reports describe traditional chromatography techniques first for separation of culture components and then quantification through comparison to a known standard or mass spectrometry.

Indeed, 1,3-BDO is described as being quantified through normal phase high performance liquid chromatography (HPLC) using an Aminex® HPX-87H anion exchange column (Nemr *et al.*, 2018) or a RSpak KC-811 ion-exclusion column (Kataoka *et al.*, 2013). Kataoka and co-workers determined the enantiomeric excess of (*R*)-1,3-BDO present in culture samples through reverse phase HPLC using a Chiralcel OB-H chiral column to achieve separation of (*R*)- and (*S*)- optical isomers. Furthermore, simultaneous separation and quantification of 1,3-BDO has been described using liquid chromatography-mass spectrometry (LC-MS) with a Hypersil Gold C_{18} column (Kim *et al.*, 2017). Quantification of 2,3-BDO through HPLC has also been described utilising an Alltech IOA-2000 organic acid column or a Aminex® HPX-87H anion exchange column (Köpke *et al.*, 2011; Kim *et al.*, 2013), also employed for 1,3-BDO separation.

Separation and quantification of 2,3-BDO through gas chromatography-mass spectrometry (GC-MS) has also been described by Xiao and co-workers. This was achieved using an Agilent GC6820 gas chromatography system with a Supelco Beta DEX™ 120 fused silica capillary column and a flame ionization detector (Xiao *et al.*, 2010).

The simultaneous separation and quantification of 1,4-BDO through LC-MS has also been described (Yim *et al.*, 2011). This was achieved using an Agilent 1200 HPLC

system with a Zorbax Eclipse XDB column. Furthermore, 1,4-BDO quantification and separation techniques using GC-MS were also described by Yim and co-workers, employing an Agilent 6890N/5973N GC-MS system with an Rtx-5SIL MS fused silica capillary column.

Very few techniques other than HPLC, LC-MS or GC-MS have been developed for the detection of BDOs. One method utilises thin layer chromatography (TLC) for detection of 2,3-BDO, but not quantification. To determine the presence of 2,3-BDO, samples are spotted onto pre-activated silica gel TLC plates that are placed in a solvent mixture of hexane, ethyl acetate and glacial acetic acid with a ratio of 140:60:3. After separation, 2,3-BDO is confirmed to be present in samples if a blue spot is present with a retention factor of 0.68 (Saran, Yadav and Saxena, 2014). Another technique that has recently been developed for detection of BDO is employment of a genetically encoded biosensor allowing *in vivo* detection of 1,4-BDO. Indeed, a 1,4-BDO inducible system found in *E. coli* MG1655 has been utilised to drive expression of *rfp* encoding the reporter red fluorescent protein for detection of 1,4-BDO (Szmidt-Middleton *et al.*, 2013).

1.3 Chemolithoautotrophic bacteria

Chemolithoautotrophic microorganisms are able to metabolise non-organic carbon sources such as CO_2 to produce biomass. To date, there are six naturally occurring metabolic pathways that have been reported for CO_2 assimilation. These are the 1. Calvin-Benson-Bassham (CBB) cycle, 2. reductive tricarboxylic acid (TCA) cycle, 3. dicarboxylate/4-hydroxybutyrate cycle, 4. 3-hydroxypropionate cycle, 5. 3-hydroxypropionate/4-hydroxybutyrate cycle and 6. reductive acetyl Co-A pathway (Wood-Ljungdahl pathway) (Gong, Cai and Li, 2016).

Of the six identified CO_2 fixation pathways, the CBB cycle is the most energy-demanding pathway of the six for CO_2 assimilation producing net one mole of glyceraldehyde 3-phosphate from three moles of CO_2, nine moles of ATP and six moles of NAD(P)H (Alagesan, Minton and Malys, 2017). Conversely, the Wood-Ljungdahl pathway first identified by Harland G. Wood and Lars G. Ljungdahl is the least energy-demanding pathway producing net one mole acetyl-CoA from two mole CO_2, one mole ATP and four mole NAD(P)H and is the only non-cyclical of the six (Ragsdale, 1997). Furthermore, the CBB, 3-hydroxyproprionate/4-hydroxybutryate and 3-hydroxypropionate pathways are considered aerobic, with the Wood-Ljungdahl, reductive TCA and dicarboxylate/4-hydroxybutyrate pathways considered anaerobic due to the presence of oxygen-sensitive enzymes for CO_2 fixation (Ducat and Silver, 2012).

Of note is the CBB cycle that is considered one of the most important CO_2 fixing pathways. Microorganisms that utilise the CBB pathway for CO_2 assimilation include the chemolithoautotrophic bacteria *Cupriavidus necator*, *Rhodobacter capsulatus* and *Nitrosomonas europaea* (Bowien and Kusian, 2002; Madigan and Gest, 1979; Chain *et al.*, 2003). The first step of the CBB cycle is capturing CO_2 by reduction and carboxylation with ribulose-1,5-bisbisphosphate facilitated by the enzyme ribulose bisphosphate carboxylase/oxygenase (Rubisco). Badger and Bek reviewed the functional significance of four Rubisco enzyme forms that have evolved in eukaryotes, archaea and bacteria with primary differences altering structure and function. Of the four Rubisco enzyme forms, Form I and Form II are reported to be the most widely distributed among proteobacteria and cyanobacteria and are directly involved in CO_2 metabolism *via* the CBB cycle (Badger and Bek, 2008). To further investigate

functionality of the crucial enzyme Rubisco, specific activity was investigated and reported to be 2.7-5 µmol min^{-1} mg^{-1} (Bar-Even *et al.*, 2010).

Chemolithoautotrophic bacterium have been employed to convert CO_2 into a variety of industrially relevant compounds. One example is production of the bioplastic (P3HB) by *C. necator* H16 accumulating up to 68 % of dry cell weight using CO_2 as a carbon source fixed *via* the CBB cycle (Tanaka *et al.*, 1995). Anaerobic acetogens such as *Clostridium ljungdahlii* have also been utilised for production of the platform chemicals acetone, ethanol and butanol that naturally accumulate during fermentation. Indeed, bioproduction of ethanol and acetate by *C. ljungdahlii* has been previously reported, reaching concentrations of 5.2 and 40.1 mM, respectively (Cotter, Chinn and Grunden, 2009). To achieve this *C. ljungdahlii* cells were cultivated using synthesis gas containing CO_2 and CO as the carbon sources that were fixed through the Wood-Ljungdahl pathway.

Improving yields and/or productivity of chemolithoautotrophic bacteria through metabolic engineering can be challenging with anaerobic bacteria able to more readily drive heterologous protein production due to smaller available thermodynamic free energy (Bar-Even, Noor and Milo, 2012). However, aerobic chemolithoautotrophs can capture larger amounts of energy compared to anaerobes by employing O_2 as an electron acceptor, thus increasing titres of energy-dense molecules. These are key factors to consider when developing chemolithoautotrophic bacteria as a production chassis.

1.3.1 The industrially relevant chassis *Cupriavidus necator* H16

Cupriavidus necator H16 (formerly *Ralstonia eutropha* H16, *Alcaligenes eutrophus*, *Wautersia eutropha* and *Hydrogenomonas eutropha*) is a facultative chemolithoautotrophic Gram-negative β-proteobacterium found in soil and freshwater. *C. necator* H16 is able to metabolise a wide range of carbon sources reaching high cell densities heterotrophically using carbohydrates such as fructose or organic acids such as gluconate as the carbon and energy sources (Volodina, Raberg and Steinbuchel, 2016). Furthermore, *C. necator* H16 can also grow autotrophically utilising CO_2 with O_2 and H_2 providing energy (Bowien and Kusian, 2002) or organoautotrophically utilising formate providing both carbon and energy (Friedrich, Bowien and Friedrich, 1979). Of particular interest is the ability to store large amounts of carbon in the form of P3HB and is considered a model organism for the study of bioplastic production (Peoples and Sinskey, 1989). In *C. necator* aerobic respiration is the primary method employed for energy generation, but under anoxic cultivation conditions nitrite (NO_2^-) and nitrate (NO_3^-) can be utilised as alternative electron acceptors *via* a complete denitrification pathway (Pfitzner and Schlegel, 1973; Aragno and Schlegel, 1992). The ability to utilise *C. necator* H16 for biotechnological applications was greatly enhanced when the fully sequenced genome was reported by Pohlmann and co-workers in 2006, elucidating genes encoding proteins potentially contributing to carbon and energy metabolism (Pohlmann *et al.*, 2006). The genome of *C. necator* H16 comprises three circular replicons consisting, two chromosomes and one megaplasmid (pHG1) containing 7,416,678 bp with a reported 6,116 putative genes. Indeed, analysis of the genome revealed chromosome 1 contains the majority of genes coding organic acid metabolism, aerobic energy metabolism and DNA replication, transcription and

translation. Present on Chromosome 2 are genes encoding sugar and sugar acid catabolism for degradation of fructose, 2-ketogluconate and glucosaminate (Pohlmann *et al.*, 2006). It should be noted the sequence of the pHG1 was reported prior to the publication of the entire *C. necator* H16 genome sequence (Schwartz *et al.*, 2003).

1.3.1.1 Carbon metabolism in *C. necator* H16

C. necator H16 is a metabolically diverse bacterium that can use various substrates including CO_2 as a carbon source. In *C. necator* H16, CO_2 assimilation occurs *via* the CBB cycle (Figure 1.8) and the first step is carboxylation of one mole of atmospheric CO_2 with one mole ribulose-1,5-bisphosphate, forming two mole 3-phospohoglycerate facilitated by a Form I Rubisco encoded by *cbbLS*. Next, 3-phosphoglycerate is converted to glyceraldehyde-3-phosphate through the Embden-Mayerhoff-Parnass (EMP) pathway *via* the intermediate 1,3-phosphoglycerate, facilitated by a 3-phosphoglycerate kinase encoded by *cbbK* and glyceraldehyde 3-phosphate dehydrogenase encoded by *cbbG*, respectively. Next, glyceraldehyde-3-phosphate is combined with another EMP pathway intermediate fructose-6-phosphate to form xylulose-5-phosphate by a transketolase encoded by *cbbT*. Glyceraldehyde-3-phosphate is also converted to dihydroxyacetone phosphate (DHAP) by a triosephosphate isomerase encoded by *tim*, which is then combined with erythrose-4-phosphate forming sedoheptulose-1,7-bisphosphate by fructose-bisphosphate aldolase encoded by *cbbA*. Sedoheptulose-1,7-bisphosphate is dephosphorylated to sedoheptulose-7-phosphate by sedoheptulose-1,7-bisphosphatase encoded by *cbbF*, which is subsequently converted to ribose-5-phosphate by a transketolase. Both ribose-5-phosphate and xylulose-5-phosphate are converted to ribulose-5-phosphate by the enzymes ribose 5-phosphate isomerase encoded by *rpiA* and ribulose-phosphate 3-

epimerase encoded by *cbbE*, respectively. Ribulose-5-phosphate is then phosphorylated by phosphoribulokinase encoded by *cbbP* regenerating ribulose-1,5-bisphosphate for assimilation of CO_2. Most enzymes required for the CBB cycle are encoded by two separate operons, with one operon located on chromosome 2 and the other located on the megaplasmid pHG1. Transcription of both CBB operons appears to be complex involving the LysR-type transcription regulator CbbR (encoded by *cbbR*) as well as transcription of regulator RegA (encoded by *regA*) that contributes to the global transcription regulation system (RegA/RegB) (Bowien and Kusian, 2002; Gruber, Schwab and Heidinger, 2017). Furthermore, induction of *cbbLS* encoding Rubisco is induced when cells are cultivated under autotrophic growth conditions and repressed when cultivated under heterotrophic conditions (Badger and Bek, 2008).

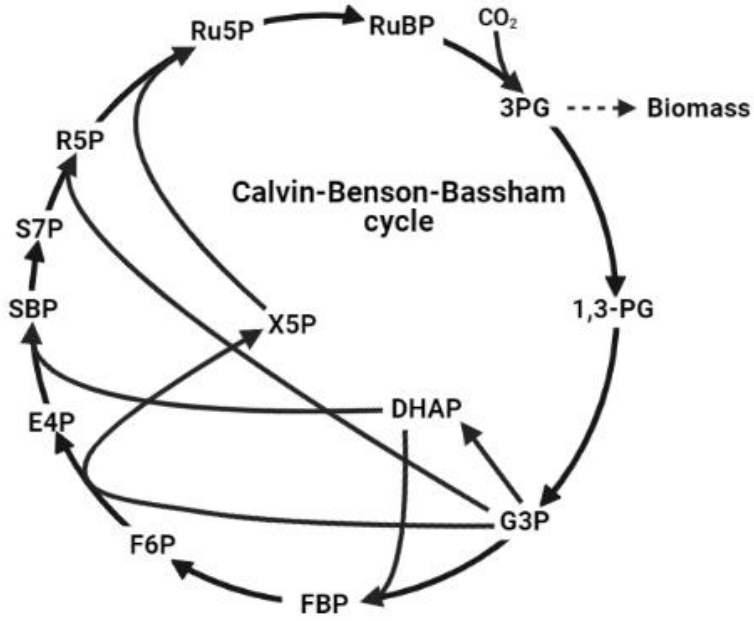

Figure 1.8 Schematic representation of the Calvin-Benson-Bassham (CBB) cycle facilitating fixation of atmospheric CO_2. Metabolite abbreviations: *3PG* 3-phosphoglycerate, *1,3-PG* 1,3-bisphosphoglycerate, *G3P* glyceraldehyde-3-phopsphate, *FBP* fructose-1,6-bisphosphate, *F6P* fructose-6-phosphate, *E4P* erythrose-4-phosphate, *SBP* sedoheptulose-1,7-bisphosphate,

S7P sedoheptulose-7-phosphate, *R5P* ribose-5-phosphate, *RuBP* ribulose-5-phosphate, *RuBP* ribulose-1,5-bisphosphate, *X5P* xylulose-5-phosphate, *DHAP* dihydroxyacetone phosphate.

C. necator H16 is also able to grow organoautotrophically by oxidising formate to CO_2 that is facilitated by a formate dehydrogenase, whilst simultaneously generating energy in the form of NADH. Subsequently, released CO_2 is assimilated *via* the CBB cycle (Bowien and Kusian, 2002). Oxidation of formate is achieved by reduction of NAD^+ by the characterised molybdenum-containing formate dehydrogenase encoded by the formate inducible *fdsGBACD* operon (Oh and Bowien, 1998). Additionally, distinct activity of three membrane-bound formate dehydrogenases has also been detected in *C. necator* H16 (Burgdorf, Bömmer and Bowien, 2001), supported by determinants for three membrane-bound formate dehydrogenases encoded by *fdh, fdo* and *fdw* (Pohlmann *et al.*, 2006).

C. necator H16 is also able to grow heterotrophically utilising a range of organic carbon and energy sources. *C. necator* H16 can reach high specific growth rates when cultivated utilising different substrates including sugar acids such as gluconic acid, organic acids, fatty acids and tricarboxylic acid (TCA) cycle intermediates (Kersters and De Ley, 1984). Specifically, gluconate is degraded through the Entner-Doudoroff (ED) pathway, with the first step enzymatic conversion to 6-phsophocluconate facilitated by gluconate kinase encoded by *gntK* (Pohlmann *et al.*, 2006). Furthermore, the only sugars that *C. necator* H16 can metabolise are fructose and *N*-acetylglucoasmine (Kersters and De Ley, 1984). Fructose is catabolised through the ED pathway, with the ED pathway considered the major degradation route of organic substrates in *C. necator* H16 (Alagesan, Minton and Malys, 2017). This is supported by *C. necator* H16 lacking genes encoding phosphfructokinase of the Emden-

Mayerhoff-Parnas (EMP) pathway or 6-phosphogluconate dehydrogenase of the oxidative pentose-phosphate pathway (Pohlmann *et al.*, 2006).

C. necator H16 is also capable of being cultivated under mixotrophic conditions. However, the carbon flux through the CBB cycle can increase or decrease dependent upon the organic substrates present during cultivation. Indeed, this can range from complete repression of the CBB cycle in the presence of pyruvate and malate to a significant increase in carbon flux in the presence of glycerol (Alagesan, Minton and Malys, 2017).

1.3.1.2 Energy metabolism in *C. necator* H16

The genome of *C. necator* H16 contains genes that encode several isoenzymes that contribute to balancing of cellular redox, indicating various ways energy sources can be harnessed for cellular function. Indeed, there are gene clusters encoding two hydrogenases responsible for the splitting of molecular hydrogen (H_2) into two protons and two electrons (Cramm, 2008). One is a membrane-bound [NiFe]-hydrogenase (*hoxKGZ*) and the other a soluble hydrogenase (*hoxFUHY*). Once H_2 has been split, proton translocation is facilitated by an NADH dehydrogenase (type I, NDH-I) complex encoded by 14 genes that simultaneously oxidises NADH (Pohlmann *et al.*, 2006). *C. necator* H16 chromosome 1 also contains a single gene (*h16_A2740*) encoding a single-subunit NADH dehydrogenase (type 2, NDH-2) that does not conserve energy during oxidation of NADH that is potentially non-functional (Cramm, 2008). Additionally, Jones and co-workers report that saturation of NADH dehydrogenase was observed for membrane-bound transhydrogenase activity in the presence of excess NAD^+ during heterotrophic cultivation, supporting NDH-I is the primary enzyme involved in

oxidation of NAD^+ (Jones *et al.*, 1975). Furthermore, NADH hydrogenase activity appears to be oxygen-dependent, with no membrane-bound transhydrogenase activity detected in *C. necator* H16 cells cultivated under anaerobic conditions (Drozd, 1977).

Of interest is the abundance of multiple putative transhydrogenase isoenzymes present in *C. necator* H16 with unknown function. One potential application may be regeneration of NADPH utilised in the reductive P3HB biosynthesis pathway (Steinbüchel and Schlegel, 1991). Present in the *C. necator* H16 are genes encoding four membrane-bound transhydrogenase's (PntAB1234) comprised of 2-3 subunits which couple proton translocation and transfer of reducing equivalents between NADH and NADPH. This reversible reaction favours formation of NADPH, providing reducing equivalents when cells are cultivated under typical physiological conditions.

Several enzymes involved in central carbon metabolism that also contribute to energy metabolism in *C. necator* H16 are listed in Supplementary Table 1.

1.3.1.3 Biotechnological applications of *C. necator* H16

C. necator H16 is a model organism for the study of polyhydroxyalkanoate (PHA) granule formation using a β-ketothiolase, NADPH-dependent acetoacetyl-CoA reductase and poly(3-hydroxybutyrate) synthase encoded by *phaA, phaB* and *phaC,* respectively. These three enzymes facilitate the conversion of two acetyl-CoA molecules to P3HB *via* the intermediates acetoacetyl-CoA and (*R*)-3-hydroxybutryl-CoA (Figure 1.9) that is used as carbon and energy storage by *C. necator* H16 (Pohlmann *et al.*, 2006). Previous reports describe nitrogen limitation in the presence of excess carbon increases carbon flux towards P3HB formation whilst simultaneously

limiting growth, accumulating up to 90 % (w/w) of dry cell weight in *C. necator* H16 (Peoples and Sinskey, 1989, Lindenkamp et al., 2013).

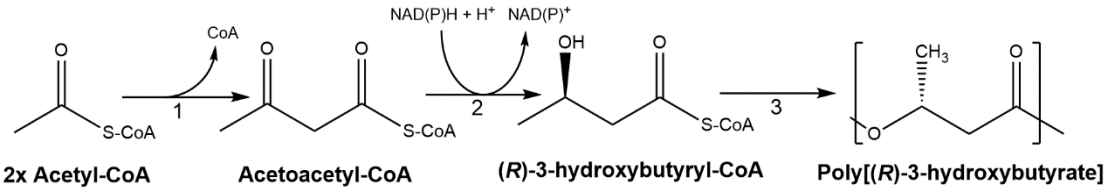

Figure 1.9 Poly[(*R*)-3-hydroxybutyrate] biosynthesis pathway with enzymatic steps: 1. two molecules of the precursor acetyl-CoA are converted to acetoacetyl-CoA by a β-ketothiolase (PhaA) encoded by *phaA*; 2. reduction of acetoacetyl-CoA to (*R*)-3-hydroxybutryl-CoA by an acetoacetyl-CoA reductase (PhaB) encoded by *phaB* and 3. polymerisation to poly[(*R*)-3-hydroxybutyrate] by poly(3-hydroxybutyrate) synthase (PhaC) encoded by *phaC*.

For production of other value-added products, genetic alterations to the P3HB pathway were undertaken for production of biodegradable plastics with more desirable characteristics than the relatively hard and brittle bioplastic P3HB. The biopolymer poly(3-hydxoxybutyrate-co-3-hydroxyhexanoate) was produced using a PHA synthase homologue encoded by *phaC* from *Aeromonas caviae* in a *C. necator* Δ*phaC* strain using palm kernel oil as the carbon source (Sato et al., 2015).

C. necator H16 has been utilised as a host chassis to produce platform chemicals isobutanol, 3-methyl-1-butanol, methyl ketones, alka(e)nes, *n*-butanol, acetoin, isoprene and isopropanol (Lu *et al.*, 2012; Müller *et al.*, 2013; Crepin, Lombard and Guillouet, 2016; Black *et al.*, 2018; Windhorst and Gescher, 2019; Alagesan *et al.*, 2018). Over the last decade, deployment of *C. necator* H16 specifically for autotrophic production of platform chemicals has seen an increase. Bioproduction of 435 mg L^{-1} alka(e)nes was reported by Crepin and co-workers using a metabolically engineered *C.*

necator H16 strain with CO_2 as the carbon source (Crepin et al., 2016). This was accomplished using an aldehyde decarboxylase oxygenase and acyl-ACP reductase encoded by two codon optimised genes *Synpcc7942_1593* and *Synpcc7942_1594* endogenous to *Synechococcus elongates*.

The production of 0.4 mM *n*-butanol from the pre-cursor 3-hydroxybutyryl-CoA by *C. necator* H16 has also been reported using formate as the carbon and energy source (Black *et al.*, 2018). First, 3-hydroxybutyryl-CoA is converted to crotonyl-CoA by a an enoyl-CoA hydratase encoded by *phaJ* from *A. caviae*. Next, crotonyl-CoA is hydrogenated to butyryl-CoA facilitated by a trans-2-enoyl-CoA reductase encoded by *ter* from *Treponema denticola*. Final conversion to *n*-butanol *via* the intermediate butanal is facilitated by a butyraldehyde dehydrogenase and aldehyde reductase encoded by *bld* from *C. saccharoperbutylacetonicum* and *yqhD* from *E. coli*, respectively. To improve *n*-butanol production, codon optimised *ter* was employed as well as overexpression of endogenous *C. necator* H16 enzymes PhaAB, resulting in a >2-fold increase in *n*-butanol concentration.

Finally, engineered *C. necator* H16 has been demonstrated to be suitable for bioproduction of acetoin achieving a titre of 44 mM from CO_2 as the carbon source (Windhorst and Gescher, 2019). Acetoin biosynthetic pathway was assembled from an α-acetolactate synthase (ALS) and α-acetolactate decarboxylase (ALD) using codon optimised *B. subtilis alsSD* . Similar to the previously reported pyruvate-dependent 2,3-BDO biosynthesis pathway, pyruvate is converted to acetoin *via* the intermediate α-acetolactate. To improve carbon flux towards acetoin, first, consumption of acetoin by *C. necator* H16 was interrupted by deletion of *acoABC* encoding enzymes responsible for degradation of acetoin. Next, two *C. necator* H16 P3HB synthase homologues

facilitating P3HB synthesis encoded by *phaC1* and *phaC2* were chromosomally deleted, further increasing carbon flux towards acetoin.

1.4 Research aims

The overall aim of this work will be to explore and engineer *C. necator* H16 for BDO biosynthesis seeking to develop strains suitable for autotrophic fermentation using carbon dioxide-as sole carbon source. This can be further divided into the following specific research aims:

First, suitability of *C. necator* H16 for deployment as a host chassis for BDO biosynthesis will be assessed. The concentration of compounds of interest (acetoin, butanediol) where toxic effect is exhibited in *C. necator* H16 will be determined. Next, synthetic biology tools for production and detection of BDO's or BDO pathway intermediates will be identified explored and developed. This will involve assembly two inducible gene expression systems for evaluation in *C. necator* H16. A 1,4-BDO-inducble gene expression system from *E. coli* or an acetoin-inducible gene expression system from *A woodii* will be assembled into a genetically encoded biosensors and characterised for BDO monitoring.

Second, a (*R*)-1,3-BDO metabolic pathway suitable for deployment in *C. necator* H16 will be identified. Candidate genes encoding (*R*)-1,3-BDO pathway enzymes will be assembled on a modular vector and screened for (*R*)-1,3-BDO production in *C. necator* H16. This will include screening of several enzyme combinations for production of (*R*)-1,3-BDO. Then, (*R*)-1,3-BDO production and limitations in *C. necator* H16 will be investigated to inform metabolic engineering strategies. To increase carbon flux towards (*R*)-1,3-BDO biosynthesis pathway, acetyl-CoA availability will be increased by chromosomal deletion of genes encoding enzymes that contribute to the TCA cycle.

Third, autotrophic production of (*R*)-1,3-BDO will be investigated using *C. necator* H16 strains chromosomally integrated with BDO pathway genes. To achieve this, strains will be constructed with chromosomally integrated BDO pathway genes encoding enzymes for production of (*R*)-1,3-BDO and subsequently evaluated. Then, BDO pathway gene copy number will be increased with simultaneous TCA cycle gene deletions to improve (*R*)-1,3-BDO production using CO_2 as the carbon source.

Finally, the energy metabolism in *C. necator* H16 will be investigated. To this end, a *C. necator* H16 transhydrogenase deficient strain will be constructed to ascertain effect on cell metabolism. Next, a NADH- or NADPH-dependent 2,3-BDO biosynthesis pathway will be employed to evaluate autotrophic production of 2,3-BDO and effect on NAD(P)H supply in *C. necator* H16 transhydrogenase deletion strain.

2 Materials and Methods

2.1 Bacterial strains and cultivation conditions

2.1.1 Bacterial strains

Bacterial strains used in this study are in Table 2.1. All bacterial strains used and developed in this study are summarised in individual chapters. For Chapter 3, Chapter 4, Chapter 5 and Chapter 6 all bacterial strains are listed in Table 3.3, Table 4.3, Table 5.3 and Table 6.3, respectively.

Table 2.1 Bacterial strains used in this study

Strain	**Genotype**	**Source**
Acetobacterium woodii	Wild type	DSM 1030
Clostridium acetobutylicum	Wild type	DSM 792
Clostridium saccharoperbutylacetonicum N1-4	Wild type	DSM 14923
Cupriavidus necator H16	Wild type	DSM 428
Escherichia coli DH5α	*lacZ*ΔM15, *rec*A1, *end*A1	Invitrogen
Escherichia coli MG1655	F- , λ-, *rph*-1	DSM 18039
Escherichia coli S17-1	λpir/pLFX	DSM 9079
Pseudomonas aeruginosa PAO1	Wild type	DSM 19880
Pseudomonas putida KT2440	Wild type	DSM 6125

All bacterial strains in this study were stored by cryopreservation in Microbank^{TM} vials (Pro-Lab Diagnostics, U.K) according to manufacturer's preparation and revival procedures. Stored strains were revived by streaking a single bead on an agar plate.

2.1.2 Cultivation media

Bacterial strains were revived on lysogeny broth (LB) solid media plates containing 10 g L^{-1} tryptone, 5 g L^{-1} yeast extract, 10 g L^{-1} NaCl and 15 g L^{-1} agar.

E. coli strains were cultivated in liquid LB or M9 minimal media (M9MM) where stated. M9MM components: 0.24 g L^{-1} $MgSO_4$, 0.011 g L^{-1} $CaCl_2$ and 200 mL L^{-1} 5X M9 salt solution (64 g L^{-1} $Na2HPO_4 \cdot 7H_2O$, 15 g L^{-1} KH_2PO_4, 2.5 g L^{-1} NaCl, 5 g L^{-1} NH_4Cl) (Sambrook, Fritsch and Maniatis, 1989) supplemented with 20 mg L^{-1} and 1 mg L^{-1} thiamine (Jensen, 1993).

C. necator H16 strains were cultivated in liquid LB, minimal media (MM) or nitrogen-limiting minimal media (NLMM) where stated. MM components: 1 g L^{-1} NH_4Cl, 9 g L^{-1} $Na_2HPO_4 \cdot 12H_2O$, 1.5 g L^{-1} KH_2PO_4, 0.2 g L^{-1} $MgSO_4 \cdot 7H_2O$, 0.02 g L^{-1} $CaCl_2$, 0.0012 g L^{-1} $(NH_4)_5[Fe(C_6H_4O_7)_2]$ (Schlegel, Kaltwasser and Gottschalk, 1961) with 1 mL L^{-1} trace element solution SL7 (25% (w/v) HCl, 0.07 g L^{-1} $ZnCl_2$, 0.1 g L^{-1} $MnCl_2 \cdot 4H_2O$, 0.06 g L^{-1} H_3BO_3, 0.2 g L^{-1} $CoCl_2 \cdot 6H_2O$, 0.02 g L^{-1} $CuCl_2 \cdot 2H_2O$, 0.02 g L^{-1} $NiCl_2 \cdot 6H_2O$, 0.04 g L^{-1} $Na_2MoO_4 \cdot 2H_2O$) (DSMZ). NLMM components different to MM: 0.6 g $L^{-1}NH_4Cl$.

2.1.3 Cultivation conditions

A single colony was used to inoculate 3 mL liquid media in a Falcon 50 mL conical centrifuge tube. Inoculated media was incubated at 30 °C with 200 rpm shaking overnight. Fresh media was used for a 20x dilution of overnight cultures for subsequent analysis.

2.2 Molecular cloning techniques

2.2.1 *In silico* techniques

Benchling software (Benchling, CA, USA, available at: www.benchling.com) was used for plasmid design, *in silico* assembly and visualisation. Gene sequences of assembled

plasmids were confirmed by aligning sequencing reads with template DNA within Benchling.

2.2.2 Purification of microbial genomic and plasmid DNA

Microbial plasmid DNA was extracted and purified using the QIAprep® Spin Miniprep Kit (Qiagen, Hilden, Germany) according to manufacturer's protocols. Microbial genomic DNA was extracted and purified using the GenElute™ Bacterial Kit (Sigma-Aldrich, Dorset, UK) according to manufacturer's protocols. All purified DNA was stored in nuclease free water at -20 °C. Purified DNA concentration was quantitated with a SimpliNano™ spectrophotometer (Biochrom, Cambridge, UK).

2.2.3 Gene sequences and codon optimisation

All gene sequences were obtained from NCBI GenBank with gene accession numbers detailed in chapter specific materials and methods sections. Genes were codon optimised for *C. necator* H16 and synthesised by Gene Art Gene Synthesis (Thermo Fisher Scientific, Waltham, MA, USA).

2.2.4 Oligonucleotide primers

Oligonucleotide primers were synthesised by Sigma-Aldrich (Dorset, UK). Annealing temperatures of oligonucleotide primers were estimated using the Thermo Fisher Scientific online T_m calculator. Restriction enzyme restriction sites were placed at least 3 bp from the 5' end of designed oligonucleotides to increase efficiency of digestion of DNA fragments. Oligonucleotide primers were stored at -20 °C. All oligonucleotide primers are provided in individual chapters. For Chapter 3, Chapter 4, Chapter 5 and

Chapter 6, oligonucleotide primers are listed in Table 3.1, Table 4.1, Table 5.1 and Table 6.1, respectively.

2.2.5 Plasmid construct assembly

All plasmids generated in this thesis were assembled through traditional cloning, USER assembly or HiFi assembly. All restriction endonucleases, T4 DNA ligase and NEBuilder® HiFi DNA Assembly Master Mix were purchased from New England Biolabs (NEB, Ipswich, MA, USA). Key features of all plasmids used and generated in this thesis are summarised in individual chapters. For Chapter 3, Chapter 4, Chapter 5 and Chapter 6, plasmids are listed in Table 3.2, Table 4.2, Table 5.2 and Table 6.2, respectively. Details of how each plasmid was assembled is provided in individual chapters.

2.2.5.1 Amplification of bacterial DNA

DNA of genes to be assembled through traditional cloning was amplified by PCR with Phusion polymerase (Invitrogen, CA, USA) in 50 µL reactions according to manufacturer's protocols.

2.2.5.2 Restriction endonuclease digestion of bacterial DNA

Restriction endonucleases were purchased from New England Biolabs (NEB, Ipswich, MA, USA) were used for digestion of DNA to be assembled. Reactions were set up according to manufacturer's protocols and incubated at 37 °C overnight.

2.2.5.3 Agarose gel purification of amplified or restriction enzyme digested DNA

Amplified and digested DNA was subjected to gel electrophoresis separation and purification. Upon completion, PCR and digestion reaction mixtures were electrophoresed using a 1 % (w/v) Tris-acetate-EDTA (TAE) agarose gel. Samples were prepared using Gel Loading Dye, Purple (NEB, Ipswich, MA, USA) and the gel was stained with SYBR™ Safe DNA Gel Stain (Thermo Fisher Scientific, Waltham, MA, USA). Quick-Load®1 kb Plus DNA Ladder purchased from NEB (Ipswich, MA, USA) was used to estimate DNA fragment size. DNA was separated by subjecting prepared gel in TAE solution to electrical current using Bio-Rad electrophoresis system with a PowerPacTM Universal Power Supply (Bio-Rad) at 100 V.

Separated DNA was analysed by imaging agarose gels using a Bio-Rad Molecular Imager GelDoc XR+ Imaging System running Image Lab™ software (Bio-Rad, CA, USA).

Separated DNA fragments were excised from agarose gels illuminated with a blue light LED transilluminator (Syngene, MD, USA) and purified using the QIAquick® Gel Extraction Kit (Qiagen, Hilden, Germany) according to the manufacturer's protocols.

Gel-extracted DNA concentrations were quantitated with a SimpliNano™ spectrophotometer (Biochrom, Cambridge, UK).

2.2.5.4 Ligation of bacterial DNA

T4 DNA ligase purchased from NEB (Ipswich, MA, USA) was used for ligation of restriction enzyme digested DNA fragments. Reactions were set up according to

manufacturer's protocols with a DNA insert to DNA vector molecular ratio of 3:1. Reactions were incubated at room temperature for 2 h.

2.2.5.5 USER construct assembly

For assembly of modular fragment constructs, the USER DNA assembly technique was employed (Bitinaite *et al.*, 2007). USER oligonucleotides were designed to contain 1 deoxyuridine (dU) residue 6 – 8 nucleotides from the 5' end with complimentary overlap sequences (Bitinaite *et al.*, 2007). Genes to be assembled were amplified with Phusion U polymerase (Invitrogen, CA, USA) using manufacturer PCR protocols from purified genomic or plasmid DNA and were digested with *DpnI* (1 U/µL) at 37 ºC for 1 h before spin column purification. 3 µg pBBR1-2USER vector was digested with *XbaI* at 37 ºC for 4 h. 10 U Nt.BbvCl was added and incubated for 1 h at 37 ºC followed by spin column purification. PCR fragments and digested pBBR1-2USER were incubated for 15 mins at 37 ºC followed by incubation at room temperature for 15 mins with 1 U USER enzyme acquired from NEB (Ipswich, MA, USA).

2.2.5.6 HiFi construct assembly

For assembly of multiple fragment constructs, the HiFi DNA assembly technique was employed. Oligonucleotide primers were designed using the NEBuilder® Assembly Tool with set parameters ensuring a DNA fragment overlap of 25 bp. Genes to be assembled were amplified with Phusion U polymerase (Invitrogen, CA, USA) using manufacturer PCR protocols from purified genomic or plasmid DNA. NEBuilder® HiFi DNA Assembly Master Mix purchased from NEB (Ipswich, MA, USA) was used for construct assembly. Reactions were set up with purified DNA fragments and linearized vector according to manufacturer's protocols.

2.2.6 DNA sequencing

Assembled construct DNA was confirmed through sequencing by Eurofins Genomics (Ebersberg, Germany).

2.3 Preparation and transformation of bacterial strains

E. coli DH5α was used for all molecular cloning.

E. coli chemical competent cells were prepared and transformed by heath shock as reported previously (Sambrook, Fritsch and Maniatis, 1989).

C. necator electrocompetent cells were prepared and transformed by electroporation as reported previously (Ausubel *et al.*, 2003). For preparation of cells, 25 mL SOB medium (20 g L^{-1} tryptone, 5 g L^{-1} yeast extract, 2.4 g L^{-1} $MgSO_4$, 0.5 g L^{-1} NaCl, 0.186 g L^{-1} KCl) was inoculated with 1 mL *C. necator* cultures grown overnight. Inoculated media was cultured at 30 °C with shaking at 200 rpm, for 4 h. Cells were then harvested by centrifugation for 10 min at 6600*g*. The supernatant was discarded and cell pellet re-suspended in 10 mL 1 mM HEPES (pH 7.0) at 4 °C. Cells were then harvested by centrifugation for 10 min at 6600*g* a second time and the supernatant was discarded. Cells were then re-suspended in 5 mL 1 mM HEPES (pH 7.0) at 4 °C. Cells were again harvested by centrifugation for 10 min at 6600*g* and the supernatant was discarded. Cells were then re-suspended in 1 mM HEPES supplemented with 10 % (v/v) glycerol to and OD_{600} of 5 at 4 °C. Cells are now considered electrocompetent and 100 µL aliquots were stored at -80 °C for subsequent transformation. For electroporation, 100 ng plasmid DNA was added to thawed 100 µL aliquot of electrocompetent cells in an electroporation cuvette with 20 mm electrode gap (Bio-Rad, CA, USA) and incubated at 4 °C for 5 min. Cuvettes containing cell and plasmid mixture were then subjected to

electroporation using a Bio-Rad Micropulser (200Ω, 25μF). After electroporation, 900 μL SOC medium (20 g L^{-1} tryptone, 5 g L^{-1} yeast extract, 4.8 g L^{-1} $MgSO_4$, 3.603 g L^{-1} dextrose, 0.5g L^{-1} NaCl, 0.186 g L^{-1} KCl) was immediately added. Transformed cells were then incubated for 2 h at 30 °C with shaking at 200 rpm with no antibiotic present. Cells were then spread on LB agar plates containing appropriate antibiotic acting as selective pressure and incubated at 30 °C for 48 h.

2.4 Analytical Techniques

2.4.1 Specific cell growth rate

Cell growth was monitored by measuring the OD at 600 nm using a BioMate™ 3S UV-Visible Spectrophotometer (Thermo Fisher Scientific, MA, USA). Specific growth rate (μ h^{-1}) was calculated from Eq. (2.1) where natural logarithm of OD_{600} at timepoint t_1 subtracted from the natural logarithm of OD_{600} at timepoint t_2 is divided by timepoint t_1 subtracted from timepoint t_2 (Widdel, 2007).

$$\mu = \frac{\ln OD_2 - \ln OD_1}{(t_2 - t_1)} \quad (2.1)$$

2.4.2 Dry cell weight estimation

To estimate dry cell weight (DCW), 1 mL of cell culture was centrifuged in pre-dried and pre-weighed 1.5 mL Eppendorf tubes for 2 min at 17000*g* and the supernatant was discarded. The cell pellet was dried for 48 h at 120 ºC in a Heratherm OGH60 gravity convection oven (Thermo Fisher Scientific, Waltham, MA, USA). Subsequently, samples were cooled in a desiccator and the DCW was determined using an analytical balance with accuracy to 0.1 mg (SI-234, Denver Instrument, Göttingen, Germany). DCW was calculated as g L^{-1}.

2.4.3 Chemicals

Sodium gluconate (cat. no. 10356290) and ethanol (cat. no. 10437341) from Fisher Scientific, Loughborough, UK; 4-hydroxy-2-butanone (Alfa Aesar, Heysham, UK; cat. no. L11456); (*R*)-(-)-1,3-Butanediol (95 % purity, cat. no. 237612), 3-hydroxybutyraldehyde (Aldol; cat. no. CDS019977) and acetic acid (cat. no. A6283) from Sigma-Aldrich, Gillingham, UK; L-arabinose (cat. no. 365185000) pyruvic acid (cat. no. 132145000) and D-fructose (cat. no. 161355000) from Arcos Organics, Geel, Belgium.

2.4.4 HPLC-UV/RI analysis

Prior to HPLC-UV/RI analysis, the cell-free supernatant samples were combined with an equal volume of mobile phase (5 mM H_2SO_4) spiked with 50 mM valerate as internal standard, the mixture was passed through a Choice™ cellulose acetate syringe filter with 0.22 μm pore size (Thermo Fisher Scientific, Waltham, MA, USA; cat. no. CH2213-CA) and stored in 2 ml snap cap vial closed with cap containing septa (Thames Restek, Saunderton, UK; cat. no. SR-0101102-AL and SR-01011TSIT, respectively).Samples were analysed using a Thermo Scientific UltiMate 3000 HPLC system equipped with a diode array detector DAD-3000 with the wavelengths set at 210 nm and 280 nm, a refractive index detector RefractoMax 521 (Thermo Fisher Scientific, Waltham, MA, USA), and Phenomenex Rezex ROA-organic acid H+ (8%) 150 mm × 7.8 mm × 8 μm column (Phenomenex, Macclesfield, UK). The column was operated at 35 °C with an isocratic flow rate of 0.5 ml/min. Samples were run for 30 min and the injection volume was 20 μl. Chromeleon Chromatography Data System software was used for HPLC system control, data processing and analysis. The

concentrations of chemical compounds were estimated from standard calibration curves generated by analysing known concentrations of commercially available chemicals.

2.5 Chemical compound yield quantification

Chemical compound yield per biomass ($Y_{P/X}$) was calculated from Eq. (2.3) where chemical concentration *P* in g L^{-1} for timepoint *t-1* subtracted from timepoint *t* is divided by the difference in biomass *X* in g L^{-1} between timepoint *t-1* and timepoint *t*.

$$Y_{P/X} = \frac{P_t^* - P_{t-1}^*}{(X_t + X_{t-1})/2} \quad (2.2)$$

Chemical compound yield per substrate ($Y_{P/S}$) was calculated from Eq. (2.3) where chemical concentration *P* in Cmol for timepoint *t-1* subtracted from timepoint *t* is divided by substrate concentration *S* in Cmol for timepoint *t-1* subtracted from timepoint *t*.

$$Y_{P/S} = \frac{P_t - P_{t-1}}{S_t - S_{t-1}} \quad (2.3)$$

2.6 Fermentation

Autotrophic fermentation was carried out in 1.3 L vessel using a DASGIP® parallel bioreactor 4-fold system with bioblock for microbiology including control modules CWD4, MP8, PH4PO4L, PH4PO4RD4, OD4, MX4/4, TC4SC4 equipped with electrodes to measure dissolved oxygen (DO) (DO Sensor MTI/VisiFerm/HMC/DASGIP), pH (405-DPAS-SC-K8S pH Probe, Mettler Toledo, Leicester, UK) and temperature Platinum RTD Temperature Sensor (100 Ohm class A?) (Eppendorf, Hamburg, Germany). DASware® control software was used for automated control of DO, temperature, and pH. The first seed culture was grown

overnight at 30 °C with 200 rpm shaking in 10 mL of LB from a single colony. Subsequently, this culture was reseeded to 120 mL of LB and grown for another 24 h in identical conditions. Resulting cells were harvested by centrifugation for 10 min at 6600*g*, washed with 10 mL of fermentation minimal media (FMM) to remove residual LB, re-suspended in 50 mL FMM and used to inoculate 700 mL FMM. If appropriate, antibiotics were added to the growth medium at the following concentrations: 10 µg mL^{-1} gentamicin or 300 µg mL^{-1} kanamycin. When cells reached DCW greater than 1 g L^{-1} protein expression was induced by addition of 0.01 % (w/v) L-arabinose. pH was controlled at 6.9 by the addition of 1 M NH_3OH until a DCW of 7.5 g L^{-1} was achieved, changing to 1 M KOH to limit nitrogen availability. DO was maintained at 10 % (v/v) by increasing air flow (8.5 – 9.5 L h^{-1}) and agitation with a Rushton-type impeller (400 – 1600 rpm) and temperature at 30 °C. Using the DASGIP MX 4/4 Gas Mixing Module CO_2, H_2 and air were continuously sparged through 0.22 µm membrane filters into the bioreactors. Gas outflow composition was analysed using a Bioprocess R&D Lab Gas Analyser, Model RLGA-9804 (Atmosphere Recovery Inc., Eden Prairie, MN, USA). 2 mL samples were taken immediately after addition of L-arabinose and then every 12 h for 120 h and subjected to HPLC-UV/RI analysis. The autotrophic fermentation data for *C. necator* H16 strains has been deposited in the public database BioStudies (https://www.ebi.ac.uk/biostudies/) under accession number S-BSST607.

FMM was composed of the following: 3.4 g L^{-1} $Na_3P_3O_9$, 1.5 g L^{-1} NH_4Cl, 0.5 g L^{-1} $MgSO_4$, 10 mg L^{-1} $CaCl_2$, 5 mg L^{-1} $MnCl_2$, 50 mg L^{-1} $(NH_4)_5[Fe(C_6H_4O_7)_2]$, 150 mg L^{-1} K_2SO_4, and 10 mL L^{-1} SL-6 trace element solution (100 mg L^{-1} $ZnSO_4$, 30 mg L^{-1} $MnCl_2$, 300 mg L^{-1} H_3BO_3, 200 mg L^{-1} $CoCl_2$, 10 mg L^{-1} $CuCl_2$, 20 mg L^{-1} $NiCl_2$ and 30 mg L^{-1} Na_2MoO_4).

3 Investigating diol toxicity and analysis of potential inducible systems for diol detection in *C. necator* H16

3.1 Introduction

Microbial production of platform chemicals on an industrial scale has become an achievable goal due to recent advances in synthetic biology. The platform chemical butanediol (BDO) has four stable structural isomers: 1,2-BDO, 1,3-BDO, 1,4-BDO and 2,3-BDO. BDO structural isomers are utilised in different industrial processes: 1,4-BDO for automotive plastics; 1,3-BDO for antibiotics; 2,3-BDO for perfumes and the 2,3-BDO pathway intermediate acetoin is used for cosmetics (Burgard *et al.*, 2016; Llarrull *et al.*, 2010; Sun *et al.*, 2015; Xiao and Lu, 2014). Bioproduction of 1,4-BDO, acetoin, 1,3-BDO or 2,3-BDO through metabolic engineering of bacteria has been previously reported (Yim *et al.*, 2011; Windhorst and Gescher, 2019; Kataoka *et al.*, 2013; Yang and Zhang, 2018). To aid development of bacterial strains engineered to produce platform chemicals, the use of genetically encoded biosensors enables real-time reporting of chemical concentrations as well as high-throughput screening (Vervoort *et al.*, 2017). Such biosensors are usually comprised of three components: a regulator which interacts with the effector, a promoter to influence gene expression, and a reporter. Indeed, one such biosensor was developed and characterised for deployment in *C. necator* H16 where the first step was identification of transcriptional regulator and inducible promoter controlling itaconate catabolism in *P. aeruginosa* (ItcR/P) (Hanko, Minton and Malys, 2018). The identified transcription factor-based inducible system was cloned upstream of *rfp* encoding red fluorescence protein (RFP) resulting in upregulation of gene expression in the presence of the effector itaconic acid

in *E. coli* MG1655. The itaconate inducible biosensor was then utilised for real-time reporting of itaconate production by engineered *C. necator* H16.

An alternative approach towards biosensor development was undertaken by Szmidt-Middleton and co-workers. Reverse transcriptase PCR was used to identify genes upregulated in *E. coli* MG1655 subjected to the effector 1,4-BDO (Szmidt-Middleton *et al.*, 2013). Which identified that the putative pyruvate transporter encoded by *yhjX* was upregulated 41-fold in the presence of 6 % (w/v) 1,4-BDO. Therefore, the promoter controlling expression of *yhjX* was an ideal candidate for development of a 1,4-BDO inducible biosensor. Characterisation of the assembled biosensor saw optimal induction of gene expression in the presence of 4 – 7 % (w/v) 1,4-BDO. Furthermore, P_{yhjX} was upregulated when cells were in the presence of 6 % (w/v) 1,3-propanediol and 4 % (w/v) 1,5-pentanediol, suggesting upregulation of *yhjX* when in the presence of other C3-C5 diols when tested in *E. coli* DH5α. Also, 1,4-BDO was found to have a negative impact on growth of *E. coli* cells at concentrations of 6 and 10 % (w/v).

In this study, *C. necator* H16 was subjected to increasing concentrations of several BDO isomers and acetoin to assess consumption and toxic effect. Next, two candidate inducible systems have been identified and characterised for potential BDO and/or acetoin detection. The first candidate comprised the *yhjX* promoter from *E. coli* and gene upregulation in the presence of several BDO isomers has been demonstrated. The second candidate comprised a two-component system formed of a transcriptional regulator and promoter from *A. woodii* where acetoin has been identified as the effector. This second system can be deployed as an acetoin biosensor or acetoin inducible system due to high specificity and wide induction range.

3.2 Materials and Methods

3.2.1 Gene sequences and codon optimisation

The sequences of genes used for identification of candidate inducible systems were retrieved from Genbank under the following accession numbers/locus tags: NP_418003.1/b3547 (*yhjX* from *E. coli*), WP_014354586.1/ Awo_c01730, WP_014354585.1/Awo_c01720 (*acoR*, *acoA* from *Acetobacterium woodii*). Gene *acoR* was codon optimised for *C. necator* H16 and synthesised by Gene Art Gene Synthesis (Thermo Fisher Scientific, Waltham, MA, USA). All codon optimised DNA sequences are listed in Section 9.1.

3.2.2 Primers used in this study

All primers used in this study are listed in Table 3.1.

Table 3.1 Primers used in this study.

Name	**Sequence 5' to 3'**
yhjXp_R	ATATATCATATGAGTATTCCTGCAGTAATAAAAAG
yhjXp_F	ATATATGACGTCGGGGTTAGCGCCAGATTT
acoR_Aat_IR_F.1	TATAGACGTCGATGTCCATCATTTCCTCCTCAACTATTG
acoR_Aat_P13_F.2	TATAGACGTCTTCCCTTTTAATCATCCGGCTCGTATAATGTGTGGAGACTTCAATCTGAACAACCCTTATTTCTGG
acoR_Nde_R.1.2	TATACATATGTTAAATGTTCTCCTTTTTTCAAATTATCCAAAGATTTTAGATGC
SC4_acoAp_Aat.Nhe_F	TATAGACGTCtatGCTAGCGAATTTTCGCATTATTGAGACAAACAATTCTCAATTATAAGATACG
SC5_acoRUPIR_Nhe_F	ATATGCTAGCCATTTCCTCCTCAACTATTGTTTTTAAATCATTTCGG
SC5_acoR_Aat_R	TATAGACGTCTCACATTTGAGACGAGCAACG
SC9_acoR_Aat_R	TATAGACGTCTCACATCTGCGACGAGCAGC

3.2.3 Plasmids used in this study

All plasmids used in this chapter are listed in Table 3.2.

Table 3.2. Plasmids used in this study. * denotes codon optimisation. Cm^R: Chloramphenicol resistance

Plasmid	**Description**	**Source**
pEH006	host plasmid with Cm^R, T_{rrnb1}-*araC*-P_{araBAD}-*rfp*-T_{dbl}	(Hanko, Minton and Malys, 2017)
pBBR1 MCS-2-P_{13}	Source of P_{13} promoter	(Alagesan *et al.*, 2018)
pJLG301	pEH006 with P_{yhjX}-*Ec*RBS2-*rfp*-T_{dbl}	This work
pJLG302	pEH006 with T_{rrnB1}-P_{acoR}-*acoR*-P_{acoA}-*rfp*-T_{dbl}	This work
pJLG303	pEH006 with T_{rrnB1}-P_{13}-*acoR*-P_{acoA}-*rfp*-T_{dbl}	This work
pJLG304	pEH006 with T_{rrnB1}-P_{acoA}-*rfp*-T_{dbl}	This work
pJLG306	pEH006 with P_{acoR}-*acoR*-T_{rrnB1}, P_{acoA}-*rfp*-T_{dbl}	This work
pJLG307	pEH006 with T_{rrnB1}-P_{acoR}-*acoR**-P_{acoA}-*rfp*-T_{dbl}	This work

3.2.4 Assembly of plasmids used in this study

For construction of expression plasmids, the previously assembled modular vector pEH006 (Hanko, Minton and Malys, 2017) was employed, utilising multiple restriction sites flanking arabinose inducible system sites upstream of *rfp*. RFP has been used to evaluate protein expression levels induced by chemicals of interest. To reduce background expression, the terminators T_{rrnb1} and T_{dbl} are placed directly upstream and downstream of designated promoter region and RFP, respectively. Native RBS were left intact.

pJLG301: Promoter P_{yhjX} consisting of 250 bp upstream of *yhjX* (b3547) start codon was amplified with yhjXp_F and yhjXp_R from *E. coli* MG1655 purified genomic DNA. The PCR product was cloned into pEH006 using restriction sites AatII and NdeI. Already present pEH006 *rfp* RBS was unchanged to ensure *C. necator* H16 plasmid-based protein expression.

pJLG302: *acoR* (Awo_C01730) as well as intergenic regions upstream and downstream of encoding DNA was amplified with acoR_Aat_IR_F.1 and acoR_Nde_R.1.2 from *A. woodii* purified genomic DNA. The PCR product was cloned into pEH006 using restriction sites AatII and NdeI.

pJLG303: *acoR* as well as intergenic region 60 bp upstream to maintain native RBS and intergenic region downstream of encoding DNA was amplified with acoR_Aat_P13_F.2 and acoR_Nde_R.1.2 from *A. woodii* purified genomic DNA. Primer acoR_Aat_P13_F.2 contains P_{13} promoter (Alagesan *et al.*, 2018) for constitutive expression of *acoR*. The PCR product was cloned into pJLG301 using restriction sites AatII and NdeI.

pJLG304: P_{acoA} was amplified with SC4_acoAp_Aat.Nhe_F and acoR_Nde_R.1.2 from *A. woodii* purified genomic DNA. The PCR product was cloned into pJLG301 using restriction sites AatII and NdeI introducing NheI restriction site.

pJLG306: *acoR* and upstream intergenic region was amplified with SC5_acoRUPIR_Nhe_F and SC5_acoR_Aat_R from *A. woodii* purified genomic DNA. The PCR product was cloned into pJLG304 using restriction sites AatII and NheI.

pJLG307: Codon optimised *acoR** was extracted from template DNA synthesised and codon optimised by Gene Art Gene Synthesis using restriction sites AatII and NdeI. The purified restriction product was then cloned into pJLG301 using restriction sites AatII and NdeI.

3.2.5 Bacterial strains used in this study

All strains used in this study are listed in Table 3.3.

Table 3.3. Strains used in this study. Square brackets represent genes under promoter (P) control. * denotes codon optimisation. Gen^R: gentamicin resistance. Cm^R: Chloramphenicol resistance

Strain	**Genotype**	**Parent Strain**	**Plasmid**	**Source**
A. woodii	wild type	-	-	DSM-1030
C. necator H16	wild type, Gen^R	-	-	DSM-428
E. coli DH5α	*lacZ*ΔM15, *rec*A1, *end*A1	-	-	Invitrogen
E. coli MG1655	F- , λ-, *rph*-1	-	-	ATCC 70096
DH5-p302	DH5α, (P_{acoR}[*acoR*], P_{acoA}[*rfp*], Cm^R)	*E. coli* DH5α	pJLG302	This work
DH5-p304	DH5α, (P_{acoA}[*rfp*], Cm^R)	*E. coli* DH5α	pJLG304	This work
MG-p301	MG1655, (P_{yhjX}[*rfp*], Cm^R)	*E. coli* MG1655	pJLG301	This work
MG-p302	MG1655, (P_{acoR}[*acoR*], P_{acoA}[*rfp*], Cm^R)	*E. coli* MG1655	pJLG302	This work
MG-p306	MG1655, (P_{acoR}[*acoR*], P_{acoA}[*rfp*], Cm^R)	*E. coli* MG1655	pJLG306	This work
H16-p301	H16, (P_{yhjX}[*rfp*], Cm^R)	*C. necator* H16	pJLG301	This work
H16-p302	H16, (P_{acoR}[*acoR*], P_{acoA}[*rfp*], Cm^R)	*C. necator* H16	pJLG302	This work
H16-p303	H16, (P_{13}[*acoR*], P_{acoA}[*rfp*], Cm^R)	*C. necator* H16	pJLG303	This work
H16-p307	H16, (P_{acoR}[*acoR**], P_{acoA}[*rfp*], Cm^R)	*C. necator* H16	pJLG307	This work

3.2.6 Diol and acetoin consumption and toxicity assays

For consumption assays, single colonies of *C. necator* H16 were used to inoculate 3 mL MM supplemented with 0.4 % (w/v) sodium gluconate in 50 mL Falcon tubes. Cultures were then incubated overnight at 30 °C with 200 rpm shaking and used to inoculate 10 mL identical fresh media and 50 mL falcon tubes. Cultures were then incubated for 6 h at 30 °C with 200 rpm shaking. Then, 1,4-BDO, 1,3-BDO, 2,3-BDO or acetoin were added to the media to a final concentration of either 0 mM or 5 mM. Cells were then incubated at for a further 72 h. Samples were taken for HPLC analysis 0, 24, 48 and 72 h after addition of diol or acetoin to the media.

For toxicity assays, single colonies of *C. necator* H16 cells were used to inoculate 3 mL MM supplemented with 0.4 % (w/v) sodium gluconate in 50 mL Falcon tubes. Cultures were then used to inoculate 10 mL fresh identical media in 50 mL Falcon tube and incubated for a further 6 h at 30 °C with 200 rpm shaking. Next, 142.5 µL of sub-cultures were aliquoted into a 96-well clear-bottom plate (Greiner Bio One, International, Germany; Cat. no 655090) with 7.5 µL fresh minimal medium containing no diol or acetoin (control), or the diol or acetoin at the desired concentration. An Infinite® M1000 PRO (Tecan, Switzerland) microplate reader was used to measure OD_{600}. Prior to normalisation, OD_{600} was corrected to autoabsorbance of the minimal media.

3.2.7 Microtiter plate fluorescence assays

Fluorescence output from the reporter protein RFP was used to estimate gene expression levels as previously described (Hanko, Minton and Malys, 2017). For time-course experiments, single colonies of *E. coli* MG1655 or *C. necator* H16 were used to inoculate 3 mL M9MM supplemented with 0.4 % (w/v) glucose or MM supplemented with 0.4 % (w/v) sodium gluconate, respectively, unless otherwise stated. Cultures were incubated overnight at 30 °C with 200 rpm shaking used to inoculate 10 mL fresh identical media to a 1:20 dilution. Sub-cultures were then incubated at 30 °C with 200 rpm shaking for a further 4 h for *E. coli* MG1655 or 6 h for *C. necator* H16 allowing cells to reach exponential growth phase. Next, 142.5 µL culture was aliquoted into a 96-well clear-bottom plate (Greiner Bio One, International, Germany; Cat. no 655090) with 7.5 µL fresh minimal medium containing no inducer (control), or the inducer at the desired concentration. An Infinite® M1000 PRO (Tecan, Switzerland) microplate reader was used to measure fluorescence with excitation at wavelength 585 nm and emission at wavelength 620 nm every 10 mins for 16 h. For normalisation of fluorescence, OD_{600} was also measured. Prior to normalisation, both OD_{600} and fluorescence values were corrected to autoabsorbance and autofluorescnce of the minimal media.

For single time-point measurements of fluorescence, first, single colonies of *E. coli* DH5α were used to inoculate 3 mL LB. Cultures incubated overnight at 30 °C with 200 rpm shaking used to inoculate 10 mL fresh LB to a 1:20 dilution. Sub-cultures were then incubated at 30 °C with 200 rpm shaking for a further 3 h allowing cells to reach exponential growth phase. Next, 0.5 mL LB containing no inducer (control), or the inducer at the desired concentration was added to the culture and incubated for a further

8 h. To a microtiter plate, 150µL culture was aliquoted and fluorescence and OD_{600} were measured and normalised as described for fluorescence time-course experiments.

3.3 Results

3.3.1 Determination of consumption and toxicity of acetoin and butanediols in *C. necator* H16

For bioproduction of target compound by a microbial chassis, a key step is to evaluate whether the targeted compound is consumed and if there is any toxic effect on the chosen strain. Indeed, understanding whether a strain consumes a compound or a toxic effect is observed by the strain informs metabolic engineering steps and/or strategies that may need to be taken for successful implementation of a synthetic metabolic pathway. For example, to engineer *C. necator* H16 to produce acetoin, endogenous genes encoding the acetoin degradation pathway were deleted (Windhorst and Gescher, 2019). Therefore, to first confirm whether *C. necator* H16 is unable to consume BDO, cells were cultivated in MM in the presence of 0.4 % (w/v) sodium gluconate and 5 mM of acetoin, (*R, R*)-2,3-BDO, *meso*-2,3-BDO, 1,4-BDO, (*R*)-1,3-BDO for 72 h (Supplementary Figure 1). No consumption of all BDO isomers tested was observed, with all acetoin consumed by the cells within 24 h increasing biomass production. Next, to evaluate the effect of acetoin and BDO on growth rate of *C. necator* H16, cells were cultivated in MM supplemented with 0.4 % (w/v) sodium gluconate and 0 – 3 % (w/v) acetoin, (*R, R*)-2,3-BDO, *meso*-2,3-BDO, 1,4-BDO or (*R*)-1,3-BDO (Table 3.4). From the data, BDOs have only a minor toxic effect on *C. necator* H16, exhibiting no growth inhibition in the presence of up to 166.4 mM (*R*)-1,3-BDO, 1,4-BDO, (*R, R*)-2,3-BDO and *meso*-2,3-BDO. No statistically significant effect on growth rate was observed in

presence of all acetoin concentrations tested, most likely due to native ability to metabolise acetoin to acetyl-CoA (Steinbüchel *et al.*, 1987).

Table 3.4 Effect on *C. necator* H16 growth rate in the presence of 0 (control), 0.375, 0.75, 1.5 or 3 % (w/v) acetoin, *meso*-2,3-BDO, (*R*, *R*)-2,3-BDO, 1,4-BDO or (*R*)-1,3-BDO. Values are relative maximum specific growth rate (%) averages ± standard error calculated from biological triplicates.

Concentration							
% (w/v)	Acetoin (mM)	Butanediol (mM)	**Acetoin**	***meso*-2,3-BDO**	**(*R*, *R*)-2,3-BDO**	**1,4-BDO**	**(*R*)-1,3-BDO**
0	0	0	100	100	100	100	100
0.375	42.6	41.6	120 ± 16	102 ± 4	136 ± 34	107 ± 5	109 ± 8
0.75	85.2	83.2	120 ± 29	97 ± 13	127 ± 21	117 ± 2	116 ± 5
1.5	170.3	166.4	109 ± 20	110 ± 1	104 ± 7	128 ± 10	126 ± 6
3	340.5	332.9	127 ± 28	75 ± 37	33 ± 25	62 ± 8	61 ± 8

3.3.2 Identifying inducible systems for the detection of BDO

3.3.2.1 Investigating *yhjX* based inducible systems from *Escherichia coli*

In order to facilitate the screening of engineered strains for BDO production and to establish if genetically encoded monitoring systems are available, a literature search was conducted. From previous reports, the promoter of a putative transporter *yhjX* (P_{yhjX}) from *E. coli* MG1655 was shown to be upregulated in the presence of 1,4-BDO (Szmidt-Middleton *et al.*, 2013). To evaluate BDO isomers other than 1,4-BDO that drive expression of P_{yhjX}, the previously studied modular vector pEH006 (Hanko, Minton and Malys, 2017) was employed. The annotated P_{yhjX} region including the native RBS (Fried, Behr and Jung, 2013) was inserted directly upstream of *rfp* gene encoding reporter RFP, resulting in plasmid pJLG301. To determine the effect other BDOs, namely (*R, R*)-2,3-BDO and (*R*)-1,3-BDO has on P_{yhjX}, *E. coli* MG1655 cells harbouring plasmid pJLG301 (MG-p301) were subjected to a microtiter plate fluorescence assay. Fluorescence normalised to absorbance (OD_{600}) of MG-p301 cells in the presence of 0, 333, 555, 777 or 1109 mM 1,4-BDO, (*R*)-1,3-BDO or (*R, R*)-2,3-BDO were measured every 4 h using a microplate reader for 16 h (Figure 3.1).

Evidently, each butanediol screened induces gene expression to a certain extent when compared to the control with no BDO isomer present. Furthermore, the optimal range of induction for 1,4-BDO is 555-777 mM, and optimal range of induction for (*R*)-1,3-BDO is 777-1109 mM. Notably, concentrations above 555 mM 1,4-BDO or 777 mM 1,3-BDO result in a lower difference in gene expression compared to the control. Furthermore, cells in the presence of 1109 mM (*R*)-1,3-BDO exhibitied lower gene expression compared to presence of 777 mM ()-1,3-BDO. This is most likely due to

increasingly toxic effect of high concentration of (*R*)-1,3-BDO inhibiting RFP biosynthesis. Overall, the highest normalised fluorescence is observed for cells in the presence of (*R*, *R*)-2,3-BDO when compared to the control.

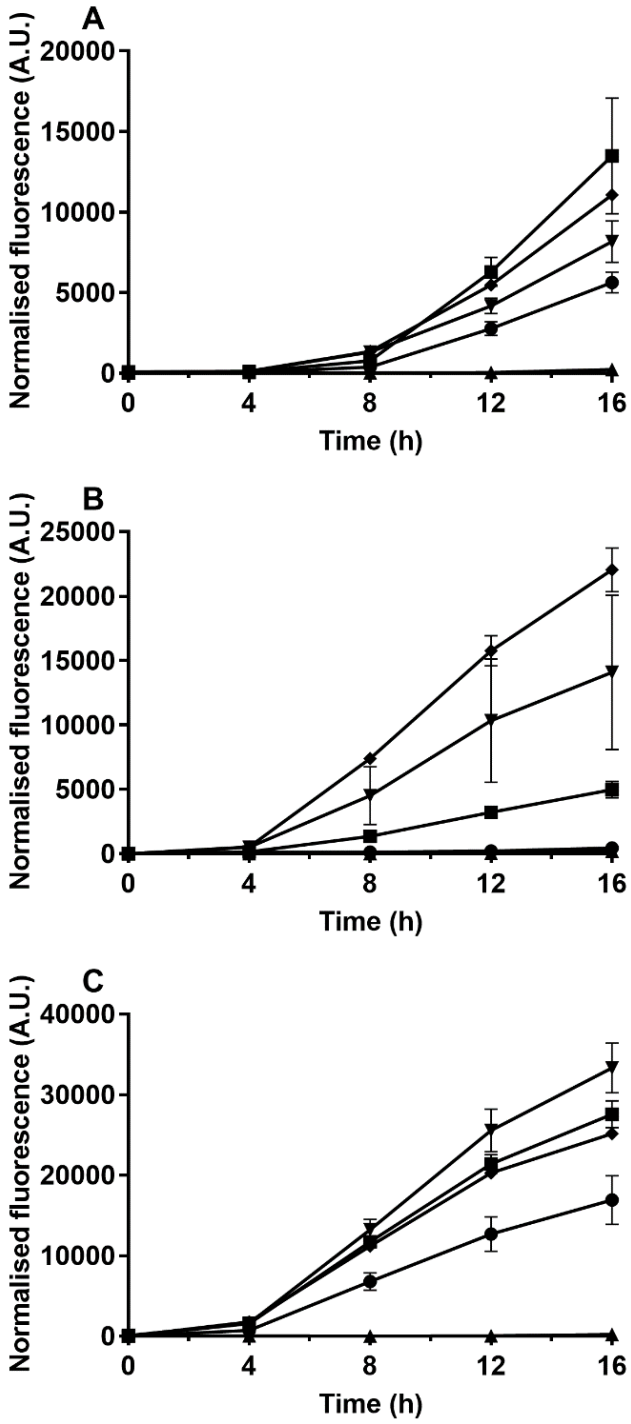

Figure 3.1 Normalised fluorescence of MG-p301 in the presence of 1,4-BDO (A), (*R*)-1,3-BDO (B) or (*R*, *R*)-2,3-BDO (C). Individual BDO was added to the medium at concentrations of 0 (triangles), 333 (circles), 555 (squares), 777 (diamonds) or 1109 (upside down triangles) mM. Error bars represent standard error calculated from biological triplicates.

It has previously been reported PyrR encoded by *pyrR* (b2381) is involved in pyruvate reutilisation within *E. coli* MG1655 and the regulator of P_{yhjX} (Miyake *et al.*, 2019). To investigate similarity of PyrR to potential *C. necator* H16 regulators, an *in-silico* alignment was carried out resulting in two native *C. necator* H16 proteins identified as similar to PyrR. Seemingly, regulatory response DNA-binding domiains ($LytT_1$ encoded by *lytT*, $LytT_2$ encoded by *h16_A3389*) possess similarity to PyrR. Indeed, $LytT_1$ and $LytT_2$ contained 26 % and 27 % identical residues and 45 % and 48 % similarity to PyrR, resepectively (Supplementary Figure 2) demonstrating presence of two *C. necator* H16 proteins with potential to regulate P_{yhjX}.

C. necator H16 is a desired chassis for BDO production and development of a biosensor for detection of BDO would allow for high-throughput screening. Therefore, the P_{yhjX}-*rfp* system confirmed to be induced by the presence of 1,4-BDO in *E. coli* MG1655 was employed in *C. necator* H16. The *C. necator* H16 wild type strain was transformed with pJLG301 (H16-p301) and the resultant strain was subjected to a fluorescence assay measuring fluorescence and absorbance of cells in the presence of 0, 111, 333 or 555 mM 1,4-BDO (Figure 3.2). During the assay, cells produced biomass and were therefore considered to be viable. However, no increase in fluorescence was observed when compared to the control containing no 1,4-BDO. This is most likely due to potential *C. necator* H16transcriptional regulators $LytT_1$ and $LytT_2$ unable to influence P_{yhjX}, rendering the biosensor non-functional.

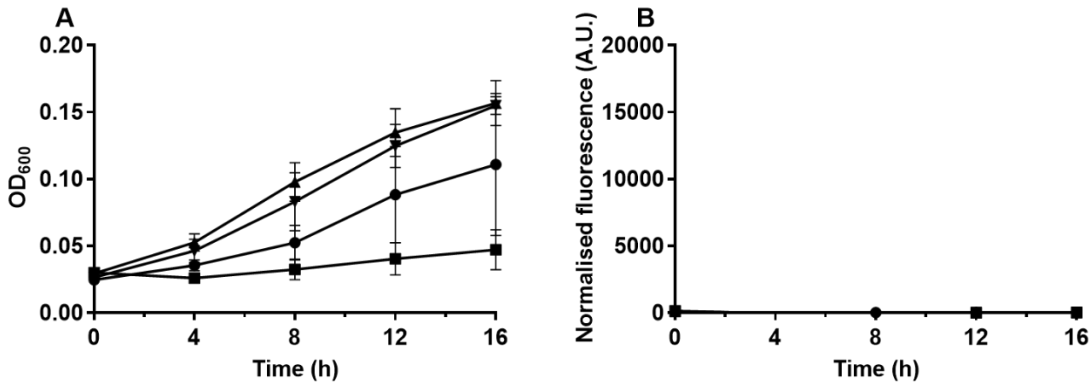

Figure 3.2 Fluorescence assay of H16-p301 with absorbance (A) and normalised fluorescence (B) represented. Strains were screened in the presence of 0 (triangles), 111 (upside down triangles), 333 (circles) or 555 (squares) mM 1,4-BDO. Error bars represent standard error calculated from at least three biological replicates.

3.3.2.2 Investigating *acoR* based inducible systems from *A. woodii*

3.3.2.2.1 Characterisation of *acoR* based inducible systems in *E. coli* MG1655

The acetogen *Acetobacterium woodii* DSM 1030 is able to metabolise 2,3-BDO as the sole carbon source *via* the Wood-Ljunghdal pathway (Hess *et al.*, 2015). This is achieved through expression of several enzymes encoded by genes *acoABCL* under the control of the transcriptional regulator *acoR*. Therefore, *acoR* was identified as a potential transcriptional regulator induced by acetoin and possibly structurally similar chemical 2,3-BDO. To evaluate response of the AcoR/P_{acoA} module in the presence of acetoin, the region encoding P_{acoR}-*acoR*-P_{acoA} identical to the orientation of the *A. woodii* DSM 1030 genome was cloned into the pEH006 backbone upstream of *rfp,* resulting in plasmid pJLG302. Next, to reduce potential constitutive impact of *acoR* promoter (P_{acoR}) on expression of *rfp*, the orientation of *acoR* was reversed compared to module in pJLG302, resulting in plasmid pJLG306 (Figure 3.3). The resultant

plasmids were then transformed into *E. coli* MG1655 (MG-p302 and MG-p306) and both strains were subjected to fluorescence assays with 0 mM (control) or 5 mM (induced) acetoin present (Figure 3.3). As postulated, presence of acetoin induces expression of the AcoR/P_{acoA} module confirmed by biosynthesis of RFP in cells harbouring pJLG302 or pJLG306. Furthermore, acetoin results in 8.4-fold or 8.9-fold increase in normalised fluorescence when compared to the control, by cells harbouring pJLG302 or pJLG306, respectively. Interestingly, reversing the direction of *acoR* from 5'→3' in pJLG302 to 3'→5' in pJLG306 results in a small decrease of uninduced gene expression. It should be noted, influence of AcoR on P_{acoA} was confirmed, with no induction of gene expression observed by strain harbouring only P_{acoA} in the presence of 5 mM acetoin (Supplementary Figure 3).

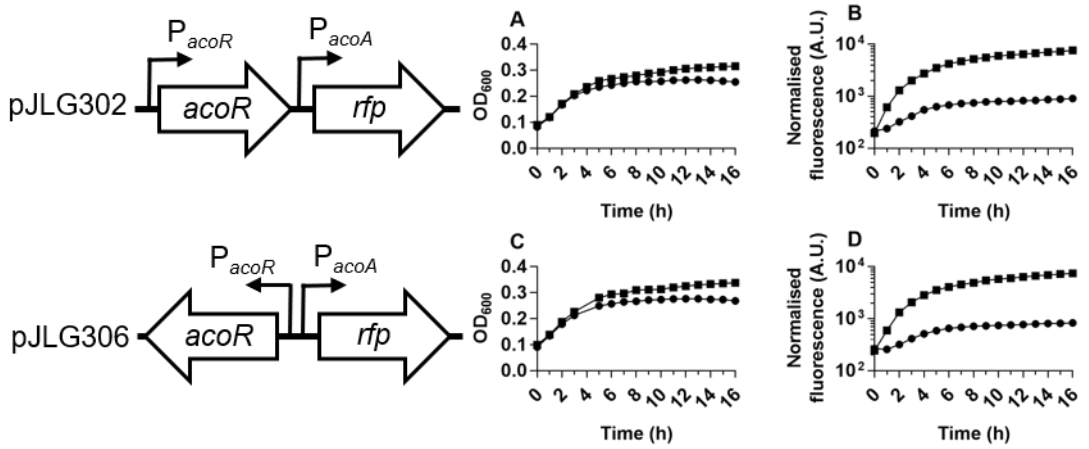

Figure 3.3 Fluorescence assay for *E. coli* MG1655 cells harbouring pJLG302 (A & B) or pJLG306 (C & D). Cells were either uninduced (circles) or induced (squares) by addition of acetoin to a final concentration of 0 or 5 mM, respectively. Absorbance values (A & C) were used to normalise fluorescence (B & D). Error bars calculated from at least two biological replicates are too small to be seen.

From the assay (Figure 3.3), expression of *rfp* was observed for both MG-p302 and MG-p306 in the presence of 0 mM acetoin indicating leaky expression of the system. Whilst reversing orientation of the P_{acoR}-*acoR* moedule in MG-p306 compared to MG-p302 did reduce basal uninduced expression to a certain extent as hypothesised, expression of *rfp* was still observed. This indicates both P_{acoR} and P_{acoA} are most likely constitutive and are upregulated in the presence of acetoin. It is also aparent P_{acoR} also influenced *rfp* expression in strain MG-p302, resulting in increased basal uninduced expression compared to strain MG-p306.

The degradation of 2,3-BDO often utilises the acetoin degradation pathway, with the first step of the pathway being conversion from to 2,3-BDO to acetoin (Hess *et al.*, 2015). Therefore, it was hypothesised that 2,3-BDO may also induce the AcoR/P_{acoA} system due to acetoin being the second intermediate during catabolism of 2,3-BDO. To determine induction of the AcoR/P_{acoA} system by 2,3-BDO, a fluorescence assay was undertaken evaluating gene expression in strains MG-p302 and MG-p306 supplemented with three 2,3-BDO optical isomers: (*R, R*)-2,3-BDO, (*S, S*)-2,3-BDO or *meso*-2,3-BDO. As a control, identical strains were cultivated with no (*R, R*)-2,3-BDO, (*S, S*)-2,3-BDO or *meso*-2,3-BDO or acetoin (Figure 3.4). From the results, no statistically significant difference in normalised fluorescence is seen between 0 and 6 h for MG-p302 or MG-p306. During later time-points, a marginal increase in fluorescence compared to the control is observed. This is most likely a result of enzymatic conversion of 2,3-BDO to acetoin by native *E. coli* MG1655 dehydrogenase(s). Seemingly, the AcoR/P_{acoA} inducible system is specific to acetoin, however screening of strains with other compounds is required to confirm this.

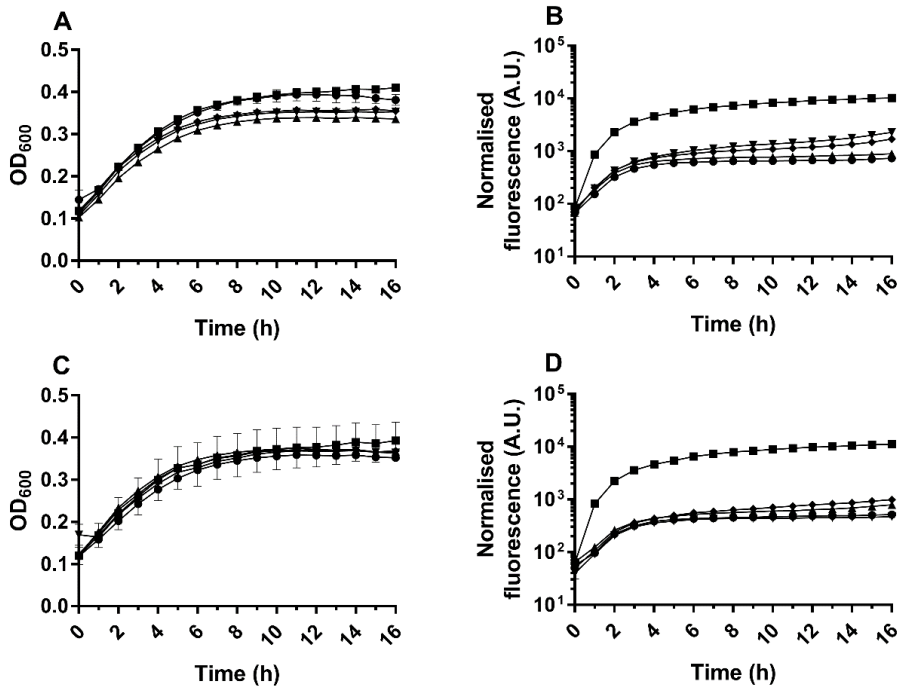

Figure 3.4 Influence of AcoR on gene expression induced by exogenous addition of (*R, R*)-2,3-BDO (triangles), (*S, S*)-2,3-BDO (upside down triangles), *meso*-2,3-BDO (diamonds) or acetoin (squares) to a final concentration of 5 mM or 0 mM (circles). Absorbance values for MG-p302 (A) and MG-p306 (C) were used to normalise fluorescence values for MG-p302 (B) and MG-p306 (D), respectively. Error bars represent standard error calculated from three biological replicates.

Due to high specificity of the AcoR/P_{acoA} system for acetoin, the optimal range of induction by acetoin and therefore potential as an inducible system for metabolic engineering applications was investigated. A fluorescence assay was undertaken utilising strain MG-p302 supplemented with a range of acetoin concentrations taking measurements after 4, 8, and 16 h (Figure 3.5). Cells were cultivated in M9MM supplemented with 0.4 % (w/v) glucose and 0, 0.005, 0.01, 0.02, 0.039, 0.078, 0.156, 0.313, 0.625, 1.25, 2.5, 5 or 10 mM acetoin. From the assay, it is evident that increasing levels of induction of gene expression are achieved between 0.02 mM and 0.625 mM

acetoin and that acetoin concentrations >1.25 mM result in no significant increase in normalised fluorescence during identical time-points indicating saturation of the system. Furthermore, the dose response curves (Figure 3.5) allowed for characterisation of half maximal effective sensitivity (EC_{50}), operating range and dynamic range of cells cultivated for 4, 8 or 16 h. For strain MG-p302 cultivated for 4 h, an EC_{50}, operating range and dynamic range of 0.092 mM, 0.020-1.250 mM acetoin and 460-2688 normalised fluorescence were observed, respectively. Cells cultivated for 8 h resulted in an EC_{50} of 0.051 mM, an operating range of 0.020-0.625 mM and a dynamic range of 738-4650 normalised floursence. Cells cultivated for 16 h resulted in an EC_{50} of 0.040 mM, an operating range also of 0.020-0.625 mM and a dynamic range of 1175 – 7255 normalised floursence, comparatively higher than cells in the presence of acetoin for 4 or 8 h.

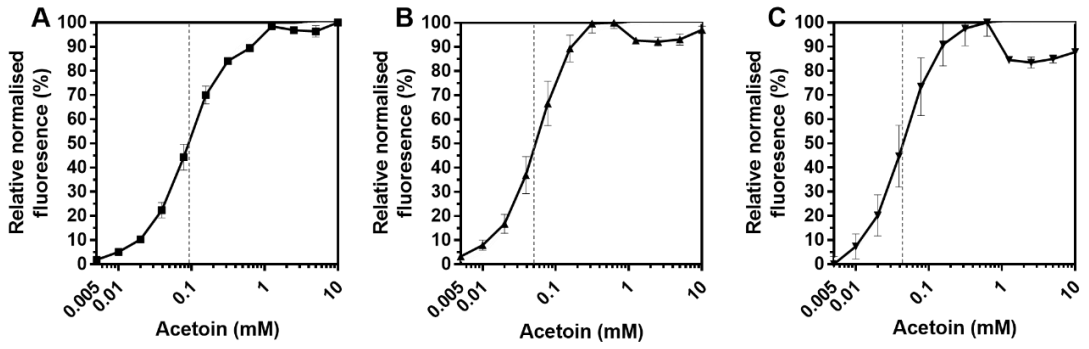

Figure 3.5 Dose response curve of MG-p302 in the presence of 0, 0.005, 0.01, 0.02, 0.039, 0.078, 0.156, 0.313, 0.625, 1.25, 2.5, 5 or 10 mM of acetoin. Measurements were taken 4 (A), 8 (B) and 16 (C) h after exogenous addition of acetoin. Error bars represent standard error calculated from three biological replicates.

3.3.2.2.2 Characterisation of *acoR* based inducible systems in *C. necator* H16

C. necator H16 is an ideal candidate for bioproduction of chemical compounds that synthetic biology tools such as genetically encoded biosensors can aid in. Therefore, to verify functionality of the AcoR/P_{acoA} inducible system in *C. necator* H16, first the wild type strain was transformed with pJLG302 (H16-p302). To minimise potential interruption of autoregulation of P_{acoR} in *C. necator* H16, the previously reported medium strength constitutive promoter P_{13} (Alagesan *et al.*, 2018) was cloned upstream of *acoR*, replacing P_{acoR}, resulting in plasmid pJLG303. Also, codon optimisation of *acoR* for *C. necator* H16 was undertaken and resulting sequence was synthesised by Gene Art Gene Synthesis, increasing GC content from 43 to 54 %. The codon optimised *acoR* gene (hereafter denoted *acoR**) was cloned into pJLG302, replacing *acoR*, resulting in plasmid pJLG307. Upon assembly, plasmids pJLG303 or pJLG307 were subsequently transformed into *C. necator* H16, generating strains H16-p303 and H16-p307, respectively.

To evaluate the acetoin inducible system in *C. necator* H16, expression of *rfp* by strains H16-p302, H16-p303 and H16-p307 was evaluated by cultivating cells in MM supplemented with 0.4 % (w/v) sodium gluconate and 0 mM (control) or 5 mM acetoin. Fluorescence measurements were taken every hour for 16 h and normalised to corresponding absorbance measurements (Figure 3.6). From the results, an increase of normalised fluorescence for strains H16-p302 and H16-p307 of 1.4-fold and 1.7-fold were observed, respectively, when compared to cells in the presence of no acetoin. However, a statistically significant difference in gene expression is only observed 4-8 h after addition of acetoin, with difference of normalised fluorescence in the control and cells in the presence of 5 mM acetoin decreasing at time-points after 7 h. This may

be due to depletion of sodium gluconate between 4 and 8 h, resulting in increased uptake of acetoin, subsequently influencing *rfp* expression regulated by the AcoR/P_{acoA} system. Interestingly, expression of *rfp* is reduced in strain H16-p302 with codon optimised *acoR** compared to strain H16-p307 with wild type *acoR* in *C. necator* H16. For cells harbouring pJLG303 with P_{13} replacing P_{acoR}, no statistically significant difference in normalised fluorescence is observed between cells in the presence of 0 mM or 5 mM acetoin.

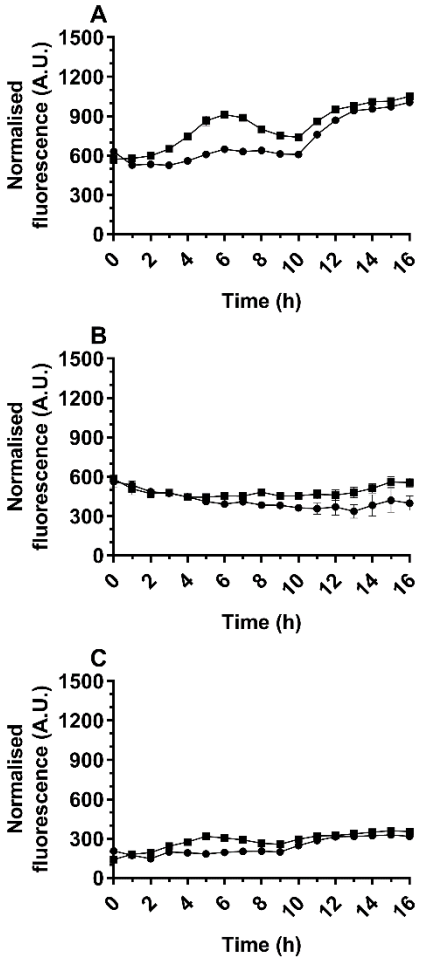

Figure 3.6 Fluorescence assay of strains H16-p302 (A), H16-p303 (B) and H16-p307 (C). Cells were cultivated in the presence of 0 mM acetoin (circles) or 5 mM acetoin (squares). Error bars represent standard error calculated from three biological triplicates.

From experimental data in Figure 3.6, consumption of both sodium gluconate and acetoin by *C. necator* H16 is potentially influencing the AcoR/P_{acoA} system. Therefore, to assess the effect on *rfp* expression in strain H16-p302 cultivated with acetoin as the sole carbon source, cells were subjected to a fluorescence assay with either 5 mM sodium gluconate or 5 mM acetoin (Figure 3.7). From the assay, cells cultivated with acetoin were observed to accumulate less biomass than cells cultivated with sodium gluconate. However, cells cultivated with acetoin resulted in a 1.7-fold to 2.1-fold increase in normalised fluorescence between 6 and 16 h, when compared to cells cultivated with sodium gluconate. These results demonstrate induction of the AcoR/P_{acoA} system by acetoin in *C. necator* H16. However, statistically significant difference is only observed in cells cultivated with acetoin as the sole carbon source at time points after 5 h.

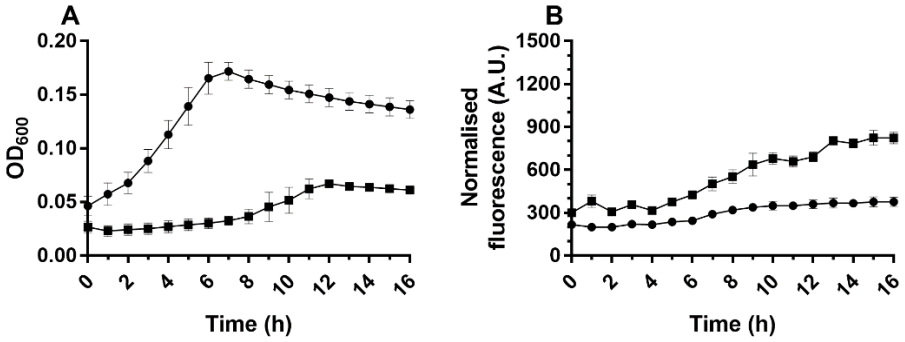

Figure 3.7 Comparison of normalised fluorescence for H16-p302 cultivated with either 5 mM sodium gluconate (circles) or 5 mM acetoin (squares) as the sole carbon source. Fluorescence was normalised (B) to absorbance (A). Error bars represent standard error calculated from three biological replicates.

3.4 Discussion

For bioproduction of compounds by microorganisms, establishing whether the target compound is consumed is important in metabolic engineering of *C. necator* H16. Indeed, metabolism of 2,3-BDO by *A. woodii* and conversion of (*S*)-1,3-BDO to 4-hydroxy-2-butanone by secondary alcohol dehydrogenase from *Candida parapsilosis* has been previously reported (Hess *et al.*, 2015; Yamamoto *et al.*, 1995) demonstrating ability of bacteria to consume various BDO isomers. Therefore, confirming 1,4-BDO, 1,3-BDO or 2,3-BDO is not consumed by *C. necator* H16 was crucial for bioproduction of BDO. Furthermore, toxicity assays indicate no toxic effect on *C. necator* H16 in the presence of any BDO at concentrations up to 166 mM, demonstrating significant titres can be produced before any negative effect on biomass production will be observed.

When metabolically engineering an organism for industrial production of chemicals, use of chromatography to determine metabolite concentrations is often the rate-limiting step. Implementation of biosensors, whilst not as accurate, can provide real-time data and enable high-throughput screening. Here, two different inducible systems have been investigated in the development of a biosensor capable of detecting butanediol isomers in *C. necator* H16.

The putative pyruvate transporter encoded by *yhjX* in *E. coli* MG1655 is a member of the major facilitator superfamily and is regulated by the two-component system PyrSR (formerly YpdAB) identified as a regulator of pyruvate reutilization and induced in the presence of concentrations of >0.1 mM pyruvate (Fried, Behr and Jung, 2013; Miyake *et al.*, 2019). However, *yhjX* appears to play a wider role during cellular stress response; an increase in expression was observed when *E. coli* MG1655 cells were in the presence

of small toxic peptides (Fozo *et al.*, 2008) or high concentrations of 1,4-BDO (Szmidt-Middleton *et al.*, 2013). Furthermore, upregulation of *yhjX* in *E. coli* W3110 occurred when cells were in the presence of benzoate (Kannan *et al.*, 2008) and *yhjX* in *E. coli* ATCC 25922 has been shown to regulate cellular growth in the presence of subinhibitory levels of gentamicin (Zhou *et al.*, 2019). Clearly, YhjX serves several functions within *E. coli* and control of expression is potentially influenced by alternative unknown transcription-factor(s). The promoter of *yhjX* (P_{yhjX}) was shown here to be induced by 1,4-BDO as previously reported (Szmidt-Middleton *et al.*, 2013), as well as (*R*)-1,3-BDO and (*R*, *R*)-2,3-BDO. From the results, presence of 2,3-BDO resulted in overall highest gene expression, compared to presence of 1,3-BDO or 1,4-BDO. This increased response is potentially a result of greater affinity for 2,3-BDO. Indeed, Szmidt-Middleton and co-workers reported a variable fluoresecnet signal of P_{yhjX} in the presence of 1,5-pentandeiol or 1,3-propanediol (Szmidt-Middleton *et al.*, 2013). Interestinly, highest response was reported in the presence of 384 mM 1,5-pentanediol, seemingly higher response than when in the presence of 777 mM 1,4-BDO demonstrating varying response of P_{yhjX} in presence of different diols.

However, the optimal concentration of BDO to be detected is greater than concentrations demonstrated to inhibit growth rate in *C. necator* H16 strains to a certain extent. This is most likely due to *yhjX* responding to cellular stress as a result of toxic concentrations of BDO isomers. To utilise the P_{yhjX} inducible promoter in *C. necator* H16 for detection of BDOs, the regulator that interacts with P_{yhjX} and regulation of *yhjX* in the presence of BDO needs to confirmed to be PyrR and optimal range of induction reduced.

There are multiple approaches that can be taken for development of a transcription factor-based inducible system responsive to a specific effector. One approach is identification of genes that are upregulated when in the presence of a specific ligand, such as *yhjX* in the presence of 1,4-BDO. An alternative approach is identification of a transcription factor responsible for regulation of an enzyme involved in enzymatic conversion of a specific effector. Here, a transcription factor-based inducible system reportedly involved in 2,3-BDO catabolism by *A. woodii* DSM1030 (Hess *et al.*, 2015) was investigated for induction by acetoin and three 2,3-BDO optical isomers in *E. coli* MG1655 and *C. necator* H16. Characterisation of the AcoR/P_{acoA} system in *E. coli* MG1655 revealed gene expression is induced by acetoin concentrations as low as 10 µM, demonstrating potential as a biosensor for real-time reporting, particularly during high through-put screening of engineered strains. Indeed, there are reports of engineering organisms to produce acetoin in recent years (Bae, Kim and Hahn, 2016; Zhang *et al.*, 2019; Drejer *et al.*, 2020), demonstrating a need for tools to aid strain development.

The AcoR/P_{acoA} inducible system from *A. woodii* DSM 1030 appears to be highly specific towards acetoin, with no induction of gene expression observed by strain MG-p302 in the presence of three 2,3-BDO optical isomers. A number of bacteria are able to natively produce 2,3-BDO, with production by *K. pneumoniae* achieving a concentration of 150 g L^{-1} previously reported (Ma *et al.*, 2009). Remarkably, the metabolic function of 2,3-BDO anabolism from pyruvate is still unconfirmed. Most likely, 2,3-BDO production aids in balancing intracellular acidification (Nakashimada *et al.*, 2000) and/or NADH/NAD^+ ratio (Bao *et al.*, 2014). The complete pathway for microbial catabolism of 2,3-BDO by *A. woodii* DSM 1030 is also unconfirmed, with

the first enzymatic step, conversion to acetoin, facilitated by an unknown alcohol dehydrogenase (Hess *et al.*, 2015). Elucidation of the regulation system of the alcohol dehydrogenase(s) responsible for conversion of 2,3-BDO to acetoin in *A. woodii* DSM 1030 may be a potential approach for developing systems induced by 2,3-BDO or other BDO isomers.

Of note, gene expression induced by presence of acetion was observed for the AcoR/P_{acoA} system when deployed in *C. necator* H16. However, this was achieved due to cultivaton of cells using acetoin as the sole carbon source. It is evident that further optimisations could be explored to improve response by AcoR/P_{acoA} system for detection of acetoin. The native RBS, P_{acoR} and P_{acoA} were utilisied in the development of the biosensor and whilst these did indicate functionality within *C. necator* H16 However, alternative RBS and/or promoters could be explored, with previous reports demonstrating influence of the role RBS plays in gene expression (Alagesan *et al.*, 2018).

3.5 Conclusion

To conclude, in this study *C. necator* H16 has been shown to not consume 1,3-BDO, 1,4-BDO or 2,3-BDO. Also, identical BDO isomers have been shown to have no toxic effect on *C. necator* H16 at concentrations up to 166 mM. Then, two systems developed towards detection of BDO in *C. necator* H16 have been investigated. The promoter of the *E. coli* gene *yhjX*, (P_{yhjX}) has been shown to increase gene expression in the presence of 1,4-BDO, 1,3-BDO and 2,3-BDO in *E. coli* MG1655. However, the mechanism for driving P_{yhjX} remains unknown and is crucial for potential deployment in *C. necator* H16. Next, an acetoin inducible system was implemented in the form of a biosensor

and characterised in *E. coli* MG1655. Finally, the acetoin inducible system was characterised in *C. necator* H16, with results indicating catabolism of acetoin interferes with the application of such system in this bacterium.

4 Metabolic engineering of *Cupriavidus necator* H16 for (*R*)-1,3-butanediol biosynthesis

4.1 Introduction

C. necator H16 is able to metabolise a wide range of carbon sources including CO_2 *via* the Calvin-Benson-Bassham (CBB) cycle (Bowien and Kusian, 2002). *C. necator* H16 has been engineered to produce a wide range of commodity chemicals including methyl ketones, alcohols, terpenes, and alkanes and alkenes (Müller *et al.*, 2013; Lu *et al.*, 2012; Crepin, Lombard and Guillouet, 2016; Grousseau *et al.*, 2014; Chakravarty and Brigham, 2018; Krieg *et al.*, 2018) demonstrating versatility as an industrial chassis.

1,3-butanediol (1,3-BDO) is an important building block for a variety of industrial applications, including as an alternative resource to produce 1,3-butadiene, a precursor for synthetic rubbers (Duan, Yamada and Sato, 2016). The optically active *R*- form of 1,3-BDO is used in the production of pheromones, fragrances and insecticides (Matsuyama, Kobayashi and Ohnishi, 1993). Also, (*R*)-1,3-BDO is of interest for its use in the production of one of the most widely prescribed antimicrobial drugs; β-lactam antibiotics (Llarrull *et al.*, 2010). Interestingly, 1,3-BDO can be oxidized to its ketone form 4-hydroxy-2-butanone (4H2B), an important precursor for the synthesis of pesticides, steroids, and anticancer drug doxorubicin (Zhang *et al.*, 2010). An NAD^+-dependent glycerol dehydrogenase (GlyDH) from *Hansenula ofunaensis* has been reported to possess low specific activity for oxidation of 1,3-BDO (Yamada-Onodera, Nakajima and Tani, 2006). Other research has shown a secondary alcohol dehydrogenase from *Candida parapsilosis* capable of converting (*S*)-1,3-BDO to 4H2B (Yamamoto *et al.*, 1999).

Both chemical and biochemical synthesis methods have been developed for (*R*)-1,3-BDO production. Chemical synthesis typically yields a mixture of *R*- and *S*-enantiomers of 1,3-BDO and requires a precursor, such as acetaldehyde, derived from petrochemical sources (Larchevêque, Mambu and Petit, 1991). Whereas, a more economical enzymatic biosynthesis of (*R*)-1,3-BDO has been achieved using either racemic 1,3-BDO or 4-hydroxy-2-butanone (4H2B) as substrates (Matsuyama *et al.*, 2001). The oxido-reduction process of (4H2B) to (*R*)-1,3-BDO has been demonstrated in a variety of microorganisms such as *Kluyveromyces*, *Candida*, *Pichia*, and others, as well as engineered *E. coli* (Matsuyama *et al.*, 2001; Matsuyama, Nikaido and Kobayashi, 1988; Okabayashi, Nakajima and Yamamoto, 2009).

Microbial bioproduction of 1,3-BDO has been first reported by Kataoka and co-workers in metabolically engineered *E. coli* (Kataoka *et al.*, 2013). A synthetic metabolic pathway, consisting of acetyl-CoA acetyltransferase (gene *phaA*) and acetoacetyl-CoA reductase (*phaB1*) from *C. necator* H16, butanal dehydrogenase (*bld*) from *Clostridium saccharoperbutylacetonicum* N1-4(HMT) and unknown endogenous *E. coli* alcohol dehydrogenase/aldehyde reductase, has been used to convert acetyl-CoA to (*R*)-1,3-BDO *via* acetoacetyl-CoA, 3-hydroxybutyryl-CoA, and 3-hydroxybutanal intermediates. Optimised fed-batch fermentation using glucose as a carbon source achieved 15.75 g/L (174.8 mmol/L) titre of 1,3-BDO with a 98.6 % enantiomeric excess and a yield of 0.18 g/g glucose (0.37 mol/mol) (Kataoka *et al.*, 2014).

Another synthetic pathway has been recently investigated demonstrating conversion of pyruvate to (*R*)-1,3-BDO through acetaldehyde and 3-hydroxybutanal intermediates (Nemr *et al.*, 2018; Kim *et al.*, 2017). Application of this pathway consisted of expression of pyruvate decarboxylase (PDC) from *Zymomonas mobilis*, deoxyribose-

5-phosphate aldolase (DERA) from *Bacillus halodurans* and aldo-keto reductase (AKR) from *Pseudomonas aeruginosa*, resulting in 2.4 g/L titre of 1,3-BDO with a yield of 56 mg/g glucose (Nemr *et al.*, 2018).

Recently, (*R*)-1,3-BDO bio-production process has been industrialised, with the US based company Genomatica, known for their industrial-scale bio-production of 1,4-butanediol, announcing large-scale production of bio-based 1,3-BDO production, branded Brontide™ BG. No details of production processes have been publicised (Genomatica, 2017b).

In this study, the production of (*R*)-1,3-BDO in *C. necator* H16 is reported. To achieve this, two alternative heterologous (*R*)-1,3-BDO biosynthetic pathways, based on utilisation of either (*R*)-3-hydroxybutyanal-CoA or pyruvate as precursors, were investigated. Initially, (*R*)-1,3-BDO biosynthesis was achieved by heterologous gene expression of either codon-optimized *bld* from *Clostridium saccharoperbutylacetonicum* encoding butanal dehydrogenase (NADH-dependent) in combination with *yqhD* from *Escherichia coli* encoding aldehyde reductase or codon-optimized *adhE2* from *Clostridium acetobutylicum* encoding bi-functional aldehyde/alcohol dehydrogenase (Figure 4.1.A). (*R*)-1,3-BDO yields were improved through the genetic inactivation of poly[(*R*)-3-hydroxybutyrate] (P3HB) biosynthesis by deleting *phaC1* gene and redirecting carbon toward diol production. (*R*)-1,3-BDO-producing strains were further improved by optimising cultivation conditions through altering carbon to nitrogen ratio and balancing levels of induced gene expression. Here, alternative 4H2B biosynthesis pathway is reported by conversion of acetyl-CoA as precursor, with intermediates acetoacetyl-CoA and 3-oxobutanal. 4H2B is formed as (*R*)-1,3-BDO biosynthesis pathway by-product as a result of increased availability of

acetoacetyl-CoA and promiscuity of Bld and YqhD. (*R*)-1,3-BDO biosynthetic pathway was also genetically engineered in *C. necator* H16 by heterologous expression of codon-optimized *pdc* (pyruvate decarboxylase from *Zymomonas mobilis*), *dra* (deoxyribose-5-phosphate aldolase; *Bacillus halodurans*) and *yqhD* (aldehyde reductase from *E. coli*) (Figure 4.1.B). The introduction of this biosynthetic pathway did not yield a detectable level of (*R*)-1,3-BDO, whereas the combination of both biosynthetic pathways resulted in highest diol yields. In conclusion, this study demonstrates that engineered *C. necator* H16 can be effectively utilised for diol production.

4.2 Materials and Methods

4.2.1 Gene sequences and codon optimisation

The sequences of genes used for generation of 1,3-BDO biosynthesis operon were retrieved from Genbank under the following accession numbers/locus tags: AY251646 (*bld* from *Clostridium saccharoperbutylacetonicum*); NP_417484/b3011, NP_416285/b1771, NP_417474/b3001, NP_416950/b2455, NP_415757/b1241 (*yqhD, ydjG, gpr, eutE, adhE* from *E. coli*); NP_744640/PP_2492 (*yqhD* from *Pseudomonas putida*); WP_077844196 (*adh* from *Clostridium beijerinckii*); CAJ92685/H16_RS07715, CAJ95981 /H16_RS24705 (*gbD, hibadh* from *Cupriavidus necator*); O32210/BSU33400, P80874/BSU09530 (*yvgN, yhdN* from *Bacillus subtilius*); ADF38510/BMD_1654, ADF39485/BMD_2640, ADF40202/BMD_3362 (ADH_1, ADH_2, *eutE* from *Bacillus megaterium*); Q9KD67/BH1352 (*dra* from *Bacillus halodurans*); AHJ73198/A265_01761 (*pdc* from *Zymomonas mobilis*), NP_249818/PA_1127 (AKR from *Pseudomonas aeruginosa*); NP_149325/CA_P0162,

NP_149199/CA_P0035 (*adhE, adhE2* from *Clostridium acetobutylicum*). Genes *bld, adhE, dra, adh* and *pdc* were codon optimised for *C. necator* H16 and synthesised by Gene Art Gene Synthesis (Thermo Fisher Scientific, Waltham, MA, USA). All codon optimised DNA sequences are listed in Section 9.1.

4.2.2 Primers used in this study

All primers used in this study are listed in Table 4.1.

Table 4.1. Primers used in this study.

Name	**Sequence 5' to 3'**
N1_u_ara_f	GGGAAAGUCTAGATTATGACAACTTGACGGCTAC
N2_u_ara_r	ATATCTCCUTCTTAAAAGATCTTTTGAATTCCC
PJG7_U_sAdh_F	AGTTAAGTAUAAGAAGGAGATATAACATGAAGGGCTTCGCCATGC
PJG8_U_sAdh_R	GGAGACAUCTCGAGTCACAGGATCACCACGGC
PJG9_U_YqhD_F	AGTTAAGTAUAAGAAGGAGATATAACATGAACAACTTTAATCTGCACACCC
PJG10_U_YqhD_R	GGAGACAUCTCGAGGCGTAAAAAGCTTAGCGG
PJG11_U_gbd_F	AGTTAAGTAUAAGAAGGAGATATAACATGGCGTTTATCTACTATCTGACCC
PJG12_U_gbd_R	GGAGACAUCTCGAGCTACATGGACTGCTCAAGCATACG
PJG13_U_HIB_F	AGTTAAGTAUAAGAAGGAGATATAACATGCATATCGCCTTCATCGGC
PJG14_U_HIB_R	GGAGACAUCTCGAGTCATTGCTTGCCCTCCTTGT
PJG15_U_Adhe_F	AGGAGATAUACATATGAAGGTGACCACCGTGAAG
PJG16_U_Adhe_R	GGAGACAUAGTCTCGAGACTAGTTCAGGGCTG
PJG17_U_Bld_F	AGGAGATAUACATATGATCAAGGACACCCTGGTG
PJG18_U_Bld_R	ATACTTAACUAGTCGAGACTAGTTCAGCCGG
P20_phaA_Xho_F	ATATCTCGAGCGCTTGCATGAGTGCCGG
P21_phaB1_NheI_R	ATATGCTAGCCAGGTCAGCCCATATGCAGGC

P22_btkB_Xho_F	ATATCTCGAGTTAGGTAAAAGTACGCTCGTTCGATTTCG
P23_btkB_SacI_R	ATATGAGCTCTAACCTCAGATACGCTCGAAGATGGC
P24_phaB1_SacI_F	ATATGAGCTCGGAAGGGGTTTTCCGGGGC
P25_YqhD.PP_SpeI_F	ATATACTAGTAAGAAGGAGATATAATGCTCAATTTTGACTTCCACAACC
P26_YqhD.PP_XhoI_R	TATACTCGAGTTAGAGGCTGGCTTCAAGCACCCTG
P27_YvgN_SpeI_F	ATATACTAGTAAGAAGGAGATATAATGCCAACAAGTTTAAAAGATACTGTAAAGTTACATAACGGAGTTG
P28_YvgN_XhoI_R	TATACTCGAGTTAAAACAGAAGCTCATCAGGATTTGGACCGAC
P29_YhdN_SpeI_F	ATATACTAGTAAGAAGGAGATATAATGGAATATACCAGTATAGCAGATACAGGAATAGAAGCCTC
P30_YhdN_XhoI_R	TATACTCGAGTTATATTTCCTCTCTGGTCGGCGGGG
P31_ydjG_SpeI_F	ATATACTAGTAAGAAGGAGATATAATGAAAAAGATACCTTTAGGCACAACGGATATTACGC
P32_ydjG_XhoI_R	TATACTCGAGTTAACGCTCCAGGGCCTCTGCC
P33_gpr_SpeI_F	ATATACTAGTAAGAAGGAGATATAATGGTCTGGTTAGCGAATCCCGAACG
p34_gpr_XhoI_R	TATACTCGAGTCATTTATCGGAAGACGCCTGCCACAG
P35_ARK.PA_SpeI_F	ATATACTAGTAAGAAGGAGATATAATGAGCGTTGAAAGCATTCGCATCGAG
P36_AKR.PA_XhoI_R	TATACTCGAGTCAGGCGTTGCGGCTGGG
P37_PDOD1_SpeI_F	ATATACTAGTAAGAAGGAGATATAATGAAAGGGTATTCAAAATTTTGTATGCCTAACTCAGTCTTTTATGG
P38_PDOD1_XhoI_R	TATACTCGAGTTAAGATTCAACAGTATTTTTGCTTCTTGAAAAATCGTAGTTATAGCAGTAATAG
P39_PDOD2_SpeI_F	ATATACTAGTAAGAAGGAGATATAATGGGAATTTATGAACTACTTGTACCACGCAC
P40_PDOD2_XhoI_R	TATACTCGAGTTAGCAGGACTTCCGCTTTGAATCGCA
P41_eutE.EC_EcoRI_F	ATATGAATTCAAAAGATCTTTTAAGAAGGAGATATACATATGAATCAACAGGATATTGAACAGGTGGTGAAAGC
P42_eutE.EC_SpeI_R	TATAACTAGTTTAAACAATGCGAAACGCATCGACTAATACACAG
P43_eutE.BMD_EcoRI_F	ATATGAATTCAAAAGATCTTTTAAGAAGGAGATATACATATGCAGTTTGATCAAGATCTTCAATCTTTACAAGAGATGC
P44_eutE.BMD_SpeI_R	TATAACTAGTTTAGTTTGTTTGATATTTTTGAAGTGCTTGATTAACCATTTCAGAAATTG

P45_adhE.EC_NdeI_F	ATATCATATGATGGCTGTTACTAATGTCGCTGAACTTAACGC
P46_adhE.EC_SpeI_R	TATAACTAGTTTAAGCGGATTTTTTCGCTTTTTTCTCAGCTTTAGC
P47_adhE2.CA_NdeI_F	ATATCATATGATGAAAGTTACAAATCAAAAAGAACTAAAACAAAAGCTAAATGAATTGAGAGAAG
P48_adhE2.CA_SpeI_R	TATAACTAGTTTAAAATGATTTTATATAGATATCCTTAAGTTCACTTATAAGTGGATACCTAGGATTAGCTGTTG
27_yqhD.EC_F	CTTTTAAGAAAGGAGATATAGAGCTCATGAACAACTTTAATCTGCACAC
303.PDCOpt_Nhe_R	ATATGCTAGCTCACAGCAGCTTGTTCAC
sucC_Sac_UP_F	ATATGAGCTCGCGCCATTACGGCCGAG
sucC_OVL_R	GGCGAGGTACGACTTACAGCATTGCGATATTCATGCGTGTTTCCTTTCGGGTAGG
sucD_OVL_F	CCTACCCGAAAGGAAACACGCATGAATATCGCAATGCTGTAAGTCGTACCTCGCC
sucD_Pac_DN_R	TATATTAATTAAAAGCGCTCCATGACCTTGAGC
sucC_UP_F	GTGGCGAGGCCTGATGCG
sucD_DN_R	AATCTCGTCAGGCGGCCTG
iclA_Sac_UP_F	ATATGAGCTCGCGCCTGCTCTTCATCGATGATCG
iclA_OVL_R	GGTTGGCGTTTTGCTTGGGGTATTACTGGTATCAGAAGGGCCATGGGAATTTCCTAAGAAGAAAG
iclA_OVL_F	CTTTCTTCTTAGGAAATTCCCATGGCCTTCTGATACCAGTAATACCCCAAGCAAAACGCCAACC
iclA_Pac_DN_R	TATATTAATTAACAACCATCGAGCAGCGAGATGTTC
iclA_UP_F	ATCGGCTGGATGGCGCC
iclA_DN_R	GGCAGGAGTGGTCACGGG
iclB_Sac_UP_F	ATATGAGCTCCGCCTTCCACCTGCCGTG
iclB_OVL_R	GGGTGACCAGGAGAGTCAGGCGGTCATGGTCACTCTCCTGATGATGC
iclB_OVL_F	GCATCATCAGGAGAGTGACCATGACCGCCTGACTCTCCTGGTCACCC
iclB_Pac_DN_R	TATATTAATTAACGTCGGGCGTCTTCAGTTC
iclB_UP_F	TCGGCCATGACTGGGGTTCG
iclB_DN_R	GGGCGCAGGGTCAGGC
phaB1_Sac_UP_F	ATATGAGCTCGCATCACCGCCGAGAACGTGGC
phaB1_OVL_R	ACCAGGCCGGCAGGTCAGCCAGTCATGTCCACTCCTTGATTGGCTTCGTTATCGTC

phaB1_OVL_F	GACGATAACGAAGCCAATCAAGGAGTGGACATGACTGGCTGACCTGCCGGCCTGGT
phaB1_Pac_DN_R	TATATTAATTAATGTTCTGGATGTCGATGAAGGCCTGGATGTTC
44.phaB1_Xho_F	ATATCTCGAGGGAAGGGGTTTTCCGGGGCC
44.phaB1_Nhe_R	TATAGCTAGCGCTAGCCAGGTCAGCCCATATGCAG

4.2.3 Plasmids used in this study

All plasmids used in this study are listed in Table 4.2.

Table 4.2. Plasmids used in this study. * denotes codon optimisation. Km^R: kanamycin resistance. Tet^R: tetracycline resistance.

Plasmid	**Description**	**Source**
pBBR1-2USER	host plasmid with Km^R and pBBR1 ori	(Alagesan *et al.*, 2018)
pJLG401	pBBR1-USER with P_{araBAD}, a*dhE**	This work
pJLG402	pBBR1-USER with P_{araBAD}, *bld**, y*qhD* (b3011)	This work
pJLG403	pBBR1-USER with P_{araBAD}, *bld**, *s-adh**	This work
pJLG404	pBBR1-USER with P_{araBAD}, *bld**, *HIBADH*	This work
pJLG405	pBBR1-USER with P_{araBAD}, *bld**, *gbd*	This work
pJLG411	pBBR1-USER with P_{araBAD}, *bld**, *yqhD* (b3011), *phaA, phaB1*	This work
pJLG414	pBBR1-USER with P_{araBAD}, *bld**	This work
pJLG415	pBBR1-USER with P_{araBAD}, *bld**, *yqhD* (PP_2492)	This work
pJLG416	pBBR1-USER with P_{araBAD}, *bld**, *yvgN*	This work
pJLG417	pBBR1-USER with P_{araBAD}, *bld**, *yhdN*	This work
pJLG418	pBBR1-USER with P_{araBAD}, *bld**, *ydjG*	This work
pJLG419	pBBR1-USER with P_{araBAD}, *bld**, *gpr*	This work
pJLG420	pBBR1-USER with P_{araBAD}, *bld**, PA1127	This work
pJLG421	pBBR1-USER with P_{araBAD}, *bld**, BMD_1654	This work
pJLG422	pBBR1-USER with P_{araBAD}, *bld**, BMD_2640	This work
pJLG423	pBBR1-USER with P_{araBAD}, *eutE* (BMD_3362), y*qhD* (b3011)	This work

pJLG424	pBBR1-USER with P_{araBAD}, *eutE* (b2455), y*qhD* (b3011)	This work
pJLG425	pBBR1-USER with P_{araBAD}, a*dhE* (b1241)	This work
pJLG426	pBBR1-USER with P_{araBAD}, a*dhE2*	This work
pJLG438	pBBR1-USER with P_{araBAD}, *bld**, *PA1127*, *phaA*, *phaB1*	This work
pJLG444	pBBR1-USER with P_{araBAD}, *bld**, y*qhD* (b3011), *dra**, *pdc**	This work
pJLG446	pBBR1-USER with P_{araBAD},, y*qhD* (b3011), *dra**, *pdc**	This work
pJLG447	pBBR1-USER with P_{araBAD}, *bld**, y*qhD* (b3011), *phaB1*	This work
pBBR1 MCS-2-P8	Source of P_8 promoter	(Alagesan *et al.*, 2018)
pLO3	host plasmid with Tet^R,, *sacB*, RP4 transfer ori, pBR322 ori	(Lenz and Friedrich, 1998)
pJLG451	pLO3, *phaB1* deletion vector	This work
pJLG452	pLO3, *iclA* deletion vector	This work
pJLG453	pLO3, *iclB* deletion vector	This work
pJLG454	pLO3, *sucCD* deletion vector	This work

4.2.4 Assembly of plasmids used in this study

Detailed molecular cloning techniques are in Materials and Methods.

Assembly of two modular vectors was undertaken to be used as a backbone for all future protein expression plasmids and were assembled using the previously described USER cloning method (Bitinaite *et al.*, 2007) for plasmids pJLG401 and pJLG402 into the pBBR1-USER (Alagesan *et al.*, 2018) host plasmid. The arabinose inducible system was combined with genes for controllable expression with restriction sites XbaI and EcoRI flanking the arabinose inducible system; EcoRI and NdeI sites flanking RBS 1; NdeI and SpeI sites flanking gene 1; an SpeI site upstream of RBS 2 and gene 2 followed by adjacent XhoI and NheI sites, where appropriate, allowing rapid assembly

of new constructs. For addition of *C. necator* genes to operon, native RBS's were utilised for translation of genes. For addition of heterologous enzyme expression, RBS 3 and RBS 4 were employed for gene 3 and gene 4 of the operon, respectively.

pJLG401: Arabinose inducible system amplified from pEH006 (Alagesan *et al.*, 2018) with N1_u_ara_f and N1_u_ara_r was combined with *adhE1* (CA_P0162) amplified with PJG15_U_Adhe_F and PJG16_U_Adhe_R from template DNA synthesised and codon optimised by Gene Art Gene Synthesis and assembled with the USER cloning protocol.

pJLG402: Arabinose inducible system amplified from pEH006 (Alagesan *et al.*, 2018) with N1_u_ara_f and N1_u_ara_r was combined with *bld* (AAP42563) amplified with PJG17_U_Bld_F and PJG18_U_Bld_R from template DNA synthesised and codon optimised by Gene Art Gene Synthesis and *yqhD* (b3011) amplified with PJG9_U_YqhD_F and PJG10_U_YqhD_R from purified *E. coli* MG1655 genomic DNA and assembled with the USER cloning protocol.

pJLG403: *s-adh* (WP_077844196) was amplified with PJG7_U_sAdh_F and PJG8_U_sAdh_R from template DNA synthesised and codon optimised by Gene Art Gene Synthesis. The PCR product was cloned into pJLG402 using restriction sites SpeI and XhoI.

pJLG404: *hibadh* (H16_RS24705) was amplified with PJG13_U_HIB_F and PJG14_U_HIB_R from purified *C. necator* H16 genomic DNA. The PCR product was cloned into pJLG402 using restriction sites SpeI and XhoI.

pJLG405: *gbD* (H16_RS07715) was amplified with PJG11_U_gbd_F and PJG12_U_gbd_R from purified *C. necator* H16 genomic DNA. The PCR product was cloned into pJLG402 using restriction sites SpeI and XhoI.

pJLG411: *phaA* and *phaB1* (H16_A1438 and H16_A1439) were amplified as one fragment with native ribosomal binding sites by P20_phaA_Xho_F and P21_phaB1_NheI_R from purified *C. necator* H16 genomic DNA. The PCR product was cloned into pJLG402 using restriction sites XhoI and NheI.

pJLG414: *bld* (AAP42563) extracted from pJLG402 was cloned into pJLG401 using restriction sites EcoRI and SpeI.

pJLG415: *yqhD* (PP_2492) was amplified with P25_YqhD.PP_SpeI_F and P26_YqhD.PP_XhoI_R from purified *P. putida* KT2440 purified genomic DNA. The PCR product was cloned into pJLG402 using restriction sites XhoI and NheI.

pJLG416: *yvgN* (BSU33400) was amplified with P27_YvgN_SpeI_F and P28_YvgN_XhoI_R from purified *B. subtilius* 168 purified genomic DNA. The PCR product was cloned into pJLG402 using restriction sites XhoI and NheI.

pJLG417: *yhdN* (BSU09530) was amplified with P29_YhdN_SpeI_F and P30_YhdN_XhoI_R from purified *B. subtilius* 168 purified genomic DNA. The PCR product was cloned into pJLG402 using restriction sites XhoI and NheI.

pJLG418: *ydjG* (b1771) was amplified with P31_ydjG_SpeI_F and P32_ydjG_XhoI_R from purified *E. coli* MG1655 genomic DNA. The PCR product was cloned into pJLG402 using restriction sites XhoI and NheI.

pJLG419: *gpr* (b3001) was amplified with P33_gpr_SpeI_F and P32_ydjG_XhoI_R from purified *E. coli* MG1655 genomic DNA. The PCR product was cloned into pJLG402 using restriction sites XhoI and NheI.

pJLG420: aldo-keto reductase PA_1127 was amplified with P35_ARK.PA_SpeI_F and P36_AKR.PA_XhoI_R from purified *P. aeruginosa* PAO1 genomic DNA. The PCR product was cloned into pJLG402 using restriction sites XhoI and NheI.

pJLG421: 1,3-propanediol dehydrogenase BMD_1654 was amplified with P37_PDOD1_SpeI_F and P38_PDOD1_XhoI_R from purified *B. megaterium* DSM319 genomic DNA. The PCR product was cloned into pJLG402 using restriction sites XhoI and NheI.

pJLG422: 1,3-propanediol dehydrogenase BMD_2640 was amplified with P39_PDOD2_SpeI_F and P40_PDOD2_XhoI_R from purified *B. megaterium* DSM319 genomic DNA. The PCR product was cloned into pJLG402 using restriction sites XhoI and NheI.

pJLG423: *eutE* (BMD_3362) was amplified with P43_eutE.BMD_EcoRI_F and P44_eutE.BMD_SpeI_R from purified *B. megaterium* DSM319 genomic DNA. The PCR product was cloned into pJLG402 using restriction sites EcoRI and SpeI.

pJLG424: *eutE* (b2455) was amplified with P41_eutE.EC_EcoRI_F and P42_eutE.EC_SpeI_R from purified *E. coli* MG1655 genomic DNA. The PCR product was cloned into pJLG402 using restriction sites EcoRI and SpeI.

pJLG425: *adhE* (b1241) was amplified with P45_adhE.EC_NdeI_F and P46_adhE.EC_SpeI_R from purified *E. coli* MG1655 genomic DNA. The PCR product was cloned into pJLG401 using restriction sites NdeI and SpeI.

pJLG426: *adhE2* (CA_P0035) was amplified with P45_adhE.EC_NdeI_F and P46_adhE.EC_SpeI_R from purified *C. acetobutylicum* ATCC 824 genomic DNA. The PCR product was cloned into pJLG401 using restriction sites NdeI and SpeI.

pJLG438: the *phaA* and *phaB* fragment was extracted from pJLG411 and cloned into pJLG420 using restriction sites XhoI and NheI.

pJLG444: the *dra* and *pdc* fragment was extracted from synthetic plasmid and cloned into pJLG402 using restriction sites XhoI and NheI.

pJLG446: the *yqhD, dra* and *pdc* operon was amplified from pJLG444 with 27.yqhD.EC_F and 303.PDCOpt_Nhe_R and cloned into pJLG401 using restriction sites NdeI and NheI.

pJLG447: *phaB1* (H16_A1439) was amplified with native ribosomal binding site by 44.phaB1_Xho_F and 44.phaB1_Nhe_R from purified *C. necator* H16 genomic DNA. The PCR product was cloned into pJLG402 using restriction sites XhoI and NheI.

The pLO3 suicide vector was utilised for all genomic manipulations of *C. necator*. With homologous recombination the primary method used for genomic manipulations, homologous chromosomal regions upstream and downstream of the desired genomic manipulation were amplified through PCR with complementary regions resulting in PCR fragment fusion through SOEing PCR or through Hi Fi assembly into the multiple cloning site of the pLO3 backbone.

pJLG451: homology arms upstream and downstream of *phaB1* were amplified with phaB1_Sac_UP_F, phaB1_OVL_R and phaB1_OVL_F, phaB1_Pac_DN_R, respectively. PCR products were then fused together using SOEing PCR with primers phaB1_Sac_UP_F and phaB1_Pac_DN_R. The fusion PCR product was cloned into pLO3 using restriction sites SacI and PacI.

pJLG452: homology arms upstream and downstream of *iclA* were amplified with iclA_Sac_UP_F, iclA_OVL_R and iclA_OVL_F, iclA_Pac_DN_R, respectively. PCR products were then fused together using SOEing PCR with primers iclA_Sac_UP_F and iclA_Pac_DN_R. The fusion PCR product was cloned into pLO3 using restriction sites SacI and PacI.

pJLG453: homology arms upstream and downstream of *iclB* were amplified with iclB_Sac_UP_F, iclB_OVL_R and iclB_OVL_F, iclB_Pac_DN_R, respectively. PCR products were then fused together using SOEing PCR with primers iclB_Sac_UP_F and iclB_Pac_DN_R. The fusion PCR product was cloned into pLO3 using restriction sites SacI and PacI.

pJLG454: homology arms upstream of *sucC* and downstream of *sucD* were amplified with sucC_Sac_UP_F, sucC_OVL_R and sucD_OVL_F, sucD_Pac_DN_R, respectively. PCR products were then fused together using SOEing PCR with primers sucC_Sac_UP_F and sucD_Pac_DN_R. The fusion PCR product was cloned into pLO3 using restriction sites SacI and PacI.

4.2.5 Bacterial strains used in this study

All bacterial strains used in this study are listed in Table 4.3.

Table 4.3. Bacterial strains used in this study. *P* denotes P_{araBAD} promoter with square brackets showing genes under promoter control. Km^R: kanamycin resistance. Gen^R: gentamicin resistance.

Strain	**Genotype**	**Parent strain**	**Plasmid**	**Source**
E. coli MG1655	F- , λ-, *rph*-1	-	-	ATCC 70096
E. coli DH5α	*lacZ*ΔM15, *rec*A1, *end*A1	-	-	Invitrogen
E.coli S17-1	λpir/pLFX	-	-	ATCC 47055
P. putida KT2440	wild type			ATCC 47054
C. necator H16	wild type, Gen^R	-	-	DSM-428
C. necator H16 *ΔphaC1*	*ΔphaC1*	-	-	(Arenas Lopez, 2018)
C. necator H16 *ΔphaC1B1*	*ΔphaC1*, *ΔphaB1*	-	-	This work
C. necator H16 Δ2	*ΔphaC1*, *ΔiclAB*	-	-	This work
C. necator H16 Δ3	*ΔphaC1*, *ΔsucCD*	-	-	This work
C. necator H16 Δ4	*ΔphaC1*, *ΔiclAB*, *ΔsucCD*	-	-	This work
MG-p411	MG1655, (*P[bld yqhD$_{Ec}$ phaA phaB1] Km^R*)	*E. coli* MG1655	pJLG411	This work
MG-p438	MG1655, (*P[bld PA1127 phaA phaB1] Km^R*)	*E. coli* MG1655	pJLG438	This work
H16ΔC-pU	H16*ΔphaC1*, *(Km^R)*	*C. necator* H16 *ΔphaC1*	pBBR1-USER	This work
H16ΔC-p402	H16*ΔphaC1*, (*P[bld yqhD$_{Ec}$] Km^R)*	*C. necator* H16 *ΔphaC1*	pJLG402	This work
H16ΔC-p415	H16*ΔphaC1*, (*P[bld yqhD$_{Pp}$] Km^R)*	*C. necator* H16 *ΔphaC1*	pJLG415	This work
H16ΔC-p420	H16*ΔphaC1*, (*P[bld PA1127] Km^R)*	*C. necator* H16 *ΔphaC1*	pJLG420	This work
H16ΔC-p426	H16*ΔphaC1*, (*P[bld adhE2] Km^R)*	*C. necator* H16 *ΔphaC1*	pJLG426	This work
H16ΔC-p444	H16*ΔphaC1*, (*P[bld yqhD$_{Ec}$ dra pdc] Km^R)*	*C. necator* H16 *ΔphaC1*	pJLG444	This work

H16ΔC-p446	H16*ΔphaC1*, (*P[yqhD$_{Ec}$ dra pdc] Km^R)*	*C. necator* H16 *ΔphaC1*	pJLG446	This work
H16ΔCB-p414	H16*ΔphaC1*, (*P[bld] Km^R)*	*C. necator* H16 *ΔphaC1*	pJLG414	This work
H16ΔCB-p402	H16*ΔphaC1*, (*P[bld yqhD$_{Ec}$] Km^R)*	*C. necator* H16 *ΔphaC1*	pJL402	This work
H16ΔCB-p447	H16*ΔphaC1*, (*P[bld yqhD$_{Ec}$ phaB1] Km^R)*	*C. necator* H16 *ΔphaC1*	pJL447	This work
H16Δ2-p402	H16*ΔphaC1ΔiclAB,* (*P[bld yqhD$_{Ec}$] Km^R*)	*C. necator* H16 Δ2	pJLG402	This work
H16Δ3-p402	H16*ΔphaC1ΔsucCD,* (*P[bld yqhD$_{Ec}$] Km^R*)	*C. necator* H16 Δ3	pJLG402	This work
H16Δ4-p402	H16*ΔphaC1ΔiclABΔsuc CD,* (*P[bld yqhD$_{Ec}$] Km^R*)	*C. necator* H16 Δ4	pJLG402	This work

4.2.6 Two-stage batch fermentation in shake-flasks

A two-stage batch fermentation in shake-flasks was employed for production of 1,3-butanediol in *E. coli* or *C. necator*. Biomass and synthetic pathway related proteins were generated by growing cells in rich media (LB) before transferring them to nutrient limited minimal media with excess carbon. 50 µg/mL or 300 µg/mL kanamycin was used throughout for *E. coli* or *C. necator*, respectively. Freshly transformed cells from single colonies were inoculated in 5 mL of LB medium and incubated for 18 h at 30°C and 200 rpm. Subsequently, cultures of *E. coli* or *C. necator* strains were re-suspended to an OD_{600} of 0.1 or 0.2 in 50 mL LB supplemented with 0.2 % (w/v) glucose or 0.2 % (w/v) sodium gluconate, respectively. The cultures were grown in 250 mL baffled shake-flasks at 30 °C and 200 rpm. At an OD_{600} of 0.6–0.8, 0.25 % (w/v) L-arabinose was added, and cultures were allowed to grow further for 4–6 h enabling heterologous gene expression. Then, *E. coli* cells were harvested by centrifugation (1700 × *g* for 6 min), re-suspended in 25 mL M9 MM supplemented with 3 % (w/v) glucose, 1 µg/mL thiamine and 20 µg/mL uracil (Jensen, 1993) to an OD_{600} of 10 and incubated in 250

mL baffled shake-flasks at 30 °C with 200 rpm shaking. Whereas *C. necator* cells were harvested by centrifugation for 10 min at 6600 × *g*, re-suspended in 25 mL MM (excluding NH_4Cl) supplemented with 2 % (w/v) sodium gluconate to an OD_{600} of 7 and incubated in 250 mL baffled shake-flasks at 30 °C with 200 rpm shaking. Samples of 0.5 mL were taken immediately, 12 and 48 h after L-arabinose supplementation, centrifuged for 5 min at 17000 × *g*, and the cell-free supernatant was subjected to HPLC-UV/RI analysis.

4.2.7 *C. necator* H16 chromosomal gene mutations

Gene deletions were performed using the pLO3 suicide vector exhibiting selection through tetracycline resistance (*tetR*) and counter-selection in the presence of sucrose (*sacB*). Chromosomal gene deletion was introduced by preserving start and stop codons of the gene. Where endogenous genes were replaced by introducing exogenous genes under control of the araC/P_{araBAD} inducible system, to eliminate potential transcriptional read-through, *rrnB* T_2 and *rrnB* T_1 terminators were incorporated upstream and downstream to the heterologous DNA region, respectively.

pLO3 suicide vector-based plasmids were transformed into *E. coli* strain S17-1 suitable for conjugative plasmid transfer to *C. necator* H16. *E. coli* and *C. necator* strains were cultivated overnight in LB supplemented with 15 µg/mL tetracycline and 10 µg/mL gentamicin, respectively. Cells were harvested by centrifugation (5000 × *g* for 10 mins) and washed before mating on LB-agar plate for 6 h at 30 °C. *C. necator* H16 transconjugants were isolated by plating onto LB-agar plates supplemented with 10 µg/mL gentamicin and 10 µg/mL tetracycline. Single colonies were then purified by re-streaking twice onto identical agar plates. Single colonies were used to inoculate 5

mL LB media in 50 mL falcon tube supplemented with 10 µg/mL gentamicin and 10 µg/mL tetracycline and incubated overnight at 30 °C with 200 rpm shaking. Cultures were then used to inoculate 5 mL low sodium-LB (2.5 g/L NaCl) supplemented with 15 % (w/v) sucrose incubated overnight at 30 °C with 200 rpm shaking. Cells were then plated onto low sodium-LB-agar plates supplemented with 15 % (w/v) sucrose and incubated at 30 °C until single colonies appeared, typically 48 – 72 h. Single-colonies were then streaked onto LB-agar plates containing no antibiotic or with antibiotic (15 µg/mL tetracycline) to establish loss of integrated chromosomal pLO3 DNA. Cells were then screened with PCR for successful mutation.

4.2.8 Protein analysis using SDS-PAGE

Relative protein concentration was analysed through SDS-PAGE protein separation. Single colonies of *C. necator* strains recovered from cryopreservation on LB agar plates supplemented with were used to inoculate duplicate 3 mL NLMM in falcon tubes supplemented with 2 % (w/v) sodium gluconate and 300 µg/mL kanamycin. Cells cultivated overnight were re-suspended in 10 mL fresh media with identical composition to an OD_{600} of 0.1. After further incubation for 4 h at 30 °C with 200 rpm shaking, gene expression was induced by addition of L-arabinose to a final concentration of 0.01 % (w/v). Samples that were not induced received no addition of L-arabinose. Cells were harvested by centrifugation (14,000 × *g* for 10 mins) after 24 h in identical cultivation conditions and supernatant discarded. Protein was then extracted from harvested cells using BugBuster Master Mix (Novagen, affiliate of Merck KGaA, Dramstadt, Germany) according to manufacturer's protocols. For analysis of soluble protein fraction, samples were combined with NuPAGE™ LDS Sample Buffer (Thermo Fisher Scientific, Waltham, MA, USA) and loaded on to

NuPAGE™ 4 – 12 %, Bis-Tris Protein Gel (Thermo Fisher Scientific, Waltham, MA, USA). PageRuler™ Prestained Protein Ladder purchased from Thermo Fisher Scientific (Waltham, MA, USA) was used to estimate protein size. Protein was separated by subjecting prepared gel in NuPAGE™ MES Running Buffer (Thermo Fisher Scientific, Waltham, MA, USA) to electrical current using XCell *SureLock*™ Mini-Cell (Thermo Fisher Scientific, Waltham, MA, USA) electrophoresis system with a PowerPac™ Universal Power Supply (Bio-Rad) at 150 V. Separated protein was then visualised with Bio-Rad Molecular Imager GelDoc XR+ Imaging System running Image Lab™ software (Bio-Rad, CA, USA) after protein staining with SimplyBlue™ SafeStain (Thermo Fisher Scientific, Waltham, MA, USA) used according to manufacturer's protocols. The protein sizes for analysed genes were obtained from UniProt using accession/locus tags stated in section 4.2.1.

4.3 Results

4.3.1 Identification of potential (*R*)-1,3-butanediol biosynthetic pathways

In order to metabolically engineer *C. necator* H16 for (*R*)-1,3-BDO production, two alternative heterologous biosynthetic pathways were considered: A) utilising (*R*)-3-hydroxybutyryl-CoA ((*R*)-3HBCoA) as a precursor and requiring two heterologous enzymatic reactions: (i) deacylation of (*R*)-3HBCoA to (*R*)-3-hydroxybutanal ((*R*)-3HBA) by butanal dehydrogenase (CoA-acylating, NADH-dependent) (Bld, EC 1.2.1.57), and (ii) reduction of (*R*)-3HBA into (*R*)-1,3-BDO by NADPH-dependent aldehyde reductase activity (YqhD, EC 1.1.1.2); B) utilising pyruvate and requiring three heterologous enzymatic reactions: (i) decarboxylation of pyruvate to acetaldehyde by pyruvate decarboxylase (PDC, EC 4.1.1.1), (ii) condensation of two acetaldehyde

molecules to (*R*)-3HBA by deoxyribose-5-phosphate aldolase (Dra/DeoC, EC 4.1.2.4); and (iii) reduction of (*R*)-3HBA into (*R*)-1,3-BDO by NADPH-dependent aldehyde reductase (Figure 4.1). Evidently, same enzymatic activity can be utilised for the final conversion of (*R*)-3HBA to (*R*)-1,3-BDO in both pathways.

Previous research has shown key TCA cycle genes (*fumA, mdh1*) are downregulated when *C. necator* cells transition from exponential to stationary growth phase, alongside the upregulation of P3HB required genes *phaAB* (Peplinski *et al.*, 2010). As one of the cells key nutrients is depleted and biomass production becomes restricted, storing carbon in the form of P3HB is triggered in *C. necator* H16 resulting in increased carbon flux towards (*R*)-3HBCoA aided by β-ketothiolase and NADPH-dependent acetoacetyl-CoA reductase activity. Whereas the deletion of Δ*phaC1* results in almost complete abolishment of poly(3-hydroxyalkanoate) polymerase activity and subsequent accumulation of (*R*)-3-HBA becoming available for biosynthesis of (*R*)-1,3-BDO.

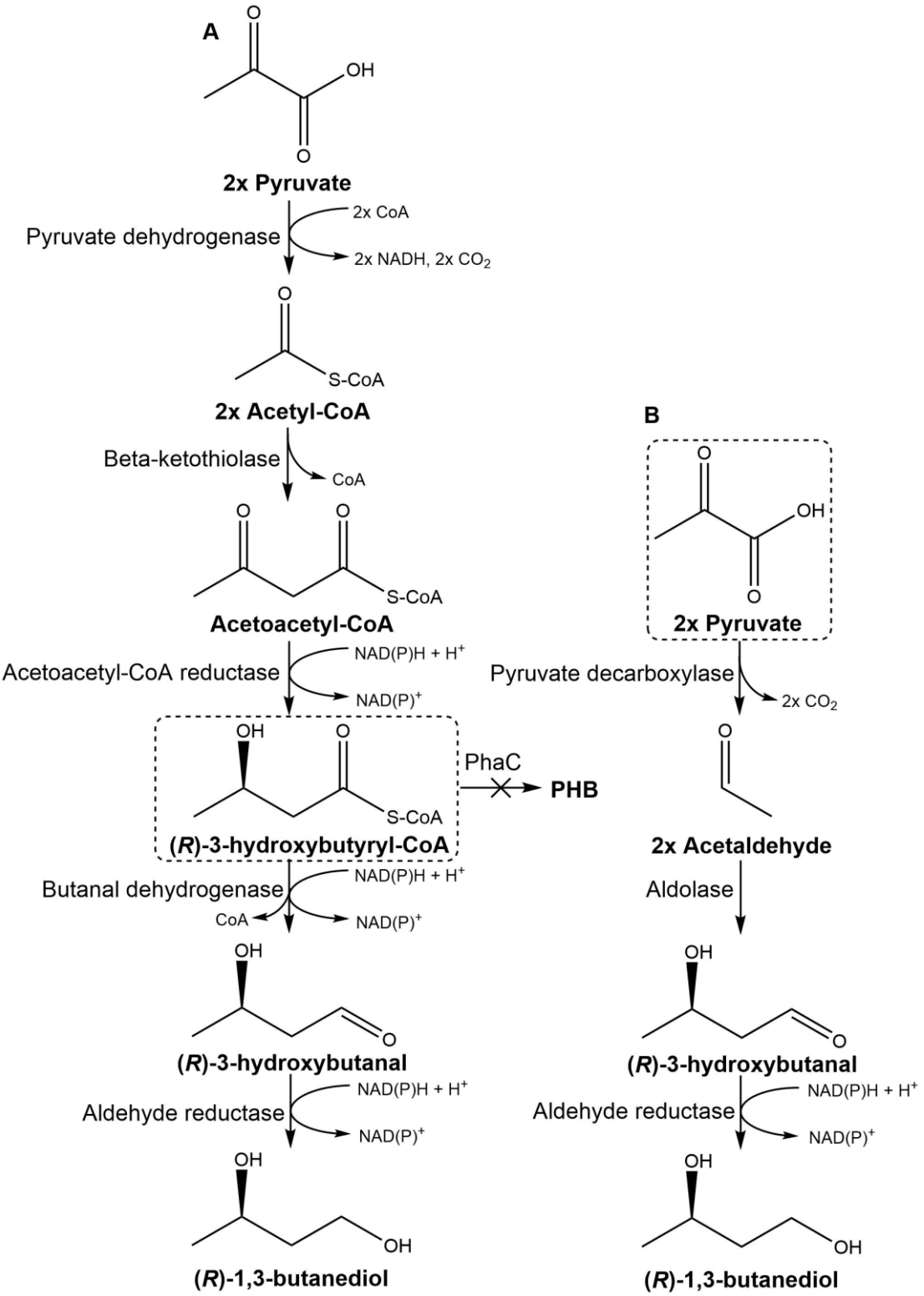

Figure 4.1. Alternative biosynthetic pathways for (*R*)-1,3-BDO production in *C. necator* H16. Required precursors (*R*)-3HBCoA (A) and pyruvate (B) are highlighted with dashed lines.

4.3.2 Screening genes for (*R*)-3HBCoA-dependent (*R*)-1,3-BDO biosynthetic pathway

To enable screening of many enzymes, a modular vector was designed and constructed with restriction sites placed strategically allowing a rapid replacement of genes by using conventional restriction-ligation methods (Figure 4.2). Medium strength ribosomal binding sites RBS1 and RBS2 (Alagesan *et al.*, 2018) were utilised to control enzyme biosynthesis from first and second heterologous genes, respectively. The *C. saccharoperbutylacetonicum* native gene *bld* possessing a very low GC content of 32.8 % was codon optimised for expression in *C. necator* H16 (66.3 % average GC content).

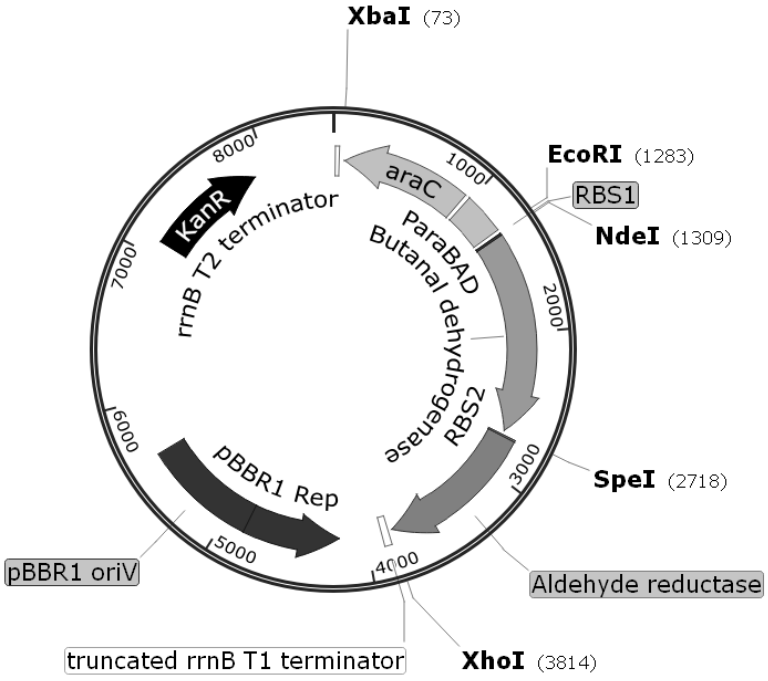

Figure 4.2. Representation of plasmid employed for (*R*)-1,3-BDO biosynthesis. Modular components *araC*/P_{araBAD}, RBS1 upstream of DNA encoding butanal dehydrogenase, RBS2 upstream of aldehyde reductase and strategically placed unique restriction enzyme recognition sites flanked by *rrnB* T_2 and truncated *rrnB* T_1 transcription termination sites, respectively. Other crucial plasmid components to ensure functionality within *C. necator* strains are the

pBBR1 origin of replication and gene facilitating kanamycin resistance (Kan^R cassette). Plasmid map visualised with SnapGene® Viewer.

Several genes encoding for alcohol dehydrogenase/aldehyde reductase enzymatic activity were screened in combination with butanal dehydrogenase (*bld*) for expression in *C. necator* H16

Table 4.4). Further to this, the widely utilised *yqhD* (b3011) gene was combined with two *eutE* (aldehyde dehydrogenase) genes for comparison with *bld* functionality. Candidates were selected due to functionality observed for similar compounds reported in the literature, such as the conversion of 4-hydroxybutyraldehyde to 1,4-butanediol (Wang *et al.*, 2017), acetoin to 2,3-butanediol (Yan, Lee and Liao, 2009) or already reported conversion of 3-hydroxybutanal to 1,3-butanediol in *E. coli* chassis (Nemr *et al.*, 2018).

(*R*)-1,3-BDO production was observed in *C. necator* H16 strains transformed with pJLG402 and pJLG415 both expressing *bld* and *yqhD*, with the latter from either *E. coli* MG1655 (hereafter denoted as $yqhD_{Ec}$; b3011) or *Pseudomonas putida* KT2440 ($yqhD_{Pp}$; PP_2492), both encoding an NADPH-dependent aldehyde reductase. *C. necator* H16 transformed with pJLG426 containing bi-functional *adhE2* from *Clostridium acetobutylicum* also produced (*R*)-1,3-BDO, as previously reported (Kataoka *et al.*, 2013). No 1,3-BDO production was detectable by HPLC-RI with strains transformed with plasmids containing other potential aldehyde reductases.

It should be noted that all constructs were tested in *C. necator* H16 wild-type (data not shown) and P3HB deficient (Δ*phaC*) mutant (hereafter denoted H16ΔC). (*R*)-1,3-BDO production was observed only in the P3HB minus strains H16ΔC-p402, H16ΔC-p415 and H16ΔC-p426., demonstrating improvement of carbon flux directed towards the diol.

Table 4.4. Constructs screened in *C. necator* H16 Δ*phaC* for (*R*)-1,3-BDO production. Cells were cultivated in 10 mL 2 % (w/v) sodium gluconate NLMM. Samples were taken 70 h after induction of gene expression by addition of L-arabinose to a final concentration of 0.1 % (w/v). * denotes codon optimised gene. N.D. denotes no 1,3-BDO detected by HPLC analysis.

Construct	Heterologous Enzyme(s)	1,3-butanediol (mM)
pJLG401	*adhE** (CA_P0162)	N.D.
pJLG402	*bld** (AAP42563) + *yqhD* (b3011)	0.237
pJLG403	*bld** (AAP42563) + *adh** (WP_077844196)	N.D.
pJLG404	*bld** (AAP42563) + *gbD* (H16_RS07715)	N.D.
pJLG405	*bld** (AAP42563) + *hibadh* (H16_RS24705)	N.D.
pJLG415	*bld** (AAP42563) + *yqhD* (PP_2492)	0.118
pJLG416	*bld** (AAP42563) + *yvgN* (BSU33400)	N.D.
pJLG417	*bld** (AAP42563) + *yhdN* (BSU09530)	N.D.
pJLG418	*bld** (AAP42563) + *ydjG* (b1771)	N.D.
pJLG419	*bld** (AAP42563) + *gpr* (b3001)	N.D.
pJLG420	*bld** (AAP42563) + PA_1127	N.D.
pJLG421	*bld** (AAP42563) + BMD_1654	N.D.
pJLG422	*bld** (AAP42563) + BMD_2640	N.D.
pJLG423	*eutE* (BMD_3362) + *yqhD* (b3011)	N.D.
pJLG424	*eutE* (b2455) + *yqhD* (b3011)	N.D.
pJLG425	*adhE* (b1241)	N.D.
pJLG426	*adhE2* (CA_P0035)	0.255

4.3.3 Evaluation of nitrogen-limiting and induced gene expression conditions for (*R*)-1,3-BDO biosynthesis

4.3.3.1 Effect of nitrogen limitation on (R)-1,3-BDO production

Previous research has shown that P3HB synthesis in *C. necator* H16 is increased under nitrogen limiting conditions with excess carbon available (Raberg *et al.*, 2008). To investigate the effect of nitrogen limitation effect (*R*)-1,3-BDO production, the H16ΔC-p402 strain was grown in minimal medium with carbon to nitrogen ratio of 6 and nitrogen-limited minimal medium (C:N = 50). Despite decrease in growth rate, more than 2-fold higher yield of (*R*)-1,3-BDO was observed under nitrogen-limiting condition (Figure 4.3). Furthermore, (*R*)-1,3-BDO yield of 0.018 Cmol $Cmol^{-1}$ was measured 24 h after induction under nitrogen limitation, whereas in non-nitrogen-limiting condition (*R*)-1,3-BDO became detectable only after 48 h. These results demonstrate that increased carbon availability for (*R*)-1,3-BDO biosynthesis in *C. necator* H16 P3HB negative strain caused by limiting nitrogen and therefore biomass.

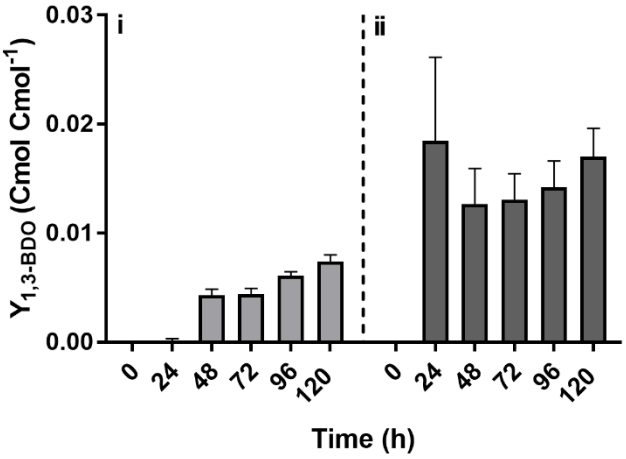

Figure 4.3. Cultivation of strain H16ΔC-p402 in minimal media with different carbon to nitrogen ratios. Conditions: i. 2 % (w/v) sodium gluconate, 5 g/L NH_3Cl (non-nitrogen

limiting), ii. 2 % (w/v) sodium gluconate, 0.6 g/L NH_3Cl (nitrogen limiting). All other minimal media components remained at identical concentrations. Cells were cultivated in 25 mL minimal media in 250 mL baffled shake-flasks in the presence of 0.01 % (w/v) arabinose. Error bars represent standard error from 3 biological replicates.

4.3.3.2 The effect of L-arabinose concentration on cell growth and (R)-1,3-BDO production

The AraC/P_{araBAD}-arabinose inducible system is relatively well repressed in uninduced state, can be fine-tuned in the range from 0.00117 to 0.15 % (w/v) of L-arabinose and allows to achieve more than 1000-fold induction in *C. necator* H16 (Alagesan et al 2018). Importantly, the monosaccharide L-arabinose is not metabolised by this bacterum. Therefore, AraC/P_{araBAD} inducible system was selected to drive overexpression of (*R*)-1,3-BDO biosynthesis genes.

To evaluate the effect of L-arabinose on cell growth and (*R*)-1,3-BDO bio-production, H16ΔC-p402 cells were grown in MM and expression of *bld* and *yqhD*$_{Ec}$ was induced by addition of L-arabinose to a final concentration of 0.005, 0.01, 0.045, 0.1 and 0.2 % (w/v) (Figure 4.4). In the first 24 h after induction, the biosynthesis levels of (*R*)-1,3-BDO correlate directly with concentration of inducer, showing the highest quantity of (*R*)-1,3-BDO synthesized by the cell culture supplemented with 0.2% of L-arabinose. However, at the later stages, a strong growth inhibition is observed in the presence of 0.045 % and higher concentrations of L-arabinose. Unsurprisingly, (*R*)-1,3-BDO when normalised to OD_{600} production is reduced at the inducer concentrations of 0.1 and 0.2 % (w/v). Further to this, the cell growth is little affected by inducer concentrations at the lower range, suggesting that 0.01 and 0.045 % of L-arabinose to be optimal for (*R*)-

1,3-BDO biosynthetic gene expression when plasmid-based system is utilized in *C. necator* H16.

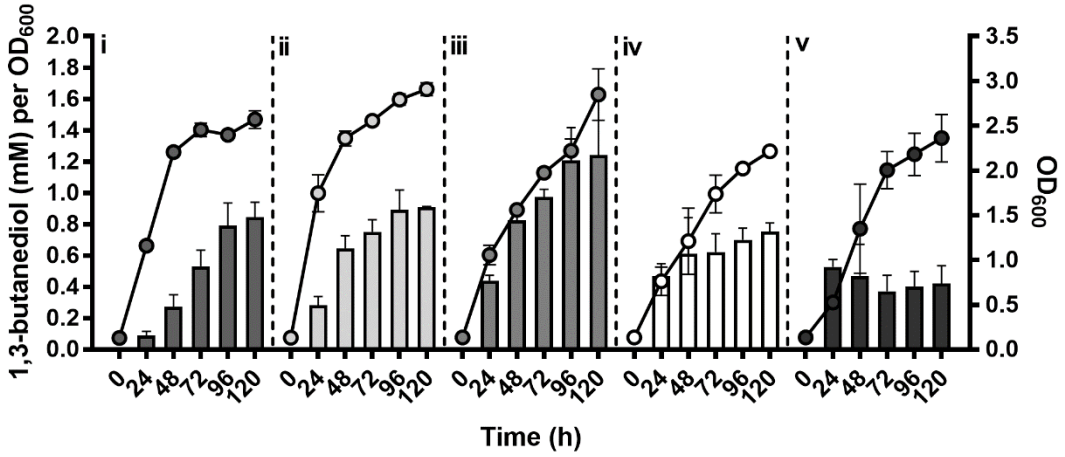

Figure 4.4. 1,3-butanediol production normalised to OD_{600} (bars) and OD_{600} (circles) by strain H16ΔC-p402 cultivated in the presence of i. 0.005, ii. 0.01, iii. 0.045, iv. 0.1 and v. 0.2 % (w/v) arabinose. Cells were grown in 25 mL 2 % (w/v) sodium gluconate NLMM in 250 mL baffled shake flasks. Error bars represent standard error calculated from biological duplicates.

4.3.4 Comparison of (*R*)-1,3-BDO-producing strains

Next, (*R*)-1,3-BDO-producing *C. necator* strains H16ΔC-p402, H16ΔC-p415 and H16ΔC-p426 were compared under heterotrophic nitrogen-limited growth conditions (Figure 4.5). Carbon yields of (*R*)-1,3-BDO were steady for the duration of 96-hours cell growth period ranging from 0.035 to 0.055 Cmol $Cmol^{-1}$, and comparable between all three strains. Carbon flux towards biomass and 1,3-BDO production – aided by the use of nitrogen-limiting condition is greatest during initial cell growth (0 - 48 h) with a highest yield of 0.055 ± 0.003 Cmol $Cmol^{-1}$ achieved between 0 and 24 h by strain H16ΔC-p402. As cells enter stationary phase (48 – 96 h) essential media components are depleted with remaining gluconate continuing to be converted into (*R*)-1,3-BDO, achieving a yield of 0.061 ± 0.030 Cmol $Cmol^{-1}$ between 72 and 96 h for strain H16ΔC-

p402. It can be concluded that of three strains possessing alternative gene combinations of (*R*)-3HBCoA-dependent pathway, the strain H16ΔC-p402 containing *bld* and $yqhD_{Ec}$ performed marginally better producing highest yields of (*R*)-1,3-BDO during early logarithmic and stationary growth periods, while exhibiting the least growth impairment. Therefore, the combination of genes *bld* and $yqhD_{Ec}$ were chosen to be utilized for (*R*)-3HBCoA-dependent biosynthetic pathway in next stages of this study.

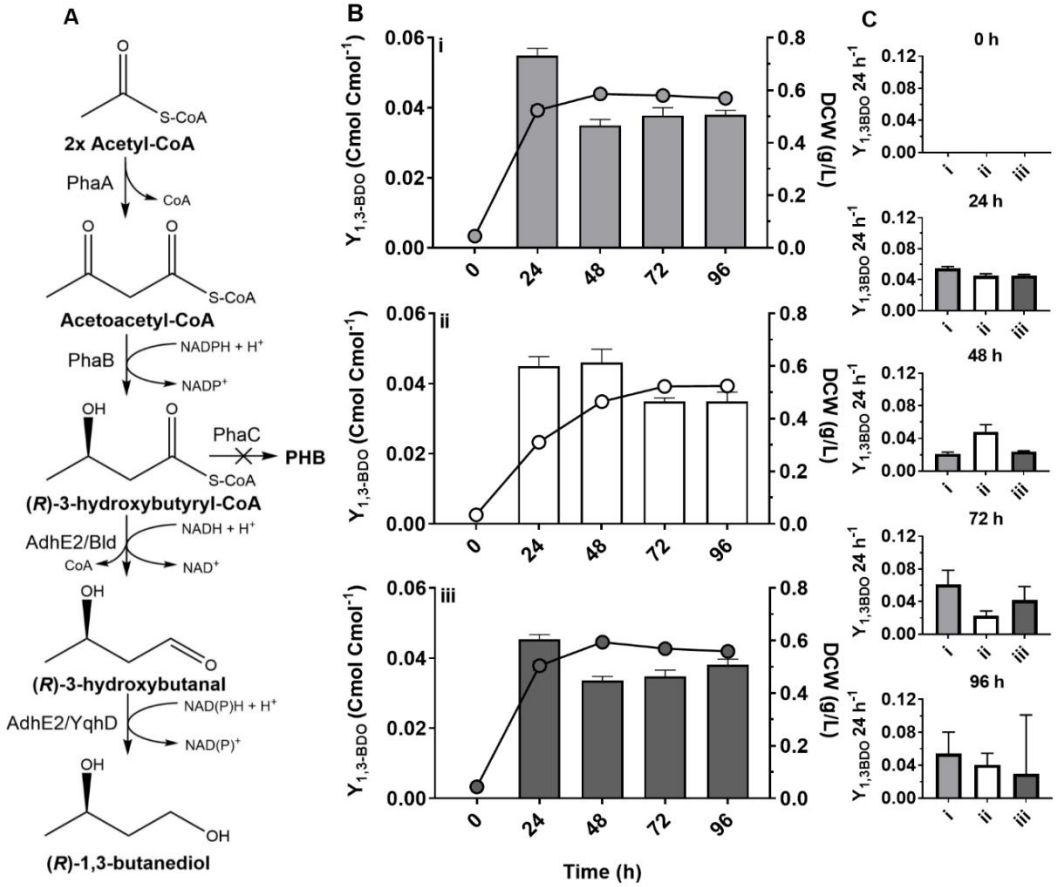

Figure 4.5. Comparison of (*R*)-1,3-BDO yields in *C. necator* expressing alternative genes of (*R*)-3HBCoA-dependent pathway. (A) The endogenous β-ketothiolase (PhaA) and NADPH-dependent acetoacetyl-CoA reductase (PhaB) provides (*R*)-3HBCoA, a precursor metabolite, which is converted by AdhE2 or combination of Bld and YqhD into (*R*)-1,3-BDO. The *phaC1* encoding a poly(3-hydroxyalkanoate) polymerase (PhaC) for P3HB synthesis is

chromosomally deleted to re-direct metabolic flux towards. (*R*)-1,3-BDO. (B) Carbon yield of (*R*)-1,3-BDO (bars) and dry cell weight (circles) in *C. necator* strains i. H16ΔC-p402, ii. H16ΔC-p415 and iii. H16ΔC-p426 (iii) 0, 24, 48, 72 and 96 h after the induction of heterologous gene expression induced with 0.01 % (w/v) L-arabinose. Yields calculated from time-point 0 (C) Carbon yield of (*R*)-1,3-BDO within specific 24 h time periods. Yields calculated from the previous time-point. Cells were grown in 2 % (w/v) sodium gluconate NLMM using 250 mL baffled shake flasks. Error bars represent standard error calculated from three biological replicates.

4.3.5 Identifying unknown metabolic by-product of the (*R*)-3HBCoA-dependent pathway

Alongside (*R*)-1,3-BDO, the 4-hydroxy-2-butanone (4H2B) was observed as a by-product in *C. necator* strains harbouring plasmids with (*R*)-3HBCoA-dependent pathway genes. Cell culture supernatant from previous experiments were compared to a 4H2B standard using HPLC as stated in Materials and Methods. Corresponding peaks for both standard and sample were observed in the RI channel and UV channel at wavelength 280 nm (Supplementary Figure 5, Supplementary Figure 6). It was hypothesized that Bld is able to acylate acetoacetyl-CoA, with unspecific functionality of Bld being previously reported demonstrating CoA-acylating capability in the biosynthesis of (*R*)-1,3-pentanediol, (*R*)-1,2,4-butanetriol and 4-methyl-(*R*)-1,3-pentanediol (Kataoka *et al.*, 2017). Acetyl-CoA produced by β-ketothiolase homologue enzymes (PhaA, BktB) present in the *C. necator* genome (Lindenkamp, Volodina and Steinbüchel, 2012) is then converted into 3-oxobutanal by Bld, which is then transformed into 4H2B by promiscuous $YqhD_{Ec}$ activity (Figure 4.7.A).

Before the hypothesised biosynthesis pathway for 4H2B could be tested, a *C. necator* H16 strain with no *phaC1* and *phaB1* gene functionality was required. Deletion of gene encoding PhaB1, responsible for conversion of acetoacetyl-CoA to (*R*)-3HBCoA will increase acetoacetyl-CoA availability for Bld. *C. necator* H16 gene deletion was achieved through an allelic exchange method employing pLO3 plasmid as suicide vector, as detailed in Materials and Methods. Schematic of method is shown in Figure 4.6. Oligonucleotide primers were designed to amplify homology arms upstream and downstream of targeted gene *phaB1*. Amplified homology arms were joined using overlap extension PCR technique, and subsequently cloned into pLO3 vector using traditional restriction ligation techniques. Gene deletion construct was then transformed into *E. coli* S-17 donor strain for conjugation with *C. necator* strain enabled by RP4 origin of transfer. Transconjugant strains were selected for using agar plated supplemented with 10 µg/mL tetracycline and 10 µg/mL gentamicin. Capitalising on *C. necator* H16 native resistance to gentamicin (Brigham *et al.*, 2010) ensured no contamination with *E. coli* donor strain, susceptible to gentamicin antibiotic. It should be noted *C. necator* strains grew much slower in presence of two antibiotics, with single colonies large enough for further testing taking at least 72, over 24 h longer than when cultivated in the presence of single antibiotic. Due to lack of functionality of pBBR32 origin of replication of in *C. necator* strains, tetracycline resistance will only be conferred by cells with successful first crossover. To complete gene deletion and remove pLO3 backbone from chromosome, secondary crossover step is executed. Cells are cultivated in presence of sucrose where *sacB*, encoding levansucrase enzyme, is used as counter-selection tool (Reyrat *et al.*, 1998). Viable cells are then screened for tetracycline resistance and those with no resistance are deemed to have lost pLO3 backbone. Mutations are then confirmed through PCR, with oligonucleotide primers

designed to amplify mutated section ± 100 bp upstream and downstream of targeted deletion, as well as small region (~500 bp) within targeted gene, ensuring no recombination of gene elsewhere in the chromosome.

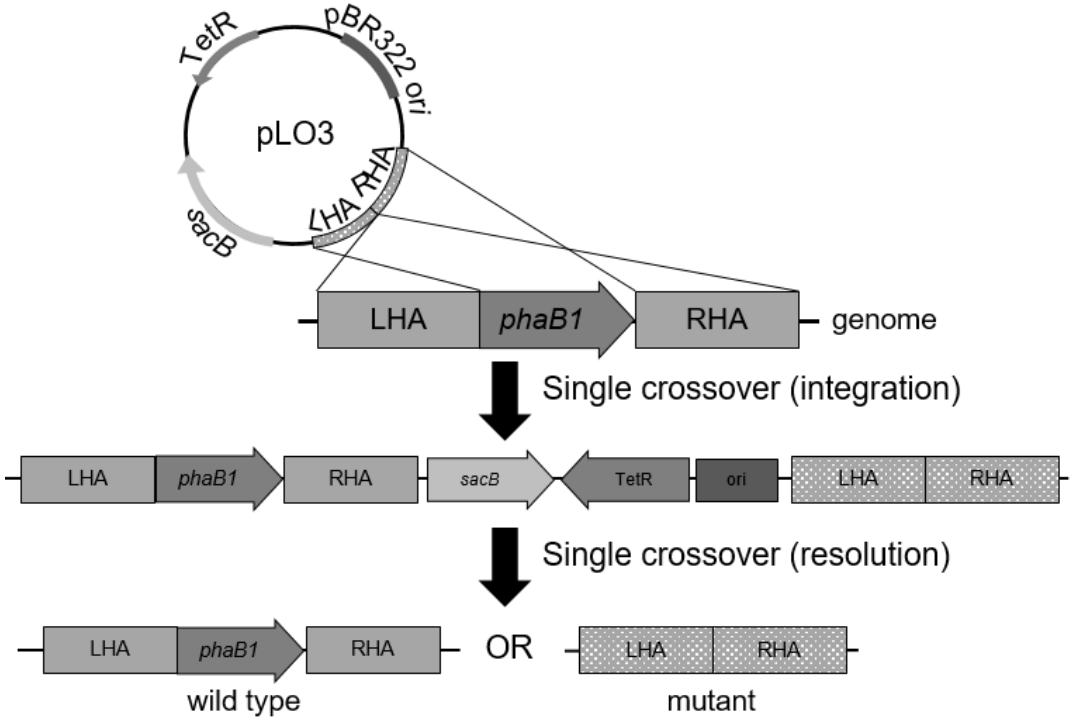

Figure 4.6. Schematic of method used for *C. necator* H16 chromosomal manipulations. Homology arms upstream (left homology arm; LHA) and downstream (right homology arm; RHA) or target manipulation site were amplified through PCR and spliced through overlap extension PCR. Spliced homology arm fragment was cloned into the pLO3 suicide vector containing *sacB* marker and tetracycline resistance (Tet^R) cassette and pBBR32 origin of replication which is non-functional in *C. necator* H16. During first stage, pLO3 backbone is integrated into chromosome through allelic exchange of left or right homology arm, conferring resistance to antibiotic tetracycline. Successfully integrated *C. necator* cells are screened for by cultivating cells on LB agar media containing tetracycline and gentamicin. The donor strain *E. coli* S-17 is unable to grow in presence of gentamicin, with no known native resistance. During second single cross over, cells are cultivated in presence of sucrose encouraging loss of pLO3

backbone containing *sacB*. This results in formation of mutant strain, with target DNA/gene removed, or reversion to wild type.

4.3.5.1 Evaluation of 4H2B production in engineered C. necator strains

To confirm 4H2B biosynthesis by *C. necator*, strain Δ*phaC1B1* was transformed either with plasmids pJLG414 containing *bld* (H16ΔCB-p414); pJLG402 with *bld* and $yqhD_{Ec}$ (H16ΔCB-p402) or pJLG447 containing *bld*, $yqhD_{Ec}$ and *phaB1* genes (H16ΔCB-p447). Results in Figure 4.7B show that neither (*R*)-1,3-BDO nor 4H2B are synthesised by H16ΔCB-p414 when $yqhD_{Ec}$ gene is absent. However, both compounds are detectable in cultures of *C. necator* transformed with plasmids containing both *bld* and $yqhD_{Ec}$. Moreover, in the absence of *phaB1* gene (strain H16ΔCB-p402), mostly 4H2B is synthesized, whereas strains H16ΔCB-p447 and H16ΔC-p402, possessing *bld*, $yqhD_{Ec}$ and *phaB1* genes, produce predominantly (*R*)-1,3-BDO. These results confirm that when NADPH-dependent acetoacetyl-CoA reductase activity is reduced by deletion of *phaB1* gene and acetoacetyl-CoA can be subsequently converted into 4H2B by Bld and $YqhD_{Ec}$ activities. Notably, even if *phaB1* gene is absent, a small quantity of (*R*)-1,3-BDO is generated, most likely through the activity of other *C. necator phaB* homologues. When Δ*phaB1* is complemented with plasmid-based *phaB1* (H16ΔCB-p447), biosynthesis of (*R*)-1,3-BDO is recovered, whereas the 4H2B yield is drastically reduced, indicating preference of Bld and $YqhD_{Ec}$ for intended (*R*)-3HBCoA-dependent pathway intermediates.

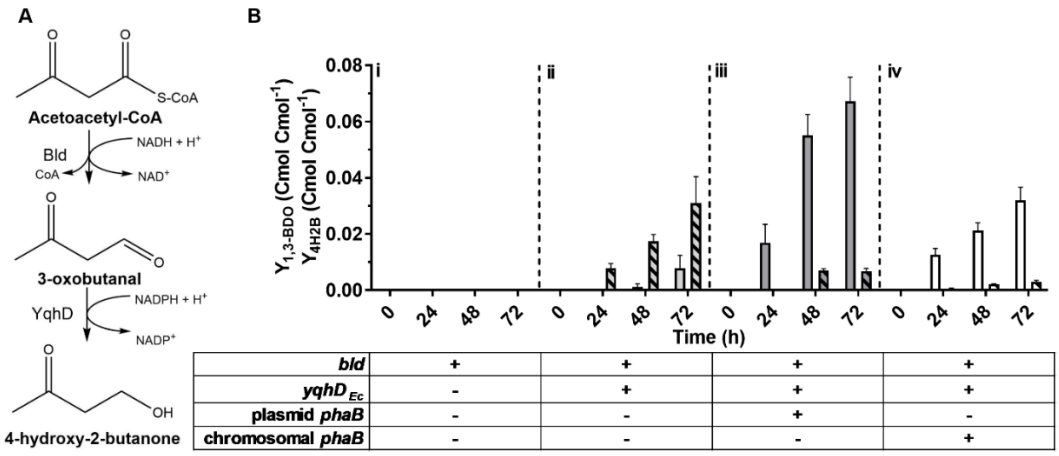

Figure 4.7. 4H2B biosynthesis in C. *necator* utilising acetoacetyl-CoA (A) Endogenous β-ketothiolase PhaA provides Acetoacetyl-CoA for conversion to 3-oxobutanal by heterologous enzyme Bld, exhibiting unspecific acylating properties. 3-oxobutanal is subsequently reduced by $YqhD_{Ec}$ to 4H2B. (B). Batch cultivation of strains i. H16ΔCB-p414, ii. H16ΔCB-p402, iii. H16ΔCB-p447 and iv. H16ΔC-p402 showing (*R*)-1,3BDO carbon yield (solid bars) and 4H2B carbon yield (striped bars). Cells were cultivated in 2 % (w/v) sodium gluconate NLMM using 250 mL baffled shake-flasks, gene expression induced by addition of 0.01 % (w/v) L-arabinose. Error bars represent standard error calculated from biological triplicates.

4.3.6 Investigating aldo-keto reductase suitability for (*R*)-1,3-butanediol biosynthesis in *C. necator* H16

An NADPH-dependent aldo-keto reductase (AKR, *PA1127*) from *Pseudomonas aeruginosa* is reported to have the highest activity for conversion of 3-HBA to 1,3-BDO in *E. coli* (Kim *et al.*, 2017), achieving a yield of 0.075 Cmol $Cmol^{-1}$-glucose (Nemr *et al.*, 2018). To compare efficiency of AKR to synthesize the 1,3-BDO in *E. coli* MG1655 and *C. necator* H16, plasmid constructs containing *PA1127* replacing $yqhD_{Ec}$ were assembled. For *E. coli*, cells harbouring plasmid pJLG438 (MG-p438 containing *PA1127*) or pJLG411 (MG-p411 containing $yqhD_{Ec}$) were cultivated in rich

media supplemented with L-arabinose to a final concentration of 0.25 % (w/v) to induce heterologous gene expression, providing optimal conditions for biomass and protein production. Cells were then re-suspended to a high cell density in minimal media with an abundance of glucose, cultured for 48 h and (*R*)-1,3-BDO cell supernatant samples measured. Similarly, *C. necator* strains harbouring plasmids with either *PA1127* (H16ΔC-p420) or $yqhD_{Ec}$ (H16ΔC-p402), were cultivated in rich media supplemented with 0.25 % (w/v) L-arabinose before re-suspension at a high cell density in minimal media with an abundance of sodium gluconate and without ammonium chloride; limiting cell growth. *E. coli* production of (*R*)-1,3-BDO is highest with strain MG-p438 harbouring plasmid with *PA1127* supporting previous work (Nemr *et al.*, 2018). Whereas *C. necator* strain H16ΔC-p420, expressing *PA1127,* produced significantly less (*R*)-1,3-BDO. Strikingly, two-stage fed-batch fermentation in a 250 mL baffled shake flask achieved (*R*)-1,3-BDO yield of 0.14 Cmol $Cmol^{-1}$ using *C. necator* strain H16ΔC-p402. Similar improvements in production using analogous fermentation approaches have been reported previously for the biosynthesis of reduced chemical compounds (Burg *et al.*, 2016; Kataoka *et al.*, 2013; Nemr *et al.*, 2018). Additionally, overexpression of $yqhD_{Ec}$ has a clear adverse effect on (*R*)-1,3-BDO production in *E. coli* but not in *C. necator*. This is likely due to $YqhD_{Ec}$ acetaldehyde dehydrogenase activity causing accumulation of extracellular acetate (El-Mansi and Holms, 1989; Jarboe, 2011) and potential depletion of NADH.

It should be noted that the induction with 0.25 % (w/v) L-arabinose produced the highest (*R*)-1,3-BDO when compared with 0.01 or 0.05 % (w/v) arabinose, likely due to reduced metabolic burden incurred by the cells when grown in rich medium compared to minimal media screening.

Table 4.5. Production of (*R*)-1,3-BDO via *in vivo* biotransformation of acetyl-CoA by *E. coli* and *C. necator* strains during two-stage batch fermentation. During first stage cells were cultivated in rich media supplemented with glucose or sodium gluconate in the presence of 0.25 % (w/v) L-arabinose. Cells were then washed and re-suspended in 3 % (w/v) glucose M9 minimal media or 2 % (w/v) sodium gluconate minimal media containing no NH_4Cl. During second stage, cells were incubated at 30 °C for 48 h in 25 mL respective media's in 250 mL baffled shake-flasks. Values are averages ± standard error of three biological replicates.

Chassis	**Strain**	**1,3-BDO (mM)**	**$Y_{1,3BDO}$ (g g^{-1})**	**$Y_{1,3BDO}$ (Cmol $Cmol^{-1}$)**	**Y_{4H2B} (Cmol $Cmol^{-1}$)**
***E. coli* MG1655**	MG-p411	1.994 ± 0.504	0.105 ± 0.028	0.035 ± 0.010	N.D.
	MG-p438	8.903 ± 0.239	0.474 ± 0.013	0.087 ± 0.019	N.D.
C. necator* H16 Δ*phaC1	H16ΔC-p402	14.805 ± 0.454	0.888 ± 0.043	0.140 ± 0.002	0.030 ± 0.001
	H16ΔC-p420	5.311 ± 0.289	0.275 ± 0.022	0.048 ± 0.003	0.024 ± 0.001

4.3.7 Increasing acetyl-CoA availability for (*R*)-1,3-BDO biosynthesis

With previous literature detailing improvement of P3HB production as a result of acetyl-CoA accumulation facilitated through gene deletions observed in *E. coli* (Centeno-Leija *et al.*, 2014), *C. necator* genes *sucCD* and *iclAB* were targeted to be deleted individually and in combination to reduce TCA cycle carbon flux, increasing acetyl-CoA pool for (*R*)-1,3-BDO production (Figure 4.8). Strains *C. necator* H16 Δ*phaC*Δ*iclAB* (H16Δ2), *C. necator* H16 Δ*phaC*Δ*sucCD* (H16Δ3) and *C. necator* H16 Δ*phaC*Δ*iclAB*Δ*sucCD* (H16Δ4) were constructed and transformed with pJLG402 for growth profiling in 250 mL baffled shake flasks. The results demonstrate that increased accumulation of extracellular pyruvate concentrations correlate with higher (*R*)-1,3-

BDO yields with strains H16Δ3-p402 and H16Δ4-p402 achieving 0.048 ± 0.002 and 0.047 ± 0.001 Cmol $Cmol^{-1}$ after 72, respectively.

As theorised, deletion of *sucCD* has increased acetyl-CoA pool for 1,3-BDO production with higher titres of (*R*)-1,3-BDO observed, complemented by the acetyl-CoA precursor pyruvate accumulating to greater concentrations and at an increased rate. Despite the loss of ATP generation by the deletion of *sucCD*, all strains exhibited similar specific growth rates with multiple homologues present in *C. necator* demonstrating capabilities of converting succinyl-CoA to succinate and thus non-essential functionality of *sucCD*. Deletion of *iclAB* resulted in no difference in (*R*)-1,3-BDO production as the sole deletion or when combined with *sucCD* gene deletions; *iclAB* has been previously reported to be primarily involved in β-oxidation pathways (Brigham *et al.*, 2010; Sharma *et al.*, 2016) and low relative mRNA levels during heterotrophic growth observed (Alagesan, Minton and Malys, 2017) indicating reduced metabolism of gluconate via the glyoxylate bypass.

However, a large amount of pyruvate is excreted from *C. necator* mutant strains harbouring plasmids with (*R*)-3HBCoA-dependent pathway genes with carbon yield of 0.201 ± 0.061 and 0.309 ± 0.024 (Cmol $Cmol^{-1}$) within the first 24 h after induction for strains H16ΔC-p402 and H16Δ3-p402, respectively. Whereas in cultures of wild type strains transformed with same plasmids pyruvate was completely absent. This indicates that the absence of poly(3-hydroxyalkanoate) polymerase activity in Δ*phaC1* strain causes the build-up of upstream metabolites of the P3HB pathway resulting in accumulation of pyruvate, potentially triggered by increase of the acetyl-CoA pool. Simultaneously, pyruvate accumulation suggests that the (*R*)-3HBCoA-dependent pathway exhibits limited capacity to drive carbon flux towards (*R*)-1,3-BDO. It should

be noted that the accumulation and excretion of pyruvate has been reported previously in *C. necator* H16 PHB^{-}4 (DSM541) and Δ*pdhL* strains (Raberg *et al.*, 2011).

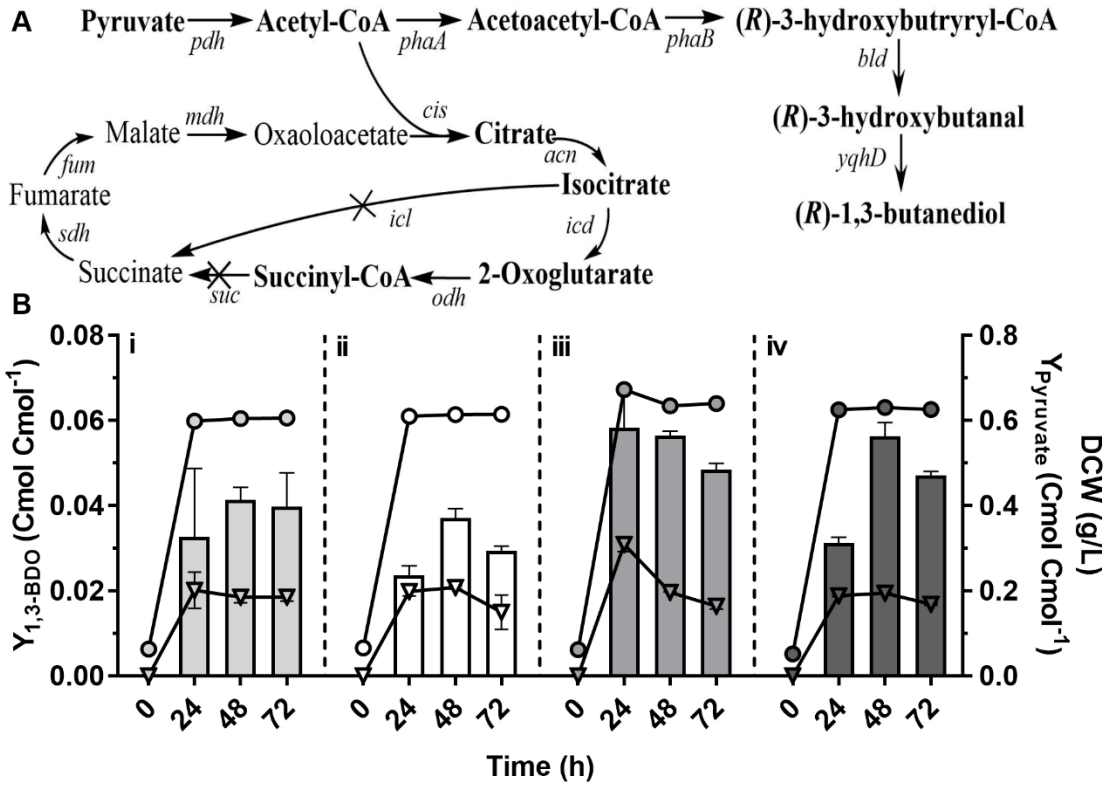

Figure 4.8. (A) Central carbon flux schematic showing gene deletions (Δ*iclAB*, Δ*sucCD*) undertaken to improve acetyl-CoA availability. Central carbon metabolites in bold demonstrate increased pool of succinyl-CoA resulting in inhibited feedback of TCA cycle, increasing availability of acetyl-CoA for (*R*)-1,3-BDO bio-production. (B) Carbon yield of 1,3-butanediol (bars) and pyruvate (upside down triangles) and dry cell weight (circles) for strains i. H16ΔC-p402, ii. H16Δ2-p402, iii. H16Δ3-p402 and iv. H16Δ4-p402. Cells were cultivated in 25 mL 2 % (w/v) sodium gluconate NLMM in 250 mL baffled shake flasks with the addition of L-arabinose to a final concentration of 0.01 % (w/v) to induce gene expression. Error bars represent standard error calculated from at least biological duplicates.

4.3.8 Implementation and characterisation of a second, pyruvate-dependent 1,3-butanediol biosynthetic pathway

To utilise accumulating pyruvate within *C. necator* H16 Δ*phaC1* strains, the previously detailed pyruvate-dependent pathway was investigated for (*R*)-1,3-BDO production. Enzyme $YqhD_{Ec}$ capable for conversion of (*R*)-3-HBA to (*R*)-1,3-BDO was combined with a pyruvate decarboxylase (PDC) sourced from *Zymomonas mobilis* ZM4 and deoxyribose-phosphatase aldolase, Dra sourced from *Bacillus holdurans* (Nemr *et al.*, 2018). The plasmid pJLG446 (containing *yqhD*$_{Ec}$*, dra, pdc*) was transformed into *C. necator* H16 Δ*phaC1* (H16ΔC_p446) to determine (*R*)-1,3-BDO producing capabilities of the pyruvate-dependent pathway (Figure 4.9). No (*R*)-1,3-BDO was detected during HPLC analysis, with plasmid presence confirmed through PCR of cells after cultivation. From metabolite analysis no pyruvate is observed, suggesting efficient conversion to acetaldehyde. However, acetate and ethanol are observed to accumulate, suggesting Dra as a pathway bottleneck. This may be caused by endogenous *C. necator* acetaldehyde dehydrogenase converting acetaldehyde into acetate (Raberg *et al.*, 2011) and YqhD known for high activity for conversion of acetate to ethanol (Jarboe, 2011). Whilst Dra was previously shown to have the highest *in vivo* specific activity of deoxy-ribose phosphatase candidates screened, (*R*)-1,3-BDO yield was seen to improve only when copy number of DERA and AKR enzymes were increased (Nemr *et al.*, 2018).

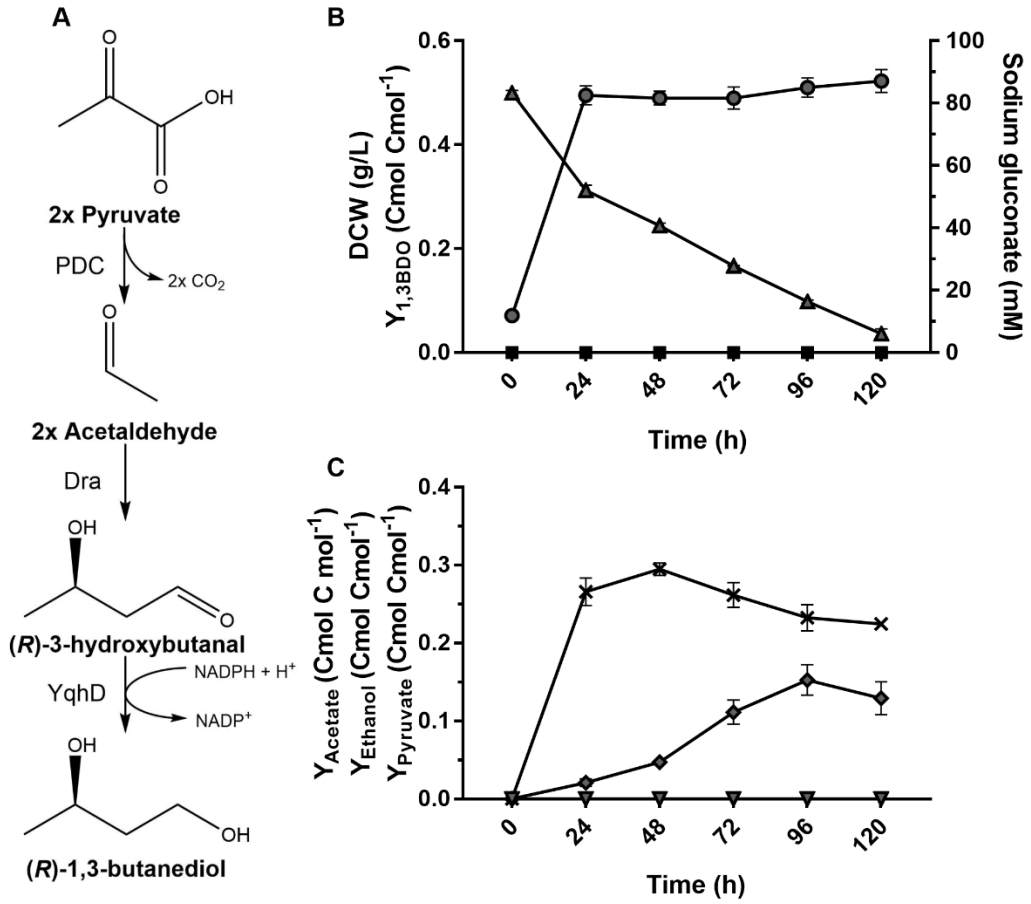

Figure 4.9. (A) Heterologous biosynthetic pathway implemented for production of 1,3-butanediol using pyruvate as a pre-cursor in strain. Data represented in (B) is DCW (circles), 1,3-butanediol carbon yield (squares), sodium gluconate (triangles) and in (C) is pyruvate (upside down triangles), acetate (crosses) and ethanol (diamonds) carbon yields. Strain H16ΔC-p446 was cultivated in 2 % (w/v) sodium gluconate NLMM in 250 mL baffled shake-flasks in the presence of 0.01 % (w/v) L-arabinose. Error bars represent standard error from biological triplicates.

With no observable (*R*)-1,3-BDO by strain harbouring only pyruvate-dependent pathway, it was theorised combining pathways would improve carbon flux towards through both 3-HBCoA and pyruvate pathways. A plasmid harbouring relevant genes *bld*, *yqhD*$_{Ec}$, *dra* and *pdc* (pJLG444) was transformed into *C. necator* H16 Δ*phaC1*

(H16ΔC_p444). This strain was screened in comparison to the control strain H16ΔC_p402, containing the 3-HBCoA-dependent pathway only, to determine (*R*)-1,3-BDO yield and other metabolite production (Table 4.6). Similar metabolite production is observed between strains H16ΔC_p444 and H16ΔC_p446, with no accumulation of pyruvate, but higher yields of acetate and ethanol. However, (*R*)-1,3-BDO carbon yield improved 1.7-fold in the strain harbouring pJLG444, confirming increase of carbon flux through both heterologous biosynthesis pathways compared with strain H16ΔC_p402.

Table 4.6. Carbon yield of (*R*)-1,3-BDO and other metabolites ± standard deviation by strains screened for 1,3-butanediol production incorporating both pathways (H16ΔC-p444) compared with the control strain H16ΔC-p402. Cells were cultivated for 72 h in 10 mL 2 % (w/v) sodium gluconate nitrogen limiting minimal media in 50 mL Falcon tubes in the presence of 0.01 % (w/v) L-arabinose.

Strain	**$Y_{1,3BDO}$ (Cmol Cmol^{-1})**	**Y_{4H2B} (Cmol Cmol^{-1})**
H16ΔC-p402	0.057 ± 0.023	0.005 ± 0.002
H16ΔC-p444	0.100 ± 0.041	0.013 ± 0.002

Strain	**$Y_{Ethanol}$ (Cmol Cmol^{-1})**	**$Y_{Pyruvate}$ (Cmol Cmol^{-1})**	**$Y_{Acetate}$ (Cmol Cmol^{-1})**
H16ΔC-p402	0.007 ± 0.0003	0.339 ± 0.062	N.D.
H16ΔC-p444	0.089 ± 0.056	N.D.	0.046 ± 0.002

Further characterisation of (*R*)-1,3-BDO production by strain H16ΔC_p444 was undertaken through cultivation in shake-flasks increasing oxygen availability to the cells (Figure 4.10). Noticeably, metabolite profiles vary considerably in an oxygen rich environment, with increased acetate yields by strain H16ΔC_p444 rising from 0.046 ± 0.002 Cmol Cmol^{-1} to 0.206 ± 0.009 Cmol Cmol^{-1}, 72 h after induction when cultivated in falcon tubes or shake-flasks, respectively. Furthermore, strain H16ΔC_p402 exhibits

higher pyruvate yields when cultivated in shake-flasks, increasing from 0.339 ± 0.062 Cmol Cmol^{-1} observed in falcon tubes to 0.515 ± 0.062 Cmol Cmol^{-1}, 72 h after induction.

Between 72 h and 120h after induction, by-product yields are observed to increase, for example, pyruvate produced by strain H16ΔC_p402 and ethanol by strain H16ΔC_p444. Continued consumption of gluconate during stationary phase with reduced carbon flux towards (*R*)-1,3-BDO indicates a reduction of enzymatic activity within the heterologous pathways implemented.

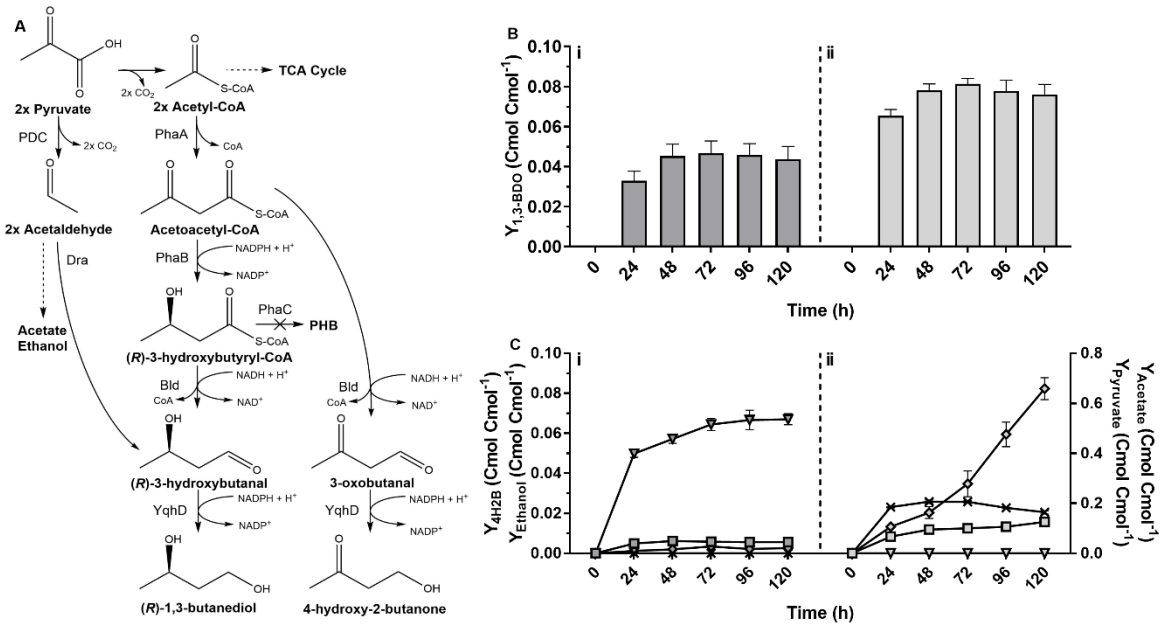

Figure 4.10. Shake-flask growth profile comparing 3HBCoA-dependent pathway and combining the 3-HBCoA-dependent and pyruvate-dependent pathways. (A) Biosynthetic pathways implemented for 1,3-BDO production in *C. necator* H16 Δ*phaC1* showing by-product metabolite formation. Strains: i. H16ΔC-p402, ii. H16ΔC-p444. Carbon yields shown (B): solid bars represent (*R*)-1,3-BDO, squares represent 4H2B, (C) crosses represent acetate, diamonds represent ethanol and upside-down triangles represent pyruvate. Cells were cultivated in 250

mL baffled shake-flasks in 2 % (w/v) sodium gluconate nitrogen-limiting minimal media at 30 °C, 200 rpm shaking in the presence of 0.01 % (w/v) L-arabinose.

With a lack of (*R*)-1,3-BDO production by strains harbouring pyruvate-dependent biosynthesis pathway and improvement of yields observed in the strains harbouring both implemented (*R*)-1,3-BDO pathways, protein analysis of strains H16ΔC-p402, H16ΔC-p446 and H16ΔC-p444 was undertaken to gain understanding of enzymes available for conversion of metabolites (Figure 4.11). Cell samples were harvested 24 h after induction of gene expression by addition of L-arabinose for comparison with cells subjected to no addition of L-arabinose enzyme synthesis. From protein analysis of strains H16ΔC-p402 and H16ΔC-p444, proteins of sizes equal to Bld (51,188 Da) and $YqhD_{Ec}$ (42,097 Da) are clearly produced. Bands showing protein of same size as PDC (60,926 Da) is observable in samples from strains H16ΔC-p444 and H16ΔC-p446.A band showing protein of same size as Dra (23,362 Da) is present for strain H16ΔC-p444, but not H16ΔC-p446, despite *dra* being present on the plasmid. Indeed, overall expression of heterologous enzymes appears to be lower in the strain H16ΔC-p446 than in strain H16ΔC-p444. Protein analysis suggests $YqhD_{Ec}$, Bld and PDC are sufficiently synthesis, whilst Dra is not and may be responsible for limiting (*R*)-1,3-BDO bioproduction in the pyruvate-dependent pathway.

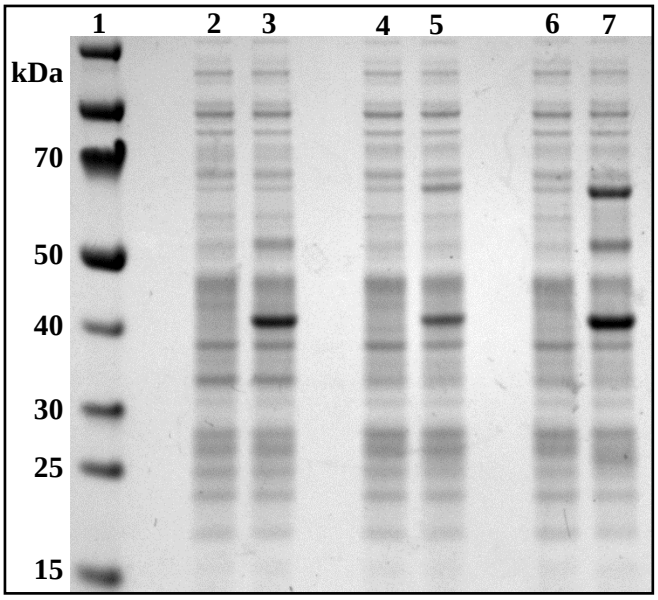

Figure 4.11. Visualisation of soluble protein expression induced by addition of L-arabinose for strains H16ΔC-p402 (lane 3), H16ΔC-p446 (lane 5) and H16ΔC-p444 (lane 7) for comparison with strains H16ΔC-p402 (lane 2), H16ΔC-p446 (lane 4) and H16ΔC-p444 (lane 6) cultivated with no L-arabinose present. PageRuler™ Protein Ladder present in lane 1 was used for estimation of protein size.

4.4 Discussion

Biosynthesis of 1,3-BDO has previously been reported in *E. coli* MG1655 utilising either pyruvate or acetyl-CoA as a precursor (Kataoka *et al.*, 2013; Kim *et al.*, 2017). This study was aimed to evaluate the capabilities of *C. necator* H16 as a chassis for bio-production of (*R*)-1,3-BDO utilising two alternative strategies individually and in combination.

When initially considering potential (*R*)-1,3-BDO biosynthesis pathways, it can be seen both pathways are NAD(P)H-consuming, with net use of three reducing cofactor molecules for each (*R*)-1,3-BDO synthesised aerobically. The (*R*)-3-HBCoA-

dependent pathway requires heterologous expression of two genes encoding a butanal dehydrogenase and NADPH-dependent aldehyde reductase. Additionally, to generate (*R*)-3-HBCoA from acetyl-CoA requires a β-ketothiolase and NADPH-dependent acetoacetyl-CoA reductase encoded by *phaAB*, respectively. The alternative pyruvate-dependent pathway requires heterologous expression of three genes encoding a pyruvate decarboxylase, deoxyribose-5-phosphate aldolase and NADPH-dependent aldehyde reductase. Bioproduction of (*R*)-1,3-BDO is therefore heavily reliant on the efficient regeneration and balance of reducing equivalent within the cell. Notably, the (*R*)-3HBCoA pathway requires two NADPH and one NADH, whereas the pyruvate pathway utilises one NADPH and two NAD^+ molecules remain unreduced due to the direct conversion of pyruvate to acetaldehyde. Given that the final reaction of the (*R*)-3HBCoA pathway requires two NADPH, the use of a NADH-dependent enzyme for (*R*)-3HBCoA conversion into (*R*)-3HBA enables balancing of NADH/NADPH ratio to some extent.

C. necator possesses metabolism which enables redirection of a large amount of carbon into P3HB, up to 90% of the CDW, if the excess carbon is available under nitrogen -limiting conditions (Lee *et al.*, 2008). This strongly suggests that a sufficiently large pool of precursor in form of 3HBCoA can be generated under nutrient-limiting conditions, generating a driving force for (*R*)-1,3-BDO biosynthesis when the (*R*)-3HBCoA-dependent pathway is utilised. Therefore, this pathway was selected for (*R*)-1,3-BDO production in *C. necator H16* heterotrophically or from CO_2.

Upon screening the various plasmids identified as exhibiting potential aldehyde reductase activity, no (*R*)-1,3-BDO production was detectable by HPLC-RI in *C. necator* wild type strain, most likely due to low (*R*)-3-HBCoA availability. However,

when screened in Δ*phaC1* mutant, detectable production of (*R*)-1,3-BDO using constructs expressing *bld* in combination with $yqhD_{Ec}$ or $yqhD_{Pp}$ was observed. Lack of diol production when Bld was combined with other reductases confirms Bld and YqhD are indispensable enzymes for (*R*)-1,3-BDO biosynthesis in *C. necator* H16.

Following confirmation of successful (*R*)-1,3-BDO production by *C. necator* strains harbouring plasmids containing genes expressing Bld and YqhD, low initial titres were surprising. Indeed, capabilities of *C. necator* cells to store large amounts of carbon and therefore generate a large pool of 3-HBCoA, cultivation conditions were investigated, and induced gene expression levels fine-tuned. Limiting nitrogen available for biomass production ensured carbon flux was re-directed towards synthetic (*R*)-1,3-BDO pathway when levels were depleted. Combined with optimisation of induced gene expression with L-arabinose, significant improvements (>2-fold) in (*R*)-1,3-BDO yields were seen.

To streamline (*R*)-1,3-BDO development, strains were compared to identify the best candidate for further advances. With similar overall (*R*)-1,3-BDO carbon yields observed by each candidate, highest productivity (Cmol $Cmol^{-1}$ 24 h^{-1}) was used as key metric to determine optimal strain. Furthermore, capability of fine-tuning individual components of biosynthesis pathway *bld* and *yqhD*, compared with single bi-functional *adhE2* gene presents greater opportunity for understanding of novel 1,3-BDO pathway.

Production of other compound of interest, 4H2B as unexpected by-product of ®-1,3-BDO biosynthesis pathway confirms promiscuity of pathway enzymes as well as increased pool of acetoacetyl-CoA, indicating carbon flux bottleneck present downstream of PhaA. Abundance of acetoacetyl-CoA is attributed to *C. necator*

endogenous carbon metabolism, with no 4H2B synthesis observed by *E. coli* strains (Table 4.5). Plasmid-based expression of *phaB1* increasi®(*R*)-1,3BDO yields compared with chromosomal expression suggests in the current system, the biosynthesis pathway is hindered by relevant protein expression levels.

To ascertain effect on (*R*)-1,3-BDO yield by increasing protein production, a two-stage fed-batch shake-flask fermentation approach was implemented, also presenting opportunity to investigate alternative AKR *PA1127* (present in pJLG420). Additionally, this style of experimentation allowed for comparison with *E. coli*, previously utilised as a chassis for all microbial (*R*)-1,3-BDO biosynthesis (Kataoka *et al.*, 2013; Kataoka *et al.*, 2014; Nemr *et al.*, 2018). By cultivating *E. coli* cells initially in rich media supplemented with preferred carbon source glucose, L-arabinose will not be catabolised and is able to induce gene expression as intended.

Highest (*R*)-1,3-BDO yields were observed during two-stage batch shake-flask fermentation, however, this included required addition of increased L-arabinose and preparation of 2 different media increasing contamination risk, becoming impractical for proposed autotrophic cultivation. Therefore, increase of pathway substrate in form of acetyl-CoA was planned, facilitated through reduction of carbon flux through TCA cycle. This strategy did improve (*R*)-1,3-BDO yields to similar levels observed by strain H16ΔCB-p447 with plasmid-based expression of *phaB1* gene. However, observation of high extracellular pyruvate levels elucidated loss of carbon from the system.

To capitalise on pyruvate accumulation in P3HB deficient *C. necator* H16 strains, implementation of pyruvate-dependent (*R*)-1,3-BDO biosynthesis pathway was attempted. Despite learnings from optimisation of (*R*)-3-HBCoA development, no

detectable levels of (*R*)-1,3-BDO were observed. However, for strain containing pyruvate-dependent pathway there was also no detectable extracellular pyruvate, instead a large accumulation of acetate or ethanol, most likely due to accumulation of toxic acetaldehyde by PDC enzyme being converted to acetate, generating extra NADH when cultivated in oxygen-rich environment of shake-flasks. With the aim to further increase (*R*)-1,3-BDO yields, plasmids containing heterologous genes expressing enzymes capable of both 3-HBCoA and pyruvate-dependent pathways were assembled and screened. Despite increased reducing power imposed on cellular metabolism by use of both pathways, (*R*)-1,3-BDO yields significantly increased. Conversely by-product formation of acetate, ethanol and 4H2B appear to be largest carbon sinks in strains expressing PDC.

4.5 Conclusion

This study has sought to determine the viability of *C. necator* as an appropriate chassis for the heterotrophic bioproduction of (*R*)-1,3-BDO, with a view to utilise native facultative autotrophic capabilities. Enzyme candidates for (*R*)-1,3-BDO production from the precursor (*R*)-3-HBCoA has been explored and cultivation conditions optimised. The pathway by-products 4H2B and pyruvate accumulated in (*R*)-1,3-BDO producing P3HB deficient *C. necator* H16 strains. Therefore, a second pyruvate-utilising (*R*)-1,3-BDO biosynthetic pathway was deployed resulting in increased yields.

5 Autotrophic fermentation of (*R*)-1,3-butanediol using engineered *C. necator* H16

5.1 Introduction

The use of industrial biotechnology to produce chemicals from waste carbon sources such as CO_2 is a promising approach to reduce atmospheric greenhouse gas levels. To achieve this, CO_2 fixing microorganisms can be employed for production of chemicals typically synthesised from non-renewable petrochemical sources. The facultative chemolithoautotrophic bacterium *C. necator* H16 is able to fix CO_2 with H_2 acting as an electron donor and O_2 acting as an electron acceptor through the CBB cycle (Bowien and Kusian, 2002). There are two copies of the *cbb* operon that encode enzymes required for CO_2 fixing in the genome of *C. necator* H16; one copy is mapped on chromosome 2 and the other on the megaplasmid pHG1 (Pohlmann *et al.*, 2006). Both *cbb* operons consist of 13 genes and are regulated by the chromosomal copy of *cbbR* (H16_B1396) encoding a transcriptional regulator (Bowien and Kusian, 2002). The megaplasmid copy of *cbbR* (PHG428) has previously been reported as defective (Windhöver and Bowien, 1991). Fixation of 1 molecule of CO_2 through CBB cycle is energy demanding, requiring 3 ATP and 2 NADH or NADPH and may present potential limitations when introducing synthetic metabolic pathways.

C. necator H16 has previously been engineered for autotrophic biosynthesis of several platform chemicals (Crepin, Lombard and Guillouet, 2016; Windhorst and Gescher, 2019; Black *et al.*, 2018). Bioproduction of the platform chemical acetoin engineered *C. necator* H16 was achieved using CO_2 as the sole carbon source yielding >100 % carbon efficiency (Windhorst and Gescher, 2019). To achieve this, cells were cultivated

in gas-tight Schott bottles continuously supplied with a gas mixture with composition: 5% CO_2, 75% H_2, 18% O_2 and 2% N_2.

C. necator H16 is also able to grow organoautotrophically using formate as both carbon and energy supply. Black and co-workers report production of 405 µM *n*-butanol using formic acid as the sole carbon and energy source in the host chassis *C. necator* H16 (Black *et al.*, 2018). Notably, the *n*-butanol titre was 6.6-fold higher in strains cultivated heterotrophically with fructose as the carbon source compared to cultivation using formic acid. Furthermore, the use of formate as carbon and energy source for autotrophic cultivation presents advantages over direct feeding of CO_2, such as reduced equipment and safety considerations for handling of gases and solubility of formate compared to CO_2. However, use of formate also presents limitations, with high sensitivity to formic acid reported for *C. necator* H16 subsequently resulting in low biomass yields (Grunwald *et al.*, 2015). An alternative approach for organoautotrophic cultivation of *C. necator* has been reported utilising an integrated electro microbial system (Al Rowaihi *et al.*, 2018). In the system, CO_2 was electrochemically converted to formate that was subsequently consumed by *C. necator* H16 resulting in P3HB production.

The global market of the platform chemical 1,3-BDO was estimated at $161.3 million in 2021 and is projected to grow to $269.1 million by 2023 (Research and Markets, 2022). Pharmaceutical-grade 1,3-BDO is widely used in the production of cosmetics and personal care products, with consumption of these products increasing and global demand of 1,3-BDO (Research and Markets, 2022). Indeed, industry-leaders including Genomatica have sought to meet this demand using bio-based production of 1,3-BDO (Genomatica, 2017b) indicating the global and economical importance of 1,3-BDO.

To date, microbial production of (*R*)-1,3-BDO has been reported using through two alternative metabolic pathways in the host chassis *E. coli*. Kataoka and co-workers report bioproduction of (*R*)-1,3-BDO from the precursor acetyl-CoA using a β-ketothiolase, acetoacetyl-CoA reductase and CoA-acylating butyraldehyde reductase (Kataoka *et al.*, 2014). For fermentation of engineered *E. coli*, cells were cultivated with LB supplemented with 222 mM glucose in baffled flasks for 36 h. The glucose concentration was maintained at 36 – 90 mM. During fermentation, the oxygen transfer coefficient (K_La) and pH were found to be optimal at values of 82.3 h^{-1} and 5.5, respectively. By optimisation of these fermentation conditions the highest concentration of 174.8 mM (*R*)-1,3-BDO was achieved.

An alternative (*R*)-1,3-BDO metabolic pathway using pyruvate as the precursor reached a concentration of 26.6 mM (*R*)-1,3-BDO during fermentation of an engineered *E. coil* strain (Nemr *et al.*, 2018). This was achieved using a pyruvate decarboxylase (PDC), 2-deoxyribose-5-phospate aldolase (DERA) and aldo-keto reductase (AKR). To increase (*R*)-1,3-BDO production, gene copy number encoding pathway enzymes DERA and AKR were doubled, improving enzyme biosynthesis. Notably, cultivation conditions had a striking effect on (*R*)-1,3-BDO production, increasing from 7.4 mM during shake flask cultivations to 26.6 mM during fermentation in bioreactors. This is most likely due to more optimal conditions within bioreactors, with increased oxygen availability and maintaining pH at 7.0.

In this study, three strains have been constructed utilising either or both the (*R*)-3HBCoA-dependent and pyruvate-dependent pathways for (*R*)-1,3-BDO biosynthesis. Genetically stable expression of heterologous genes was achieved through chromosomal integration. This presented an opportunity to identify pathway-limiting

enzymes that were addressed by increasing individual gene copy number through plasmid-based expression. Chromosomal copy number of genes encoding pathway-limiting enzymes was then doubled to improve (*R*)-1,3-BDO yields in genetically stable strains. Increase of carbon flux towards (*R*)-1,3-BDO was also achieved by increasing pool of precursors pyruvate and acetyl-CoA by deletion of *sucCD*. Developed strains were then subjected to autotrophic fermentation where first production of (*R*)-1,3-BDO from CO_2 is reported. Furthermore, a technoeconomic analysis was undertaken to evaluate the minimum estimated selling price (MESP) of (*R*)-1,3-BDO produced by *C. necator* H16 cultivated under autotrophic conditions.

5.2 Materials and Methods

5.2.1 Primers used in this study

All primers used in this study are listed in Table 5.1.

Table 5.1 Primers used in this study.

Name	**Sequence 5' to 3'**
45.dra_Spe_F	TATAACTAGTAAAAGATCTTTAAAGGAGATATAGATGTCGCGCTCG
45.dra_Xho_R	ATATCTCGAGTCAGTACGAGCCCTCCGAGCG
47.dra_Eco_F	TATAGAATTCAAAAGATCTTTTAAGAAGGAGATATACATATGTCGCGCTCGATCGCC
47.dra_Spe_R	ATATACTAGTTCAGTACGAGCCCTCCGAGCG
phaC_750Up_SacI_F	TATAGAGCTCCCGACGCCGGTCGCTTCTACTCCTATC
phaC_OVL_R	GGCACTCATGCAAGCGTCATGCATACCTCAGGATACTCGAGATATTAATTAAATACGCCATGATTTGATTGTCTCTCTGCCG
phaC_OVL_F	CGGCAGAGAGACAATCAAATCATGGCGTATTTAATTAATATCTCGAGTATCCTGAGGTATGCATGACGCTTGCATGAGTGCC
phaC_750DN_PmeI_R	ATATGTTTAAACGCACGAACTCGTCGGTCTTGAAGGC

pLO3_pJLGPacT_F	TATATTAATTAAAGAAGGCCATCCTGACGGATGGC
pLO3_pJLGBsu36I_R	ATATCCTCAGGCATTTGAGAAGCACACGG
sucC_UP.HiFi_F	CACCTAGATCCTTTTAATTCGAGCTCTCGCGTTCGGTCGTCGGCAAGATCA
sucC_UP.HiFi_R	TTAATTTGGTACCTTATGCGTGTTTCCTTTCGGGTAGGCGTAAAAGG
P8.HiFi_F	AAAGGAAACACGCATAAGGTACCAAATTAAGCAGAAGGCCATC
P8.HiFi_R	TAAAAGATCTTTTGAATTCTAAGATGAATCTATTATATCGCCG
bld.HiFi_F	CATCTTAGAATTCAAAAGATCTTTTAAGAATACATATGATCAAGGACACCC
bld.HiFi_R	CGTTTTATTTGATGCTAGCCTCGAGACTAGTTCAGCCGGCCAGC
sucD_DN.HiFi_F	AACTAGTCTCGAGGCTAGCATCAAATAAAACGAAAGGCCTTCGGGCCTTTCGTTTTATCTGTTGTTTACCGGTGTCGTACCTCGCCATTCCAGCGAGCGCTGG
sucD_DN.HiFi_R	TTAAACAGTCGACTCTAGACTTAATTAATCAGGCGGCCTGTGCCGACCGGCGG

5.2.2 Plasmids used in this study

All plasmids used in this study are listed in Table 5.2.

Table 5.2 Plasmids used in this study. * denotes codon optimisation, Km^R: kanamycin resistance, Tet^R: tetracycline resistance.

Plasmid	**Description**	**Source**
pJLG402	pBBR1-USER with P_{araBAD}, *bld**, y*qhD* (b3011)	This work
pJLG414	pBBR1-USER with P_{araBAD}, *bld**	This work
pJLG501	pBBR1-USER with P_{araBAD}, *bld**, *dra**	This work
pJLG502	pBBR1-USER with P_{araBAD}, *dra**	This work
pBBR1MCS-2-P8	Source of P_8 promoter	(Alagesan *et al.*, 2018)
pLO3	host plasmid with Tet^R, *sacB*, RP4 transfer ori, pBR322 ori	(Lenz and Friedrich, 1998)

pLO3-phaC	pLO3, *phaC1* deletion vector with multiple cloning site	This work
pJLG503	pLO3, *phaC1::*(P_{araBAD}, *bld**, *yqhD* (b3011)) deletion/integration vector	This work
pJLG504	pLO3, *phaC1::*(P_{araBAD}, *yqhD* (b3011), *dra**, *PDC*) deletion/integration vector	This work
pJLG505	pLO3, *phaC1::*(P_{araBAD}, *bld**, *yqhD* (b3011), *dra**, *PDC*) deletion/integration vector	This work
pJLG506	pLO3, *sucCD::*(P_8, *bld**) deletion/integration vector	This work
pJLG507	pLO3, *sucCD::*(P_8, *bld**, *dra**) deletion/integration vector	This work

5.2.3 Assembly of plasmids used in this study

Generic molecular cloning techniques are described in Materials and Methods of Chapter 2.

pJLG501: *dra* (BH1351) was amplified with 45.dra_Spe_F and 45.dra_Xho_R from template DNA synthesised and codon optimised by Gene Art Gene Synthesis. The PCR product was cloned into pJLG414 using restriction sites SpeI and XhoI.

pJLG502: *dra* (BH1351) was amplified with 47.dra_Eco_F and 47.dra_Spe_R from template DNA synthesised and codon optimised by Gene Art Gene Synthesis. The PCR product was cloned into pJLG401 using restriction sites EcoI and SpeI.

Assembly of *phaC* deletion vector was undertaken with PacI, XhoI and Bsu36I restriction sites placed between upstream and downstream homology arms in the pLO3 suicide vector (pLO3-phaC) to allow (*R*)-1,3-BDO producing operons to be rapidly inserted. Homology arms upstream and downstream of *phaC* were amplified with phaC_750Up_SacI_F, phaC_OVL_R and phaC_OVL_F, phaC_750DN_PmeI_R from purified *C. necator* H16 genomic DNA, respectively. PCR products were then fused

together using SOEing PCR with primers phaC_750Up_SacI_F and phaC_OVL_F, phaC_750DN_PmeI_R. The fusion PCR product was cloned into pLO3 using restriction sites SacI and PmeI.

pJLG503: the P_{araBAD}, *bld* and $yqhD_{Ec}$ operon was amplified from pJLG402 with pLO3_pJLGPacT_F and pLO3_pJLGBsu36I_R. The PCR product was cloned into pLO3-phaC using restriction sites PacI and PmeI.

pJLG504: the P_{araBAD}, $yqhD_{Ec}$, *dra* and *PDC* operon was amplified from pJLG446 with pLO3_pJLGPacT_F and pLO3_pJLGBsu36I_R. The PCR product was cloned into pLO3-phaC using restriction sites PacI and PmeI.

pJLG505: the P_{araBAD}, *bld*, $yqhD_{Ec}$, *dra* and *PDC* operon was amplified from pJLG444 with pLO3_pJLGPacT_F and pLO3_pJLGBsu36I_R. The PCR product was cloned into pLO3-phaC using restriction sites PacI and PmeI.

Assembly of pJLG506 was undertaken using HiFi assembly procedure into pLO3 suicide vector. Homology arms upstream of *sucC* and downstream of *sucD* were amplified with sucC_UP.HiFi_F, sucC_UP.HiFi_R and sucD_DN.HiFi_F, sucD_DN.HiFi_R from purified *C. necator* H16 genomic DNA, respectively. Strong constitute P_8 promoter was amplified with P8.HiFi_F and P8.HiFi_R from pBBR1MCS-2-P8. Gene *bld* was amplified with bld.HiFi_F and bld.HiFi_R from template DNA synthesised and codon optimised by Gene Art Gene Synthesis. The PCR products were then assembled into pLO3 backbone linearized with SacI and XbaI.

pJLG507: *dra* (BH1351) was amplified with 45.dra_Spe_F and 45.dra_Xho_R from template DNA synthesised and codon optimised by Gene Art Gene Synthesis. The PCR product was cloned into pJLG506 using restriction sites SpeI and XhoI.

5.2.4 Bacterial strains used in this study

All bacterial strains used in this study are listed in Table 5.3.

Table 5.3 Bacterial strains used in this study. *P* denotes P_{araBAD} promoter with square brackets showing genes under promoter control. Km^R: kanamycin resistance. Gen^R: gentamicin resistance.

Strain	**Genotype**	**Parent strain**	**Plasmid**	**Source**
E. coli DH5α	*lacZ*ΔM15, *rec*A1, *end*A1	-	-	Invitrogen
E.coli S17-1	λpir/pLFX	-	-	ATCC 47055
C. necator H16	wild type, Gen^R	-	-	DSM-428
C. necator H16 Δ*phaC1*	Δ*phaC1*	-	-	(Arenas Lopez, 2018)
H16-501	H16Δ*phaC1::P*[*bld yqhD*$_{Ec}$ *phaAB*]	-	-	This work
H16-501-p414	H16Δ*phaC1::P*[*bld yqhDEc phaAB*], (*P*[*bld*] *Km*^{R})	H16-501	pJLG414	This work
H16-501-p402	H16Δ*phaC1::P*[*bld yqhDEc phaAB*], (*P*[*bld yqhD*$_{Ec}$] *Km*^{R})	H16-501	pJLG402	This work
H16-502	H16Δ*phaC1::P*[*yqhD*$_{Ec}$ *dra PDC*]			This work
H16-502-p502	H16Δ*phaC1::P*[*yqhD*$_{Ec}$ *dra PDC*] (*P*[*dra*] *Km*^{R})	H16-502	pJLG502	This work
H16-503	H16Δ*phaC1::P*[*bld yqhD*$_{Ec}$ *dra PDC phaAB*]	-	-	This work
H16-503-p414	H16Δ*phaC1::P*[*bld yqhD*$_{Ec}$ *dra PDC phaAB*] (*P*[*bld*] *Km*^{R})	H16-503	pJLG414	This work
H16-503-p501	H16Δ*phaC1::P*[*bld yqhD*$_{Ec}$ *dra PDC phaAB*] (*P*[*bld dra*] *Km*^{R})	H16-503	pJLG501	This work
H16-504	H16Δ*phaC1::P*[*bld yqhD*$_{Ec}$ *phaAB*] Δ*sucCD::P*$_8$[*bld*]	-	-	This work
H16-505	H16Δ*phaC1::P*[*bld yqhD*$_{Ec}$ *dra PDC phaAB*] Δ*sucCD::P*$_8$[*bld dra*]	-	-	This work

5.2.5 Estimation of carbon uptake rate during autotrophic fermentation

Carbon uptake rate (CUR) was estimated analysing off gas composition using a Bioprocess R&D Lab Gas Analyser, Model RLGA-9804 (Atmosphere Recovery Inc., Eden Prairie, MN, USA). Amount of CO_2 entering bioreactors was set to 1.35 L h^{-1} (3% of total airflow) with additional CO_2 entering bioreactor in form of 3.4 % of air. Percentage of nitrogen leaving bioreactors was used to normalise CO_2 (L h^{-1}) leaving bioreactors. Carbon transfer rate (CTR, M h^{-1}) was determined using Equation 5.1 where $CO2_{IN}$ and $CO2_{OUT}$ are CO_2 flow rates in L h^{-1} and V represents bioreactor culture volume normalised to 1 L. All flow rates are converted to M h^{-1} using the Ideal Gas Law where 1 mol gas is equivalent to 22.4 L (Doran, 1995). Carbon uptake rate (CUR, mM h^{-1}) was estimated by subtracting average CTR for first 6 h of fermentation where CO_2 uptake is negligible due to low biomass production, from subsequent CTR values.

$$CTR = \frac{CO2_{IN} - CO2_{OUT}}{22.4 \times V} \quad (5.1)$$

5.2.6 Technoeconomic analysis of (*R*)-1,3-BDO production using CO_2 as sole carbon source

A technoeconomic analysis (TEA) was undertaken to determine minimum estimated selling price (MESP) using the Biorenewable Process Evaluation Tool (BioPET), a spreadsheet-based early-stage cost estimation tool developed by Claypool and Raman (Claypool and Raman, 2013; Claypool and Raman, 2015). The tool allows key parameters to be defined and estimates capital investment, labour, utilities, feedstock, nutrients and MESP. Key parameters include plant operating days, plant lifetime, internal rate of return, annual production, feedstock costs, purification stages and yields, and Lang factor that relates purchased equipment cost to total capital investment and

fixed capital investment. To calculate MESP within the BioPET tool for production of (*R*)-1,3-BDO from CO_2, plant operating days of 330, plant lifetime of 30 years, internal rate of return of 10 %, and a Lang factor of 5 were used (Satam, Daub and Realff, 2019). Annual production was assumed to be 10,000 tonne (Genomatica, 2017a) and CO_2 price set to \$2.12 USD kg^{-1} (BOC, 2022). Downstream processing for purification of (*R*)-1,3-BDO was modelled within BioPET to entail three unit operations, with the first step being centrifugation for separation of biomass and extra-cellular products. The resulting supernatant would then undergo two column distillation steps yielding 99 % purity of (*R*)-1,3-BDO. Previous reports have detailed similar approaches to purification of BDO, including a patented approach for 1,3-BDO purification from fermentation broth (Baldassarre, Cesana and Bordes, 2021) and Satam and co-workers who analysed technoeconomic feasibility and downstream processing of production of 1,4-BDO (Satam, Daub and Realff, 2019). It should be noted that MESP has been adjusted for inflation since development of BioPET in 2015 seeing an increase of 26% to 2021.

5.3 Results

5.3.1 Chromosomal integration of exogenous genes for production of (*R*)-1,3-BDO

In Chapter 4, the (*R*)-1,3-BDO yield of 0.081 ± 0.005 Cmol $Cmol^{-1}$ from sodium gluconate was achieved using *C. necator* H16 that was carrying (*R*)-1,3-BDO biosynthetic pathway genes on the plasmid. The expression plasmid pJLG444 contained *bld* (encoding a butanal dehydrogenase) from *C. saccharoperbutylacetonicum*, *yqhD* (NADP-dependent aldehyde reductase) from *E. coli*, *dra* (aldolase) from *B. halodurans* and *pdc* (pyruvate decarboxylase) from *Z.*

mobilis under control of arabinose-inducible system *araC*/P_{araBAD}. Synthesis of enzymes Bld, YqhD, Dra and PDC in combination with *C. necator* H16 enzymes PhaAB results in carbon flux through two alternative (*R*)-1,3-BDO metabolic pathways with either (*R*)-3HBCoA or pyruvate as precursor. When investigating individual pathways, the (*R*)-3HBCoA-dependent pathway achieved (*R*)-1,3-BDO yield of 0.047 Cmol $Cmol^{-1}$. Of note, pyruvate was observed as the major by-product of this pathway. Therefore, pyruvate-dependent pathway was investigated but was unable to produce detectable levels of (*R*)-1,3-BDO, despite a lack of pyruvate present in samples. A *C. necator* H16 strain that utilises both (*R*)-1,3-BDO pathways was developed (H16ΔC-p444) where improvement in (*R*)-1,3-BDO yield was observed. Primary by-products in this system are 4-hydroxy-2-butanone (4H2B), acetate and ethanol.

To achieve continuous production of platform chemical (*R*)-1,3-BDO, fermentation is ideal method of cultivation allowing control of bioreactor conditions such as oxygen transfer and pH and increased culture volumes. However, genetic stability for enzyme biosynthesis during continuous cultivation is a concern. Previous reports indicate chromosomal integration can improve stability of heterologous gene expression in *C. necator* H16 strains, compared with plasmid-based expression, particularly during large scale cultivations (Voss and Steinbüchel, 2006). Therefore, to increase (*R*)-1,3-BDO pathway enzyme synthesis, exogenous genes were inserted through homologous recombination on chromosome 1 of *C. necator* H16. The dispensable *phaC1* locus was employed as an integration site resulting in simultaneous gene deletion and integration. For tuneable expression of chromosomally integrated genes, the terminator (*rrnB* T_2) was placed upstream of the arabinose inducible system (*araC*/P_{araBAD}) reducing influence of constitutive *phaC* promoter (P_{phaC}). By design, utilisation of the *phaC* locus

as a target integration site allows for inducible expression of *phaA* and *phaB1*, also required for (*R*)-1,3-BDO biosynthesis through the (*R*)-3HBCoA-dependent pathway (strain H16-501). The strain H16-502 was assembled in the same manner integrating *yqhD*$_{Ec}$, *dra* and *PDC* downstream of *araC*/P$_{araBAD}$ in the *phaC* locus to utilise the pyruvate-dependent pathway. Strain H16-503 was also assembled integrating *bld*, *yqhD*$_{Ec}$, *dra* and *PDC* downstream of *araC*/P$_{araBAD}$ in the *phaC* locus to utilise both (*R*)-3HBCoA-dependent and pyruvate-dependent (*R*)-1,3-BDO pathways.

To assess ability to produce (*R*)-1,3-BDO, constructed strains H16-501, H16-502 and H16-503 were cultivated in NLMM supplemented with 2 % (w/v) sodium gluconate for 72 h (Table 5.4). During screening, strains H16-501 and H16-503 produced (*R*)-1,3-BDO achieving yields comparatively lower than strains with plasmid-based gene expression. As expected, strain H16-502 produced no detectable levels of (*R*)-1,3-BDO. Interestingly, by-product profiles were similar to previous observations (Section 4.3.8) with acetate and ethanol yields being much higher in strains H16-502 and H16-503 containing *PDC*, whereas pyruvate is the main byproduct produced by H16-501. Overall, production of (*R*)-1,3-BDO by strains with heterologous genes chromosomally integrated was achieved, but yields are significantly lower when compared with plasmid-based gene expression (Table 4.6). This is most likely due to a reduction in gene dosage, with chromosomal integrations resulting in single copies of *bld*, *yqhD*$_{Ec}$, *dra* and *PDC* compared with plasmid-based expression where the pBBR1 *ori* is reported to reach 30-45 copies per cell in *C. necator* H16 (Bi *et al.*, 2013).

Table 5.4 Screening of strains with chromosomally integrated (*R*)-1,3-BDO-biosynthesis pathway. Cells were cultivated in 10 mL NLMM supplemented with 2 % (w/v) sodium gluconate and 10 µg mL^{-1} gentamicin in 50 mL falcon tubes. Samples were taken 72 h after L-

arabinose was added to a final concentration of 0.1 % (w/v) to induce gene expression. All yields (Y) are averages ± standard deviation calculated from at least 2 biological replicates in units Cmol Cmol^{-1}.

Strain	$\mathbf{Y_{1,3BDO}}$	$\mathbf{Y_{4H2B}}$	$\mathbf{Y_{Acetate}}$	$\mathbf{Y_{Ethanol}}$	$\mathbf{Y_{Pyruvate}}$
H16-501	0.008 ± 0.0004	N.D.	0.022 ± 0.0003	0.004 ± 0.0001	0.345 ± 0.005
H16-502	N.D.	N.D.	0.188 ± 0.026	0.063 ± 0.013	N.D.
H16-503	0.012 ± 0.001	N.D.	0.182 ± 0.010	0.054 ± 0.006	N.D.

5.3.2 Combining plasmid and chromosomal based expression of heterologous genes to improve (*R*)-1,3-BDO yields

It was hypothesised in Chapter 4 that low expression of genes *bld* and *dra* may be the limiting factor of the (*R*)-3HBCoA-dependent and pyruvate-dependent (*R*)-1,3-BDO pathways, respectively. Chromosomal integration of all heterologous genes for (*R*)-1,3-BDO biosynthesis described in Section 5.3.1 allows for a unique opportunity to greatly increase copy number of a specific gene by plasmid-based expression. Therefore, to evaluate effect of increase in *bld* gene dosage on (*R*)-1,3-BDO yields for (*R*)-3HBCoA-dependent pathway, strain H16-501 was transformed with pJLG414 for increased copy number of *bld* or *bld* and $yqhD_{Ec}$, respectively. Transformed strains H16-501-p414 and H16-501-p402 and the control strain H16-501 were then screened by cultivation in NLMM supplemented with 2 % (w/v) sodium gluconate for 120 h (Figure 5.1).

From the data, strain H16-501-p414 and H16-501-p402 yielded similar levels of (*R*)-1,3-BDO, producing 0.184 ± 0.003 and 0.163 ± 0.017 Cmol Cmol^{-1}, respectively. This represents an 18- to 20-fold increase in (*R*)-1,3-BDO yield compared to 0.009 ± 0.0006

Cmol Cmol^{-1} achieved by the control H16-501. The by-product 4H2B was also produced by strains H16-501-p414 and H16-501-p402 yielding 0.052 ± 0.003 and 0.050 ± 0.011 Cmol Cmol^{-1}, respectively. However, no detectable levels of 4H2B were observed for strain H16-501. As previously discussed, pyruvate is the primary by-product of (*R*)-3HBCoA-dependent pathway. Strain H16-501 accumulated the most pyruvate yielding 0.094 ± 0.012 Cmol Cmol^{-1}. Strain H16-501-p414 also accumulated pyruvate yielding 0.041 Cmol Cmol^{-1} that is significantly less than strain H16-501. Notably, no statistically significant difference in (*R*)-1,3-BDO yields is observed between strains H16-501-p414 and H16-501-p402, indicating Bld as primary limitation of the pathway. Evidently, only a single chromosomal-based copy of *yqhD*$_{Ec}$ is sufficient to convert (*R*)-3-hydroxybutanal to (*R*)-1,3-BDO.

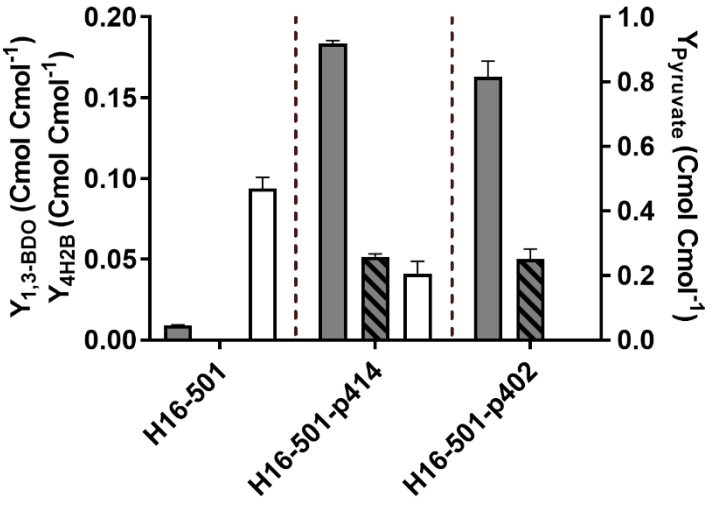

Figure 5.1 Screening strain H16-501 transformed with pJLG414 or pJLG402 increasing *bld* or *bld* and *yqhD*$_{Ec}$ gene copy number for (*R*)-1,3-BDO biosynthesis *via* the (*R*)-3HBCoA-dependent pathway. Grey bars represent (*R*)-1,3-BDO, striped bars represent 4H2B and white bars represent pyruvate. Cells were cultivated in 10 mL NLMM in 50 mL falcon tubes for 120

h after addition of L-arabinose to a final concentration of 0.05 % (w/v). Error bars represent standard error calculated from three biological replicates.

During protein analysis of strain H16ΔC-p446 containing *yqhD*$_{Ec}$, *dra* and *PDC*, relatively low synthesis of Dra was observed, indicating potential limitation in the pyruvate-dependent (*R*)-1,3-BDO pathway (Figure 4.11). Also, accumulation of pyruvate is significantly reduced in strains expressing *PDC*, indicating efficient conversion to acetaldehyde by PDC. This supports the hypothesis *dra* expression is the most likely limiting factor in the pyruvate-dependent pathway. To confirm this, the copy number of *dra* was increased in strain H16-502 through transformation with pJLG502 (H16-502-p502) assembled to contain *dra* downstream of the arabinose inducible system. Strains H16-502 and H16-502-p502 were then screened through cultivation in NLMM supplemented with 2 % (w/v) sodium gluconate for 120 h (Figure 5.2).

From HPLC analysis, strain H16-502-p502 yielded 0.002 ± 0.001 Cmol Cmol^{-1} (*R*)-1,3-BDO, with no detectable levels produced by strain H16-502. Yield of by-product ethanol was for both H16-502 and H16-502-p502. However, statistically lower acetate yield was seen by strain H16-502-p502 reaching 0.112 ± 0.018 Cmol Cmol^{-1} compared to H16-502-502 producing 0.193 ± 0.019. Thus, an increase in *dra* copy number appears to increase conversion of acetaldehyde to (*R*)-3-hydroxybutanal for subsequent conversion to detectable levels of (*R*)-1,3-BDO. This is further supported by a reduction in accumulated acetate, most likely due to natural conversion of pathway intermediate acetaldehyde by native *C. necator* H16 enzymes.

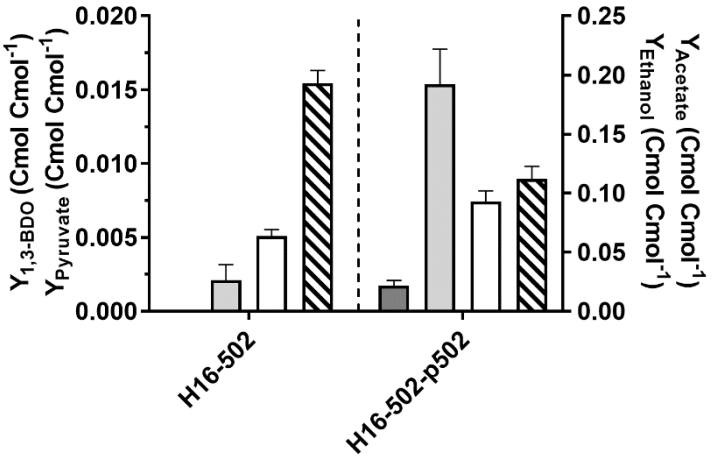

Figure 5.2 Screening chromosomally integrated strain H16-502 transformed with pJLG502 to increase *dra* copy number for (*R*)-1,3-BDO biosynthesis *via* the pyruvate-dependent pathway. Dark grey bars represent (*R*)-1,3-BDO, light grey bars represent pyruvate, white bars represent ethanol and striped bars represent acetate. Cells were cultivated in 10 mL NLMM in 50 mL falcon tubes for 120 h after addition of L-arabinose to a final concentration of 0.05 % (w/v). Error bars represent standard error calculated from three biological replicates.

Increasing copy number of *bld* or *dra* significantly improved (*R*)-1,3-BDO yields by strains H16-501 and H16-502, respectively. To assess the effect of increasing gene copy number of *bld* or *bld* and *dra* within a strain utilising both (*R*)-3HBCoA-dependent and pyruvate-dependent pathways, strain H16-503 was transformed with pJLG414 containing *bld* or plasmid pJLG501 containing *bld* and *dra* downstream of the arabinose inducible system (H16-503-p414 and H16-503-p501, respectively). Transformed strains H16-503-p414 and H16-503-p501 and the control strain H16-503 were subsequently screened for (*R*)-1,3-BDO (Figure 5.3).

Upon screening, strains H16-503-p414 and H16-503-p501 yielded 0.122 ± 0.012 and 0.146 ± 0.05 Cmol Cmol^{-1} (*R*)-1,3-BDO after 120 h of cultivation, respectively. The control strain H16-503 yielded 0.004 ± 0.002 Cmol Cmol^{-1}. Clearly increasing copy

number of *bld* greatly increases (*R*)-1,3-BDO yield. Also, there is no accumulation of by-product acetate by strains H16-503-p414 and H16-503-p501, presumably due to re-direction of carbon flux towards (*R*)-1,3-BDO.

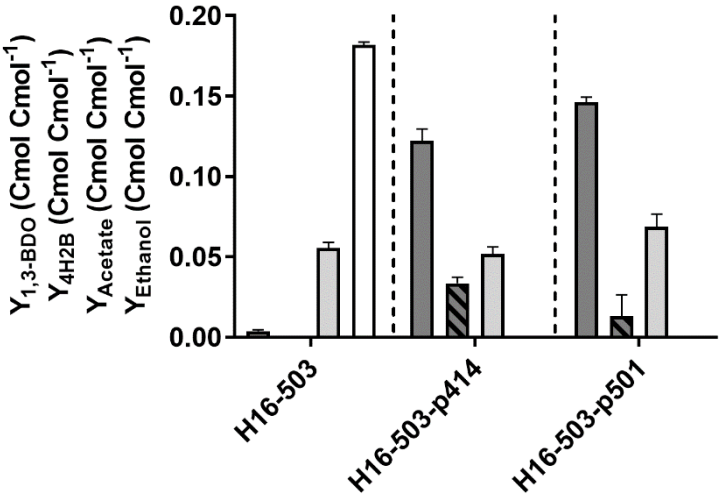

Figure 5.3 Screening chromosomally integrated strain H16-503 transformed with pJLG414 or pJLG501 for (*R*)-1,3-BDO biosynthesis *via* both the (*R*)-3HBCoA-dependent and pyruvate-dependent pathways. Dark grey bars represent (*R*)-1,3-BDO, striped bars represent 4H2B, light grey bars represent ethanol and white bars represent acetate. Cells were cultivated in 10 mL NLMM in 50 mL falcon tubes for 120 h after addition of L-arabinose to a final concentration of 0.05 % (w/v). Error bars represent standard error calculated from three biological replicates.

From the (*R*)-1,3-BDO yields achieved by the pyruvate-dependent pathway, it is evident there are limitations impacting (*R*)-1,3-BDO biosynthesis. Indeed, strain H16-502-p502 yielded only 0.002 ± 0.001 Cmol Cmol^{-1} (*R*)-1,3-BDO, with strain H16-503-p414 and H16-503-p501 achieving significantly higher yields using when increasing gene copy number of pathway-limiting enzyme. However, as observed previously, introducing the pyruvate-dependent pathway results in efficient conversion of pyruvate to acetaldehyde facilitated by PDC. This typically results in a marginal improvement

of (*R*)-1,3-BDO biosynthesis compared to strains utilising only the (*R*)-3HBCoA-dependent pathway. Therefore, only strains utilising the (*R*)-3HBCoA-depdentent pathway or both the (*R*)-3HBCoA-dependent and pyruvate-dependent pathway were employed for further development.

5.3.3 Increasing copy number of chromosomally integrated heterologous genes to improve (*R*)-1,3-BDO yields

It was postulated an extra copy of genes *bld* and *dra* encoding pathway-limiting enzymes Bld and Dra could be integrated into the *sucCD* locus to improve (*R*)-1,3-BDO yields. This would result in simultaneous doubling of gene copy number and an increase in acetyl-CoA and pyruvate pool available for (*R*)-1,3-BDO biosynthesis. To achieve this, strains H16-501 (Δ*phaC1::bld, yqhD*$_{Ec}$) and H16-503 (Δ*phaC1::bld, yqhD*$_{Ec}$*, dra, PDC*) were used to construct strains H16-504 (Δ*phaC1::bld, yqhD*$_{Ec}$; Δ*sucCD::bld*) and H16-505 (Δ*phaC1::bld, yqhD*$_{Ec}$*, dra, PDC;* Δ*sucCD::bld, dra*) by integrating a second copy of *bld* or *bld* and *dra* into the *sucCD* locus, respectively. Genes *dra* and/or *bld* were integrated downstream of a previously reported strong constitutive promoter (P_8) to achieve high levels of expression (Alagesan *et al.*, 2018). Strains H16-501, H16-503, H16-504 and H16-505 were then screened to investigate (*R*)-1,3-BDO yields and pathway by-products (Figure 5.4). For strains H16-501 and H16-504 utilising only the (*R*)-3HBCoA-dependent pathway, (*R*)-1,3-BDO yields of 0.009 ± 0.001 and 0.010 ± 0.003 Cmol Cmol^{-1} were achieved, respectively. For strains utilising both the (*R*)-3HBCoA-depdentent and pyruvate-dependent pathways, H16-503 and H16-505 yielded 0.004 ± 0.002 and 0.012 ± 0.009 Cmol Cmol^{-1} (*R*)-1,3-BDO, respectively. From the results, when comparing (*R*)-1,3-BDO yields, it is apparent increasing *dra* and/or *bld* copy number in conjunction with *sucCD* gene deletion has no

statistically significant effect when cells are cultivated under heterotrophic conditions. Notably, pyruvate accumulation decreased in strain H16-504, despite Δ*sucCD* potentially increasing acetyl-CoA pool and may cause of detectable levels of 4H2B that was not observed for strain H16-501.

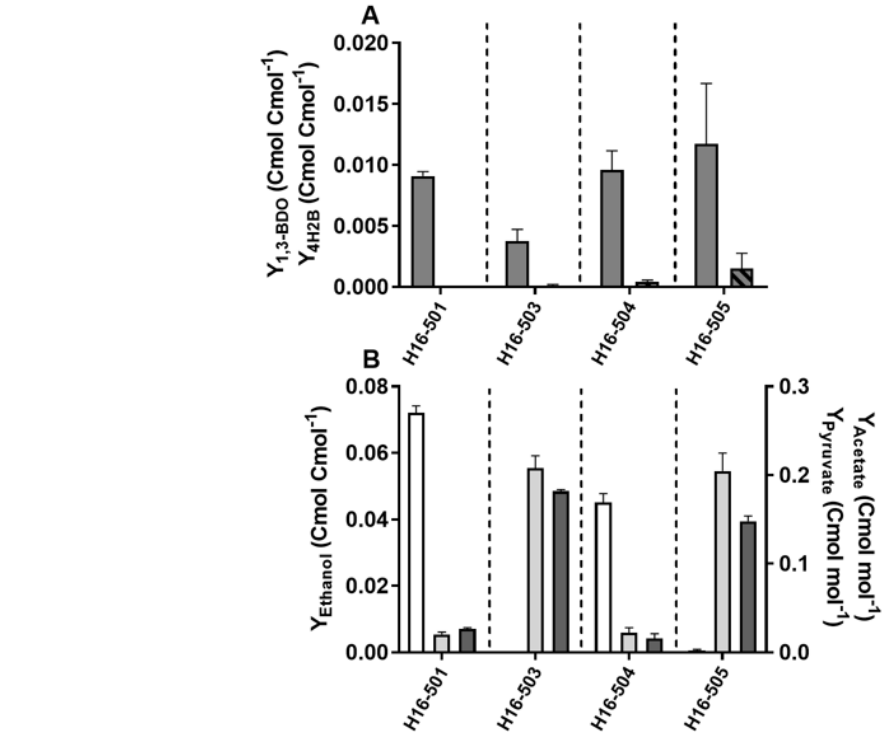

Δ*phaC::P[bld, yqhD$_{Ec}$]*	+	-	+	-
Δ*phaC::P[bld, yqhD$_{Ec,}$ dra, PDC]*	-	+	-	+
Δ*sucCD::P$_{δ}$[bld]*	-	-	+	-
Δ*sucCD::P$_{δ}$[bld, dra]*	-	-	-	+

Figure 5.4. Metabolite profiles for strains H16-501, H16-503, H16-504 and H16-505 screened in 50 mL falcon tubes for stable (*R*)-1,3-BDO production. Cells were cultivated for 120 h in 10 mL NLMM supplemented with 2 % (w/v) sodium gluconate. (A) Solid bars represent (*R*)-1,3-BDO and striped bars represent 4H2B carbon yields. (B) White bars represent pyruvate, light grey bars represent ethanol and dark grey bars represent acetate carbon yields. Error bars represent standard error from three biological replicates.

5.3.4 Autotrophic fermentation of *C. necator* H16 for (*R*)-1,3-BDO production

To evaluate production of (*R*)-1,3-BDO from CO_2, engineered *C. necator* H16 strains H16-501, H16-503, H16-504 and H16-505 were subjected to autotrophic fermentation. This was undertaken through batch fermentation where cells were cultivated in 750 mL FMM supplemented with addition of 0.1 % (w/v) L-arabinose to induce gene expression in 1.2 L bioreactors. A gas mixture composed of 3% CO_2, 19% air and 78 % H_2 (Bommareddy *et al.*, 2020) was continuously supplied to the bioreactors. Dissolved oxygen was maintained at 10 % (v/v) by increasing impeller agitation speed and air flow rate. Samples were taken every 12 h for 120 h for HPLC analysis and gas composition leaving the bioreactor was analysed to determine (*R*)-1,3-BDO production rate from CO_2, (*R*)-1,3-BDO titres and by-product titres (Figure 5.5).

Strain H16-504 containing extra copy of *bld* achieved highest overall production rate of 0.41 Cmol Cmol^{-1} h^{-1} between 48 and 60 h, an 8-fold increase compared with strain H16-501 reaching 0.05 Cmol Cmol^{-1} h^{-1}. Strain H16-505 also saw large increase in yield compared with H16-503, yielding 0.27 and 0.07 Cmol Cmol^{-1} h^{-1} (*R*)-1,3-BDO (48 – 60 h), respectively. Contrary to heterotrophic cultivation of identical strains, increased availability of key pathway enzymes Dra and/or Bld considerably improves (*R*)-1,3-BDO titres and carbon yields. Strains H16-504 and H16-505 with *sucCD* deletion exhibited slower growth rate when compared with strains H16-501 and H16-503, respectively. This may be attributed to reduced ATP production during conversion of succinyl-CoA to succinate. As previously observed, pyruvate is the main by-product of the (*R*)-3HBCoA-dependent pathway and accumulation is increased in strain H16-504 compared with strain H16-501. However, detectable levels of pyruvate are not observed for strains containing the pyruvate-dependent pathway, presumably due to

utilisation of pyruvate for (*R*)-1,3-BDO production. Notably, strains containing both the (*R*)-3HBCoA-dependent and pyruvate-dependent pathways exhibit initially high production of acetate (0 – 48 h), with later stages seeing increase in ethanol production. This activity corresponds with increased biomass, depleting excess oxygen demonstrating preference for acetate production in oxygen rich environment and preference for ethanol production in oxygen limiting conditions.

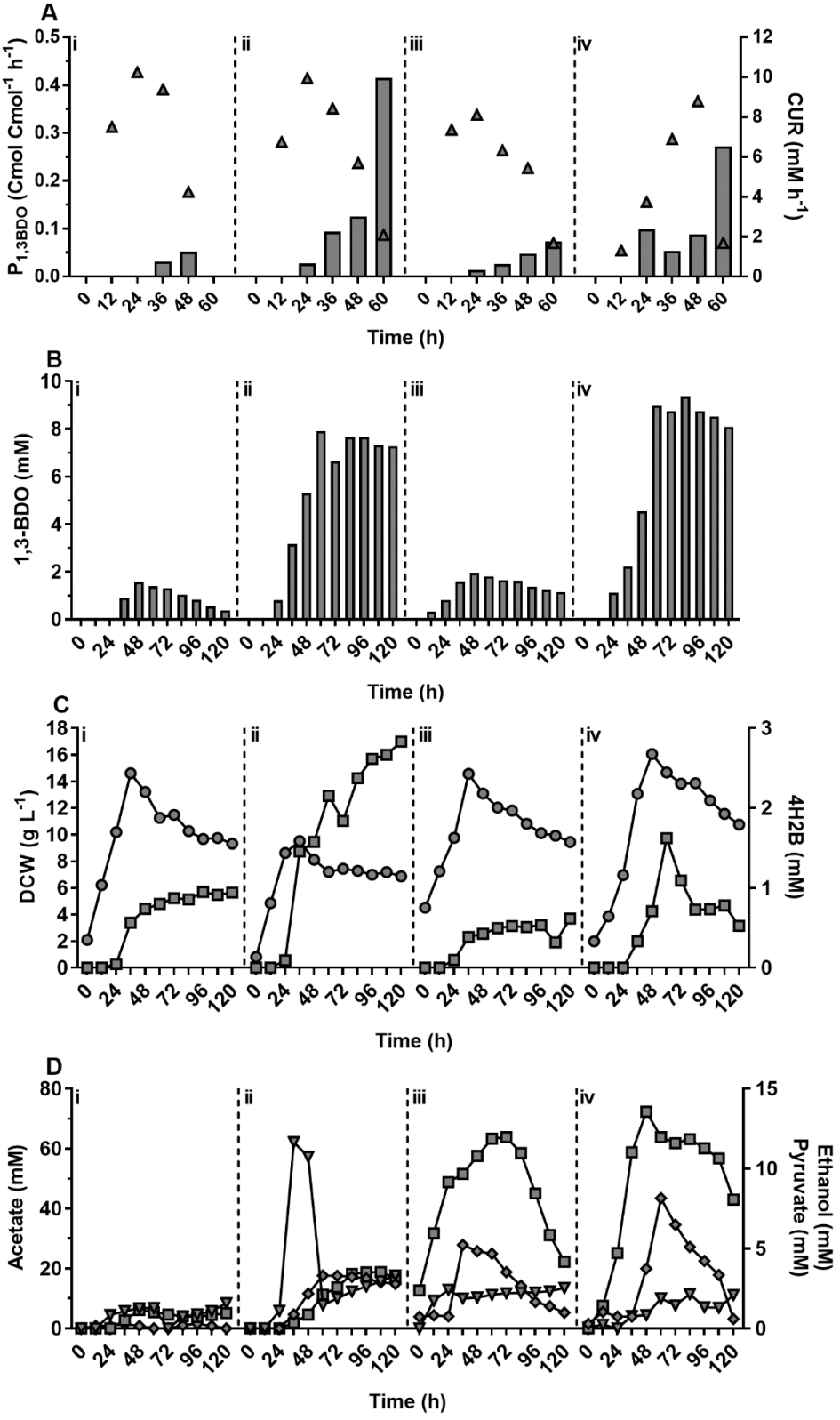

Figure 5.5 Batch autotrophic fermentation of strains i. H16-501, ii. H16-504, iii. H16-503 and iv. H16-505 for production of (*R*)-1,3-BDO from CO_2. Strains contained either single or

double copy of chromosomally integrated genes encoding pathway-limiting enzymes Bld or Dra in combination with *sucCD* and/or *phaC* gene deletions. Bars represent (*R*)-1,3-BDO production rate (P) calculated from carbon uptake rate (CUR) represented by triangles (A). Titres shown: bars represent (*R*)-1,3-BDO titres (B), circles represent biomass (DCW, g L^{-1}) and squares represent 4H2B (C), upside down triangles represent pyruvate, squares represent acetate and diamonds represent ethanol (D).

During earlier stages of strain development, engineered strains H16-501-p414 and H16-503-p501 achieved overall highest (*R*)-1,3-BDO yields so far when cultivated heterotrophically. This is most likely due to plasmid-based overexpression of *dra* and/or *bld* increasing biosynthesis of pathway-limiting enzymes and subsequent carbon flux towards (*R*)-1,3-BDO. Therefore, to determine strains H16-501-p414 and H16-503-p501 were fermented under autotrophic conditions to investigate optimisation of integrated chassis towards fermentation for continuous (*R*)-1,3-BDO production (Figure 5.6).

During fermentation, strain H16-501-p414 achieved the highest (*R*)-1,3-BDO titre at 33 mM with a production rate of 0.77 Cmol $Cmol^{-1}$ h^{-1} between 72 and 84 h after addition of L-arabinose to the media to induce gene expression. Furthermore, 4H2B production also achieved high titres at 19.7 mM with a production rate of 0.57 Cmol $Cmol^{-1}$ h^{-1} between 72 and 84 h. Notably, 4H2B titre increases during later time-points, indicating insufficient conversion of acetoacetyl-CoA to 3-hydroxybutanal facilitated by PhaB. During autotrophic fermentation of H16-501-p414, no other by-products, namely pyruvate, ethanol or acetate were detected, indicating significantly increased carbon flux towards (*R*)-1,3-BDO and 4H2B as cells being to reach stationary phase. However, a significant proportion of carbon is used to reach high cell densities of >9.5

g L^{-1} DCW prior to (*R*)-1,3-BDO production. Furthermore, (*R*)-1,3-BDO titres reach approximately maximum after 84 h production, suggesting another limitation is placed on the system, such as reduced activity of pathway enzymes or depletion of reducing power in form of NADPH. It should be noted H16-503-p501 demonstrated significantly impaired growth and no detectable levels of (*R*)-1,3-BDO or other metabolites (data not shown), despite successful production of (*R*)-1,3-BDO during fermentation by H16-501-p414 handled in identical manner. This is most likely due to plasmid loss rendering the cells no longer viable, demonstrating genetic stability is key for continuous fermentation of *C. necator* H16.

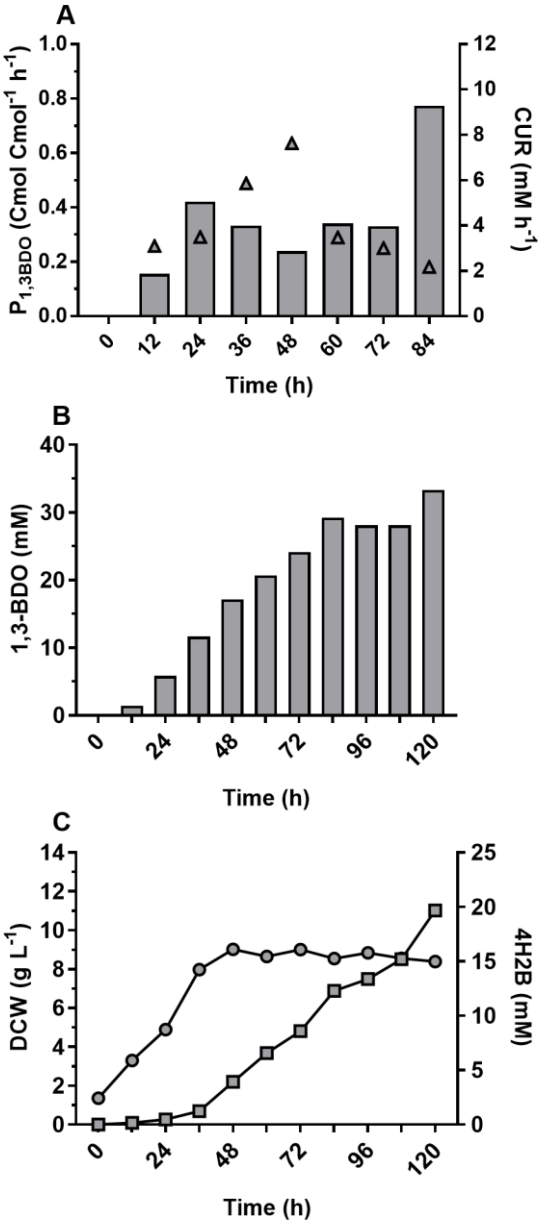

Figure 5.6 Autotrophic fermentation of strain H16-501-p414 cultivated in a bioreactor for production of (*R*)-1,3-BDO. Introduction of plasmid-based *bld* (pJLG414) increases gene copy number in strain H16-501 to identify limitations in chromosomally integrated strains. Bars represent (*R*)-1,3-BDO production rate (P) calculated from CUR represented by triangles. (A). Titres shown: bars represent (*R*)-1,3-BDO titres (B), circles represent biomass (DCW, g L^{-1}) and squares represent 4H2B (C). Pyruvate, acetate and ethanol were not detected during HPLC analysis of samples.

5.3.5 Economic feasibility of (*R*)-1,3-BDO produced using CO_2

A technoeconomic analysis (TEA) was undertaken using the BioPET tool to determine minimum estimated selling price (MESP) of large-scale production of (*R*)-1,3-BDO (10,000 tonne per annum) from CO_2 using engineered *C. necator* H16 as host chassis. BioPET was developed and validated by Claypool and Raman and allows process modelling of bio-based chemical production (Claypool and Raman, 2013). In addition to the key parameters outlined in Section 5.2.6, BioPET requires productivity, titre and yield to calculate MESP. Therefore, MESP was calculated using data generated in this study for production of (*R*)-1,3-BDO by strains H16-504, H16-505 and H16-501-p414 using CO_2 as the sole carbon source (Table 5.5).

Table 5.5 Minimum estimated selling price for (*R*)-1,3-BDO produced by engineered *C. necator* H16 strains cultivated under autotorophic conditions

Strain	Productivity g L^{-1} h^{-1}	Titre g L^{-1}	Yield g g^{-1}	MSP ($/kg)
H16-504	0.012	0.71	0.041	112,790.31
H16-505	0.013	0.81	0.050	95,843.65
H16-501-p414	0.030	2.63	0.17	31,847.72

Evidently, it can be seen that higher productivity and titres of (*R*)-1,3-BDO correlate to a lower MESP $ kg^{-1} value, with production by strain H16-501-p414 resulting in the lowest MESP of $31,847.72 USD kg^{-1}. From the BioPET tool, CO_2 is the single largest cost contributing to 54 % of MESP for production of (*R*)-1,3-BDO by strain H16-501-p414.

5.4 Discussion

Microbial production of (*R*)-1,3-BDO has been previously achieved using *E. coli* as host chassis with glucose as the carbon source. First (*R*)-1,3-BDO bioproduction reports utilised acetyl-CoA as a pathway pre-cursor and cells were fermented in rich media supplemented by feeding of glucose (Kataoka *et al.*, 2014). Then, Nemr and co-workers investigated an alternative pathway resulting in production of (*R*)-1,3-BDO by fermentation of cells in a defined minimal media, preferred for industrial production of chemicals due to reduced downstream processing steps required (Nemr *et al.*, 2018). This study has demonstrated ability of engineered *C. necator* strains to produce (*R*)-1,3-BDO from CO_2 by cells cultured in a defined minimal media.

Continuous fermentation of *C. necator* cells engineered to produce (*R*)-1,3-BDO from waste resources is the ultimate aim for industrialisation of strains developed in Chapter 4 requiring stable gene expression (Li *et al.*, 2014). To achieve this, *C. necator* H16 strain containing chromosomally integrated heterologous genes encoding Bld and YqhD required for production of (*R*)-1,3-BDO was assembled. Integration into the *phaC* locus allowed for the entire (*R*)-1,3-BDO operon to be expressed by the arabinose inducible system, including *C. necator* H16 *phaA* and *phaB1*. One advantage of this is better balancing of gene expression, with *phaAB1* previously under control of the relatively weak constitutive promoter P_{phaC} (Alagesan *et al.*, 2018; Johnson *et al.*, 2018). The effects of this balanced gene expression are observed by no detectable levels of 4H2B produced by strains H16-501 or H16-503. This is most like a result of decreased accumulation of acetoacetyl-CoA, suggesting improvement in expression of *phaB1*.

Moving from plasmid-based gene expression to chromosomal integration of heterologous genes significantly reduced gene copy number and subsequent (*R*)-1,3-BDO yield achieved by strains H16-501, H16-502 or H16-503. However, this did allow for identification of pathway-limiting enzymes that was investigated by increasing gene copy number through plasmid-based overexpression that also significantly increased (*R*)-1,3-BDO yield. Indeed, increasing gene copy number to improve (*R*)-1,3-BDO yields has been reported previously (Nemr *et al.*, 2018). Upon analysis, Bld was found to be the primary enzyme within the (*R*)-3HBCoA-dependent pathway and Dra was found to be the primary limiting enzyme within the pyruvate-dependent pathway. Notably, to improve pyruvate-dependent pathway (*R*)-1,3-BDO yield in *E. coli*, PDC was mutated to reduce enzymatic activity and two plasmid-based copies of *dra* were utilised (Nemr *et al.*, 2018). Despite a large accumulation of pyruvate in *C. necator* H16 Δ*phaC* strains, there are clear limitations with the pyruvate-dependent pathway, with (*R*)-3HBCoA-dependent pathway becoming preferred (*R*)-1,3-BDO biosynthesis pathway. Strain H16-505 utilising both (*R*)-3HBCoA-dependent and pyruvate-dependent pathways saw a minor increase in (*R*)-1,3-BDO yield compared strain H16-504 utilising only (*R*)-3HBCoA-dependent pathway. This is most likely due to an increase in pyruvate precursor as a result of reduced TCA flux caused by *sucCD* gene deletion.

Fermentation of *C. necator* strains H16-501, H16-503, H16-504 for production of (*R*)-1,3-BDO produced from CO_2 is the first step towards engineering a stable strain for continuous bioproduction. Furthermore, fermentation allows for constant monitoring and control of pH, DO and continuous supply of carbon source, particularly when compared to shake-flask cultivations. During fermentation cells are able to reach a high

DCW achieving >9.5 g L^{-1} after 36 h, much higher than shake-flask cultivations, presumably due to constant supply of carbon and energy sources. From the data, production of the majority of biomass is followed by a decrease in CUR and increase in (*R*)-1,3-BDO production. As the cells enter the stationary phase of during fermentation, there is optimal production of (*R*)-1,3-BDO. Biomass production becomes limited due to complete consumption of a key media element, most likely nitrogen, resulting in carbon flux being re-directed from biomass towards (*R*)-1,3-BDO. By limiting the supply of nitrogen, biomass can be controlled and exploited for increased yields (Section 4.3.3).

To further understand autotrophic production of (*R*)-1,3-BDO by engineered *C. necator* H16, strains H16-501-p414 and H16-503-p501 were subjected to fermentation. Strain H16-501-p414 achieved the highest yields and titres of all developed strains. Evidently, the majority of (*R*)-1,3-BDO is produced within 24 h period following the cells entering stationary phase, with little to no further production during later time points. For strain H16-501-p414 to exhibit this trait, there are two potential reasons, pathway enzyme activity is reduced, that is supported by increase in production of 4H2B suggesting reduction in PhaB1 activity. Or, reducing power in form of NADPH within the cells is depleted as the reductive pathway for (*R*)-1,3-BDO bioproduction competes with the CBB cycle that also requires a significant amount of reducing power for fixation of CO_2.

When developing production processes with industrial relevance, economic feasibility of the product plays a substantial role in scale-up and subsequent commercialisation. In this study, a TEA indicated production of (*R*)-1,3-BDO by strain H16-501-p414 is economically feasible, with an MESP of $31,847.72 USD kg^{-1} comparable to market

price of 95 % (*R*)-1,3-BDO at ~$43,500 USD kg^{-1} (Sigma-Aldrich, 2022). Whilst the BioPET model employed for MESP calculation was validated against previous reports and alternative TEA tool SuperPro Designer®, several assumptions and limitations are made within the model to allow MESP to be generated at the early-stage of process development, relying on definition of key parameters, rather than generated data.

Furthermore, seemingly only possible economically feasible strain saw deployment of plasmid-based *bld* allowing for highest titres, with strains with chromosomally integrated (*R*)-1,3-BDO pathway-related genes in strains H16-504 and H16-505 seeing MESP >2-fold higher than market price. Whilst utilising a plasmid-based system increases titres, further strain is placed on the overall with regards to potential industrial scale-up, including requiring antibiotics as well as batch fermentation for production.

5.5 Conclusion

To conclude, in this study, genetically stable *C. necator* H16 strains required for reliable (*R*)-1,3-BDO production were developed through chromosomal integration of 1,3-BDO biosynthetic pathway genes. Utilizing engineered *C. necator* H16, it has been demonstrated a sustainable production of (*R*)-1,3-BDO from CO_2 as the sole carbon source. (*R*)-1,3-BDO yields have been further improved by increasing a copy number of genes encoding pathway-limiting enzymes. The engineered and genetically stable *C. necator* H16 strains can potentially be utilized for continuous autotrophic (*R*)-1,3-BDO fermentation.

6 Investigating transhydrogenase influence on NAD(P)H co-factor supply in *C. necator* H16 using model diol production system

6.1 Introduction

The biosynthesis of compounds such as chiral alcohols and PHA's requires co-factors such as nicotinamide adenine dinucleotide (NAD) or nicotinamide adenine dinucleotide phosphate (NADP) in their reduced form (NADH and NADPH, respectively) to aid oxidoreductase enzymatic activity on pathway intermediates (Weckbecker and Hummel, 2004; Sanchez *et al.*, 2006). Arguably, efficient regeneration of co-factor(s) can be a crucial aspect when developing a strain for production of an energy-intensive compound. Previous studies have reported various methods of engineering intracellular redox metabolism to improve product yield; A) overexpression of co-factor regeneration systems including *E. coli* soluble transhydrogenase UdhA (Jan *et al.*, 2013) and *E. coli* NAD kinase encoded by *yfjB* (Li *et al.*, 2009); B) modification of alcohol dehydrogenase YqhD co-factor preference from NADPH to NADH through saturation mutagenesis (Wu *et al.*, 2016); and C) modification of malic enzyme co-factor preference from NAD to synthetic co-factor nicotinamide flucytosine dinucleotide (NFD), also achieved by saturation mutagenesis (Ji *et al.*, 2011).

As previously reported, *C. necator* H16 is able to accumulate up to 90 % (w/w) of DCW in form of P3HB through conversion of acetyl-CoA to acetoacetyl-CoA by β-ketothiolase (PhaA), reduction of acetoacetyl-CoA to (*R*)-3-hydroxybutyruly-CoA by NADP-dependent acetoacetyl-CoA reductase (PhaB1) and polymerisation by poly(3-hydroxyalkonoate) polymerase (PhaC2) (Lindenkamp, Volodina and Steinbüchel, 2012). To achieve high P3HB yields, regeneration of reducing power in form of

NADPH is crucial. Several activities can contribute to the availability and balance of $NAD(P)^+$ and NAD(P)H pools in *C. necator* H16 including the following enzyme complexes: one membrane-bound [NiFe]-hydrogenase encoded by *hoxKGZ*; one soluble hydrogenase encoded by *hoxFUHY*; one large membrane-bound Type I NADH dehydrogenase encoded by *nuoABCDEFGHIJKLMN*; one Type II NADH dehydrogenase encoded by *ndh*; and four proton-translocating membrane-bound transhydrogenase's encoded by *pntAaAbB1*, *pntAaAbB2*, *pntAaAbB3* and *pntAB4* (hereafter denoted as *pntAB1234*).

Energy-dependent membrane-bound proton translocating transhydrogenases PntAB1234 facilitate transfer of electrons between NAD^+ and $NADPH^+$ by a process that is coupled to the proton translocation across the membrane ($[NADP^+] + [NADH] + [H^+_{out}] \leftrightarrow [NADPH] + [NAD^+] + [H^+_{in}]$). Furthermore, a membrane-bound transhydrogenase in *E. coli* MG1655 ($PntAB_{Ec}$) is reported to drive regeneration of NADPH by reduction of $NADP^+$ (Sauer *et al.*, 2004; Spielmann, Baumgart and Bott, 2019). In *C. necator* H16 membrane-bound transhydrogenase activity has been detected when cultivated under heterotrophic conditions demonstrating faster oxidisation of NADH than NADPH (Jones *et al.*, 1975) suggesting a similar function to $PntAB_{Ec}$. However, *C. necator* H16 PntAB1234 functionality has not been characterised when cultivated under autotrophic conditions.

Other *C. necator* H16 enzymes involved in central carbon metabolism and capable of contributing to the $NAD(P)^+$/NAD(P)H balance include: three glutamate dehydrogenases (GD) encoded by *gdhA12* (NADP-dependent); gluathionine reductase encoded by *lpdaA* (NADP-dependent); three glucose-6-phosphate 1-dehydrogenases (G6PD) encoded by *zwf123* (NADP-dependent), three isocitrate dehydrogenases

encoded by *icd12* (NADP-dependent) and *icd3* (NAD-dependent) (Obruca *et al.*, 2013); two malate dehydrogenases encoded by *maeA* (NAD-dependent) and *maeB* (NADP-dependent) (Bruland *et al.*, 2010); three glyceraldehyde-3-phosphate dehydrogenases (GAPD) encoded by *gapA*, *cbbG2* and *cbbGp* (NAD-dependent) (Pohlmann *et al.*, 2006) and L-lactate dehydrogenase encoded by *ldh* (NAD-dependent) (Jendrossek, Kratzin and Steinbüchel, 1993).

One platform chemical that has been extensively studied for microbial fermentation and biosynthesis is 2,3 BDO. There are three different stereoisomers of 2,3-BDO: (*S, S*)-2,3-BDO, (*R, R*)-2,3-BDO and *meso*-(2,3)-BDO and biosynthesis from the precursor requires energy in the form of NAD(P)H as a co-factor. The chemical 2,3-BDO is commonly used as a component in antifreeze or for conversion to 1,3-butadiene, an organic intermediate for synthetic rubber (Białkowska, 2016). Of the four butanediol structural isomers (1,2-BDO, 1,3-BDO, 1,4-BDO and 2,3-BDO), biosynthesis of 2,3-BDO is the most widely researched and understood. Indeed, several reviews summarise metabolic engineering strategies for improving 2,3-BDO yield in non-modified microorganisms, as well as strains expressing heterologous genes for biosynthesis of different 2,3-BDO stereoisomers (Sun *et al.*, 2015; Hakizimana, Matabaro and Lee, 2020; Ji, Huang and Ouyang, 2011). Notably, productivity of 2,3-BDO by engineered *Saccharomyces cerevisiae* was improved from 0.26 g/L h^{-1} to 0.44 g/L h^{-1} as a direct result of NAD^+ regeneration facilitated by heterologous expression of water-forming NADH oxidase encoded by *noxE* from *Lactococcus lactis* (Kim and Hahn, 2015) demonstrating importance of cellular redox balancing when engineering cells to produce chemicals *via* energy intensive pathways.

C. necator H16 has been engineered to produce acetoin, a key 2,3-BDO pathway intermediate, achieving acetoin yields of 0.42 Cmol $Cmol^{-1}$ from fructose and >1 Cmol $Cmol^{-1}$ from CO_2 (Windhorst and Gescher, 2019). This was achieved through heterologous expression of *B. subtilis* acetolactate dehydrogenase and acetolactate decarboxylase encoded by codon optimised *alsS* and *alsD*. To improve the yield, *C. necator* H16 genes *acoABC* encoding genes facilitating acetoin consumption and *phaC12* encoding poly(3-hydroxyalkanoate) polymerase homologues PhaC1 and PhaC2 were deleted, increasing carbon flux toward acetoin.

Recently, heterotrophic and continuous autotrophic production of (*R, R*)-2,3-BDO by implementation of synthetic metabolic pathway has been reported in *C. necator* H16 (Bommareddy *et al.*, 2020). Heterologous expression of acetolactate dehydrogenase and acetolactate decarboxylase encoded by codon optimised *B. subtilis alsSD* combined with NADP-dependent secondary-alcohol dehydrogenase encoded by codon optimised by *adh* from *Clostridium beijerinckii* enabled conversion of acetoin to stereoisomer (*R, R*)-2,3-BDO. To increase carbon flux towards 2,3-BDO biosynthesis pathway, acetoin consumption genes *acoXABC* and P3HB producing operon *phaCAB* were deleted. (*R, R*)-2,3-BDO yields of 0.16 ± 0.002 Cmol $Cmol^{-1}$ from fructose and 0.21 ± 0.003 Cmol C-mol^{-1} from CO_2 were achieved by strains expressing chromosomally integrated 2,3-BDO pathway genes (Bommareddy *et al.*, 2020).

In this chapter, the role of four proton-translocating membrane-bound transhydrogenases present in *C. necator* H16 genome has been investigated. A *C. necator* H16 mutant strain was generated by subsequently deleting all transhydrogenase gene. The transhydrogenase minus strain was engineered by introducing biosynthetic pathways enabling *C. necator* H16 to produce one of two 2,3-BDO stereoisomers;

either *meso*-2,3-BDO or (*R, R*)-2,3-BDO. Strain specific growth rate, acetoin yield and 2,3-BDO yield have been evaluated to determine effect on NAD(P)H availability in transhydrogenase deleted strains. Furthermore, role of *E. coli* soluble transhydrogenase UdhA in cell metabolism was determined. The transcriptome analysis of transhydrogenase negative and positive strains containing (*R, R*)-2,3-BDO biosynthesis pathway was conducted to investigate the transhydrogenase's role in the cellular metabolism under autotrophic conditions.

6.2 Materials and Methods

6.2.1 Gene sequences and codon optimisation

The sequences of *C. necator* H16 transhydrogenase genes were retrieved from Genbank under the following accession numbers/locus tags: CAJ91997/H16_A0850 (*pntAa1*), CAJ91998/H16_A0851 (*pntAb1*), CAJ91999/H16_A0852 (*pntB1*), CAJ92404/H16_A1264 (*pntAa2*), CAJ92405/H16_A1265 (*pntAb2*), CAJ92406/H16_A1266 (*pntB2*), CAJ94203/H16_A3128 (*pntAa3*), CAJ94204/H16_A3129 (*panD*), CAJ94205/H16_A3130 (*pntAb3*), CAJ94206/H16_A3131 (*pntB3*), CAJ96500/H16_B1715 (*pntA4*), CAJ96499/H16_B1714 (*pntB4*).

The sequences of *E. coli* MG1655 transhydrogenase genes were retrieved from Genbank under the following accession numbers/locus tags: NP_416120/b1603 (*pntA*), NP_416119/b1602 (*pntB*), NP_418397/b3962 (*udhA*)

The sequences of genes for 2,3-BDO biosynthesis operon were retrieved from Genbank under the following accession numbers/locus tags: NP_391482/BSU_36010, NP_391481/BSU_36000 (*alsS* and *alsD* from *Bacillus subtilis* 168); AAA23199 (*adh*

from *Clostridium beijerinckii*), KPR_3097/WP_004145378 (*budC* from *Klebsiella pneumoniae* subsp. rhinoscleromatis SB3432). Genes *alsS, alsD, budC,* and *adh* were codon optimised for *C. necator* H16 and synthesised (GeneArt, Thermo Fisher Scientific, Waltham, MA, USA). All codon optimised DNA sequences are listed in Section 9.1.

The sequences of *C. necator* H16 reference genome were retrieved from Genbank under the following accession numbers/locus tags: NC_008313 (chromosome 1), NC_008314 (chromosome 2), NC_005241 (megaplasmid pHG).

6.2.2 Primers used in this study

All primers used in this study are listed in Table 6.1.

Table 6.1. Primers used in this study.

Name	**Sequence 5' to 3'**
pntA1_UP_F	ACGTCCTGCGTTGACTCCG
pntA1_Sac_F	ATATGAGCTCCTTCACGCCTGGGGCACGCGTG
pntA1_OVL_R	CGGTCTTCGTCGGGATCAGTCTTGCATATCGATAGATCC CCTTGCACcg
pntB1_OVL_F	cGGTGCAAGGGGATCTATCGATATGCAAGACTGATCCCG ACGAAGACCG
pntB1_Pac_R	TATATTAATTAAGTCGACGTAGCCTTGCGCATC
pntB1_DN_R	ggAAGTGCTCGCGATCGGTG
pntA2_UP_F	GTGTTGCTGGTCGACTGATTCCAC
pntA2_Sac_F	atatGAGCTCCATGGCGTGCTGGTGTTCCg
pntA2_OVL_R	CTCCTCTGCATCGGGCTCAGGCCTGCATTTCAATCTCCTT TGGTcccgtgc
pntB2_OVL_F	GCACGGGACCAAAGGAGATTGAAATGCAGGCCTGAGCC CGATGCAGAGGAG
pntB2_Pac_R	TATATTAATTAATGGGCTCAGAGCGAGCTGACC
pntB2_DN_R	TTCTGCGTGCAGCAGCGTC
pntA3_UP_F	TGAACAGTACTCGCTGTCGTC
pntA3_Sac_F	ATATGAGCTCGCGTGTACAAGGCGTCCAGC
pntA3_OVL_R	CATGGCGCCCGTGGAAATTACGCCGCGGGATGCCGATG TACATCGTC

pntA3_OVL_F	GACGATGTACATCGGCATCCCGGCGTAATTTCCACGGGC GCCATG
pntA3_Pac_R	TATATTAATTAATACCGTCCAGACCACGTGGTAACC
pntA3_DN_R	CTGACAAGACCGGTCATCACGCAC
pntA4_UP_F	ACGATCCCATTTCTTCCAAGATcc
pntA4_Sac_F	ATATgagctcGTGTCGTCGAATATGACGGCGAC
pntA4_OVL_R	TCGACTCGACCAACTCAGGCTGGCATGGCATTCACCGTT T
pntB_OVL_F	AAACGGTGAATGCCATGCCAGCCTGAGTTGGTCGAGTC GA
pntB4_Pac_R	TATATTAATTAAAGGTCCCATAGACACCGCCC
pntB4_DN_R	AAGATGCACACGCCCTGCAG

6.2.3 Plasmids used in this study

All strains used in this study are listed in Table 3.2.

Table 6.2. Plasmids used in this study. * denotes codon optimisation. Tet^R: Tetracycline resistance

Plasmid	**Description**	**Source**
pLO3	host plasmid with Tet^R,, *sacB*, RP4 transfer ori, pBR322 ori	(Lenz and Friedrich, 1998)
pJLG601	pLO3, *pntAaAbB1* deletion vector	This work
pJLG602	pLO3, *pntAaAbB2* deletion vector	This work
pJLG603	pLO3, *pntAa3* deletion vector	This work
pJLG604	pLO3, *pntAB4* deletion vector	This work
pJLG605	pLO3, *maeB* deletion vector	This work

6.2.4 Assembly of plasmids used in this study

Detailed molecular cloning techniques are in Materials and Methods of Chapter 2.

As previously described in Chapter 4, the pLO3 suicide vector was utilised for *C. necator* H16 gene deletions. Genes were deleted through homologous recombination,

DNA regions upstream and downstream of the desired gene deletion were amplified through PCR with oligonucleotides used for amplification containing complementary regions allowing PCR fragment fusion through SOEing PCR into the multiple cloning site of the pLO3 backbone. The following plasmids were assembled by utilising this strategy.

pJLG601: homology arms upstream of *pntAa1* and downstream of *pntB1* were amplified with pntA1_Sac_F, pntA1_OVL_R and pntB1_OVL_F, pntB1_Pac_R, respectively. PCR products were then fused together using SOEing PCR with primers pntA1_Sac_F and pntB1_Pac_R. The fusion PCR product was cloned into pLO3 using restriction sites SacI and PacI.

pJLG602: homology arms upstream of *pntAa2* and downstream of *pntB2* were amplified with pntA2_Sac_F, pntA2_OVL_R and pntB2_OVL_F, pntB2_Pac_R, respectively. PCR products were then fused together using SOEing PCR with primers pntA2_Sac_F and pntB2_Pac_R. The fusion PCR product was cloned into pLO3 using restriction sites SacI and PacI.

pJLG603: homology arms upstream and downstream of *pntAa3* were amplified with pntA3_Sac_F, pntA3_OVL_R and pntA3_OVL_F, pntA3_Pac_R, respectively. PCR products were then fused together using SOEing PCR with primers pntA3_Sac_F and pntA3_Pac_R. The fusion PCR product was cloned into pLO3 using restriction sites SacI and PacI.

pJLG604: homology arms upstream of *pntA4* and downstream of *pntB4* were amplified with pntA4_Sac_F, pntA4_OVL_R and pntB4_OVL_F, pntB4_Pac_R, respectively. PCR products were then fused together using SOEing PCR with primers pntA4_Sac_F

and pntB4_Pac_R. The fusion PCR product was cloned into pLO3 using restriction sites SacI and PacI.

6.2.5 Bacterial strains used in this study

All strains used in this study are listed in Table 6.3.

Table 6.3. Bacterial strains used in this study. Square brackets represent genes under promoter control. Gen^R: gentamicin resistance. Production of either (*R, R*)-2,3-BDO or *meso*-2,3-BDO by individual strains also represented.

Strain	**Genotype**	**(*R, R*)-2,3-BDO production**	***meso*-2,3-BDO production**	**Source**
C. necator H16	wild type, Gen^R	-	-	DSM-428
H16-601	H16, Δ*pntAaAbB1*, Δ*pntAaAbB2*, Δ*pntAa3*, Δ*pntAB4*	-	-	This work
H16-602	H16, Δ*acoXABC*, Δ*phaCAB::*P_{araBAD}*[alsS alsD budC]*	-	+	Bommareddy *et al.*, unpublished
H16-603	H16, Δ*acoXABC*, Δ*phaCAB::*P_{araBAD}*[alsS alsD adh]*	+	-	(Bommareddy *et al.*, 2020)
H16-604	H16, Δ*pntAaAbB1*, Δ*pntAaAbB2*, Δ*pntAa3*, Δ*pntAB4*, Δ*acoXABC*, Δ*phaCAB::*P_{araBAD}*[alsS alsD budC]*	-	+	This work
H16-605	H16, Δ*pntAaAbB1*, Δ*pntAaAbB2*, Δ*pntAa3*, Δ*pntAB4*, Δ*acoXABC*, Δ*phaCAB::*P_{araBAD}*[alsS alsD adh]*	+	-	This work
H16-606	H16, Δ*pntAaAbB1*, Δ*pntAaAbB2*, Δ*pntAa3*, Δ*pntAB4*, Δ*acoXABC*, Δ*phaCAB::*P_{araBAD}*[alsS alsD adh udhA]*	+	-	This work

6.2.6 Alignment of multiple protein coding sequences

Web-based software Clustal Omega (Madeira *et al.*, 2019) was employed to estimate similarities/difference between multiple sequences coding for proteins of interest. Protein Multiple Sequence Alignment was undertaken with sequences identified using accession tags stated in Section 6.2.1 with Output format set to ClustalW with character counts. Alignments were visualised where '*' indicates perfect alignment; ':' indicates strong similarity and '.' indicates weak similarity. Phylogenetic trees were visualised with branch length displayed as real branch length.

6.2.7 Chemostat fermentation of *C. necator* H16

Single colonies picked from an LB agar plate were used to inoculate 10 mL LB as first seed culture and were incubated overnight at 30 °C with shaking at 200 rpm. Second seed culture of 120 mL LB in baffled shake-flask was inoculated with 1 mL of first seed culture and incubated in identical conditions overnight. 100 mL second seed culture was used to inoculate 650 mL FMM present in fermentation vessel. For continuous autotrophic fermentation of *C. necator* H16 strains fermenter vessels were prepared as described in Section 2.6 with addition of LIC100 conductivity probe (Mettler Toledo, Leicester, UK) to control vessel media volume. Once cells reached a DCW of 1.5 g L^{-1}, FMM containing arabinose to a final concentration of 0.1 % (w/v) was fed at a rate of 7 mL h^{-1}. Media containing cells was removed from the vessel at a rate determined by the conductivity probe, ensuring a minimum volume in the vessel was maintained. pH was maintained at 6.9 by addition of NH_3OH for entire duration of fermentation. Gentamicin was present in all cultures at a concentration of 10 µg mL^{-1}

to reduce risk of contamination. Samples were collected for analysis every 24 h for 312 h ensuring steady state was reached.

6.2.8 Extraction and quantification of *C. necator* H16 transcriptome

During autotrophic fermentation when cells had reached stationary phase, 2 mL of cell culture was taken. Cells were separated from liquid media by centrifugation at 16,000 ×*g* for 1 min. The supernatant was discarded, and cells were flash-frozen by submersion in liquid nitrogen for 1 min to preserve RNA. Samples were then stored at – 80 °C. The RNA was then extracted along with evaluation of quality and quantity by GENEWIZ® (Leipzig, Germany) with samples achieving RNA Integrity Number (RIN) >7 selected for further processing, indicating high quality of RNA (Jahn, Charkowski and Willis, 2008). Extracted RNA was then sequenced and a cDNA library was prepared, also by GENEWIZ®. The resulting library was mapped to *C. necator* H16 reference genome (Pohlmann *et al.*, 2006; Schwartz *et al.*, 2003). RNA-Seq data was analysed by normalisation of raw counts using the median of ratios methods represented by Equation 6.1. Estimated logarithmic fold change in RNA expression levels (FC) were calculated from log base 2 of normalised count for gene *X* present in mutant strain (X_1) divided by normalised count for gene *X* in the control strain (X_2). The FC values for *C. necator* H16 transcriptome has been deposited in the public database BioStudies (https://www.ebi.ac.uk/biostudies/) under accession number S-BSST607.

$$FC = log_2\left(\frac{X_1}{X_2}\right) \tag{6.1}$$

6.3 Results

6.3.1 Construction of transhydrogenase deletion *C. necator* H16 strains

Remarkably, *C. necator* H16 genome possesses multiple genes encoding subunits of four putative transhydrogenases (Figure 6.1B Figure 6.1C) (Pohlmann *et al.*, 2006; Hoppensack, Rehm and Steinbuchel, 1999). To investigate amino acid sequence similarity to the membrane-bound transhydrogenase characterised previously (Sauer *et al.*, 2004), multiple sequence alignments (Supplementary Figure 8, Supplementary Figure 9, Supplementary Figure 10, Supplementary Figure 11 and Supplementary Figure 12) were undertaken using protein sequences for $PntA_{Ec}$ (b1603) or $PntB_{Ec}$ (b1602) as the consensus sequences (Table 6.4). *C. necator* H16 sequences for subunits PntAB4 showed highest identity and similarity percentages to $PntAB_{Ec}$ subunit sequences, most likely due to due to lack of an α-subunit 2 for PntAB4 (Pohlmann *et al.*, 2006). Indeed, protein alignment for subunits PntAb123 and PntA4 demonstrates high homology between amino acid residues 439 to 479, indicative of similar enzymatic functionality. Therefore it can be concluded eleven coding regions express subunits for four membrane-bound proton-translocating transhydrogenase's in agreement with previous reports (Pohlmann *et al.*, 2006).

Table 6.4 Identity and similarity of *C. necator* H16 PntAa1234 or PntB1234 subunit protein sequences aligned to *E. coli* MG1655 PntA or PntB protein sequences, respectively.

***C. necator* H16 transhydrogenase subunit**	**Locus tag**	**Identity to *E. coli* PntA (%)**	**Similarity to *E. coli* PntA (%)**	**Identity to *E. coli* PntB (%)**	**Similarity to *E. coli* PntB (%)**
PntAa1	H16_A0850	44	63	-	-
PntB1	H16_A0852	-	-	49	66
PntAa2	H16_A1264	43	63	-	-

PntB2	H16_A1266	-	-	50	67
PntAa3	H16_A3128	43	62	-	-
PntB3	H16_A3131	-	-	51	68
PntA4	H16_B1715	58	73	-	-
PntB4	H16_B1714	-	-	62	74

To understand role of PntAB1234 in *C. necator* H16 metabolism, the first step was to assemble a mutant transhydrogenase negative strain. This was achieved using the gene deletion method described in Section 4.2.7 and Section 4.3.5. Employing pLO3 suicide vector-based system, transhydrogenase genes *pntAaAbB1*, *pntAaAbB2*, *pntAa3* and *pntAB4* were systematically deleted, hereafter denoted Δ*pntAB1234*. First, four strains were assembled with single transhydrogenase deletions which were then used to assemble subsequent double and triple transhydrogenase deletion strains. Next quadruple transhydrogenase deletion strain H16-601 was assembled for use in all further experimentation. It should be noted PntAB3 is encoded by three genes (*pntAa3*, *pntAb3* and *pntB3*) that flank *panD* which encodes aspartate 1-decarboxylase (Figure 6.1.B). It is suggested a transcriptional unit is formed with PntAB3 encoding genes and *panD* (Cramm, 2008) and attempts to delete *pntAbB3* were unsuccessful. However, it is reported that deletion of *pntA* subunit in *E. coli* W3110 (Chin *et al.*, 2009) or deletion of both *pntAB* subunits in *E. coli* MG1655 (Sauer *et al.*, 2004) results in a similar reduction in transhydrogenase activity, suggesting all subunits are essential to form a functioning transhydrogenase. To confirm successful deletion of *pntAB1234* from *C. necator* H16 genome, PCR was employed to amplify the regions encoding transhydrogenase's for comparison to wild type *C. necator* H16. A reduction in amplified PCR fragment from Δ*pntAB1234* strain when compared to wild type indicates deletion of targeted genes (Figure 6.1.A). A band of approximately 3.1 Kb

corresponding to expected wild type fragment (3.079 Kb) and band of approximately 2 Kb corresponding to expected gene deletion fragment (1.957 Kb) is seen in.

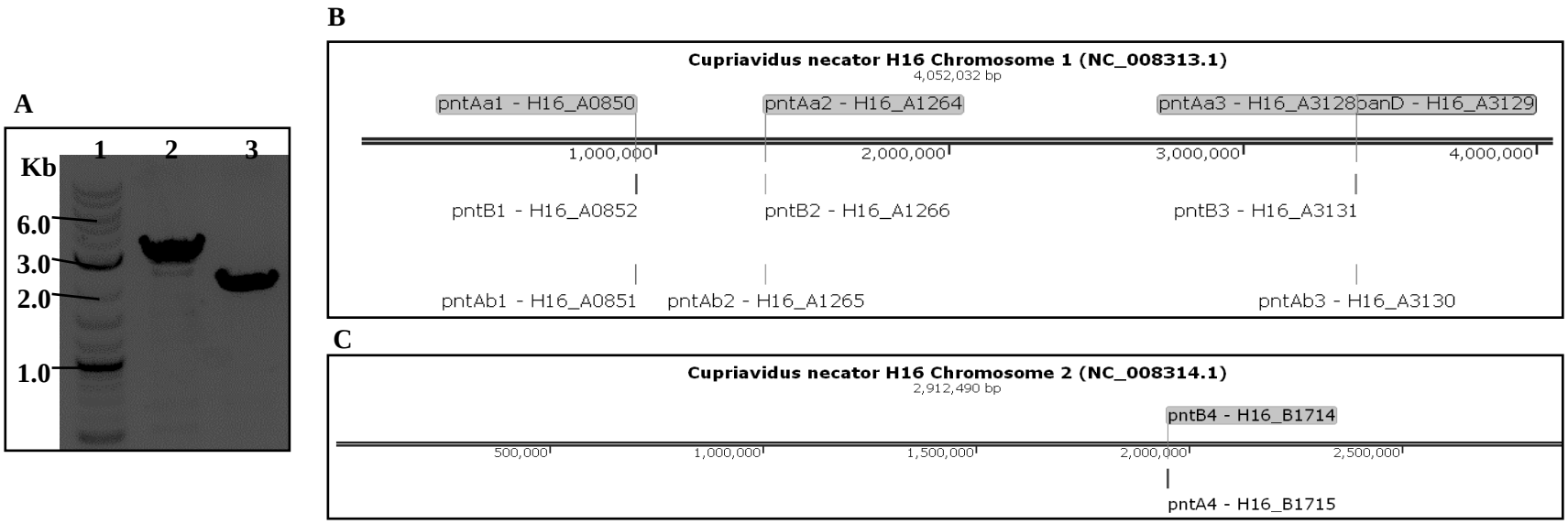

Figure 6.1 (A) Visualisation of DNA fragments amplified with Primers pntA3_UP_F and pntA3_DN_R, subsequently separated by gel electrophoresis. Wild type *C. necator* H16 strain (lane 2) was amplified for comparison with H16-601 strain (lane 3) DNA Ladder present in lane 1 was used for estimation of DNA fragment size. (B & C) Visual representation of *C. necator* H16 chromosome 1 and chromosome 2 with transhydrogenase encoding genes highlighted. PntAB123 are encoded by genes present on chromosome 1 (B). PntA1 is encoded by 3 subunits *pntAa1*, *pntAb1 pntB1;* PntAB2 encoded 3 subunits *pntAa2*, *pntAb2*, *pntB2* and PntAB3 encoded by 3 subunits *pntAa3*, *pntAb3*, *pntB3*. *pntAa3* α-subunit 1 and *pntAb3* α-subunit 2 flank *panD* encoding aspartate 1-decarboxylase. PntAB4 is encoded by 2 subunits *pntA4*, *pntB4* present on chromosome 2 (C). Chromosome images were produced with SnapGene Viewer.

To evaluate the effect of transhydrogenase gene deletions on *C. necator* H16 metabolism, wild type and Δ*pntAB1234* strain (H16-601) were compared by cultivating both strains under heterotrophic conditions. The maximum specific growth rate (μ_{max} h^{-1}) and biomass yield (DCW) were used as a metabolism efficiency indicator. For heterotrophic growth conditions, 25 mL fresh MM was inoculated to an OD_{600} of 0.1 using an overnight pre-culture. Samples were taken immediately, 12, 24, 36 and 48 h after re-suspension in fresh media. Maximum specific growth rate for both strains was observed between 0 and 12 h (Table 6.5), with no increase in biomass observed between 24 and 48 h, indicating stationary phase was reached after 24 h. Therefore, final DCW (g L^{-1}) values were calculated from samples taken after 48 h of cultivation. From the data, no statistically significant difference is observed between strains for growth rate or biomass production.

Table 6.5 Maximum specific growth rate (μ_{max}) and total biomass production by strains *C. necator* H16 and H16-601 cultivated for 48 h in 250 mL baffled shake-flasks in MM supplemented with 0.4 % (w/v) sodium gluconate and 10 µg mL^{-1} gentamicin.

Strain	**μ_{max} (h^{-1})**	**DCW (g L^{-1})**
C. necator H16	0.249 ± 0.005	0.947 ± 0.046
H16-601	0.243 ± 0.006	0.972 ± 0.039

6.3.2 Construction and characterisation of 2,3-BDO biosynthesis by Δ*pntAB1234 C. necator*

As no statistically significant difference in biomass yield or maximum specific growth rate were observed between *C. necator* H16 wild type and Δ*pntAB1234* strain, it was hypothesised that by increasing demand of cellular NADH or NADPH, it would be

possible to establish if PntAB1234 contribute to the NAD(P)H co-factor supply. To achieve this, model biosynthesis pathway for production of *meso*-2,3-BDO or (*R, R*)-2,3-BDO utilising NADH or NADPH, respectively, was introduced into *C. necator* H16 wild type and transhydrogenase negative strains. For production of 2,3-BDO, pyruvate is converted to (*R, R*)- or *meso*-2,3-BDO by three enzymatic reactions: (i) conversion of pyruvate to (*S*)-2-acetolactate by acetolactate synthase (Mg^{2+} binding, thiamine diphosphate binding) (AlsS, EC 2.2.1.6), (ii) decarboxylation of (*S*)-2-acetolactate to (*R*)-acetoin by acetolactate decarboxylase (AlsD, EC 4.1.1.5) and (iii) reduction of (*R*)-acetoin to *meso*-2,3-BDO by acetoin reductase (NAD-dependent) (BudC, EC 1.1.1.303) or to (*R, R*)-2,3-BDO by alcohol dehydrogenase (NADP-dependent) (ADH, EC 1.1.1.80) (Figure 6.2).

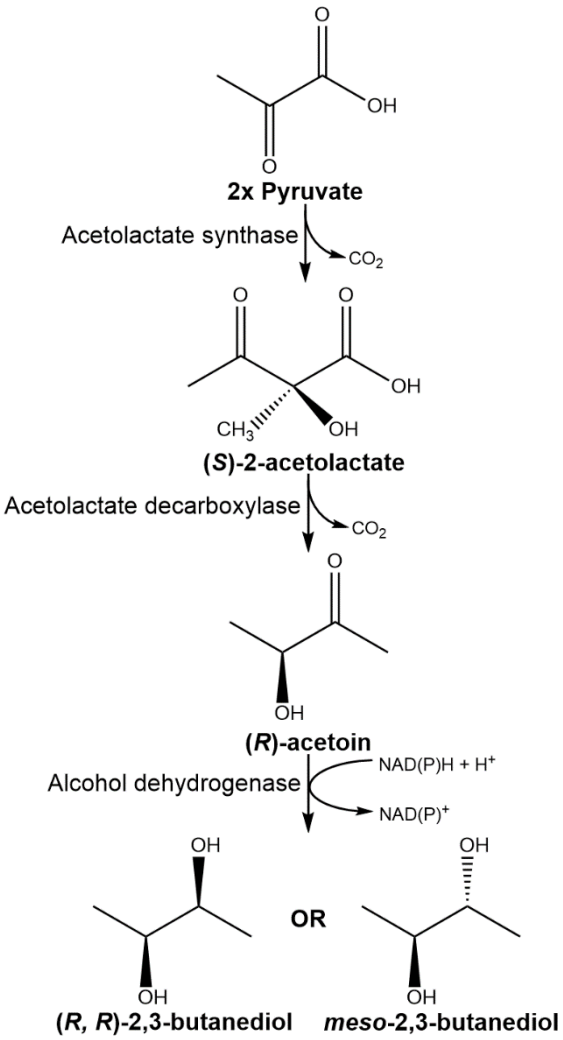

Figure 6.2 Biosynthetic pathway for synthesis of either (*R, R*)-2,3-BDO or *meso*-2,3-BDO stereoisomers from pre-cursor pyruvate in *C. necator* H16.

There have been previous reports that deletion of two *C. necator* H16 metabolic pathways can improve production of the 2,3-BDO pathway intermediate acetoin (Windhorst and Gescher, 2019). The pathways deleted were responsible for acetoin degradation encoded by *acoABC* and P3HB biosynthesis by deletion of genes *phaC12*. A similar *C. necator* H16 strain deficient the acetoin degradation pathway and P3HB biosynthesis pathway has been engineered for (*R, R*)-2,3-BDO production (Bommareddy *et al.*, 2020). *C. necator* H16 strains with chromosomal integration of

(*R, R*)-2,3-BDO or *meso*-2,3-BDO biosynthesis operons in addition to *acoXABC* and *phaC1AB1* gene deletions were assembled and kindly donated by Dr. Rajesh Bommareddy (Synthetic Biology Research Centre, University of Nottingham). These strains were confirmed to produce either *meso*-2,3-BDO or (*R, R*)-2,3-BDO when cultivated under heterotrophic conditions and were deployed for further development (Table 3.3). Strain H16-602 was used to generate strain H16-604 exhibiting Δ*pntAB1234*, Δ*acoXABC* and Δ*phaC1AB1* in conjunction with integrated NADH-dependent 2,3-BDO operon. Strain H16-603 was used to generate strain H16-605 exhibiting Δ*pntAB1234*, Δ*acoXABC* and Δ*phaC1AB1* in conjunction with integrated NADPH-dependent 2,3-BDO operon. Finally, strain H16-603 was also used to generate strain H16-606 exhibiting Δ*pntAB1234*, Δ*acoXABC* and Δ*phaC1AB1* in conjunction with integrated NADPH-dependent 2,3-BDO operon including soluble hydrogenase UdhA from *E. coli* MG1655.

To investigate the effect of transhydrogenase gene deletions on *meso*-2,3-BDO production by engineered *C. necator* H16, strains H16-602 and H16-604 were cultivated under heterotrophic conditions (Figure 6.3). Characterisation of both strains revealed that the strain H16-604 (Δ*pntAB1234*) exhibited a lower maximum specific growth rate. In particular, strain H16-604 reached stationary phase after 48 hours, whereas the control strain H16-602 entered the stationary phase after 24 hours. A reduction in growth rate in *E. coli* MG1655 Δ*pntAB* mutants has also been previously reported (Jan *et al.*, 2013; Sauer *et al.*, 2004). However, once stationary phase is reached by strain H16-604, production of *meso*-2,3-BDO improves after 96 h achieving 0.037 ± 0.002 Cmol Cmol^{-}1. This is a >1.7-fold increase in yield compared with strain H16-602 producing 0.021 ± 0.001 Cmol Cmol^{-1}. Interestingly, acetoin yield exhibits no

statistically significant difference 72 – 96 h after induction of heterologous enzyme expression, suggesting improvement in conversion of acetoin to *meso*-2,3-BDO during later time-points and therefore overall increased NADH availability.

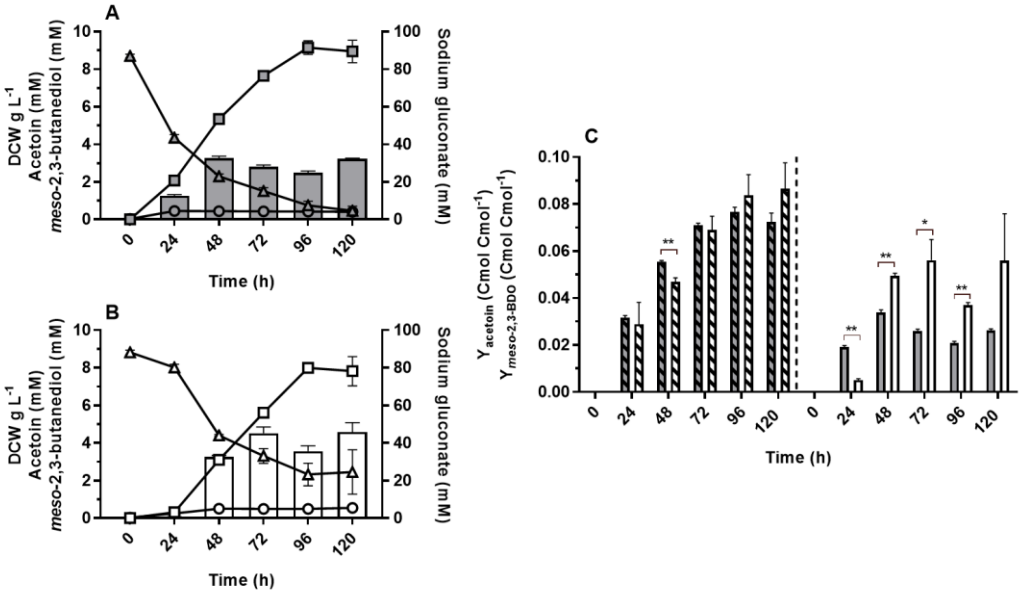

Figure 6.3 Effect of *pntAB1234* deletion on cell growth and *meso*-2,3-BDO biosynthesis. Batch cultivation data showing *meso*-2,3-BDO (bars), acetoin (squares), DCW (circles) and sodium gluconate (triangles) of strains H16-602 (A) and H16-604 (B). Carbon yields of acetoin (striped bars) and *meso*-2,3-BDO for strains H16-602 (grey) (A) and H16-604 (white) (C). Yields for all metabolites were calculated from time point 0 h. Cells were cultivated in 25 mL NLMM supplemented with 2 % (w/v) sodium gluconate and 10 µg mL^{-1} gentamicin using 250 mL baffled shake-flasks. Gene expression was induced by addition of L-arabinose to a final concentration of 0.1 % (w/v). Error bars represent standard error calculated from biological triplicates. An unpaired t-test was carried out comparing metabolite carbon yield values for each time-point; statistically significant differences are shown where ** represents a P value <0.01 and * represents a P value <0.05.

From the results, it appears that in transhydrogenase deletion *C. necator* H16 strain *meso*-2,3-BDO production is increased, indicating increased supply of NADH compared to the transhydrogenase positive strain. Therefore, (*R, R*)-2,3-BDO production utilising NADP-dependent enzyme in strains H16-603, H16-605 and H16-606 cultured under heterotrophic conditions was also evaluated (Figure 6.4). As previously observed by strain H16-604, transhydrogenase deletion strains H16-605 and H16-606 exhibit reduced maximum specific growth rate reaching stationary phase after 48 h when compared to H16-603. Deletion of *C. necator* H16 transhydrogenase's appears to somewhat improve (*R, R*)-2,3-BDO yield. The control strain H16-603 reached 0.046 ± 0.006 Cmol $Cmol^{-1}$ compared to strain H16-605 achieving 0.064 ± 0.005 Cmol $Cmol^{-1}$ (*R, R*)-2,3-BDO after 120 h of cultivation. There is no statistically significant difference in acetoin yields between strains H16-603 and H16-605, however higher (*R, R*)-2,3-BDO yielded by H16-605 suggests increased conversion of acetoin to (*R, R*)-2,3-BDO during final enzymatic step of biosynthesis pathway and therefore increased NADPH supply.

Interestingly, strain expressing UdhA (H16-606) employed to increase balance cellular redox as a substitute for PntAB1234 yielded 0.030 ± 0.003 Cmol $Cmol^{-1}$ (*R, R*)-2,3-BDO after 120 h cultivation. This is >2-fold decrease compared with (*R, R*)-2,3-BDO yield achieved by strain H16-605. Furthermore, increased acetoin yields are observed in strain H16-606, reaching 0.144 ± 0.024 Cmol $Cmol^{-1}$ after 72 h cultivation, 1.9-fold higher than strain H16-605 (0.074 ± 0.003 Cmol $Cmol^{-1}$). Conversion of accumulated acetoin to (*R, R*)-2,3-BDO is evident in both H16-603 and H16-605 strains. However, strain H16-606 appears to accumulate acetoin, indicating NADPH is depleted by UdhA and cells are unable to synthesise (*R, R*)-2.3-BDO. This observation is in agreement

with previous reports that UdhA acts in a divergent function to PntAB reducing NAD^+ through oxidation of NADPH to $NADP^+$ (Sauer *et al.*, 2004).

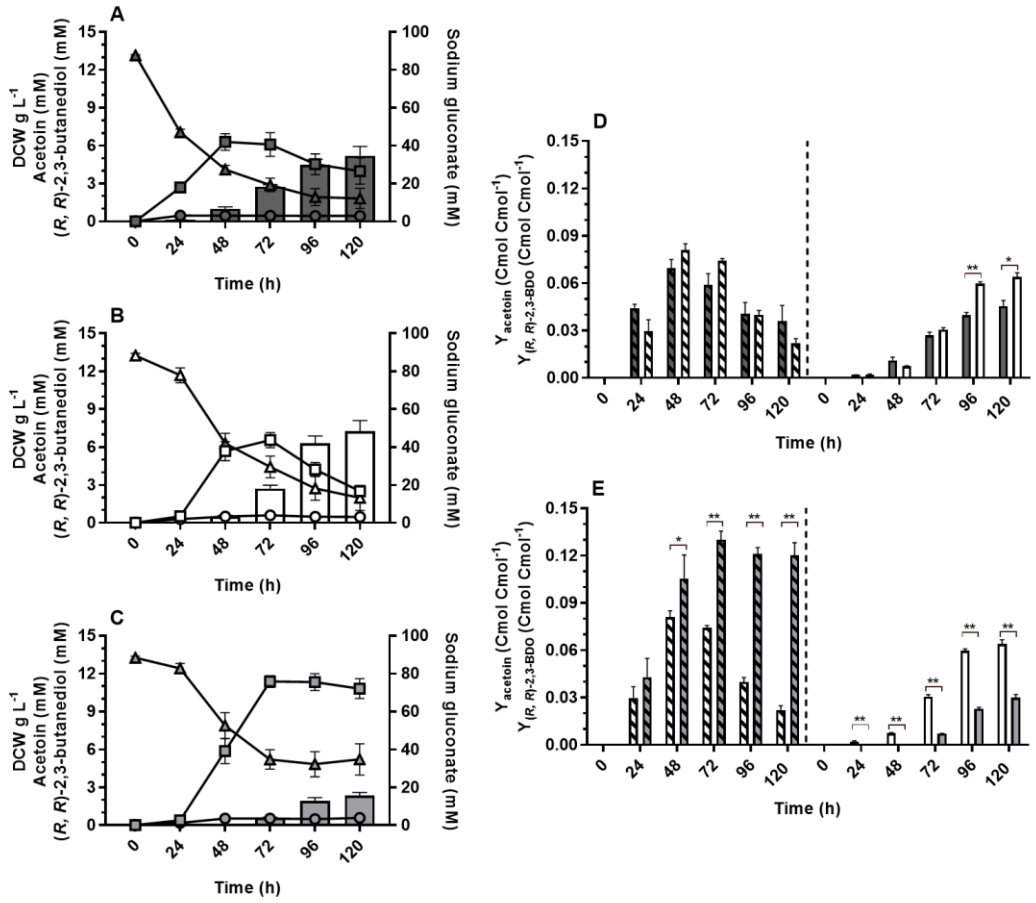

Figure 6.4 Effect of *pntAB1234* deletion and heterologous expression of *udhA* on cell growth and (*R, R*)-2,3-BDO biosynthesis. Batch cultivation data showing (*R, R*)-2,3-BDO (bars), acetoin (squares), DCW (circles) and sodium gluconate (triangles) of strains H16-603 (A), H16-605 (B) and H16-606 (C). Carbon yields of acetoin (striped bars) and (*R, R*)-2,3-BDO for strains H16-603 (dark grey) and H16-605 (white) (D). Carbon yields of acetoin (striped bars) and (*R, R*)-2,3-BDO for strains H16-605 (white) and H16-606 (light grey) (E) Yields for all metabolites were calculated from time point 0 h. Cells were cultivated in 25 mL NLMM supplemented with 2 % (w/v) sodium gluconate and 10 µg mL^{-1} gentamicin using 250 mL baffled shake-flasks. Gene expression was induced by addition of L-arabinose to a final concentration of 0.1 % (w/v).

Error bars represent standard error calculated from biological triplicates. An unpaired t-test was carried out comparing metabolite carbon yield values for each time-point; statistically significant differences are shown where ** represents a P value <0.01 and * represents a P value <0.05.

6.3.3 Autotrophic production of (*R, R*)-2,3-BDO by *C. necator* strains

To gain further insights into the role of transhydrogenases during autotrophic cultivation of *C. necator* H16, strains H16-603, H16-605 and H16-606 were cultivated autotrophically using CO_2 as the sole carbon source with H_2 and O_2 supplied for energy metabolism (Table 6.6).

From the results, a reduction in specific growth rate by strain H16-605 is observed, as seen during heterotrophic cultivation. However, this phenotypic behaviour was not observed by alternative Δ*pntAB1234* strain H16-606, suggesting UdhA is able to balance redox metabolism which is disrupted in Δ*pntAB1234* cells. Interestingly, despite comparable specific growth rate for strains H16-606 and H16-603, (*R, R*)-2,3-BDO yield is increased 1.9-fold, indicating that UdhA contributes to reduction of NADPH, required for (*R, R*)-2,3-BDO biosynthesis, regenerating co-factor NADH as reported previously (Sauer *et al.,* 2004). The resulting increase in NADH supply is utilised by the CBB cycle achieving higher specific growth rates and reduced (*R, R*)-2,3-BDO production rates. Indeed, acetoin accumulation in strain H16-606 compared with strain H16-603 also indicates reduced NADPH availability. Autotrophic cultivation of strain H16-605 results in accumulation of acetoin and (*R, R*)-2,3-BDO yield decreasing 0.7-fold when compared with strain H16-603. This is in contrast to production of (*R, R*)-2,3-BDO by strains H16-603 and H16-605 when cultivated under

heterotrophic conditions. These findings confirm PntAB1234 contribute to balance of $NADP^+$/NADPH ratio when cells are cultivated under autotrophic conditions.

Table 6.6 Autotrophic fermentation of 2,3-BDO producing strains H16-604, H16-605 and H16-606. Metabolite titres, biomass and calculated yield product (g L^{-1}) per biomass (g g^{-1}) (Y). Samples were taken when cells were in a steady state, 13 d after supply of fresh minimal media supplemented with 0.1 % (w/v) L-arabinose to induce gene expression.

Strain	**DCW (g/L)**	**Acetoin (mM)**	**(*R*, *R*)-2,3-BDO (mM)**	**$Y_{acetoin}$ (g g^{-1})**	**$Y_{(R, R)\text{-}2,3\text{-}BDO}$ (g g^{-1})**
H16-603	8.8	7.2	243.8	0.07	2.51
H16-605	2.9	28.5	60.4	0.87	1.88
H16-606	8.4	49.4	118.5	0.52	1.28

6.3.4 Insights from *C. necator* transcriptome during autotrophic production of (*R*, *R*)-2,3-BDO

To further understand cellular response to transhydrogenase encoding gene deletions in (*R*, *R*)-2,3-BDO producing strain the transcriptome of H16-603 and H16-605 was analysed. This was achieved by using RNA-Seq next generation sequencing (Wang, Gerstein and Snyder, 2009) and mapping reads to *C. necator* H16 reference genome (Pohlmann *et al.*, 2006; Schwartz *et al.*, 2003). Logarithmic fold change estimations (FC) in gene transcription were determined from raw counts which were normalised using the median of ratios method (Love, Huber and Anders, 2014). This allowed identification of gene up- and down-regulation by strain H16-605 compared to the control strain H16-603 (Figure 6.5). Upon analysis, genes encoding enzymes involved in central carbon metabolism capable of regenerating NADPH, namely *zwf123* encoding glucose-6-phosphate 1-dehydrogenase (G6PD), *maeAB* encoding malate dehydrogenase encoded and *icd123* encoding isocitrate dehydrogenase saw no

significant difference in expression levels. Overall CBB cycle appears to only be margianally upregulated in strain H16-605, seeing only FC value of 1.27 for *cbbX2* encoding rubisco accessory protein. However, there was no significant increase in expression of other genes in *cbb* operon. Of note is the significant increase in expression of copper resistance encoding genes *copABCD* indicating increase of intracellular Cu^{+}. The gene *copA* encoding a copper resistance protein reportedly facilitates transport of monovalent Cu from the cytoplasm to maintain intracellular homeostasis (Bondarczuk and Piotrowska-Seget, 2013).

Other insights from transcriptome analysis is *ccoNOQP* encoding a *cbb3*-type cytochrome oxidase encoded (Cramm, 2008) exhibits significant decrease in expression. Interestingly, this *cbb3*-type cytochrome oxidase requires copper ions during assembly to act as a terminal oxidoreductase for aerobic respiration (Pitcher and Watmough, 2004). From analysis of the H16-505 transcriptome, it appears transhydrogenase's play a vital role in *C. necator* H16 energy metabolism, with no apparent alternative present to facilitate $NADP^{+}$/NADPH balancing when cultivated under autotrophic conditions.

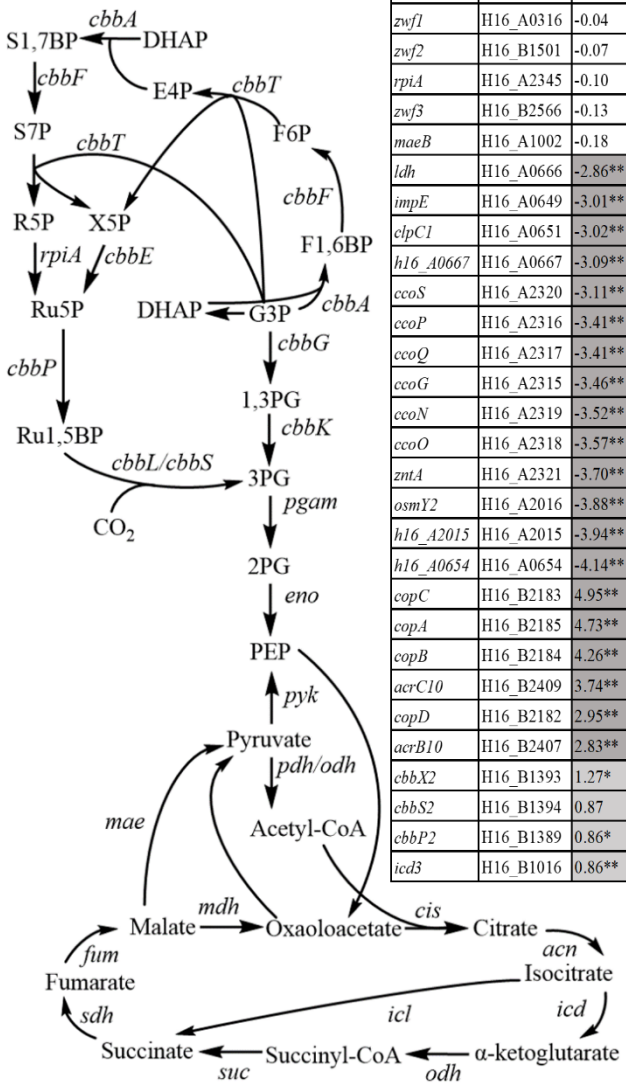

Gene	Locus	FC	Gene	Locus	FC	Gene	Locus	FC
maeA	H16_A3153	0.08	*cbbY2*	H16_B1392	0.84	*flgE*	H16_B0264	-3.82**
ppnK	H16_A1132	0.03	*cbbB*	H16_B1383	0.84	*adhP*	H16_B1433	-3.99**
h16_A3004	H16_A3004	0.03	*cbbG2*	H16_B1386	0.72	*fhaB*	H16_B0247	-4.07**
icd1	H16_A3056	0.02	*cbbA2*	H16_B1384	0.70	*fnr4*	H16_B1540	-4.43**
zwf1	H16_A0316	-0.04	*cbbE2*	H16_B1391	0.64	*ompW2*	H16_B0080	-4.56**
zwf2	H16_B1501	-0.07	*cbbF2*	H16_B1390	0.63	*flhD2*	H16_B1539	-4.59**
rpiA	H16_A2345	-0.10	*pyk3*	H16_B0961	0.62	*kdpD2*	H16_B0895	-6.79**
zwf3	H16_B2566	-0.13	*cbbT2*	H16_B1388	0.53	*dapA3*	H16_B0891	-6.98**
maeB	H16_A1002	-0.18	*cbbK2*	H16_B1385	0.45	*kdpC*	H16_B0896	-7.43**
ldh	H16_A0666	-2.86**	*cbbZ2*	H16_B1387	0.42	*kdpB*	H16_B0897	-8.41**
impE	H16_A0649	-3.01**	*icd2*	H16_B1931	0.30	*kdpA*	H16_B0898	-8.85**
clpC1	H16_A0651	-3.02**	*cbbR*	H16_B1396	0.15	*cbbXp*	PHG425	0.92
h16_A0667	H16_A0667	-3.09**	*tar2*	H16_B2122	-3.01**	*cbbL*	PHG427	0.80
ccoS	H16_A2320	-3.11**	*flhF*	H16_B0254	-3.02**	*cbbYp*	PHG424	0.79
ccoP	H16_A2316	-3.41**	*motR*	H16_B0255	-3.07**	*cbbPp*	PHG421	0.76
ccoQ	H16_A2317	-3.41**	*fliO*	H16_B0564	-3.09**	*cbbSp*	PHG426	0.76
ccoG	H16_A2315	-3.46**	*fliN*	H16_B0565	-3.16**	*cbbGp*	PHG418	0.64
ccoN	H16_A2319	-3.52**	*fhaC*	H16_B0248	-3.21**	*cbbFp*	PHG422	0.62
ccoO	H16_A2318	-3.57**	*fliF*	H16_B2368	-3.27**	*cbbKp*	PHG417	0.59
zntA	H16_A2321	-3.70**	*fliI*	H16_B2371	-3.27**	*cbbAp*	PHG416	0.52
osmY2	H16_A2016	-3.88**	*fliG*	H16_B2369	-3.30**	*cbbEp*	PHG423	0.42
h16_A2015	H16_A2015	-3.94**	*flhA*	H16_B0253	-3.30**	*cbbZp*	PHG419	0.30
h16_A0654	H16_A0654	-4.14**	*fliE*	H16_B2367	-3.32**	*nosC*	PHG253	-3.08**
copC	H16_B2183	4.95**	*flgI*	H16_B0268	-3.34**	*phaP2*	PHG202	-3.10**
copA	H16_B2185	4.73**	*h16_B1434*	H16_B1434	-3.34**	*nosX*	PHG254	-3.16**
copB	H16_B2184	4.26**	*csgG*	H16_B0249	-3.38**	*nrdG*	PHG238	-3.23**
acrC10	H16_B2409	3.74**	*fliH*	H16_B2370	-3.38**	*dmrD*	PHG262	-3.24**
copD	H16_B2182	2.95**	*flgC*	H16_B0262	-3.50**	*narX*	PHG265	-3.35**
acrB10	H16_B2407	2.83**	*flgF*	H16_B0265	-3.55**	*nosD*	PHG250	-3.51**
cbbX2	H16_B1393	1.27*	*flgB*	H16_B0261	-3.58**	*nosZ*	PHG252	-3.84**
cbbS2	H16_B1394	0.87	*flgH*	H16_B0267	-3.60**	*nosR*	PHG251	-3.97**
cbbP2	H16_B1389	0.86*	*flgD*	H16_B0263	-3.63**	*nosF*	PHG249	-4.14**
icd3	H16_B1016	0.86**	*flgG*	H16_B0266	-3.64**			

Figure 6.5 Schematic of central carbon metabolism in *C. necator* for fixation of CO_2 during autotrophic cultivation with accompanying tabulated FC values for H16-605. Present in the table are genes involved in CO_2 fixation, genes that encode enzymes that contribute to energy metabolism and all genes with FC values greater than 2.5 or less than -3.0 that are not hypothetical or predicted genes. Samples were taken from the fermenters for RNA-sequencing after 13 d of autotrophic cultivation. Central carbon metabolites represented in the schematic: phosphoenolpyruvate (PEP), 2-phosphoglycerate (2PG), 3-phosphoglycerate (3PG), 1,3-bisphosphoglycerate (1,3PG), glyceraldehyde 3-phosphate (G3P), fructose 1,6-bisphosphate

(F1,6BP), fructose 6-phosphate (F6P), erythrose 4-phosphate (E4P), sedoheptulose 1,7-bisphosphate (S1,7BP), sedoheptulose 7-phosphate (S7P), ribose 5-phosphate (R5P), xylulose 5-phosphate (X5P), ribulose 5-phosphate (Ru5P), ribulose 1,5-bisphosphate (Ru1,5BP), dihydroxyacetone phosphate (DHAP). Light grey shading indicates FC value above 0.5 and below -0.5 and dark grey indicates FC value above 2.0 and below -2.0. A t-test was carried out to determine statistical significance of FC where ** represents a P value <0.01 and * represents a P value <0.05

6.4 Discussion

The primary focus of this study was to improve understanding of how membrane-bound energy-dependent transhydrogenases PntAB1234 contributes to the NAD(P)H co-factor supply in *C. necator* H16. Each transhydrogenase is formed of 2-3 subunits that are encoded by genes present on chromosome 1 or chromosome 2 of *C. necator* H16 genome. Genes that encode PntAB1234 were systematically deleted generating a Δ*pntAB1234* strain. and specific growth rate and biomass yield were compared to wild type strain, with no statistically significant difference observed. This result indicated a no effect on redox metabolism placed on the cells that would typically be observed by limited biomass production (Gu *et al.*, 2019).

C. necator H16 strains were assembled expressing heterologous genes encoding enzymes for biosynthesis of *meso*-2,3-BDO or (*R, R*)-2,3-BDO utilising co-factor NADH or NADPH, respectively. Introducing either *meso*-2,3-BDO or (*R, R*)-2,3-BDO biosynthesis pathways allowed comparison of NADH and NADPH availability within *C. necator* H16 strains. This strategy resulted in 2,3-BDO yields being directly impacted by changes in redox, due to a single enzyme co-factor preference in the implemented biosynthetic pathway. Upon testing, Δ*pntAB1234* strains expressing

either *meso*-2,3-BDO or (*R, R*)-2,3-BDO biosynthesis pathways exhibited a reduction in maximum specific growth rate, compared with strains still containing genes encoding transhydrogenase's. Interestingly, deletion of *pntAB1234* marginally improved *meso*-2,3-BDO titre suggesting increased availability of NADH. This is in agreement with reports PntAB in *E. coli* MG1655 regenerates NADPH. However, (*R, R*)-2,3-BDO yields was also increased in Δ*pntAB1234* strains indicating increase in NADPH availability. This is possibly due to other enzymatic activities being more efficient at regenerating NADPH than the energy-dependent PntAB1234 when cultivated under heterotrophic conditions.

When strain H16-605 was cultivated under autotrophic conditions, specific growth rate and (*R, R*)-2,3-BDO yield was significantly reduced compared to strain H16-603. This result is in contrast to results observed for strain H16-605 when cultivated under heterotrophic conditions, indicating a burden was placed on cells in the form of diminished NADPH supply by *pntAB1234* deletion. Thus, under autotrophic conditions, it can be concluded PntAB1234 contributes to cellular NADPH regeneration in *C. necator* H16. To investigate further, analysis of the *C. necator* H16 transcriptome was undertaken that yielded no obvious alternative for regeneration of NADPH when cultivated under autotrophic conditions. However, increased expression of *icd3* encoding NAD^+-dependent isocitrate dehydrogenase Icd3 was observed that suggests in Δ*pntAB1234* strains there is an increase in NAD^+ which is then reduced to NADH by Icd3. This increase in NAD^+ is most likely a result of increased expression of the *cbb* operon oxidising NADH during fixation of CO_2.

Further analysis of the *C. necator* H16 transcriptome revealed reduced expression of *ccoNOQP* operon encoding *cbb3*-type cytochrome oxidase in strain H16-605 cultivated

under autotrophic conditions when compared to strain H16-603. Simultaneously, increased expression of *copABCD* encoding copper resistance proteins can be seen, suggesting accumulation of intracellular copper ions Interestingly, the *ccb3*-type cytochrome oxidase is a member of the heme-copper superfamily and requires uptake and metabolism of copper for assembly of its dinuclear centre (Pitcher and Watmough, 2004). Indeed, it appears that in Δ*pntAB1234* strain the reduction in expression of genes encoding *cbb3*-type cytochrome oxidase leads to an accumulation of copper ions, suggesting importance of PntAB1234 *C. necator* H16 energy metabolism through NADPH regeneration.

The soluble transhydrogenase UdhA from *E. coli* MG1655 has been reported to reduce NAD^+ with NADPH regenerating NADH (Sauer *et al.*, 2004). In this study, *udhA* was heterologously expressed in *C. necator* H16 Δ*pntAB1234* (*R, R*)-2,3-BDO producing strain (H16-606) to investingate preference for NADH or NADPH regeneration in an alternative microorganism. Strain H16-606 was cultivated under both heterotrophic and autotrophic conditions where similar phenotypic qualities were observed. Indeed, expression of *udhA* resulted in specific growth rate reduced in Δ*pntAB1234* strains being restored to growth rates seen by strains with transhydrogenases still present. Also, expression of *udhA* resulted in the lowest (*R, R*)-2,3-BDO yields and highest acetoin yields. This is in agreement with previous reports by Sauer and co-workers that UdhA transfers reducing power from NADPH to NADH.

6.5 Conclusion

To conclude, in this study the regeneration of NADPH during production of 2,3-BDO from CO_2 has been investigated. This involved first generating a *C. necator* H16

tranhysdrogenase deletion strain (Δ*pntAB1234*) and subsequent characterisation compared to the wild type strain. The Δ*pntAB1234* deletion had no statistically significant effect on specific growth rate or biomass yield. Two heterologous operons were then introduced for biosynthesis of either *meso*-2,3-BDO or (*R, R*)-2,3-BDO *via* either a strictly NADH or NADPH pathway, respectively. Engineered *C. necator* H16 strains producing (*R, R*)-2,3-BDO were then characterised under heterotrophic and autotrophic conditions. During cultivation, heterologous expression of *udhA* encoding a soluble transhydrogenase from *E. coli* MG1655 was shown to regenerate NADH by oxidation of NADPH, as previously reported (Sauer *et al.*, 2004). Analysis of the *C. necator* H16 transcriptome confirmed PntAB1234 plays an important role in NADPH regeneration when cultivated under autotrophic conditions. Overall, advances have been made to understand transhydrogenase role on *C. necator* H16 metabolism.

7 Conclusions

The research aim of this work was to explore and engineer *C. necator* H16 for production of butanediol (BDO) using carbon dioxide (CO_2) as the carbon source. The development of bacterial strains suitable for utilisation and biological conversion of CO_2 to platform chemicals such as BDO can facilitate reducing current fossil fuel dependence and greenhouse gas emissions.

In this context, *C. necator* H16 was established as a viable chassis for production of BDO demonstrating no consumption of BDO structural isomers and no inhibitory effect on growth rate in the presence of <166.4 mM acetoin or BDO. When deploying a microbial chassis for production of a foreign compound, consumption of the desired product can severely hamper strain development requiring identification of enzymes responsible and implementation of strategies to reduce compound degradation. Indeed, Arenas-Lopez and co-workers report consumption of 3-hydroxypropionic acid by *C. necator* H16 that was identified as potential target compound for bioproduction. This required first the identification and systematic removal of enzymes responsible for compound degradation (Arenas-López *et al.*, 2019).

An initial part of the research was dedicated to identification and characterisation of genetically encoded biosensors that can potentially be used for BDO detection and monitoring, allowing high-throughput BDO sample analysis during *C. necator* H16 strain development. Two inducible systems were developed into *E. coli* MG1665- and *C. necator* H16-based whole cell biosensors that were evaluated in the presence of either acetoin or 1,3-BDO, 1,4-BDO or 2,3-BDO. Unfortunately, neither of two *C. necator* H16-based biosensors showed reliably measurable response to these

compounds. To date, there have been only a few reports of biosensors used for detection of BDO isomers, with one instance being work by Szmidt-Middleton and co-workers deploying a biosensor for detection of 1,4-BDO in *E. coli* DH5α and *E. coli* MG1655 (Szmidt-Middleton *et al.*, 2013). This is surprising considering the microbial production of 2,3-BDO has been reported for several decades, and more recently there is increased interest in microbial production of 1,4-BDO and 1,3-BDO. Development of biosensors for detection of specific BDO structural isomers within *C. necator* H16 could aid in advancing strain development for BDO bioproduction.

Previously, individual (*R*)-3-HBCoA- or pyruvate-dependent pathways have been deployed in *E. coli* for bioproduction of (*R*)-1,3-BDO using glucose as the carbon source. Here, both the (*R*)-3-HBCoA-depdendent and pyruvate-dependent pathways have been deployed in *C. necator* H16 for (*R*)-1,3-BDO bioproduction using gluconate or CO_2 as the carbon source. Notably, *C. necator* H16 can accumulate high cell densities with up to 90 % (w/w) DCW in the form of P3HB when cultured under nitrogen limiting conditions. The P3HB pathway intermediate (*R*)-3-HBCoA was therefore ideal precursor for (*R*)-1,3-BDO biosynthetic pathway with the potential to redirect large amounts of carbon. Initially, the (*R*)-3-HBCoA-depdenendet pathway was investigated establishing successful production of (*R*)-1,3-BDO using of a butanal dehydrogenase and NADP-dependent aldehyde reductase in a P3HB deficient *C. necator* H16 strain. However, in this system pyruvate was found to be the primary by-product. Therefore, to utilise accumulating pyruvate and increase carbon flux towards (*R*)-1,3-BDO, a pyruvate decarboxylase and DERA were used to direct carbon through the pyruvate-dependent biosynthetic pathway.

To achieve the autotrophic fermentation using engineered *C. necator* H16 stains, genes encoding both (*R*)-1,3BDO biosynthesis pathways were chromosomally integrated increasing genetic stability during fermentation. Subsequent strains were cultivated heterotrophically and autotrophically with (*R*)-1,3-BDO production decreasing due to reduced gene dosage. To increase (*R*)-1,3-BDO production, multiple gene copies encoding pathway-limiting enzymes Bld and Dra were chromosomally integrated to increase enzyme synthesis. Whilst this strategy did increase (*R*)-1,3-BDO yield as also reported by Nemr and co-workers (Nemr *et al.*, 2018), optimal bioproduction of (*R*)-1,3-BDO from CO_2 was observed in a chromosomally integrated *C. necator* strain also harbouring plasmid containing gene encoding key pathway enzyme Bld.

Previous investigations of whole-cell bioproduction of (*R*)-1,3-BDO have deployed *E. coli* as the host chassis utilising pyruvate or acetyl-CoA as the precursor for (*R*)-1,3-BDO synthesis pathway using glucose as carbon source, with highest titres of 174 mM from acetyl-CoA precursor and 26.6 mM from pyruvate precursor reported (Nemr *et al.*, 2018; Kataoka *et al.*, 2014). In comparison, in this study *C. necator* H16 was engineered to produce (*R*)-1,3-BDO utilising both described pathways, reaching a highest titre of 20 mM when cultivated heterotrophically and a highest titre of 33 mM when cultivated autotrophically. Interestingly, highest titre is observed when cultivated under autotrophic conditions and is most likely due to continuous supply of carbon and energy sources compared to autotrophic cultivation. Furthermore, Kataoka and co-workers were able to achieve highest titre when cultivating cells using fed-batch fermentation, allowing for increased carbon flux towards (*R*)-1,3-BDO when cells reached stationary growth phase. Further strain engineering and/or optimisation of fermentation conditions would be required to achieve productions levels seen by

engineered *E. coli*, with the potential of several approaches to be undertaken to increase overall titres and yields. Employing these approaches would also further improve economic feasibility.

Two alternative strategies were deployed for optimisation of production of (*R*)-1,3-BDO, with Kataoka and co-workers optimising fermentation parameters (K_La and pH), whereas Nemr and co-workers aimed to reduce production of by-products and increase pathway-related enzyme production, with both approaches resulting in significant increase in (*R*)-1,3-BDO titres.

Overall, highest producing *C. necator* H16 strain developed in this study achieved a titre and yield that are seemingly economically feasible and indicate a first step towards industrial production. However, further optimisations could be made to increase (*R*)-1,3-BDO produced from CO_2. These could include implementation of a plasmid addiction system to allow for stable expression of pathway-related genes during continuous cultivation of engineered *C. necator* H16 strains (Pan *et al.*, 2021). Furthermore, optimal oxygen transfer coefficient (K_La) and pH could be investigated as undertaken by Kataoka and co-workers who reported a >1.5-fold increase in (*R*)-1,3-BDO bioproduction. Another approach to increasing (*R*)-1,3-BDO bioproduction would see reduction of by-product 4H2B, whether through enzyme engineering of Bld to increase specific enzymatic activity (Hwang et al., 2014), or through bioconversion of 4H2B to (*R*)-1,3-BDO using whole cell biocatalysis (Zheng *et al.*, 2012). Finally, Yim and co-workers demonstrated the power of metabolic modelling of *E. coli* using in-house SimPheny Biopathway Predictor software to optimise 1,4-BDO production (Yim *et al.*, 2011), with a similar approach deployed for *C. necator* H16 to further increase (*R*)-1,3-BDO bioproduction.

Finally, investigation into alternative waste feedstocks could also be potential route towards industrial bioproduction of (*R*)-1,3-BDO, with *C. necator* H16 capable of using multiple carbon sources including glycerol (González-Villanueva *et al.*, 2019) and syngas (Shin *et al.*, 2021). However, this would most likely require further *C. necator* H16 strain development and optimisation, but would be the ideal industrial process for production of (*R*)-1,3-BDO from renewable carbon sources.

Large amounts of reducing power in the form of NAD(P)H is required for (*R*)-1,3-BDO biosynthesis. One approach to increase (*R*)-1,3-BDO may be regeneration of NAD(P)H providing sufficient reducing power as to not limit production. However, energy metabolism of *C. necator* H16 has not been comprehensively studied, in particular when cultivated under autotrophic conditions. Therefore, in this study the potential sources of NADPH regeneration in the bacterium *C. necator* H16 when cultured using sodium gluconate or CO_2 as the sole carbon source were investigated. Specifically, the role of four energy-dependent transhydrogenase's (PntAB1234) in energy metabolism was explored. The systematic deletion of genes encoding PntAB1234 and increase in metabolic burden through introduction of a 2,3-BDO biosynthetic pathway resulted in a minor effect on cell metabolism. However, 2,3-BDO production indicated sufficient NAD(P)H regeneration in *C. necator* H16 demonstrating robust energy metabolism mechanisms, particularly during heterotrophic cultivation. Gaining further understanding of the key components of *C. necator* H16 energy metabolism, particulalrly during autotrophic cultivation, may prove invaluable in the deployment of synthetic metabolic pathways.

In conclusion, this research advances our abilities to utilise carbon dioxide-fixing bacteria such as *C. necator* H16 for BDO production and through this perspective

improves understanding of chemolithoautotroph metabolism and NAD(P)H co-factor supply requirements. The design-build-test-learn approach deployed in this work allowed development of *C. necator* H16 strains suitable for production of (*R*)-1,3-BDO from CO_2.

8 References

Al Rowaihi, I. S., Paillier, A., Rasul, S., Karan, R., Grötzinger, S. W., Takanabe, K. and Eppinger, J. (2018) 'Poly(3-hydroxybutyrate) production in an integrated electromicrobial setup: Investigation under stress-inducing conditions', *PLOS One*, 13(4), pp. e0196079.

Alagesan, S., Hanko, E. K. R., Malys, N., Ehsaan, M., Winzer, K. and Minton, N. P. (2018) 'Functional Genetic Elements for Controlling Gene Expression in Cupriavidus necator H16', *Applied Environmental Microbiology*, 84(19).

Alagesan, S., Minton, N. P. and Malys, N. (2017) '13C-assisted metabolic flux analysis to investigate heterotrophic and mixotrophic metabolism in Cupriavidus necator H16', *Metabolomics*, 14(1), pp. 9.

Aragno, M. and Schlegel, H. G. (1992) 'The mesophilic hydrogen-oxidizing (knallgas) bacteria'. New York: Springer-Verlag Inc., pp. 344-384.

Arenas Lopez, C. (2018) *The genetic basis of 3-hydroxypropanoate metabolism in Cupriavidus necator H16.* Doctoral Thesis, University of Nottingham.

Arenas-López, C., Locker, J., Orol, D., Walter, F., Busche, T., Kalinowski, J., Minton, N. P., Kovács, K. and Winzer, K. (2019) 'The genetic basis of 3-hydroxypropanoate metabolism in Cupriavidus necator H16', *Biotechnology for Biofuels*, 12(1), pp. 150.

Atsumi, S., Wu, T.-Y., Eckl, E.-M., Hawkins, S. D., Buelter, T. and Liao, J. C. (2010) 'Engineering the isobutanol biosynthetic pathway in Escherichia coli by comparison of three aldehyde reductase/alcohol dehydrogenase genes', *Applied Microbiology and Biotechnology*, 85(3), pp. 651-657.

Ausubel, F., Brent, R., Kingston, R. E., Moore, D. D., Seidman, J., Smith, J. A. and Struhl, K. (2003) 'Current protocols in molecular biology', *NY: Wiley*.

Badger, M. R. and Bek, E. J. (2008) 'Multiple Rubisco forms in proteobacteria: their functional significance in relation to CO2 acquisition by the CBB cycle', *Journal of Experimental Botany*, 59(7), pp. 1525-1541.

Bae, S.-J., Kim, S. and Hahn, J.-S. (2016) 'Efficient production of acetoin in Saccharomyces cerevisiae by disruption of 2,3-butanediol dehydrogenase and expression of NADH oxidase', *Scientific Reports*, 6(1), pp. 27667.

Baldassarre, M., Cesana, A. and Bordes, F. (2021) 'Process for Bio - 1,3 - butanediol purification from a fermentation broth. USA Patent. US 2021/0380512 A1'.

Bao, T., Zhang, X., Rao, Z., Zhao, X., Zhang, R., Yang, T., Xu, Z. and Yang, S. (2014) 'Efficient Whole-Cell Biocatalyst for Acetoin Production with NAD+ Regeneration System through Homologous Co-Expression of 2,3-Butanediol Dehydrogenase and NADH Oxidase in Engineered Bacillus subtilis', *PLOS One*, 9(7), pp. e102951.

Bar-Even, A., Noor, E., Lewis, N. E. and Milo, R. (2010) 'Design and analysis of synthetic carbon fixation pathways', *Proceedings of the National Academy of Sciences*, 107(19), pp. 8889-8894.

Bar-Even, A., Noor, E. and Milo, R. (2012) 'A survey of carbon fixation pathways through a quantitative lens', *Journal of Experimental Botany*, 63(6), pp. 2325-2342.

Bi, C., Su, P., Müller, J., Yeh, Y.-C., Chhabra, S. R., Beller, H. R., Singer, S. W. and Hillson, N. J. (2013) 'Development of a broad-host synthetic biology toolbox for Ralstonia eutropha and its application to engineering hydrocarbon biofuel production', *Microbial Cell Factories*, 12, pp. 107-107.

Białkowska, A. M. (2016) 'Strategies for efficient and economical 2,3-butanediol production: new trends in this field', *World Journal of Microbiology and Biotechnology*, 32(12).

Bitinaite, J., Rubino, M., Varma, K. H., Schildkraut, I., Vaisvila, R. and Vaiskunaite, R. (2007) 'USER™ friendly DNA engineering and cloning method by uracil excision', *Nucleic Acids Research*, 35(6), pp. 1992-2002.

Black, W. B., Zhang, L., Kamoku, C., Liao, J. C. and Li, H. (2018) 'Rearrangement of Coenzyme A-Acylated Carbon Chain Enables Synthesis of Isobutanol via a Novel Pathway in Ralstonia eutropha', *ACS Synthetic Biology*, 7(3), pp. 794-800.

BOC (2022) *Carbon Dioxide Cylinder, Industrial Grade, Compressed Gas*. Available at: https://www.boconline.co.uk/shop/en/uk/carbon-dioxide-cylinder (Accessed: 12/12/2022).

Bommareddy, R. R., Wang, Y., Pearcy, N., Hayes, M., Lester, E., Minton, N. P. and Conradie, A. V. (2020) 'A Sustainable Chemicals Manufacturing Paradigm Using CO(2) and Renewable H(2)', *iScience*, 23(6), pp. 101218-101218.

Bondarczuk, K. and Piotrowska-Seget, Z. (2013) 'Molecular basis of active copper resistance mechanisms in Gram-negative bacteria', *Cell Biology and Toxicology*, 29(6), pp. 397-405.

Bowien, B. and Kusian, B. (2002) 'Genetics and control of CO2 assimilation in the chemoautotroph Ralstonia eutropha', *Archives of Microbiology*, 178(2), pp. 85-93.

Brigham, C. J., Budde, C. F., Holder, J. W., Zeng, Q., Mahan, A. E., Rha, C. and Sinskey, A. J. (2010) 'Elucidation of β-Oxidation Pathways in Ralstonia eutropha H16 by Examination of Global Gene Expression', *Journal of Bacteriology*, 192(20), pp. 5454-5464.

Bruland, N., Voss, I., Brämer, C. and Steinbüchel, A. (2010) 'Unravelling the C3/C4 carbon metabolism in Ralstonia eutropha H16', *Journal of Applied Microbiology*, 109(1), pp. 79-90.

Burg, J. M., Cooper, C. B., Ye, Z., Reed, B. R., Moreb, E. A. and Lynch, M. D. (2016) 'Large-scale bioprocess competitiveness: the potential of dynamic metabolic control in two-stage fermentations', *Current Opinion in Chemical Engineering*, 14, pp. 121-136.

Burgard, A., Burk, M. J., Osterhout, R., Van Dien, S. and Yim, H. (2016) 'Development of a commercial scale process for production of 1,4-butanediol from sugar', *Current Opinion in Biotechnology*, 42, pp. 118-125.

Burgard, A. P., Burk, M. J., Osterhout, R. E., Sun, J. and Pharkya, P. (2012) 'Microorganisms for Producing 1, 3-Butanediol and Methods Related Thereto. USA Patent. US 2012/0329113 A1.'.

Burgdorf, T., Bömmer, D. and Bowien, B. (2001) 'Involvement of an unusual mol operon in molybdopterin cofactor biosynthesis in Ralstonia eutropha', *Journal of Molecular Microbiology and Biotechnology*, 3(4), pp. 619-629.

Burk, M. J., Burgard, A. P., Osterhout, R. E. and Sun, J. (2010) 'Microorganisms for the production of 1, 4-butanediol. USA Patent. US 7,858,350 B2'.

Centeno-Leija, S., Huerta-Beristain, G., Giles-Gómez, M., Bolivar, F., Gosset, G. and Martinez, A. (2014) 'Improving poly-3-hydroxybutyrate production in Escherichia coli by combining the increase in the NADPH pool and acetyl-CoA availability', *Antonie van Leeuwenhoek*, 105(4), pp. 687-696.

Chain, P., Lamerdin, J., Larimer, F., Regala, W., Lao, V., Land, M., Hauser, L., Hooper, A., Klotz, M., Norton, J., Sayavedra-Soto, L., Arciero, D., Hommes, N., Whittaker, M. and Arp, D. (2003) 'Complete Genome Sequence of the Ammonia-Oxidizing Bacterium and Obligate Chemolithoautotroph Nitrosomonas europaea', *Journal of Bacteriology*, 185(9), pp. 2759-2773.

Chakravarty, J. and Brigham, C. J. (2018) 'Solvent production by engineered Ralstonia eutropha: channeling carbon to biofuel', *Applied Microbiology and Biotechnology*, 102(12), pp. 5021-5031.

Chin, J. W., Khankal, R., Monroe, C. A., Maranas, C. D. and Cirino, P. C. (2009) 'Analysis of NADPH supply during xylitol production by engineered Escherichia coli', *Biotechnology and Bioengineering*, 102(1), pp. 209-220.

Claypool, J. and Raman, D. (2015) 'Biorenewable Process Evaluation Tool'.

Claypool, J. T. and Raman, D. R. (2013) 'Development and validation of a technoeconomic analysis tool for early-stage evaluation of bio-based chemical production processes', *Bioresour Technol*, 150, pp. 486-95.

Cotter, J. L., Chinn, M. S. and Grunden, A. M. (2009) 'Ethanol and acetate production by Clostridium ljungdahlii and Clostridium autoethanogenum using resting cells', *Bioprocess and Biosystems Engineering*, 32(3), pp. 369-380.

Cramm, R. (2008) 'Genomic view of energy metabolism in Ralstonia eutropha H16', *Journal of Molecular Microbiology and Biotechnology*, 16(1-2), pp. 38-52.

Crepin, L., Lombard, E. and Guillouet, S. E. (2016) 'Metabolic engineering of Cupriavidus necator for heterotrophic and autotrophic alka(e)ne production', *Metabolic Engineering*, 37, pp. 92-101.

Doran, P. M. (1995) '2 - Introduction to Engineering Calculations', in Doran, P.M. (ed.) *Bioprocess Engineering Principles*. London: Academic Press, pp. 9-26.

Drejer, E. B., Chan, D. T. C., Haupka, C., Wendisch, V. F., Brautaset, T. and Irla, M. (2020) 'Methanol-based acetoin production by genetically engineered Bacillus methanolicus', *Green Chemistry*, 22(3), pp. 788-802.

Drozd, J. 'Growth energetics in Alcaligenes eutrophus H16'. *Proceedings of the Society for General Microbiology*, 72.

Duan, H., Yamada, Y. and Sato, S. (2016) 'Future Prospect of the Production of 1,3-Butadiene from Butanediols', *Chemistry Letters*, 45(9), pp. 1036-1047.

Ducat, D. C. and Silver, P. A. (2012) 'Improving carbon fixation pathways', *Current Opinion in Chemical Biology*, 16(3), pp. 337-344.

El-Mansi, E. M. T. and Holms, W. H. (1989) 'Control of Carbon Flux to Acetate Excretion During Growth of Escherichia coli in Batch and Continuous Cultures', *Microbiology*, 135(11), pp. 2875-2883.

Emptage, M., Haynie, S. L., Laffend, L. A., Pucci, J. P. and Whited, G. (2003) *Proces for the biological production of 1,3-propanediol with high titer*. [Online].

Fozo, E. M., Kawano, M., Fontaine, F., Kaya, Y., Mendieta, K. S., Jones, K. L., Ocampo, A., Rudd, K. E. and Storz, G. (2008) 'Repression of small toxic protein synthesis by the Sib and OhsC small RNAs', *Molecular Microbiology*, 70(5), pp. 1076-1093.

Fried, L., Behr, S. and Jung, K. (2013) 'Identification of a target gene and activating stimulus for the YpdA/YpdB histidine kinase/response regulator system in Escherichia coli', *Journal of Bacteriology*, 195(4), pp. 807-815.

Friedrich, C. G., Bowien, B. and Friedrich, B. (1979) 'Formate and Oxalate Metabolism in Alcaligenes eutrophus', *Microbiology*, 115(1), pp. 185-192.

Genomatica 2017a. Genomatica delivers on plant performance guarantees. *In:* Weiss, S. (ed.) *Novamont confirms Bottrighe plant meets performance parameters.* https://www.genomatica.com/wp-content/uploads/2017/01/Genomatica-delivers-on-performance-guarantees-1.pdf: Genomatica.

Genomatica 2017b. Genomatica introduces next process technology. *In:* Weiss, S. (ed.) *GENO BG™ process delivers naturally sourced, sustainable butylene glycol for personal care; proven bioengineering capabilities drive rapid commercilaization of another high-yield process.* https://www.genomatica.com/products/: Genomatica.

Gong, F., Cai, Z. and Li, Y. (2016) 'Synthetic biology for CO(2) fixation', *Science China Life Sciences*, 59(11), pp. 1106-1114.

González-Villanueva, M., Galaiya, H., Staniland, P., Staniland, J., Savill, I., Wong, T. S. and Tee, K. L. (2019) 'Adaptive Laboratory Evolution of Cupriavidus necator H16 for Carbon Co-Utilization with Glycerol', *International Journal of Molecular Sciences*, 20(22), pp. 5737.

Grousseau, E., Lu, J., Gorret, N., Guillouet, S. E. and Sinskey, A. J. (2014) 'Isopropanol production with engineered Cupriavidus necator as bioproduction platform', *Applied Microbiology and Biotechnology*, 98(9), pp. 4277-4290.

Gruber, S., Schwab, H. and Heidinger, P. (2017) 'CbbR and RegA regulate cbb operon transcription in Ralstonia eutropha H16', *Journal of Biotechnology*, 257, pp. 78-86.

Grunwald, S., Mottet, A., Grousseau, E., Plassmeier, J. K., Popović, M. K., Uribelarrea, J. L., Gorret, N., Guillouet, S. E. and Sinskey, A. (2015) 'Kinetic and stoichiometric characterization of organoautotrophic growth of Ralstonia eutropha on formic acid in fed-batch and continuous cultures', *Microbial Biotechnology*, 8(1), pp. 155-63.

Gu, Y., Lv, X., Liu, Y., Li, J., Du, G., Chen, J., Rodrigo, L.-A. and Liu, L. (2019) 'Synthetic redesign of central carbon and redox metabolism for high yield production of N-acetylglucosamine in Bacillus subtilis', *Metabolic Engineering*, 51, pp. 59-69.

Hakizimana, O., Matabaro, E. and Lee, B. H. (2020) 'The current strategies and parameters for the enhanced microbial production of 2,3-butanediol', *Biotechnology Reports*, 25, pp. e00397.

Hanko, E. K. R., Minton, N. P. and Malys, N. (2017) 'Characterisation of a 3-hydroxypropionic acid-inducible system from Pseudomonas putida for orthogonal gene expression control in Escherichia coli and Cupriavidus necator', *Scientific Reports*, 7(1), pp. 1724.

Hanko, E. K. R., Minton, N. P. and Malys, N. (2018) 'A Transcription Factor-Based Biosensor for Detection of Itaconic Acid', *ACS Synthetic Biology*.

Hess, V., Oyrik, O., Trifunović, D. and Müller, V. (2015) '2,3-Butanediol Metabolism in the Acetogen Acetobacterium woodii', *Applied and Environmental Microbiology*, 81(14), pp. 4711-4719.

Hoppensack, A., Rehm, B. H. and Steinbuchel, A. (1999) 'Analysis of 4-phosphopantetheinylation of polyhydroxybutyrate synthase from Ralstonia eutropha: generation of beta-alanine auxotrophic Tn5 mutants and cloning of the panD gene region', *Journal of Bacteriology*, 181(5), pp. 1429-35.

'Horizon 2020: EU framework programme for research and innovation', (2014) *International Journal of Disaster Resilience in the Built Environment*, 5(2).

Hwang, H. J., Park, J. H., Kim, J. H., Kong, M. K., Kim, J. W., Park, J. W., Cho, K. M. and Lee, P. C. (2014) 'Engineering of a butyraldehyde dehydrogenase of Clostridium saccharoperbutylacetonicum to fit an engineered 1,4-butanediol pathway in Escherichia coli', *Biotechnology and Bioengineering*, 111(7), pp. 1374-1384.

Jahn, C. E., Charkowski, A. O. and Willis, D. K. (2008) 'Evaluation of isolation methods and RNA integrity for bacterial RNA quantitation', *J Microbiol Methods*, 75(2), pp. 318-24.

Jan, J., Martinez, I., Wang, Y., Bennett, G. N. and San, K. Y. (2013) 'Metabolic engineering and transhydrogenase effects on NADPH availability in Escherichia coli', *Biotechnol Progress*, 29(5), pp. 1124-1130.

Jarboe, L. R. (2011) 'YqhD: A broad-substrate range aldehyde reductase with various applications in production of biorenewable fuels and chemicals', *Applied Microbiology and Biotechnology*, 89(2), pp. 249-257.

Jendrossek, D., Kratzin, H. D. and Steinbüchel, A. (1993) 'The Alcaligenes eutrophus ldh structural gene encodes a novel type of lactate dehydrogenase', *FEMS Microbiology Letters*, 112(2), pp. 229-235.

Jensen, K. F. (1993) 'The Escherichia coli K-12 "wild types" W3110 and MG1655 have an rph frameshift mutation that leads to pyrimidine starvation due to low pyrE expression levels', *Journal of Bacteriology*, 175(11), pp. 3401-3407.

Ji, D., Wang, L., Hou, S., Liu, W., Wang, J., Wang, Q. and Zhao, Z. K. (2011) 'Creation of bioorthogonal redox systems depending on nicotinamide flucytosine dinucleotide', *Journal of the American Chemical Society*, 133(51), pp. 20857-20862.

Ji, X.-J., Huang, H. and Ouyang, P.-K. (2011) 'Microbial 2,3-butanediol production: A state-of-the-art review', *Biotechnology Advances*, 29(3), pp. 351-364.

Johnson, A. O., Gonzalez-Villanueva, M., Tee, K. L. and Wong, T. S. (2018) 'An Engineered Constitutive Promoter Set with Broad Activity Range for Cupriavidus necator H16', *ACS Synthetic Biology*, 7(8), pp. 1918-1928.

Jones, C. W., Brice, J. M., Downs, A. J. and Drozd, J. W. (1975) 'Bacterial Respiration-Linked Proton Translocation and Its Relationship to Respiratory-Chain Composition', *European Journal of Biochemistry*, 52(2), pp. 265-271.

Kannan, G., Wilks, J. C., Fitzgerald, D. M., Jones, B. D., BonDurant, S. S. and Slonczewski, J. L. (2008) 'Rapid acid treatment of Escherichia coli: transcriptomic response and recovery', *BMC Microbiology*, 8(1), pp. 37.

Kataoka, N., Vangnai, A. S., Pongtharangkul, T., Yakushi, T. and Matsushita, K. (2017) 'Production of 1, 3-diols in Escherichia coli', *Bioresource Technology*.

Kataoka, N., Vangnai, A. S., Tajima, T., Nakashimada, Y. and Kato, J. (2013) 'Improvement of (R)-1,3-butanediol production by engineered Escherichia coli', *Journal of Bioscience and Bioengineering*, 115(5), pp. 475-480.

Kataoka, N., Vangnai, A. S., Ueda, H., Tajima, T., Nakashimada, Y. and Kato, J. (2014) 'Enhancement of (R)-1,3-butanediol production by engineered Escherichia coli using a bioreactor system with strict regulation of overall oxygen transfer coefficient and pH', *Bioscience, Biotechnology, and Biochemistry*, 78(4), pp. 695-700.

Kersters, K. and De Ley, J. (1984) 'Bergey's Manual of Systematic Bacteriology Volume 1 (Krieg, NR and Holt, JG eds.)', *The Williams & Wilkins Co., Baltimore*, 1, pp. 224-254.

Kim, S. and Hahn, J.-S. (2015) 'Efficient production of 2,3-butanediol in Saccharomyces cerevisiae by eliminating ethanol and glycerol production and redox rebalancing', *Metabolic Engineering*, 31, pp. 94-101.

Kim, S. J., Seo, S. O., Jin, Y. S. and Seo, J. H. (2013) 'Production of 2,3-butanediol by engineered Saccharomyces cerevisiae', *Bioresour Technology*, 146, pp. 274-281.

Kim, T., Flick, R., Brunzelle, J., Singer, A., Evdokimova, E., Brown, G., Joo, J. C., Minasov, G. A., Anderson, W. F., Mahadevan, R., Savchenko, A. and Yakunin, A. F. (2017) 'Novel aldo-keto reductases for the biocatalytic conversion of 3- hydroxybutanal to 1,3-butanediol: Structural and biochemical studies', *Applied and Environmental Microbiology*, 83(7).

Krieg, T., Sydow, A., Faust, S., Huth, I. and Holtmann, D. (2018) 'CO2 to Terpenes: Autotrophic and Electroautotrophic alpha-Humulene Production with Cupriavidus necator', *Angewandte Chemie (International ed. in English)*, 57(7), pp. 1879-1882.

Köpke, M., Mihalcea, C., Liew, F., Tizard, J. H., Ali, M. S., Conolly, J. J., Al-Sinawi, B. and Simpson, S. D. (2011) '2,3-Butanediol Production by Acetogenic Bacteria, an Alternative Route to Chemical Synthesis, Using Industrial Waste Gas', *Applied and Environmental Microbiology*, 77(15), pp. 5467-5475.

Larchevêque, M., Mambu, L. and Petit, Y. (1991) 'Preparation of Enantiomerically Pure 1,3-Butanediol from Threonine', *Synthetic Communications*, 21(22), pp. 2295-2300.

LBNet (2017) *UK Top Bio-based Chemicals Opportunities*. Available at: https://www.bbnet-nibb.co.uk/wp-content/uploads/2019/08/LBNet-UKBioChem10_UK-Top-Bio-based-Chemicals-Opportunities_Dec2017.pdf (Accessed: 02/11/2020).

Lee, W.-H., Loo, C.-Y., Nomura, C. T. and Sudesh, K. (2008) 'Biosynthesis of polyhydroxyalkanoate copolymers from mixtures of plant oils and 3-hydroxyvalerate precursors', *Bioresource Technology*, 99(15), pp. 6844-6851.

Lenz, O. and Friedrich, B. (1998) 'A novel multicomponent regulatory system mediates H2 sensing in Alcaligenes eutrophus', *Proceedings of the National Academy of Sciences of the United States of America*, 95(21), pp. 12474-12479.

Li, H., Chen, J. and Li, Y. (2008) 'Enhanced activity of yqhD oxidoreductase in synthesis of 1,3-propanediol by error-prone PCR', *Progress in Natural Science*, 18(12), pp. 1519-1524.

Li, T., Chen, X. B., Chen, J. C., Wu, Q. and Chen, G. Q. (2014) 'Open and continuous fermentation: products, conditions and bioprocess economy', *Biotechnology Journal*, 9(12), pp. 1503-1511.

Li, Z. J., Cai, L., Wu, Q. and Chen, G. Q. (2009) 'Overexpression of NAD kinase in recombinant Escherichia coli harboring the phbCAB operon improves poly(3-hydroxybutyrate) production', *Applied Microbiology and Biotechnology*, 83(5), pp. 939-947.

Lindenkamp, N., Volodina, E. and Steinbüchel, A. (2012) 'Genetically modified strains of Ralstonia eutropha H16 with β- ketothiolase gene deletions for production of copolyesters with defined 3-hydroxyvaleric acid contents', *Applied and Environmental Microbiology*, 78(15), pp. 5375-5383.

Llarrull, L. I., Testero, S. A., Fisher, J. F. and Mobashery, S. (2010) 'The future of the β-lactams', *Current Opinion in Microbiology*, 13(5), pp. 551-557.

Love, M. I., Huber, W. and Anders, S. (2014) 'Moderated estimation of fold change and dispersion for RNA-seq data with DESeq2', *Genome Biology*, 15(12), pp. 550.

Lu, J., Brigham, C. J., Gai, C. S. and Sinskey, A. J. (2012) 'Studies on the production of branched-chain alcohols in engineered Ralstonia eutropha', *Applied Microbiology and Biotechnology*, 96(1), pp. 283-297.

Ma, C., Wang, A., Qin, J., Li, L., Ai, X., Jiang, T., Tang, H. and Xu, P. (2009) 'Enhanced 2,3-butanediol production by Klebsiella pneumoniae SDM', *Applied Microbiology and Biotechnology*, 82(1), pp. 49-57.

Madeira, F., Park, Y. M., Lee, J., Buso, N., Gur, T., Madhusoodanan, N., Basutkar, P., Tivey, A. R. N., Potter, S. C., Finn, R. D. and Lopez, R. (2019) 'The EMBL-EBI search and sequence analysis tools APIs in 2019', *Nucleic Acids Research*, 47(W1), pp. W636-W641.

Madigan, M. T. and Gest, H. (1979) 'Growth of the photosynthetic bacterium Rhodopseudomonas capsulata chemoautotrophically in darkness with H<inf>2</inf> as the energy source', *Journal of Bacteriology*, 137(1), pp. 524-530.

Matsuyama, A., Kobayashi, Y. and Ohnishi, H. (1993) 'Microbial Production of Optically Active 1,3-Butanediol from 4-Hydroxy-2-butanone', *Bioscience, Biotechnology, and Biochemistry*, 57(2), pp. 348-349.

Matsuyama, A., Nikaido, T. and Kobayashi, Y. (1988) 'Production of optically active 1,3-butanediol by asymmetric assimilation or reduction of 4-hydroxy-2-butanone. USA Patent. US 5219757 A'.

Matsuyama, A., Yamamoto, H., Kawada, N. and Kobayashi, Y. (2001) 'Industrial production of (R)-1,3-butanediol by new biocatalysts', *Journal of Molecular Catalysis B: Enzymatic*, 11(4), pp. 513-521.

Miller, E. N., Jarboe, L. R., Yomano, L. P., York, S. W., Shanmugam, K. T. and Ingram, L. O. (2009) 'Silencing of NADPH-Dependent Oxidoreductase Genes (yqhD and dkgA in Furfural-Resistant Ethanologenic Escherichia coli', *Applied and Environmental Microbiology,* 75(13), pp. 4315-4323.

Miyake, Y., Inaba, T., Watanabe, H., Teramoto, J., Yamamoto, K. and Ishihama, A. (2019) 'Regulatory roles of pyruvate-sensing two-component system PyrSR (YpdAB) in Escherichia coli K-12', *FEMS Microbiology Letters,* 366(2).

Müller, J., MacEachran, D., Burd, H., Sathitsuksanoh, N., Bi, C., Yeh, Y. C., Lee, T. S., Hillson, N. J., Chhabra, S. R., Singer, S. W. and Beller, H. R. (2013) 'Engineering of Ralstonia eutropha H16 for autotrophic and heterotrophic production of methyl ketones', *Applied and Environmental Microbiology,* 79(14), pp. 4433-4439.

Nakashimada, Y., Marwoto, B., Kashiwamura, T., Kakizono, T. and Nishio, N. (2000) 'Enhanced 2,3-butanediol production by addition of acetic acid in Paenibacillus polymyxa', *Journal of Bioscience and Bioengineering,* 90(6), pp. 661-664.

Nemr, K., Muller, J. E. N., Joo, J. C., Gawand, P., Choudhary, R., Mendonca, B., Lu, S., Yu, X., Yakunin, A. F. and Mahadevan, R. (2018) 'Engineering a short, aldolase-based pathway for (R)-1,3-butanediol production in Escherichia coli', *Metabolic Engineering,* 48, pp. 13-24.

Nybo, S. E., Khan, N. E., Woolston, B. M. and Curtis, W. R. (2015) 'Metabolic engineering in chemolithoautotrophic hosts for the production of fuels and chemicals', *Metabolic Engineering,* 30, pp. 105-120.

Obruca, S., Snajdar, O., Svoboda, Z. and Marova, I. (2013) 'Application of random mutagenesis to enhance the production of polyhydroxyalkanoates by Cupriavidus necator H16 on waste frying oil', *World Journal of Microbiology and Biotechnology,* 29(12), pp. 2417-2428.

Oh, J. I. and Bowien, B. (1998) 'Structural analysis of the fds operon encoding the NAD+-linked formate dehydrogenase of Ralstonia eutropha', *Journal of Biological Chemistry,* 273(41), pp. 26349-26360.

Okabayashi, T., Nakajima, T. and Yamamoto, H. (2009) 'Recombinant microorganisms with 1,3-butanediol-producing function and uses thereof. USA Patent. US 20120276606 A1'.

Oliver, J. W. K., Machado, I. M. P., Yoneda, H. and Atsumi, S. (2013) 'Cyanobacterial conversion of carbon dioxide to 2,3-butanediol', *Abstracts of Papers of the American Chemical Society,* 246.

Opgenorth, P., Costello, Z., Okada, T., Goyal, G., Chen, Y., Gin, J., Benites, V., de Raad, M., Northen, T. R., Deng, K., Deutsch, S., Baidoo, E. E. K., Petzold, C. J., Hillson, N. J., Garcia Martin, H. and Beller, H. R. (2019) 'Lessons from Two Design–Build–Test–Learn Cycles of Dodecanol Production in Escherichia coli Aided by Machine Learning', *ACS Synthetic Biology,* 8(6), pp. 1337-1351.

Pan, H., Wang, J., Wu, H., Li, Z. and Lian, J. (2021) 'Synthetic biology toolkit for engineering Cupriviadus necator H16 as a platform for CO(2) valorization', *Biotechnology for Biofuels,* 14(1), pp. 212.

Peoples, O. P. and Sinskey, A. J. (1989) 'Poly-β-hydroxybutyrate (PHB) biosynthesis in Alcaligenes eutrophus H16. Identification and characterization of the PHB polymerase gene (phbC)', *Journal of Biological Chemistry,* 264(26), pp. 15298-15303.

Peplinski, K., Ehrenreich, A., Doring, C., Bomeke, M., Reinecke, F., Hutmacher, C. and Steinbuchel, A. (2010) 'Genome-wide transcriptome analyses of the 'Knallgas' bacterium Ralstonia eutropha H16 with regard to polyhydroxyalkanoate metabolism', *Microbiology*, 156(Pt 7), pp. 2136-2152.

Perez, J. M., Arenas, F. A., Pradenas, G. A., Sandoval, J. M. and Vasquez, C. C. (2008) 'Escherichia coli YqhD exhibits aldehyde reductase activity and protects from the harmful effect of lipid peroxidation-derived aldehydes', *J Biol Chem*, 283(12), pp. 7346-7353.

Pfitzner, J. and Schlegel, H. G. (1973) 'Denitrifikation bei Hydrogenomonas eutropha Stamm H16', *Archiv für Mikrobiologie*, 90(3), pp. 199-211.

Pitcher, R. S. and Watmough, N. J. (2004) 'The bacterial cytochrome cbb3 oxidases', *Biochimica et Biophysica Acta*, 1655, pp. 388-399.

Pohlmann, A., Fricke, W. F., Reinecke, F., Kusian, B., Liesegang, H., Cramm, R., Eitinger, T., Ewering, C., Potter, M., Schwartz, E., Strittmatter, A., Vosz, I., Gottschalk, G., Steinbuchel, A., Friedrich, B. and Bowien, B. (2006) 'Genome sequence of the bioplastic-producing "Knallgas" bacterium Ralstonia eutropha H16', *Nature Biotechnology*, 24(10), pp. 1257-1262.

Raberg, M., Bechmann, J., Brandt, U., Schluter, J., Uischner, B., Voigt, B., Hecker, M. and Steinbuchel, A. (2011) 'Versatile metabolic adaptations of Ralstonia eutropha H16 to a loss of PdhL, the E3 component of the pyruvate dehydrogenase complex', *Appl Environ Microbiol*, 77(7), pp. 2254-63.

Raberg, M., Reinecke, F., Reichelt, R., Malkus, U., König, S., Pötter, M., Fricke, W. F., Pohlmann, A., Voigt, B., Hecker, M., Friedrich, B., Bowien, B. and Steinbüchel, A. (2008) 'Ralstonia eutropha H16 Flagellation Changes According to Nutrient Supply and State of Poly(3-Hydroxybutyrate) Accumulation', *Applied and Environmental Microbiology*, 74(14), pp. 4477-4490.

Ragsdale, S. W. (1997) 'The Eastern and Western branches of the Wood/Ljungdahl pathway: how the East and West were won', *BioFactors*, 6(1), pp. 3-11.

Research and Markets (2022) *1,3-Butylene Glycol Market Research Report: By Product, Function, Application - Global Industry Size and Demand Forecast to 2030*. Research and Markets. Available at: https://www.researchandmarkets.com/reports/5184612/13-butylene-glycol-market-research-report-by (Accessed: 02/01/2023).

Reyrat, J. M., Pelicic, V., Gicquel, B. and Rappuoli, R. (1998) 'Counterselectable markers: untapped tools for bacterial genetics and pathogenesis', *Infection and immunity*, 66(9), pp. 4011-4017.

Sabra, W., Groeger, C. and Zeng, A. P. 2016. Microbial cell factories for diol production. *Advances in Biochemical Engineering/Biotechnology*.

Sadaharu, U. I., Okajima, Y., Mimura, A., Kanai, H. and Kudo, T. (1997) 'Molecular generation of an Escherichia coli strain producing only the meso-isomer of 2,3-butanediol', *Journal of Fermentation and Bioengineering*, 84(3), pp. 185-189.

Sambrook, J., Fritsch, E. F. and Maniatis, T. (1989) *Molecular cloning: a laboratory manual*. Cold Spring Harbor, NY: Cold Spring Harbor Laboratory Press.

Sanchez, A. M., Andrews, J., Hussein, I., Bennett, G. N. and San, K. Y. (2006) 'Effect of overexpression of a soluble pyridine nucleotide transhydrogenase (UdhA) on the production of poly(3-hydroxybutyrate) in Escherichia coli', *Biotechnology Progress,* 22(2), pp. 420-425.

Saran, S., Yadav, S. and Saxena, R. (2014) 'Development of a highly sensitive, fast and efficient screening technique for the detection of 2, 3-butanediol by thin layer chromatography', *Journal of Chromatography & Separation Techniques,* 5(6), pp. 1.

Satam, C. C., Daub, M. and Realff, M. J. (2019) 'Techno-economic analysis of 1,4-butanediol production by a single-step bioconversion process', *Biofuels, Bioproducts and Biorefining,* 13(5), pp. 1261-1273.

Sauer, U., Canonaco, F., Heri, S., Perrenoud, A. and Fischer, E. (2004) 'The soluble and membrane-bound transhydrogenases UdhA and PntAB have divergent functions in NADPH metabolism of Escherichia coli', *Journal of Biological Chemistry,* 279(8), pp. 6613-6619.

Schlegel, H., Kaltwasser, H. and Gottschalk, G. (1961) 'Ein Submersverfahren zur Kultur wasserstoffoxydierender Bakterien: Wachstumsphysiologische Untersuchungen', *Archiv für Mikrobiologie,* 38(3), pp. 209-222.

Schwartz, E., Henne, A., Cramm, R., Eitinger, T., Friedrich, B. and Gottschalk, G. (2003) 'Complete Nucleotide Sequence of pHG1: A Ralstonia eutropha H16 Megaplasmid Encoding Key Enzymes of H2-based Lithoautotrophy and Anaerobiosis', *Journal of Molecular Biology,* 332(2), pp. 369-383.

Sharma, P. K., Fu, J., Spicer, V., Krokhin, O. V., Cicek, N., Sparling, R. and Levin, D. B. (2016) 'Global changes in the proteome of Cupriavidus necator H16 during poly-(3-hydroxybutyrate) synthesis from various biodiesel by-product substrates', *AMB Express,* 6(1), pp. 36-36.

Shin, S. K., Ko, Y. J., Jeong, D. W., Lee, M.-E., You, S. K., Hyeon, J. E. and Han, S. O. (2021) 'Enhanced production of polyhydroxybutyrate from syngas by using nanoscaled cellulose particles with a syngas-converting enzyme complex immobilized on Ralstonia eutropha', *Journal of Cleaner Production,* 285, pp. 124903.

Sigma-Aldrich (2022) *(R)-(−)-1,3-Butanediol, 95 %*. Available at: https://www.sigmaaldrich.com/GB/en/product/aldrich/237612 (Accessed: 12/12/2022).

Solomon, S., Plattner, G.-K., Knutti, R. and Friedlingstein, P. (2009) 'Irreversible climate change due to carbon dioxide emissions', *Proceedings of the National Academy of Sciences,* 106(6), pp. 1704-1709.

Spielmann, A., Baumgart, M. and Bott, M. (2019) 'NADPH-related processes studied with a SoxR-based biosensor in Escherichia coli', *MicrobiologyOpen,* 8(7).

Steinbüchel, A., Fründ, C., Jendrossek, D. and Schlegel, H. G. (1987) 'Isolation of mutants of Alcaligenes eutrophus unable to derepress the fermentative alcohol dehydrogenase', *Archives of Microbiology,* 148(3), pp. 178-186.

Steinbüchel, A. and Schlegel, H. G. (1991) 'Physiology and molecular genetics of poly(β-hydroxyalkanoic acid) synthesis in Alcaligenes eutrophus', *Molecular Microbiology,* 5(3), pp. 535-542.

Sun, X., Shen, X., Jain, R., Lin, Y., Wang, J., Sun, J., Wang, J., Yan, Y. and Yuan, Q. (2015) 'Synthesis of chemicals by metabolic engineering of microbes', *Chemical Society Reviews*, 44(11), pp. 3760-3785.

Szmidt-Middleton, H. L., Ouellet, M., Adams, P. D., Keasling, J. D. and Mukhopadhyay, A. (2013) 'Utilizing a highly responsive gene, yhjX, in E. coli based production of 1,4-butanediol', *Chemical Engineering Science*, 103, pp. 68-73.

Tai, Y. S., Xiong, M., Jambunathan, P., Wang, J., Wang, J., Stapleton, C. and Zhang, K. (2016) 'Engineering nonphosphorylative metabolism to generate lignocellulose-derived products', *Nat Chemical Biology*, 12(4), pp. 247-253.

Tanaka, K., Ishizaki, A., Kanamaru, T. and Kawano, T. (1995) 'Production of poly(D-3-hydroxybutyrate) from CO2, H2, and O2 by high cell density autotrophic cultivation of Alcaligenes eutrophus', *Biotechnology and Bioengineering*, 45(3), pp. 268-275.

UNFCCC (2015) *Adoption of the Paris Agreement. Proposal by the President. Draft decision -/CP.21*. Available at: https://unfccc.int/resource/docs/2015/cop21/eng/l09r01.pdf.

Vemuri, G. N., Altman, E., Sangurdekar, D. P., Khodursky, A. B. and Eiteman, M. A. (2006) 'Overflow Metabolism in Escherichia coli during Steady-State Growth: Transcriptional Regulation and Effect of the Redox Ratio', *Applied and Environmental Microbiology*, 72(5), pp. 3653-3661.

Vervoort, Y., Linares, A. G., Roncoroni, M., Liu, C., Steensels, J. and Verstrepen, K. J. (2017) 'High-throughput system-wide engineering and screening for microbial biotechnology', *Current Opinion in Biotechnology*, 46, pp. 120-125.

Volodina, E., Raberg, M. and Steinbuchel, A. (2016) 'Engineering the heterotrophic carbon sources utilization range of Ralstonia eutropha H16 for applications in biotechnology', *Critical Reviews in Biotechnology*, 36(6), pp. 978-991.

Volova, T. G., Zhila, N. O., Kalacheva, G. S., Brigham, C. J. and Sinskey, A. J. (2013) 'Effects of intracellular poly(3-hydroxybutyrate) reserves on physiological–biochemical properties and growth of Ralstonia eutropha', *Research in Microbiology*, 164(2), pp. 164-171.

Voss, I. and Steinbüchel, A. (2006) 'Application of a KDPG-aldolase gene-dependent addiction system for enhanced production of cyanophycin in Ralstonia eutropha strain H16', *Metabolic Engineering*, 8(1), pp. 66-78.

Wang, J., Jain, R., Shen, X., Sun, X., Cheng, M., Liao, J. C., Yuan, Q. and Yan, Y. (2017) 'Rational engineering of diol dehydratase enables 1,4-butanediol biosynthesis from xylose', *Metabolic Engineering*, 40, pp. 148-156.

Wang, Z., Gerstein, M. and Snyder, M. (2009) 'RNA-Seq: a revolutionary tool for transcriptomics', *Nature Reviews Genetics*, 10(1), pp. 57-63.

Weckbecker, A. and Hummel, W. (2004) 'Improved synthesis of chiral alcohols with Escherichia coli cells co-expressing pyridine nucleotide transhydrogenase, NADP+-dependent alcohol dehydrogenase and NAD+-dependent formate dehydrogenase', *Biotechnology Letters*, 26(22), pp. 1739-44.

Widdel, F. (2007) 'Theory and measurement of bacterial growth', *Di dalam Grundpraktikum Mikrobiologie*, 4(11).

Windhorst, C. and Gescher, J. (2019) 'Efficient biochemical production of acetoin from carbon dioxide using Cupriavidus necator H16', *Biotechnology for Biofuels*, 12(1), pp. 163.

Windhöver, U. and Bowien, B. (1991) 'Identification of cfxR, an activator gene of autotrophic CO2 fixation in Alcaligenes eutrophus', *Molecular Microbiology*, 5(11), pp. 2695-2705.

Wu, W., Tran-Gyamfi, M. B., Jaryenneh, J. D. and Davis, R. W. (2016) 'Cofactor engineering of ketol-acid reductoisomerase (IlvC) and alcohol dehydrogenase (YqhD) improves the fusel alcohol yield in algal protein anaerobic fermentation', *Algal Research*, 19, pp. 162-167.

Xiao, Z. and Lu, J. R. (2014) 'Strategies for enhancing fermentative production of acetoin: A review', *Biotechnology Advances*, 32(2), pp. 492-503.

Xiao, Z., Lv, C., Gao, C., Qin, J., Ma, C., Liu, Z., Liu, P., Li, L. and Xu, P. (2010) 'A Novel Whole-Cell Biocatalyst with NAD+ Regeneration for Production of Chiral Chemicals', *PLOS One*, 5(1), pp. e8860.

Yamada-Onodera, K., Nakajima, A. and Tani, Y. (2006) 'Purification, characterization, and gene cloning of glycerol dehydrogenase from Hansenula ofunaensis, and its expression for production of optically active diol', *Journal of Bioscience and Bioengineering*, 102(6), pp. 545-551.

Yamamoto, H., Kawada, N., Matsuyama, A. and Kobayashi, Y. (1999) 'Cloning and expression in Escherichia coli of a gene coding for a secondary alcohol dehydrogenase from Candida parapsilosis', *Bioscience, Biotechnology, and Biochemistry*, 63(6), pp. 1051-1055.

Yamamoto, H., Matsuyama, A., Kobayashi, Y. and Kawada, N. (1995) 'Purification and characterization of (S)-1,3-butanediol dehydrogenase from Candida parapsilosis', *Bioscience, Biotechnology, and Biochemistry*, 59(9), pp. 1769-1770.

Yan, Y., Lee, C.-C. and Liao, J. C. (2009) 'Enantioselective synthesis of pure (R,R)-2,3-butanediol in Escherichia coli with stereospecific secondary alcohol dehydrogenases', *Organic & Biomolecular Chemistry*, 7(19), pp. 3914-3917.

Yang, T., Man, Z., Rao, Z., Xu, M., Zhang, X. and Xu, Z. (2014) 'Asymmetric reduction of 4-hydroxy-2-butanone to (R)-1,3-butanediol with absolute stereochemical selectivity by a newly isolated strain of Pichia jadinii', *Journal of Industrial Microbiology & Biotechnology*, 41(12), pp. 1743-1752.

Yang, Z. and Zhang, Z. (2018) 'Production of (2R, 3R)-2,3-butanediol using engineered Pichia pastoris: strain construction, characterization and fermentation', *Biotechnology for Biofuels*, 11(1), pp. 35.

Yim, H., Haselbeck, R., Niu, W., Pujol-Baxley, C., Burgard, A., Boldt, J., Khandurina, J., Trawick, J. D., Osterhout, R. E., Stephen, R., Estadilla, J., Teisan, S., Schreyer, H. B., Andrae, S., Yang, T. H., Lee, S. Y., Burk, M. J. and Van Dien, S. (2011) 'Metabolic engineering of Escherichia coli for direct production of 1,4-butanediol', *Nature Chemical Biology*, 7(7), pp. 445-452.

Zhang, H., Lountos, G. T., Ching, C. B. and Jiang, R. (2010) 'Engineering of glycerol dehydrogenase for improved activity towards 1, 3-butanediol', *Applied Microbiology and Biotechnology*, 88(1), pp. 117-124.

Zhang, X., Han, R., Bao, T., Zhao, X., Li, X., Zhu, M., Yang, T., Xu, M., Shao, M., Zhao, Y. and Rao, Z. (2019) 'Synthetic engineering of Corynebacterium crenatum to selectively produce acetoin or 2,3-butanediol by one step bioconversion method', *Microbial Cell Factories,* 18(1), pp. 128.

Zheng, R.-C., Ge, Z., Qiu, Z.-K., Wang, Y.-S. and Zheng, Y.-G. (2012) 'Asymmetric synthesis of (R)-1,3-butanediol from 4-hydroxy-2-butanone by a newly isolated strain Candida krusei ZJB-09162', *Applied Microbiology and Biotechnology,* 94(4), pp. 969-976.

Zhou, S., Zhuang, Y., Zhu, X., Yao, F., Li, H., Li, H., Zou, X., Wu, J., Zhou, H., Nuer, G., Huang, Y., Li, S. and Peng, Q. (2019) 'YhjX Regulates the Growth of Escherichia coli in the Presence of a Subinhibitory Concentration of Gentamicin and Mediates the Adaptive Resistance to Gentamicin', *Frontiers in Microbiology,* 10, pp. 1180-1180.

9 Appendix

9.1 Codon optimised DNA sequences

A. woodii acoR codon optimised for *C. necator* H16.

```
ATGGAACCGAACCTGAAGAAGCTGGCCGACAACTGGAAGAACTACCTGGACCACGACATCCT
GGACGAGAACACGCGCCCGATCATCCAGCGCTCGTGGTCGTACTGCAAGAAGCACGGCATCG
ACGTGAACGAAGGCAAGGGCGCCGCCATCGACTCGGCCCAGATCGAGCAGATCCTGGAAAAG
AACCAGGAACTGCTGAAGATCGCGCGCCCCATCATGCAGAACCTGTACGAGATCGTGCTGTC
GTCGCACTTCGTGCTGGTGCTGACCGACAAGAACGGCATCCTGCTGGACACCATCGGCGACG
AAATCGTGTCGATGCGCGCCTCGGAGCTGCGCTTCCTGAAGGGCACCGTGTGGACCACCGAC
GCCGTGGGCACCAACGCCATCGGCCTGGCGCTGGACGAGGACGCCCCGGTGCACGTGGTGGG
CGCCGAACACTACTGCATCTCGCACCACACCTGGACCTGCTCGGCCACCACCATCCACAACG
TGAAGGGCGAAGTGATCGGCTGCCTGAACATGTCGGGCGAGTCGCGCAAGCTGCACTCGCAC
ACGCTGGGCATCGTGGTCGCCGCCGCCTACAGCATCGAGAACGAGCTGGCCCTGTCGCACAC
CTACCGCTCGATGAACGCCTCGCTGAACTCGACCGAGGACGGCATCTTCGTGACCGACGAAA
ACCTGAACCTGCAGTGGATGAACTATGGCGCCCAGAAGGTGCTGCATCTGAACATGGACCAG
TTCAACGCGATCGGCTTCAACAACATCTTCAAGAAGATGGACGTGTCGGACGAGAGCTGGAA
CCCGGGCGAGAGCACCCGCTACTACACCGACGTGACCGCCTTCATCGGCAACCAGAAGATCC
CGTGCAGCGCCAACATCTCGCGCATCCTGGAAAACGACAAGATCCAGGGCTACTCGATCGGC
ATCCGCGAGATCAAGCATCTGCACACCGCCGTGAACCGCGTGTCGGGCAACGTGGCCTCGTA
CACCTTCGACGACATCATCACCCAGAACGCCGAGATGAAGATCATCATCAAGACCGCCGAAA
AGATGGCCCGCTTCAAGAAGTGCATCCTGATCGAGGGCGAAAGCGGCACCGGCAAGGAAATG
TTCGCCCACTCGATCCACAAGGCCTCGCACTTCTCGGCGGGCCCGTTCATCGTGGTGAACTG
CGCCTGCCTGCCGCGCGACCTGGTGGAATCGGAGCTGTTCGGCTACGTCAAGGGCGCGTTCA
CCGGCGCGCTGAACGAGGGCAAGCCGGGCAAGTTCGAGCTGGCGGAAGGCGGCACCATCTTC
CTGGACGAAATCGGCGAGCTGCCGCTGGAAATCCAGGCCAAGCTGCTGCGCGTGGTGGAAAC
CTACTCGGTGTCGCGCATCGGCTCGCAGTCGGAACGCAAGCTGAACATCCGCATCATCGTGG
CCACCAACCGCAACCTGGAACAGGAAGTGCAGAACAAGAACTTCCGCGAGGACCTGTACTTC
CGCCTGAACGTGATCTACCTGCACATCCCGCCGCTGCGCGTCCGCGGCGACGACATCCTGTG
GACCGCCTGCTACTTCCTGGACCGCCTGAACCTGGAATACCCGGAACACGCCAAGACCTTCG
CGCCGGACTTCCTGGAAGGCCTGAAGTTCCACCACTGGCCGGGCAACGTCCGCGAGCTGCAG
AACTTCGTGGAACGCACCTTCTACCTGTGCACCGAAACCGTGATCTCGAAGGACTACCTGCC
GCTGTCGGAGCGCAAGAACGTGACGATCAACAACGTGCTGCCCCTGACGCATAACCCGAGCC
TGGACGACCTGGTCAAGTCGAACCTGGAAAAGATCCTGAAGCAGACCCACGGCAGCGTGGAA
GCCAGCGCCGAGATCATGGGCCTGTCGCGCGCCAGCCTGTACCGCAAGATCAAGAAGTACAA
GATCGACATCAAGAACTATCGCTGCTCGTCGCAGATGTGA
```

C. acetobutylicum adhE codon optimised for *C. necator* H16.

```
ATGAAGGTGACCACCGTGAAGGAACTGGACGAGAAGCTGAAGGTGATCAAGGAAGCCCAGAA
GAAGTTCAGCTGCTACTCGCAGGAAATGGTCGACGAGATCTTCCGCAATGCCGCCATGGCCG
CCATCGATGCCCGCATCGAACTGGCCAAGGCCGCCGTGCTGGAAACCGGCATGGGCCTGGTC
GAGGACAAGGTCATCAAGAACCACTTCGCGGGCGAGTACATCTACAACAAGTACAAGGACGA
AAAGACCTGCGGCATCATCGAGCGCAACGAACCGTACGGCATCACCAAGATCGCCGAACCGA
```

TCGGCGTGGTGGCCGCGATCATCCCGGTGACGAATCCGACCTCGACCACCATCTTCAAGTCG
CTGATCTCGCTGAAGACCCGCAACGGCATCTTCTTCTCGCCGCATCCGCGCGCCAAGAAGTC
GACCATCCTGGCCGCCAAGACGATCCTGGATGCCGCCGTGAAGTCGGGCGCCCCGGAAAACA
TCATCGGCTGGATCGACGAGCCGAGCATCGAGCTGACCCAGTACCTGATGCAGAAGGCCGAC
ATCACCCTGGCCACCGGCGGCCCGTCGCTGGTCAAGTCGGCCTATTCGTCGGGCAAGCCGGC
CATCGGCGTCGGCCCGGGCAACACCCCGGTGATCATCGACGAGTCGGCCCACATCAAGATGG
CCGTGTCGTCGATCATCCTGAGCAAGACCTACGACAACGGCGTGATCTGCGCCTCGGAGCAG
TCGGTGATCGTGCTGAAGTCGATCTATAACAAGGTGAAGGACGAGTTCCAGGAACGCGGCGC
CTACATCATCAAGAAGAACGAGCTGGACAAGGTGCGCGAGGTGATCTTCAAGGACGGCTCGG
TGAACCCGAAGATCGTGGGCCAGAGCGCCTACACGATCGCGGCCATGGCGGGCATCAAGGTG
CCCAAGACCACGCGCATCCTGATCGGCGAGGTGACCAGCCTGGGCGAAGAGGAACCGTTCGC
GCACGAAAAGCTGTCGCCGGTGCTGGCCATGTACGAGGCCGACAACTTCGACGACGCCCTGA
AGAAGGCGGTCACCCTGATCAACCTGGGCGGCCTGGGCCACACCTCGGGCATCTACGCGGAC
GAGATCAAGGCCCGCGACAAGATCGACCGCTTCAGCTCGGCCATGAAGACCGTGCGCACCTT
CGTGAACATCCCGACCTCGCAGGGCGCCTCGGGCGACCTGTACAACTTCCGCATCCCGCCGT
CGTTCACCCTGGGCTGCGGCTTCTGGGGCGGCAACTCGGTGTCGGAAAACGTGGGCCCGAAG
CATCTGCTGAACATCAAGACCGTGGCCGAACGCCGCGAGAACATGCTGTGGTTCCGCGTGCC
GCACAAGGTGTACTTCAAGTTCGGCTGCCTGCAGTTCGCGCTGAAGGACCTGAAGGATCTGA
AGAAGAAGCGCGCCTTCATCGTCACCGACTCGGACCCGTACAACCTGAACTACGTGGACTCG
ATCATCAAGATCCTGGAACACCTGGACATCGACTTCAAGGTGTTCAACAAGGTGGGCCGCGA
GGCCGACCTGAAGACCATCAAGAAGGCCACCGAAGAGATGTCGTCGTTCATGCCGGACACCA
TCATCGCCCTGGGCGGCACCCCGGAAATGTCGTCGGCCAAGCTGATGTGGGTGCTGTACGAA
CACCCGGAAGTGAAGTTCGAGGACCTGGCCATCAAGTTCATGGACATCCGCAAGCGCATCTA
CACGTTCCCGAAGCTGGGCAAGAAGGCCATGCTGGTCGCCATCACCACCTCGGCCGGCTCGG
GCAGCGAAGTGACGCCCTTCGCGCTGGTGACCGACAACAACACCGGCAACAAGTATATGCTG
GCCGACTACGAGATGACCCCGAACATGGCCATCGTGGACGCGGAGCTGATGATGAAGATGCC
CAAGGGCCTGACCGCCTACAGCGGCATCGACGCCCTGGTGAACAGCATCGAGGCCTACACCA
GCGTGTACGCCAGCGAGTACACCAACGGCCTGGCGCTGGAAGCCATCCGCCTGATCTTCAAG
TACCTGCCGGAAGCCTACAAGAATGGCCGCACCAACGAAAAGGCGCGCGAGAAGATGGCCCA
CGCCAGCACCATGGCCGGCATGGCCTCGGCCAACGCCTTCCTGGGCCTGTGCCACTCGATGG
CGATCAAGCTGTCGTCGGAGCACAACATCCCGTCGGGCATCGCCAACGCGCTGCTGATCGAG
GAAGTGATCAAGTTCAACGCCGTGGACAACCCGGTGAAGCAGGCCCCGTGCCCGCAGTACAA
GTACCCGAATACCATCTTCCGCTATGCCCGCATCGCCGACTACATCAAGCTGGGCGGCAACA
CCGACGAGGAAAAGGTGGACCTGCTGATCAATAAGATCCACGAACTGAAGAAGGCCCTGAAT
ATCCCGACGTCGATCAAGGATGCCGGCGTCCTGGAAGAGAACTTCTACTCGTCGCTGGACCG
CATCTCGGAGCTGGCCCTGGACGATCAGTGCACCGGCGCCAATCCGCGCTTCCCGCTGACCT
CGGAAATCAAGGAAATGTACATCAACTGCTTCAAGAAGCAGCCCTGA

C. saccharoperbutylacetonicum bld codon optimised for *C. necator* H16.

ATGATCAAGGACACCCTGGTGTCGATCACCAAGGACCTGAAGCTGAAGACCAACGTGGAAAA
CGCCAACCTGAAGAACTACAAGGACGACTCGTCGTGCTTCGGCGTGTTCGAGAACGTCGAGA
ATGCCATCTCGAACGCCGTGCACGCCCAGAAGATCCTGTCGCTGCACTACACCAAGGAACAG
CGCGAGAAGATCATCACCGAGATCCGCAAGGCCGCGCTGGAAAACAAGGAAATCCTGGCCAC
CATGATCCTGGAAGAAACCCACATGGGCCGCTACGAGGACAAGATCCTGAAGCACGAACTGG
TGGCCAAGTACACCCCGGGCACCGAGGATCTGACCACCACCGCCTGGTCGGGCGACAACGGC
CTGACCGTGGTGGAAATGAGCCCGTACGGCGTGATCGGCGCGATCACCCCGAGCACGAACCC
GACCGAAACCGTGATCTGCAACTCGATCGGCATGATCGCCGCCGGCAACACCGTGGTGTTCA
ACGGCCATCCGGGCGCCAAGAAGTGCGTCGCCTTCGCCGTCGAGATGATCAACAAGGCCATC
ATCTCGTGCGGCGGCCCGGAAAACCTGGTGACCACCATCAAGAACCCGACGATGGACTCGCT

GGACGCCATCATCAAGCATCCGTCGATCAAGCTGCTGTGCGGCACCGGCGGCCCCGGCATGG
TCAAGACCCTGCTGAACTCGGGCAAGAAGGCCATCGGCGCCGGCGCGGGCAATCCGCCGGTG
ATCGTGGATGACACCGCCGACATCGAGAAGGCCGGCAAGTCGATCATCGAGGGCTGCTCGTT
CGACAACAACCTGCCGTGCATCGCGGAGAAGGAAGTGTTCGTCTTCGAAAACGTGGCCGACG
ACCTGATCTCGAACATGCTGAAGAACAATGCCGTGATCATCAACGAGGACCAGGTGTCGAAG
CTGATCGACCTGGTGCTGCAGAAGAACAACGAAACCCAGGAATACAGCATCAACAAGAAGTG
GGTCGGCAAGGACGCCAAGCTGTTCCTGGACGAGATCGACGTGGAATCGCCGTCGTCGGTGA
AGTGCATCATCTGCGAGGTGTCGGCCCGCCATCCGTTCGTGATGACCGAGCTGATGATGCCC
ATCCTGCCGATCGTGCGCGTGAAGGACATCGACGAGGCCATCGAGTACGCCAAGATCGCCGA
GCAGAACCGCAAGCACTCGGCCTACATCTACTCGAAGAACATCGACAACCTGAACCGCTTCG
AGCGCGAAATCGACACGACCATCTTCGTGAAGAACGCCAAGTCGTTCGCCGGCGTGGGCTAC
GAGGCCGAGGGCTTCACCACCTTCACGATCGCCGGCTCCACCGGCGAGGGCATCACCTCGGC
GCGCAATTTCACCCGCCAGCGCCGCTGCGTGCTGGCCGGCTGA

B. halodurans dra codon optimised for *C. necator* H16.

ATGTCGCGCTCGATCGCCCAGATGATCGACCACACGCTGCTGAAGCCGAACACCACCGAGGA
CCAGATCGTGAAGCTGTGCGAGGAAGCCAAGGAATACTCGTTCGCCTCGGTGTGCGTGAACC
CGACCTGGGTCGCCCTGGCCGCGCAGCTGCTGAAGGATGCCCCGGACGTGAAGGTGTGCACC
GTGATCGGCTTCCCGCTGGGCGCCACCACGCCGGAAGTGAAGGCGTTCGAAACCACCAACGC
CATCGAGAATGGCGCCACCGAGGTGGACATGGTGATCAACATCGGCGCCCTGAAGGACAAGC
AGTACGAACTGGTGGGCCGCGACATCCAGGCCGTGGTGAAGGCCGCCGAAGGCAAGGCCCTG
ACCAAGGTGATCATCGAAACCTCGCTGCTGACCGAGGAAGAGAAGAAGGCGGCCTGCGAGCT
GGCCGTGAAGGCGGGCGCCGACTTCGTCAAGACCTCGACGGGCTTCAGCGGCGGCGGCGCGA
CCGCGGAAGATATCGCCCTGATGCGCAAGGTGGTGGGCCCGAACCTGGGCGTCAAGGCCTCC
GGCGGCGTCCGCGACCTGTCGGACGCCAAGGCCATGATCGATGCGGGCGCCACGCGCATCGG
CGCGTCGGCCGGCGTGGCCATCGTGAACGGCGAACGCTCGGAGGGCTCGTACTGA

Z. mobilis pdc codon optimised for *C. necator* H16.

ATGTCGTACACCGTGGGCACCTACCTGGCCGAGCGCCTGGTGCAGATCGGCCTGAAGCACCA
CTTCGCCGTGGCCGGCGACTACAACCTGGTGCTGCTGGATAATCTGCTGCTGAACAAGAACA
TGGAACAGGTGTACTGCTGCAACGAGCTGAACTGCGGCTTCTCGGCGGAGGGCTATGCCCGC
GCCAAGGGCGCCGCGGCCGCCGTCGTGACCTACTCGGTGGGCGCCCTGTCGGCCTTCGACGC
CATCGGCGGCGCCTACGCCGAAAACCTGCCGGTGATCCTGATCTCGGGCGCCCCGAACAACA
ACGACCATGCCGCCGGCCATGTGCTGCATCACGCCCTGGGCAAGACCGACTACCACTACCAG
CTGGAAATGGCCAAGAACATCACCGCGGCGGCCGAGGCCATCTACACCCCGGAAGAAGCCCC
GGCCAAGATCGACCATGTGATCAAGACCGCGCTGCGCGAGAAGAAGCCGGTCTACCTGGAAA
TCGCCTGCAATATCGCCTCGATGCCGTGCGCGGCGCCCGGCCCGGCCTCGGCGCTGTTCAAC
GACGAAGCCTCGGACGAGGCCAGCCTGAATGCCGCCGTGGAAGAAACCCTGAAGTTCATCGC
CAACCGCGACAAGGTGGCCGTGCTGGTCGGCTCGAAGCTGCGCGCCGCCGGCGCCGAGGAAG
CGGCCGTCAAGTTCGCGGATGCCCTGGGCGGCGCGGTGGCCACGATGGCGGCGGCCAAGTCG
TTCTTCCCGGAAGAGAACCCGCACTACATCGGCACCTCGTGGGGCGAAGTGTCGTATCCGGG
CGTCGAAAAGACCATGAAGGAAGCCGACGCCGTGATCGCGCTGGCCCCGGTGTTCAATGACT
ACTCGACCACCGGCTGGACGGACATCCCGGATCCGAAGAAGCTGGTCCTGGCCGAACCGCGC
AGCGTGGTGGTGAATGGCGTGCGCTTCCCGTCGGTGCATCTGAAGGACTACCTGACGCGCCT
GGCGCAGAAGGTGTCGAAGAAGACCGGCGCGCTGGATTTCTTCAAGTCGCTGAATGCGGGCG
AGCTGAAGAAGGCCGCGCCGGCGGACCCGTCGGCGCCGCTGGTGAACGCCGAAATCGCCCGC
CAGGTGGAAGCCCTGCTGACCCCGAACACGACGGTGATCGCGGAAACCGGCGACTCGTGGTT

CAACGCCCAGCGCATGAAGCTGCCGAATGGCGCGCGCGTGGAATACGAGATGCAGTGGGGCC
ACATCGGCTGGTCGGTGCCGGCCGCGTTCGGCTACGCCGTGGGCGCCCCGGAACGCCGCAAT
ATCCTGATGGTCGGCGACGGCTCGTTCCAGCTGACCGCGCAGGAAGTGGCCCAGATGGTGCG
CCTGAAGCTGCCCGTGATCATCTTCCTGATCAACAACTACGGCTACACCATCGAGGTGATGA
TCCATGATGGCCCGTACAACAACATCAAGAACTGGGACTATGCCGGCCTGATGGAAGTGTTC
AACGGCAATGGCGGCTACGACTCCGGCGCCGGCAAGGGCCTGAAGGCCAAGACCGGCGGCGA
ACTGGCCGAGGCGATCAAGGTGGCGCTGGCCAATACGGATGGCCCGACGCTGATCGAGTGCT
TCATCGGCCGCGAGGACTGCACCGAGGAACTGGTGAAGTGGGGCAAGCGCGTGGCCGCCGCG
AACTCGCGCAAGCCGGTGAACAAGCTGCTGTGA

C. beijerinckii adh codon optimised for *C. necator* H16.

ATGAAGGGCTTCGCCATGCTGGGCATCAACAAGCTGGGCTGGATCGAGAAGGAACGCCCGGT
GGCCGGCAGCTACGATGCCATCGTGCGCCCGCTGGCCGTGTCGCCGTGCACCTCGGATATCC
ACACCGTGTTCGAAGGCGCCCTGGGCGACCGCAAGAACATGATCCTGGGCCACGAGGCCGTG
GGCGAAGTGGTGGAAGTGGGCAGCGAGGTGAAGGACTTCAAGCCCGGCGACCGCGTGATCGT
GCCGTGCACGACCCCGGACTGGCGCTCGCTGGAAGTGCAGGCCGGCTTCCAGCAGCACTCGA
ACGGCATGCTGGCCGGCTGGAAGTTCTCGAACTTCAAGGACGGCGTGTTCGGCGAGTACTTC
CACGTGAACGACGCCGACATGAACCTGGCCATCCTGCCGAAGGACATGCCGCTGGAAAACGC
CGTGATGATCACCGACATGATGACCACGGGCTTCCATGGCGCCGAGCTGGCCGACATCCAGA
TGGGCTCGTCGGTGGTGGTGATCGGCATCGGCGCCGTGGGCCTGATGGGCATCGCCGGCGCC
AAGCTGCGCGGCGCCGGCCGCATCATCGGCGTGGGCTCGCGCCCGATCTGCGTGGAAGCGGC
CAAGTTCTATGGCGCCACCGACATCCTGAACTACAAGAACGGCCACATCGTGGACCAGGTGA
TGAAGCTGACCAACGGCAAGGGCGTCGACCGCGTCATCATGGCCGGCGGCGGCTCGGAAACC
CTGTCGCAGGCCGTGAGCATGGTCAAGCCCGGCGGCATCATCTCGAACATCAACTACCACGG
CTCGGGCGACGCCCTGCTGATCCCGCGCGTGGAATGGGGCTGCGGCATGGCCCACAAGACCA
TCAAGGGCGGCCTGTGCCCGGGCGGCCGGCTGCGCGCCGAAATGCTGCGCGACATGGTGGTG
TACAACCGCGTGGACCTGTCGAAGCTGGTGACCCACGTGTACCATGGCTTCGACCACATCGA
AGAGGCCCTGCTGCTGATGAAGGACAAGCCCAAGGACCTGATCAAGGCCGTGGTGATCCTGT
GA

B. subtilis alsS codon optimised for *C. necator* H16.

ATGACCAAGGCCACCAAGGAACAGAAGTCGCTGGTCAAGAATCGCGGCGCCGAACTGGTGGT
GGACTGCCTGGTGGAACAGGGCGTGACCCACGTGTTCGGCATCCCGGGCGCCAAGATCGACG
CCGTGTTCGACGCGCTGCAGGACAAGGGCCCCGAGATCATCGTGGCCCGCCACGAGCAGAAT
GCCGCCTTCATGGCCCAGGCGGTGGGCCGCCTGACCGGCAAGCCGGGCGTCGTGCTGGTGAC
GAGCGGCCCGGGCGCGAGCAACCTGGCCACCGGCCTGCTGACCGCCAACACCGAAGGCGACC
CGGTGGTGGCCCTGGCCGGCAACGTGATCCGCGCCGACCGCCTGAAGCGCACCCATCAGTCG
CTGGACAATGCCGCGCTGTTCCAGCCGATCACCAAGTACTCGGTGGAAGTGCAGGACGTGAA
GAACATCCCGGAAGCCGTGACCAACGCCTTCCGCATCGCCTCGGCCGGCCAGGCCGGCGCCG
CCTTCGTGTCGTTCCCGCAGGACGTCGTGAACGAGGTGACCAACACCAAGAACGTGCGCGCC
GTGGCCGCGCCGAAGCTGGGCCCCGCCGCCGACGACGCCATCTCGGCCGCGATCGCCAAGAT
CCAGACCGCCAAGCTGCCGGTGGTGCTGGTCGGCATGAAGGGCGGCCGGCCGGAAGCGATCA
AGGCCGTGCGCAAGCTGCTGAAGAAGGTGCAGCTGCCGTTCGTGGAAACCTACCAGGCCGCG
GGCACCCTGTCGCGCGATCTGGAAGATCAGTACTTCGGCCGCATCGGCCTGTTCCGCAACCA
GCCGGGCGACCTGCTGCTGGAACAGGCGGATGTGGTGCTGACCATCGGCTACGACCCGATCG
AGTACGACCCCAAGTTCTGGAACATCAACGGCGACCGCACCATCATCCACCTGGACGAAATC
ATCGCCGACATCGACCACGCCTACCAGCCGGACCTGGAACTGATCGGCGACATCCCGAGCAC

GATCAACCACATCGAGCATGACGCCGTGAAGGTCGAGTTCGCCGAGCGCGAGCAGAAGATCC
TGTCGGACCTGAAGCAGTACATGCACGAGGGCGAACAGGTGCCGGCCGACTGGAAGTCGGAT
CGCGCCCATCCGCTGGAAATCGTGAAGGAACTGCGCAACGCCGTGGACGACCACGTGACCGT
GACCTGCGACATCGGCTCGCACGCCATCTGGATGTCGCGCTACTTCCGCAGCTACGAGCCGC
TGACGCTGATGATCAGCAACGGCATGCAGACCCTGGGCGTCGCCCTGCCGTGGGCCATCGGC
GCCTCGCTGGTGAAGCCCGGCGAAAAGGTGGTGTCGGTGAGCGGCGATGGCGGCTTCCTGTT
CTCGGCCATGGAACTGGAAACCGCCGTGCGCCTGAAGGCCCCGATCGTGCACATCGTGTGGA
ACGACTCGACCTACGACATGGTGGCCTTCCAGCAGCTGAAGAAGTACAACCGCACCTCGGCC
GTGGACTTCGGCAACATCGACATCGTGAAGTACGCCGAGTCCTTCGGCGCCACGGGCCTGCG
CGTGGAATCGCCGGACCAGCTGGCCGACGTGCTGCGCCAGGGCATGAACGCGGAAGGCCCGG
TGATCATCGACGTGCCGGTGGACTACTCGGACAACATCAACCTGGCGTCGGACAAGCTGCCC
AAGGAGTTCGGCGAGCTGATGAAGACCAAGGCGCTGTGA

B. subtilis alsD codon optimised for *C. necator* H16.

ATGAAGCGCGAGTCGAACATCCAGGTGCTGTCGCGCGGCCAGAAGGACCAGCCGGTCAGCCA
AATCTACCAGGTGTCGACCATGACCTCGCTGCTGGACGGCGTGTACGACGGCGACTTCGAGC
TGTCGGAGATCCCGAAGTACGGCGATTTCGGCATCGGCACCTTCAACAAGCTGGATGGCGAG
CTGATCGGCTTCGACGGCGAGTTCTACCGCCTGCGCTCGGATGGCACCGCCACGCCGGTGCA
GAACGGCGATCGCAGCCCGTTCTGCTCGTTCACCTTCTTCACCCCGGACATGACCCACAAGA
TCGACGCCAAGATGACCCGCGAGGACTTCGAGAAGGAAATCAACTCGATGCTGCCGTCGCGC
AACCTGTTCTACGCCATCCGCATCGACGGCCTGTTCAAGAAGGTGCAGACCCGCACCGTGGA
ACTGCAGGAAAAGCCCTACGTCCCGATGGTGGAAGCCGTCAAGACCCAGCCGATCTTCAACT
TCGACAACGTGCGCGGCACCATCGTGGGCTTCCTGACGCCGGCCTACGCCAACGGCATCGCC
GTGTCGGGCTACCATCTGCACTTCATCGACGAAGGCCGCAACAGCGGCGGCCACGTGTTCGA
CTACGTGCTGGAAGATTGCACCGTGACCATCTCGCAGAAGATGAACATGAACCTGCGCCTGC
CGAACACCGCCGATTTCTTCAACGCCAACCTGGACAACCCGGACTTCGCCAAGGACATCGAA
ACCACCGAGGGCTCGCCGGAATGA

K. pneumoniae budC codon optimised for *C. necator* H16.

ATGAAGAAGGTGGCCCTGGTCACCGGCGCCGGCCAGGGCATCGGCAAGGCGATCGCGCTGCG
CCTGGTGAAGGATGGCTTCGCCGTGGCGATCGCCGACTACAACGACACCACCGCCAAGGCCG
TGGCCTCGGAGATCAACCAGGCCGGCGGCCGGGCGATGGCCGTGAAGGTGGACGTGTCGGAC
CGCGACCAGGTGTTCGCCGCCGTGGAACAGGCCCGCAAGACCCTGGGCGGCTTCGACGTGAT
CGTGAACAATGCCGGCGTGGCCCCGAGCACGCCGATCGAATCGATCACCCCGGAAATCGTGG
ACAAGGTGTACAACATCAACGTGAAGGGCGTGATCTGGGGCATCCAGGCCGCGGTGGAAGCC
TTCAAGAAGGAAGGCCACGGCGGCAAGATCATCAACGCCTGCTCGCAGGCCGGCCACGTGGG
CAACCCGGAACTGGCCGTGTACTCGTCGTCGAAGTTCGCCGTGCGCGGCCTGACGCAGACCG
CCGCGCGCGACCTGGCGCCGCTGGGCATCACCGTGAATGGCTACTGCCCCGGCATCGTCAAG
ACCCCGATGTGGGCCGAGATCGACCGCCAGGTGTCGGAAGCCGCCGGCAAGCCGCTGGGCTA
CGGCACCGCCGAGTTCGCCAAGCGCATCACCCTGGGCCGCCTGTCGGAGCCGGAAGATGTGG
CCGCGTGCGTGTCGTATCTGGCCTCGCCGGACTCGGACTACATGACCGGCCAGTCGCTGCTG
ATCGATGGCGGCATGGTGTTCAACTGA

9.2 Supplementary Tables

Supplementary Table 1 List of enzymes that contribute to carbon and energy metabolism in *C. necator* H16 as previously reported (Pohlmann *et al.*, 2006; Cramm, 2008).

Enzyme	**Gene(s)**	**Locus tag(s)**	**EC Number**
Glucosamine specific phosphotransferase system	*nagFE*	H16_A0311, H16_A0312	2.7.1.193
N-acetylglucosamine-6-phosphate deacetylase	*nagA*	H16_A0314	3.5.1.25
Glucosamine-6-phosphate deaminase	*nagB*	H16_A0315	2.6.1.16
Glucose-6-phosphate 1-dehydrogenase isoenzyme 1	*zwf1*	H16_A0316	1.1.1.49/1.1.1.363
Phosphoglycerate mutase 1	*pgam1*	H16_A0332	5.4.2.11
Glutamate dehydrogenase	*gdhA1*	H16_A0471	1.4.1.3
Phosphoglycerate mutase 2	*pgam2*	H16_A0493	5.4.2.11
Succinyl-CoA synthetase	*sucCD*	H16_A0547, H16_A0548	6.2.1.5
Phosphoglycerate kinase	*pgk*	H16_A0566	2.7.2.3
Pyruvate kinase isoenzyme 1	*pyk1*	H16_A0567	2.7.1.40
Fructose-bisphosphate aldolase	*fba*	H16_A0568	4.1.2.13
Mo-formate dehydrogenase (NAD^+-dependent)	*fdsGBACD*	H16_A0640 - H16_A0644	1.17.1.9
L-lactate dehydrogenase (NAD-dependent)	*ldh*	H16_A0666	1.1.1.27
Membrane-bound transhydrogenase isoenzyme 1	*pntAa1, pntAb1, pntB1*	H16_A0850 - H16_A0852	1.6.1.2/7.1.1.1
Malate dehydrogenase ($NADP^+$-dependent)	*maeB*	H16_A1002	1.1.1.40
Triosephosphate isomerase	*tim*	H16_A1047	5.3.1.1
NAD dehydrogenase (type I)	*nuoABCDEFGHIJKLMN*	H16_A1050 - H16_A1063	7.1.1.2

Phosphogluconate dehydratase	*edd1*	H16_A1178	4.2.1.12
Gluconate kinase	*gntK*	H16_A1179	2.7.1.12
Phosphopyruvate hydratase	*eno*	H16_A1188	4.2.1.11
Membrane-bound transhydrogenase isoenzyme 2	*pntAa2, pntAb2, pntB2*	H16_A1264 - H16_A1266	1.6.1.2/7.1.1.1
Pyruvate dehydrogenase E1 component	*pdhA12*	H16_A1374, H16_A1753	1.2.4.1
Pyruvate dehydrogenase E2 component	*pdhB*	H16_A1375	2.3.1.12
Pyruvate dehydrogenase E3 component	*pdhL*	H16_A1377	1.8.1.4
Glucose-6-phosphate isomerase	*pgi1*	H16_A1502	5.3.1.9
D-lactate dehydrogenase isoenzyme 1	*ldhA1*	H16_A1681	1.1.1.28
D-lactate dehydrogenase isoenzyme 2	*ldhA2*	H16_A1682	1.1.1.28
Citrate synthase	*cisY*	H16_A1906	2.3.3.1
2-oxoglutarate dehydrogenase E3 component	*odhL*	H16_A2323	1.8.1.4
2-oxoglutarate dehydrogenase E2 component	*odhB*	H16_A2324	2.3.1.61
2-oxoglutarate dehydrogenase E1 component	*odhA*	H16_A2325	1.2.4.2
Pentose-5-phosphate isomerase isoenzyme 1	*rpiA*	H16_A2345	5.3.1.6
Transaldolase	*tai*	H16_A2346	2.2.1.2
Fumarate hydratase class I	*fumA*	H16_A2528	4.2.1.2
Succinate dehydrogenase	*sdhBADC*	H16_A2629 - H16_A2632	1.3.5.1/1.3.5.4
Malate dehydrogenase isoenzyme 1	*mdh12*	H16_A2634, H16_B0334	1.1.1.37
Aconitate hydratase	*acnA*	H16_A2638	4.2.1.3
NAD dehydrogenase (type 2)	*ndh*	H16_A2740	7.1.1.2

Membrane-bound formate dehydrogenase isoenzyme 1	*fhdD1, fdhC, fdhB1, fdhA1, fdhD2, fdhA2*	H16_A2932, H16_A2934, H16_A2936, H16_A2937, H16_B1470, H16_B1471	1.17.1.9
Isocitrate dehydrogenase (NADP-dependent) isoenzyme 1	*icd1*	H16_A3056	1.1.1.42
Membrane-bound transhydrogenase isoenzyme 3	*pntAa3, pntAb3, pntB3*	H16_A3128, H16_A3130, H16_A3131	1.6.1.2/7.1.1.1
Glyceraldehyde-3-phosphate dehydrogenase isoenzyme 1	*gapA*	H16_A3146	1.2.1.12
Malate dehydrogenase (NAD^+-dependent)	*maeA*	H16_A3153	1.1.1.40
Pyruvate kinase isoenzyme 2	*pyk2*	H16_A3602	2.7.1.40
Glutathionine reductase (NADPH-dependent)	*lpdaA*	H16_A3724	1.8.1.7
Fumarate hydratase class II	*fumC*	H16_B0103	4.2.1.2
Aconitate hydratase 2	*acnB*	H16_B0568	4.2.1.3/4.2.1.99
Pyruvate kinase isoenzyme 3	*pyk3*	H16_B0961	2.7.1.40
Isocitrate dehydrogenase (NAD^+-dependent)	*icd3*	H16_B1016	1.1.1.41
2-Amino-2-keto-gluconate hydrolase	*h16_B1211*	H16_B1211	4.3.1.18
2-keto-3-deoxygluconate kinase	*kdgK*	H16_B1212	2.7.1.45
2-keto-3-deoxy-6-phosphogluconate aldolase	*eda*	H16_B1213	4.1.2.14/4.1.3.42
Fructose-1,6-/sedoheptulose-1,7-bisphosphate aldolase isoenzyme 1	*cbbA2*	H16_B1384	4.1.2.13
Phosphoglycerate kinase isoenzyme 1	*cbbK2*	H16_B1385	2.7.2.3
Glyceraldehyde-3-phosphate dehydrogenase isoenzyme 2	*cbbG2*	H16_B1386	1.2.1.12

Transketolase isoenzyme 1	*cbbT2*	H16_B1388	2.2.1.1
Pentose-5-phosphate 3-epimerase isoenzyme 1	*cbbP2*	H16_B1389	2.7.1.19
Fructose-1,6-/seduheptulose-1,7-bisphosphatase isoenzyme 1	*cbbF2*	H16_B1390	3.1.3.11/3.1.3.37
Ribulose-phosphate 3-epimerase isoenzyme 1	*cbbE2*	H16_B1391	5.1.3.1
Ribulose-bisphosphate carboxylase isoenzyme 1	*cbbS2*	H16_B1394	4.1.1.39
Ribulose-bisphosphate carboxylase isoenzyme 3	*cbbL2*	H16_B1395	4.1.1.39
Membrane-bound formate dehydrogenase isoenzyme 2	*fdoGHIE*	H16_B1452-B16_B1455	1.17.1.9
Glucose-6-phosphate 1-dehydrogenase isoenzyme 2	*zwf2*	H16_B1501	1.1.1.49/1.1.1.363
Glucose-6-phosphate isomerase	*pgi2*	H16_B1502	5.3.1.9
Fructokinase	*frcK*	H16_B1503	2.7.1.4
Membrane-bound formate dehydrogenase isoenzyme 3	*fdwAB*	H16_B1700, H16_B1701	1.17.1.9
Membrane-bound transhydrogenase isoenzyme 4	*pntA4, pntB4*	H16_B1714-H16_B1715	1.6.1.2/7.1.1.1
Isocitrate dehydrogenase (NADP-dependent) isoenzyme 1	*icd2*	H16_B1931	1.1.1.42
Glutamate dehydrogenase ($NADP^+$-dependent)	*gdhA2*	H16_B1945	1.4.1.4
Glucokinase	*glk*	H16_B2564	2.7.1.2
6-Phosphogluconolactonase	*pgl*	H16_B2565	3.1.1.31
Glucose-6-phosphate 1-dehydrogenase isoenzyme 3	*zwf3*	H16_B2566	1.1.1.49/1.1.1.363
Phosphogluconate dehydratase	*edd2*	H16_B2567	4.2.1.12

Membrane-bound [NiFe]-hydrogenase	*hoxKGZ*	PHG001-PHG003	1.12.99.6
Soluble hydrogenase	*hoxFUHY*	PHG088-PHG091	1.12.1.2
Fructose-1,6-/sedoheptulose-1,7-bisphosphate aldolase isoenzyme 2	*cbbAp*	PHG416	4.1.2.13
Phosphoglycerate kinase isoenzyme 2	*cbbKp*	PHG417	2.7.2.3
Glyceraldehyde-3-phosphate dehydrogenase (NAD-dependent)	*cbbGp*	PHG418	1.2.1.12
Transketolase isoenzyme 2	*cbbTp*	PHG420	2.2.1.1
Pentose-5-phosphate 3-epimerase isoenzyme 2	*cbbPp*	PHG421	2.7.1.19
Fructose-1,6-/seduheptulose-1,7-bisphosphatase isoenzyme 2	*cbbFp*	PHG422	3.1.3.11/3.1.3.37
Ribulose-phosphate 3-epimerase isoenzyme 2	*cbbEp*	PHG423	5.1.3.1
Ribulose-bisphosphate carboxylase isoenzyme 2	*cbbSp*	PHG426	4.1.1.39
Ribulose-bisphosphate carboxylase isoenzyme 4	*cbbLp*	PHG427	4.1.1.39

9.3 Supplementary Figures

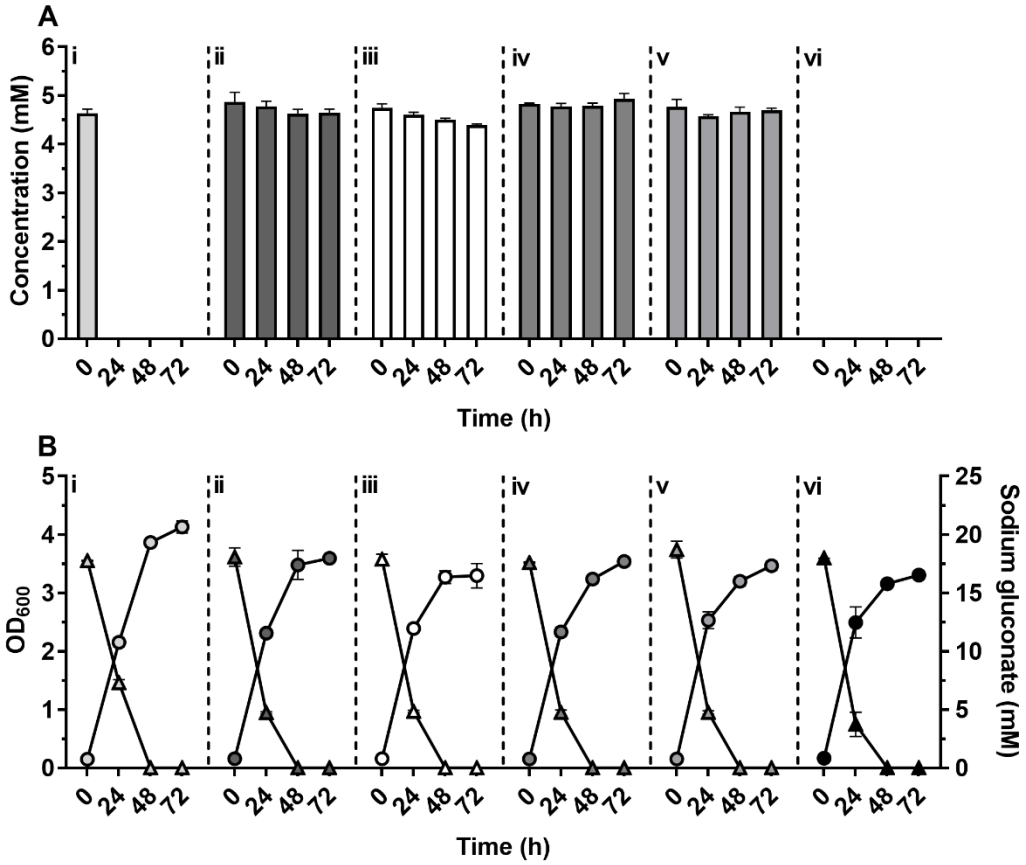

Supplementary Figure 1 Co-consumption assay screening *C. necator* in the presence of several diol isomers and acetoin exogenously added to a final concentration of 5 mM (A). Compounds tested: i. acetoin, ii. *meso*-2,3-BDO, iii. (*R*, *R*)-2,3-BDO, iv. 1,4-BDO, v. (*R*)-1,3-BDO, vi. control containing no BDO or acetoin. Biomass production was also measured with circles representing OD_{600} and triangles represent sodium gluconate (B). Cells were cultivated in falcon tubes in 10 mL MM supplemented with 0.4 % (w/v) sodium gluconate at 30 °C, 200 rpm shaking. Error bars represent standard error calculated from three biological replicates.

```
b2381:PyrR          --MKVIIVE-DEFLAQQELSWLIKEHSQMEIVGTFDDGLDVLKFLQHNRVDAIFLDINIP        57
H16_A2233:LytT      MTPTLLIADDEALLARVLESELMSLWPEARIVSVVHDGVAALAAAREHQPRVAFLDIRMP        60
H16_A3389:LytT      MTPTALIADDEEHLRAYLRSKLQRHWPELQIVAEATNGIEAADAIARLSPSVAFLDIKMP        60
                       . :*.: :  *     * *     : .**.   :*: .     .    . ****.:*

b2381:PyrR          SLDGVLLAQNISQFAHKPFIVFITAWKEHAVEAFELEAFDYILKPYQESRITGMLQKLEA        117
H16_A2233:LytT      GMSGMDVARELIEFDTPPLVVFVTAYDQFALEAFERAAVDYVLKPVQRERLEATVQRLKD        120
H16_A3389:LytT      GLSGLEVAQGI---ETDTRLVFVTAYDEFALDAFERAAVDYLVKPVSEERLGRTIERLRK        117
                    .:.*: :*: :        :**:**:.:.*::***  *.**::** ...*:   :::*.

b2381:PyrR          AWQQQQTSS--------------------------TPAATVTREN---DTINLVKDERI        147
H16_A2233:LytT      RLAGPADDEDTEAEASIAETDRLGQLLARLESLEHATPGPGGAPQRQYLRFIKALVGQEV        180
H16_A3389:LytT      ALQEAAPL------------PELAQLLSQ---LTRAQPR---AESGGQLRWVRASRGNTT        159
                                                    *    : .      :.   .:

b2381:PyrR          IVTPINDIYYAEAHEKMTFVYTRRESYVMPMNITEFCSKLPPSHFFRCHRSFCVNLNKIR        207
H16_A2233:LytT      RIIPVDEVIYLEATDKYVNVVSGAGEALIRTSLRELTQQLDPERFWQVHRGTVVNITCVA        240
H16_A3389:LytT      SHVPIQEVMYFQSDDKYVVVHTRDGEHLIRTPLAELIAGLDPEVFWQIHRSSIVNMEYVA        219
                       *:::: * :: :* . * :   . ::   : *:   * *. *:: **.  **:  :

b2381:PyrR          EIEPWFNNTYILRLKDLDFEVPVSRSKVKEFRQLMHL       244
H16_A2233:LytT      SAVNQSLGRLSLRLRDRPELLPVARQYAHLFKQM---       274
H16_A3389:LytT      GTRRDEAGRLFVRMRDSEAELPVSRAYMHRFRQM---       253
                           .   :*::*    :**:*   : *:*:
```

Supplementary Figure 2 Alignment of the amino acid sequences for transcription factor PyrR from from *E. coli* MG1655 and two LytT response regulator proteins containing LytTR DNA-binding domains ($LytT_1$, $LytT_2$) from *C. necator* H16. Protein sequence alignments were completed and visualised using Clustal Omega software.

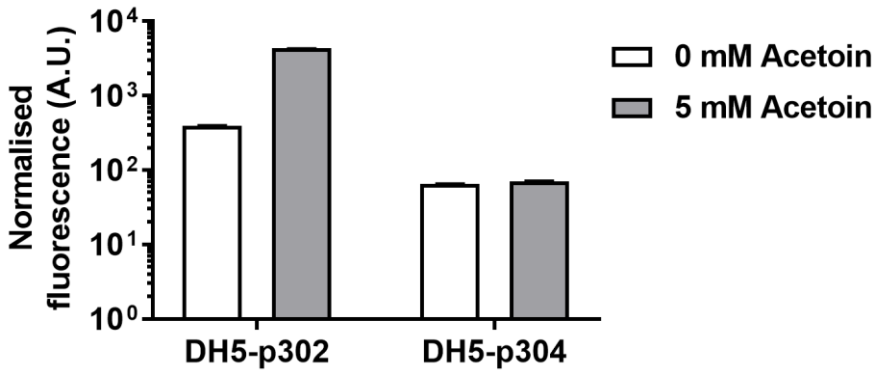

Supplementary Figure 3 Confirmation of AcoR influence on P_{acoA} for induction of gene expression by effector acetoin. Normalised fluorescence of strains DH5-p302 and DH5-p304 harbouring AcoR/P_{acoA} inducible system or promoter only (P_{acoA}), respectively. Single fluorescence measurement was taken 8 h after exogenous addition of 0 mM (control) or 5 mM

acetoin to cells cultivated in LB. Error bars represent standard error calculated from three biological replicates.

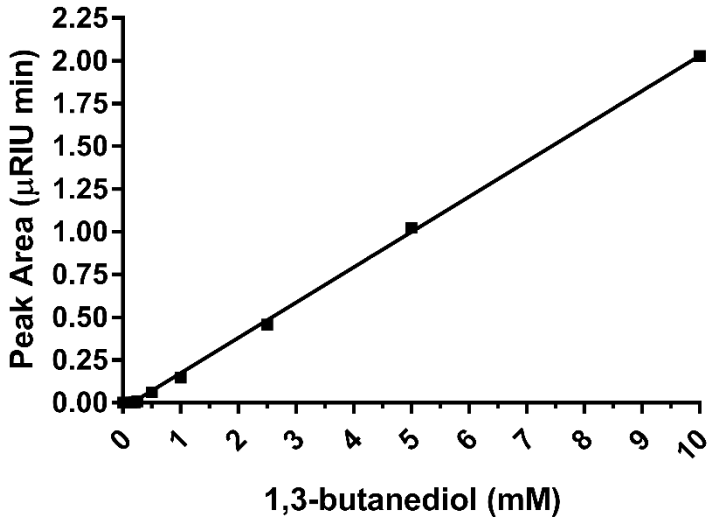

Supplementary Figure 4. Integrated peak area obtained from HPLC-RI chromatography analysis plotted against known concentrations of 1,3-BDO standard.

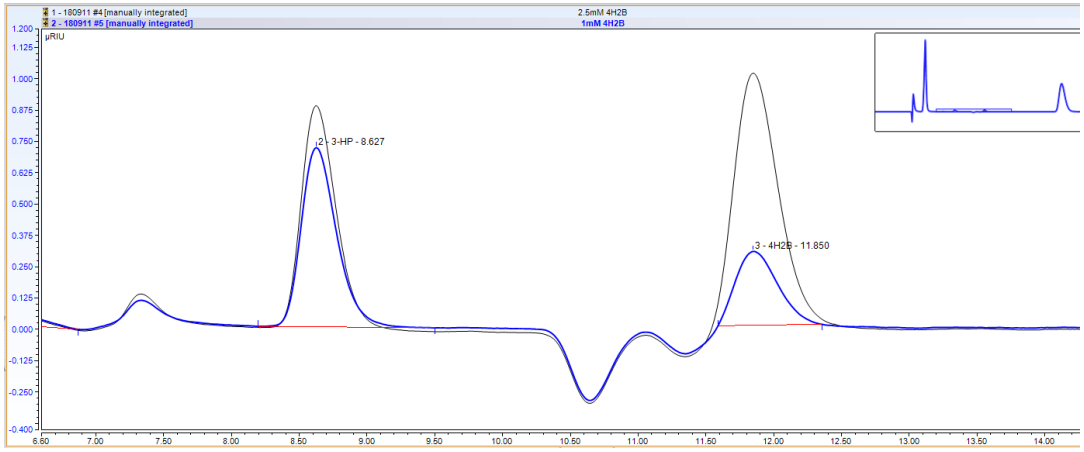

Supplementary Figure 5. Chromatogram of 1 mM and 2.5 mM 4-hydroxy-2-butanone standards with peaks observed in the RI channel

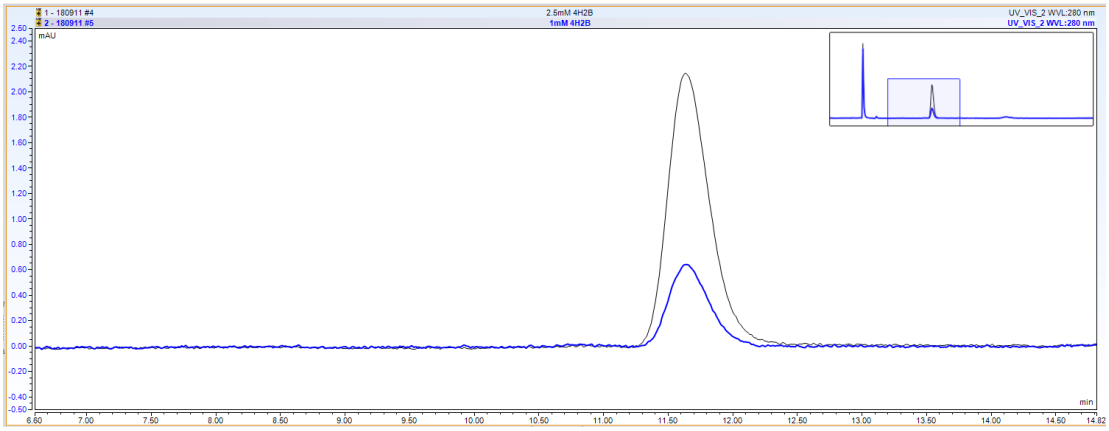

Supplementary Figure 6. Chromatogram of 1 mM and 2.5 mM 4-hydroxy-2-butanone standards with peaks observed in the UV channel at wavelength 280 nm

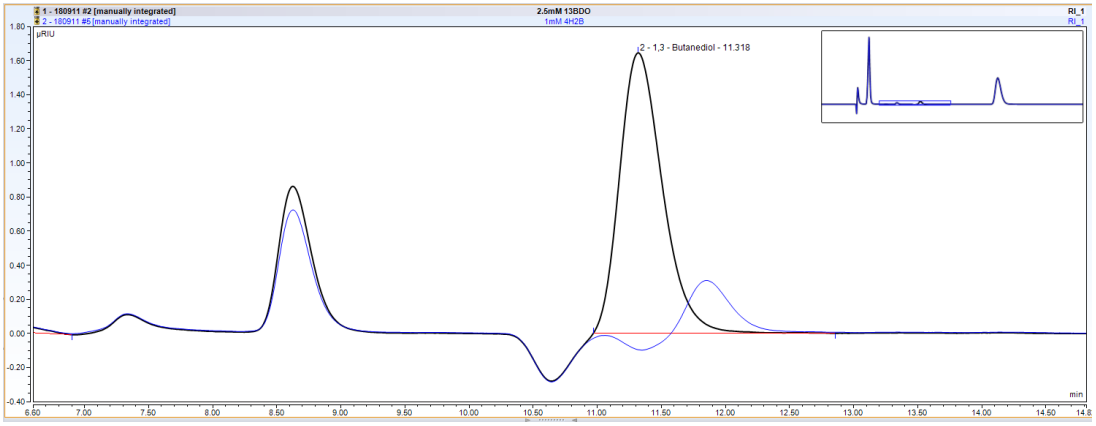

Supplementary Figure 7. Overlaid chromatograms of 2.5 mM 1,3-butanediol and 1 mM 4-hydroxy-2-butanone standards with peaks observed in the RI channel

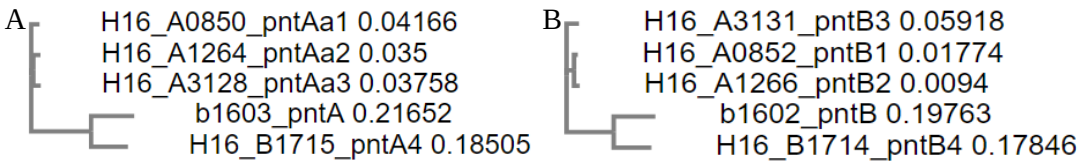

Supplementary Figure 8. Phylogenetic tree of membrane-bound transhydrogenase subunits PntA (A) and PntB (B) for *E. coli* (PntAB) and *C. necator* (PntAa1234, pntB1234). Phylogenetic tree was visualised using Clustal Omega software.

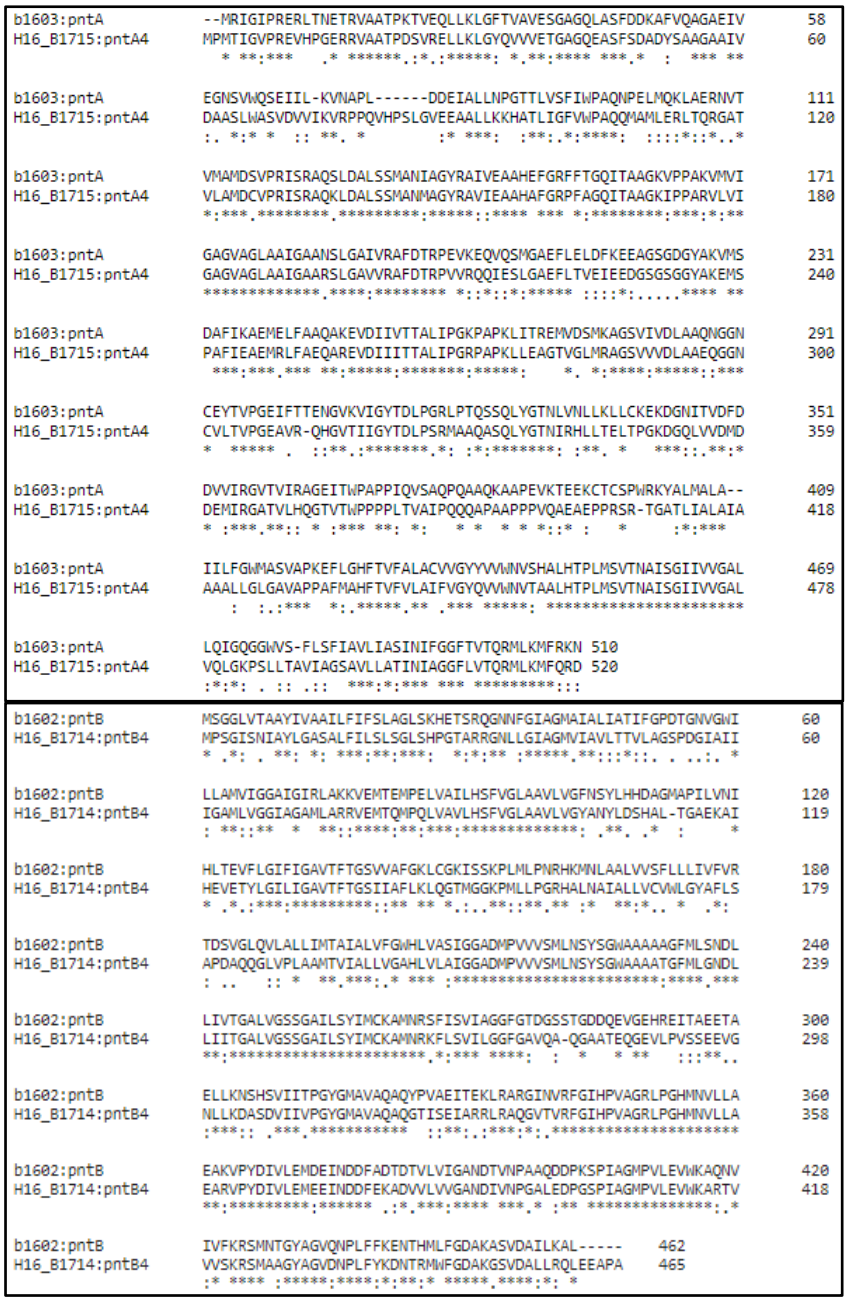

Supplementary Figure 9. Alignment of the amino acid sequences for transhydrogenase subunits PntAB from *E. coli* MG1655 and PntAB4 from *C. necator* H16. Protein sequence alignments were completed and visualised using Clustal Omega software.

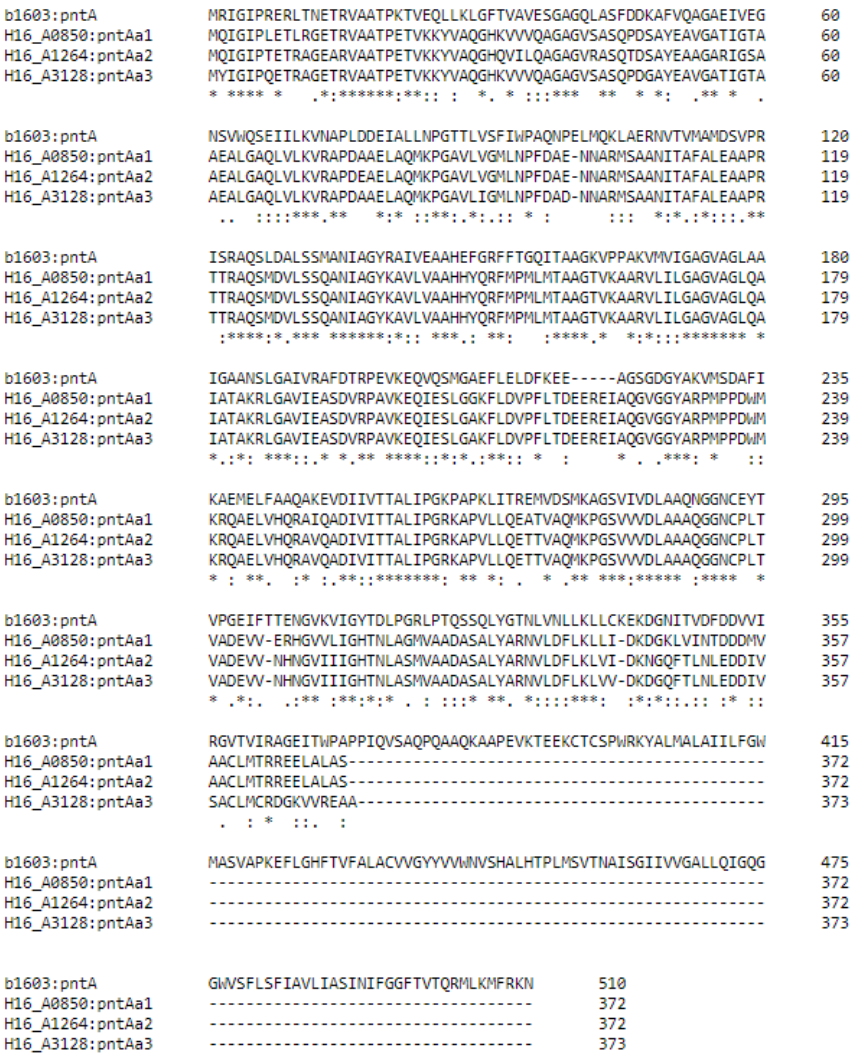

Supplementary Figure 10 Alignment of the amino acid sequences for transhydrogenase subunits PntA from *E. coli* MG1655 and PntAa123 from *C. necator* H16. Protein sequence alignments were completed and visualised using Clustal Omega software.

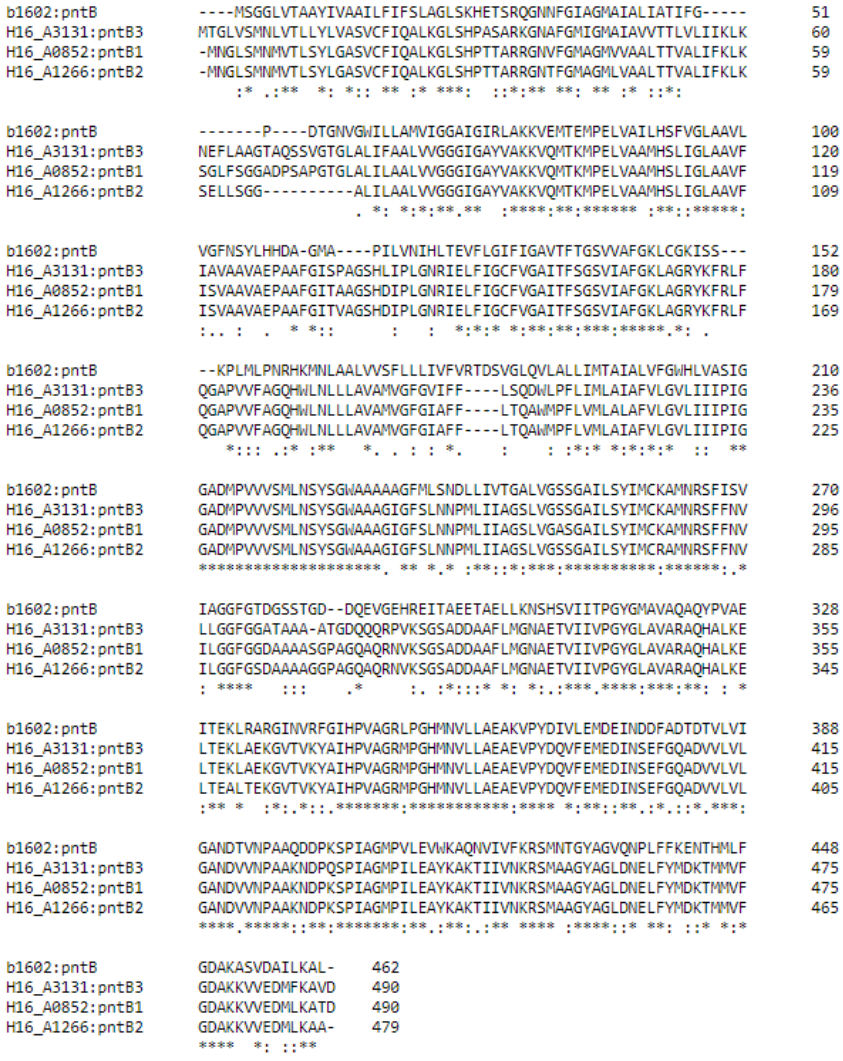

Supplementary Figure 11. Alignment of the amino acid sequences for transhydrogenase subunits PntB from *E. coli* MG1655 and PntB123 from *C. necator* H16. Protein sequence alignments were completed and visualised using Clustal Omega software.

```
H16_B1715:pntA4       MPMTIGVPREVHPGERRVAATPDSVRELLKLGYQVVVETGAGQEASFSDADYSAAGAAIV     60
H16_A3130:pntAb3      ------------------------------------------------------------     0
H16_A0851:pntAb1      ------------------------------------------------------------     0
H16_A1265:pntAb2      ------------------------------------------------------------     0

H16_B1715:pntA4       DAASLWASVDVVIKVRPPQVHPSLGVEEAALLKKHATLIGFVWPAQQMAMLERLTQRGAT     120
H16_A3130:pntAb3      ------------------------------------------------------------     0
H16_A0851:pntAb1      ------------------------------------------------------------     0
H16_A1265:pntAb2      ------------------------------------------------------------     0

H16_B1715:pntA4       VLAMDCVPRISRAQKLDALSSMANMAGYRAVIEAAHAFGRPFAGQITAAGKIPPARVLVI     180
H16_A3130:pntAb3      ------------------------------------------------------------     0
H16_A0851:pntAb1      ------------------------------------------------------------     0
H16_A1265:pntAb2      ------------------------------------------------------------     0

H16_B1715:pntA4       GAGVAGLAAIGAARSLGAVVRAFDTRPVVRQQIESLGAEFLTVEIEEDGSGSGGYAKEMS     240
H16_A3130:pntAb3      ------------------------------------------------------------     0
H16_A0851:pntAb1      ------------------------------------------------------------     0
H16_A1265:pntAb2      ------------------------------------------------------------     0

H16_B1715:pntA4       PAFIEAEMRLFAEQAREVDIIITTALIPGRPAPKLLEAGTVGLMRAGSVVVDLAAEQGGN     300
H16_A3130:pntAb3      ------------------------------------------------------------     0
H16_A0851:pntAb1      ------------------------------------------------------------     0
H16_A1265:pntAb2      ------------------------------------------------------------     0

H16_B1715:pntA4       CVLTVPGEAVRQHGVTIIGYTDLPSRMAAQASQLYGTNIRHLLTELTPGKDGQLVVDMDD     360
H16_A3130:pntAb3      ------------------------------------------------------------     0
H16_A0851:pntAb1      ------------------------------------------------------------     0
H16_A1265:pntAb2      ------------------------------------------------------------     0

H16_B1715:pntA4       EMIRGATVLHQGTVTWPPPPLTVAIPQQQAPAAPPPVQAEAEPPRSRTGATLIALAIAAA     420
H16_A3130:pntAb3      ------------------------------------------------------------     0
H16_A0851:pntAb1      ------------------------------------------------------------     0
H16_A1265:pntAb2      ------------------------------------------------------------     0

H16_B1715:pntA4       ALLGLGAVAPPAFMAHFTVFVLAIFVGYQVVWNVTAALHTPLMSVTNAISGIIVVGALVQ     480
H16_A3130:pntAb3      ------MEMVNHTVINLIIFVLAIYVGYHVVWTVTPALHTPLMAVTNAISAIIIVGAMLA     54
H16_A0851:pntAb1      ------MEMVSHTVINLIIFVLAIYVGYHVVWTVTPALHTPLMAVTNAISAIIIVGAMLA     54
H16_A1265:pntAb2      ------MEMVSHTVFNLIIFVLAIYVGYHVVWTVTPALHTPLMAVTNAISAIIIVGAMLA     54
                            : :: :*****:***:***.** *******:******.**:***::

H16_B1715:pntA4       LGKPSLL-TAVIAGSAVLLATINIAGGFLVTQRMLKMFQRD------------------     520
H16_A3130:pntAb3      AGLTEGGVGRVMGTLAVALAAVNVFGGFLVTQRMLEMFKKKEPKAKAPESKPALAREGA-     113
H16_A0851:pntAb1      AGLTEGYVGRAMGTLAVALAAVNVFGGFLVTQRMLEMFRKKAPKAQPEAKGQPGGKLAEV     114
H16_A1265:pntAb2      AGLTEGYVGRSMGTLAVALAAVNVFGGFLVTQRMLEMFRKKAPKAQPEAKGQPGGKLAEV     114
                       *  .      :.  ** **::*: **********:**::.

H16_B1715:pntA4       --        520
H16_A3130:pntAb3      --        113
H16_A0851:pntAb1      AQ        116
H16_A1265:pntAb2      AQ        116
```

Supplementary Figure 12. Alignment of the amino acid sequences for transhydrogenase subunits PntA4 and PntAb123 from *C. necator* H16. Protein sequence alignments were completed and visualised using Clustal Omega software